Fall 12-18-2015

An Assessment Of The Accuracy Of The Euler-Bernoulli Beam Theory For Calculating Strain and Deflection in Composite Sandwich Beams

Qhinhon D. Ho
qdhce@uno.edu

An Assessment Of The Accuracy Of The Euler-Bernoulli Beam Theory For Calculating Strain and Deflection in Composite Sandwich Beams

A Thesis

Submitted to the Graduate Faculty of the
University of New Orleans
in partial fulfillment of the
requirements for the degree of

Master of Science
In
Engineering

by

Ho Dac Qui Nhon

B.S., University of New Orleans, 2001

December 2015

Dedication

This thesis is dedicated to my loving and supportive wife, and to my always encouraging, ever faithful parents.

ACKNOWLEDGEMENT

I would like to thank my supervising Professor, Dr. Norma Jean Mattei for her continuous guidance and encouragement throughout the duration of this thesis.

I would like to express my gratitude to Dr. John A. McCorquodale, and Dr. Malay Ghose Hajra for taking the time to serve on my committee.

I am truly grateful for the enduring generosity, faith, and superb guidance from my professors at the University of New Orleans.

For their generous assistance in various stages of this project, I would like to acknowledge Mr. Burnell Thibodeaux, Civil Engineer, former H&H Branch Chief—U.S. Army Corps of Engineers, New Orleans District, Mr. Edward Blodgett, Civil Engineer—U.S. Army Corps of Engineers, New Orleans District, Dr. William Middleton, former Director of the Learning Resource Center-University of New Orleans, and his wife Anne Middleton, Ms. Sandra Hinton, former Executive Assistant-Learning Resource Center-University of New Orleans.

To those who have been there along the way, I am forever thankful for the reflections I have seen in you.

TABLE OF CONTENTS

LIST OF TABLES

LIST OF FIGURES

NOMENCLATURE

E_{skin}	Modulus of Elasticity-Skin Material (psi)
E_{core}	Modulus of Elasticity-Core Material (psi)
n	Ratio of Moduli of Elasticity
t_{core}	Core Thickness (in)
t_{skin}	Skin Thickness (in)
b	Composite Sandwich Beam Width (in)
$b_{transformed}$	Effective Laminated Skin Width (in)
I	Moment of Inertia (in^4)
EI_{eq}	Equivalent Flexural Rigidity ($lbf*in^2$)
M_{center}	Bending Moment due to Center-Point Load (lbf*in)
$M_{quarter}$	Bending Moment due to Quarter-Point Load (lbf*in)
P	Experimental Load (lbf)
L	Length of Composite Sandwich Beam (in)
L_{span}	Length of Composite Sandwich Beam under support (in)
ε	Normal Strain (in/in)
c	Distance from Neutral Surface to Outermost Fiber of Skin Layers (in)
ρ	Radius of Curvature (in)
ε_{center}	Normal Strain due to Center-Point Load (in/in)
$\varepsilon_{quarter}$	Normal Strain due to Quarter-Point Load (in/in)
D_{center}	Deflection due to Center-Point Load (in)
$D_{quarter}$	Deflection due to Quarter-Point Load (in)

ABSTRACT

ABSTRACT

This study focuses on assessing the accuracy of the Euler-Bernoulli beam theory as computational bases to calculate strain and deflection of composite sandwich beam subjected to three-point and four-point bending. Two groups of composite sandwich beams tests results will be used for comparison purposes. Mechanical properties for the laminated skin are provided by researchers from University of Mississippi (Ellen Lackey et al., 2000). Mechanical properties for the balsa wood core are provided by Alcan Baltek Corporation. Appropriate material properties and test geometries are then used in the Euler-Bernoulli-based algorithm in order to generate analytical data for comparison to experimental data provided by researchers from University of New Orleans (UNO, 2005). The resulting single material cross section is then analyzed in the traditional manner using the Euler-Bernoulli beam theory. In general, the Euler-Bernoulli beam theory provides an appropriate analytical approach in predicting flexural behavior of composite sandwich beams.

Keywords: composite sandwich beams, Euler-Bernoulli Beam Theory, laminated skin, center-point load configuration, quarter-point load configuration

OBJECTIVE OF RESEARCH

The objective of this research is to determine if a less complex theory yields acceptable results when compared to experimental results. In this thesis, Euler-Bernoulli based algorithm will be used to estimate flexure responses for composite sandwich beams subjected to various loading conditions. This thesis will incorporate mechanical properties for laminated skin from University of Mississippi (Ellen Lackey et al., 2000), mechanical properties for end grain balsa wood (Alcan Baltek Corporation), and experimental data provided by researchers from University of New Orleans (UNO, 2005). This thesis will provide algorithm development of the Euler-Bernoulli beam theory and introduces established criteria for employing the theory. For analysis purposes, this thesis will introduce composite sandwich beam mechanical properties, geometry, loading configurations, and related parameters. Analytical data, generated by applying the Euler-Bernoulli based algorithm, are then compared to experimental data recorded by researchers from the University of New Orleans (UNO, 2005). Finally, the validity and applicability of this single approach are investigated for future reference.

METHODOLOGY ADOPTED

The methodology that will be used to assess the accuracy of Euler-Bernoulli beam theory in generating acceptable results when compared to experimental results is a series of bending analysis of composite sandwich beams. Analytical data such as normal strain and deflection will be compared to experimental strain and deflection data (UNO, 2005). These composite sandwich beams will be subjected to center-point loading and quarter-point loading in accordance with ASTM C 393-00-a standard testing method for flexural properties of sandwich constructions.

LITERATURE REVIEW

At its simplest, a composite sandwich beam consists of a lightweight core sandwiched between two stiff facesheets (Francisco A. et al., 2000). A composite sandwich beam, with appropriate stiffness-density ratio, can be strong and stiff enough to withstand loading conditions while remaining relatively light compared to beams of similar geometry of different materials. For structural engineers, durability and lightweight are desirable characteristics in modern construction.

As the use of composite materials increases, so do the challenges of developing robust modeling and analysis tools that incorporate important material characteristics and behavioral response features. The fundamentals of sandwich construction and reviews of analytical and computational methods are described in recent works by Zenkert (1997). Many of the models proposed to date are approximations to the three-dimensional elasticity theory based on assumptions for the displacements, strains and/or stresses through the thickness. The need for composite beam, plate, and shell theories with better predictive capabilities has led to the development of higher-order theories. In these refined theories, commonly known as refined equivalent single-layer theories, higher-order kinematic terms (Eugenio Oñate, 2009), with respect to the beam-depth, have been added to the expressions for the transverse displacement. Similar contributions were also made by Ambartsumian (Ambartsumian S. A., 1953) that incorporated deformation characteristics of the individual layers of the structure. These models use power law and exponential fitting equations, but they have limited correlation. Still, while added variables provide excellent fit to the data, they may not necessarily relate to physical properties or characteristics (Hunt et al., 2015). While notable improvements have been achieved, these higher-order theories are cumbersome and computationally demanding, due to additional unknowns introduced into the theory (Alexander Tessler et al., 2007).

Of the existing beams theories, the Euler–Bernoulli and Timoshenko beam theories are most popular among scientists and engineers. It is widely known that the Euler-Bernoulli beam theory properly models the behavior of flexure-dominated (or ‘‘long”) beams. The Timoshenko theory is known to apply for shear-dominated (or ‘‘short”) beams. In the mid-length range, both

theories should be equivalent, and some agreement between them would be expected (André Teófilo Beck et al., 2009). The differences are in the assumptions of both theories. In the Euler-Bernoulli beam theory, under loading conditions the cross sections are perpendicular to the neutral axis. In other words, the two fundamental assumptions of the classical Euler-Bernoulli beam theory are that the transverse shear and through-the-depth normal strains are negligible, compared to the axial strain associated with bending action (Alexander Tessler et al., 2003). The Timoshenko beam theory, on the other hand, assumes rotation between the cross sections and the neutral axis, under transverse loads. Essentially, the Timoshenko beam theory takes into account shear deformation and rotational inertia effects, making it suitable for describing the behavior of short beams. Between the two theories, the Euler-Bernoulli beam theory is a simplification of the linear theory of elasticity, and the kinematic assumptions, upon which the Euler-Bernoulli beam theory is founded, that can also be extended to the analysis of composite sandwich beams.

CHAPTER I

INTRODUCTION

1.1 Composite Material Overview

Composite sandwich beams and panels, comprised of strong outer skins and low-density cores, are well known in many areas of engineering. In construction, sandwich structures offer improved stiffness and strength to weight ratios compared to monolithic materials (E.E. Gdoutos et al., 2008). The advantage is in the separation of the skins by a low-density core that increases the moment of inertia of the beam with minimal increase in weight. By design, the relatively high tensile strength skin layers will carry most of the bending moments while the core material will stabilize the skin layers and carry all transverse shear force (E.E. Gdoutos et al., 2008). Composite sandwich beams can be stronger in shear and bending as the density of the core material increases. Typical sandwich construction exhibits high transverse stiffness when compared to materials with similar weight. The high stiffness to weight ratio makes sandwich construction a very attractive design option in weight critical structures and is often incorporated in certain construction practices. Common products such as composite wood panels, home furniture, etc. are often comprised of resin infused laminates bonded to balsa wood core or rigid polyurethane foam core. Similarly, many functional parts of modern sea, land, air, and space vehicles are made of composite materials to take advantage of high tensile characteristics and significant weight reduction.

1.2 Computational History

As laminate structure, become more and more complex, so has the theories used in predicting composite behaviors under various loads. Depending on the application, the computational effort to obtain analytical values is a daunting task that has been avoided when considering laminated-composite structures in flexure. Instead, to overcome certain computational inflexibility, the focus has shifted to conducting experiments and making adjustments as deemed necessary to eventually arrive at an optimal composite material

combination as well as precise composite geometry (Issac M. Daniel et al., 2000). Typically, materials for composite sandwich beams are chosen for an experiment. From the selected materials, composite sandwich beams of certain geometry would be constructed. Based on the selected composite beam geometry, loading experiments are conducted according to suitable ASTM procedures. Data such as loading values, deflection, and normal strain are collected via computerized data acquisition systems. The data are then analyzed using current theories or completely new algorithms in order to identify optimal composite constituents and over all geometry. Over the years, it is well known within the composite industry, that employing classical theories to solve non-traditional structural systems often lead to considerable errors. Considering how difficult a problem it has been in predicting and analyzing data such as normal stress, normal strain, and deflections for composite sandwich structures, the objective of this research is to determine if a less complex theory yields acceptable results when compared to experimental flexure bending tests of composite panels.

1.3 Organization of Thesis

This thesis will compare experimental load and strain data from flexural bending tests performed at the University of New Orleans with those predicted using the fairly simple Euler-Bernoulli theory and the equivalent area method to "transform" one of the composite material into an equivalent amount of the other. In this thesis, the composite panel is made of a laminated skin (itself a composite) and a balsa wood core. For simplicity, the laminate skin will be modeled as a uniform, homogeneous material.

Chapter I: Introduction to composite materials, mechanical properties for laminated skin material provided by researchers from University of Mississippi (Ellen Lackey et al., 2000), mechanical properties for end grain balsa wood (Alcan Baltek Corporation) and experimental data provided by researchers from the University of New Orleans (UNO, 2005).

Chapter II: Introduction to composite sandwich beam geometry and loading configurations provided by researchers from the University of New Orleans (UNO, 2005).

Chapter III: Introduction to Euler-Bernoulli beam theory, algorithm development, and normal strain and deflection analysis.

Chapter IV: Compare analytical and experimental data.

Chapter V: Recommendations and Conclusions

1.4 Characterization of Constituent Materials

1.4.1 Laminated Skin

In polymeric composite terms, a fabric is defined as a manufactured assembly of long fibers of carbon, aramid or glass, or a combination of these, to produce a flat sheet of one or more layers of fibers (USDOD, 2002). These layers are held together either by mechanical interlocking of the fibers themselves or with a secondary material to bind these fibers together and hold them in place, giving the assembly sufficient integrity to be handled. Fabric types are categorized by the orientation of the fibers used, and by the various construction methods used to hold the fibers together. The four main fiber orientation categories are: unidirectional, 0/90 (woven, stitched or hybrid), multi-axial, woven fabrics, and other/random. The fabric's integrity is maintained by the mechanical interlocking of the fibers. All of the different fibers used in composites have different properties and so affect the properties of the composite in different ways. (Wim Van Paepegem, 2004)

The matrix material used was Derakane 510A-40 Vinyl ester resin, a brominated bisphenol-A based vinyl ester, designed to offer increased adhesive strength, superior resistance to abrasion and severe mechanical stress, while giving greater toughness and elongation. (Ashland Composite Polymers, 2005)

In this research, the laminated skin panels are made of 24 oz. woven fabric with Dow Derakane 510A Vinyl ester resin. These sample skin specimens were fabricated at Ingalls Shipbuilding facility and tested for flexural strength at University of Mississippi (Ellen Lackey et

al., 2000). According to ASTM D790-10 guidelines, samples of dimensions 5 in. length, 1 in. width, and 0.25 in. thick, were cut from the panels and subjected to flexural testing using MTS universal test machines. These samples were then subjected to environmental conditioning-room temperature and humidity-to examine secondary bonding concerns. E_{RT1}, E_{RT2}, E_{RT3}, and E_{RT5} are flexural modulus for each tested laminated skin panel. For this research, only the average modulus of elasticity, $E_{average}$, for the laminated skin material is to be used in assessing the accuracy of the Euler-Bernoulli beam theory. The average modulus of elasticity value for the laminated skin is given in Table 1. Additional data is included in Appendix I.

Table 1. Laminated Skin Flexural Moduli and Average Flexural Modulus

LAMINATED PANEL #	ELASTICITY
	(psi)
RT 1	E_{RT1} = 5479452
RT 2	E_{RT2} = 4854369
RT 3	E_{RT3} = 5405405
RT 5	E_{RT5} = 4878048
	$E_{average}$= 5154319

1.4.2 End Grain Balsa Wood Core

Regarding composite sandwich beams, the consensus on core material selection is that a stiff core that transmits the load to the other face of the laminate causes fracture or delamination, while a core that deforms will absorb the impact preventing further damage. The properties of balsa make it ideal as a core for sandwich construction. It has extremely high strength and stiffness to weight ratios, and achieves an excellent bond with all types of resins and adhesives (Ashish, 2007). Balsa wood is known to be compatible with a variety of manufacturing processes and is resistant to temperature changes, or exposure to fire or chemicals such as styrene. Generally, core density is of significant influence on the overall strength of a composite sandwich beam. For the selected end grain balsa wood core materials, mechanical properties of core material with designations S 56, D 100, and S 1415 are given in Table 2 (Alcan Baltek Corporation, 2000).

Table 2. End-grain balsa wood core properties

BALSA WOOD PROPERTIES	S 56	D 100	S 1415
Nominal Density, lbf/ft^3	6.07	9.4	15
Compressive Strength, psi (Perpendicular to plane)	961	1837	3617
Compressive Modulus, psi (Perpendicular to plane)	302664	568661	1115647
Tensile Strength, psi (Perpendicular to plane)	1114	1886	3309
Tensile Modulus, psi (Perpendicular to plane)	**329443**	**510176**	**814110**
Ultimate Shear Strength, psi	271	427	693
Shear Modulus, psi	15696	22829	42864
Thermal Conductivity, $(BTU*in)/(ft^2*h*^{\circ}F)$	0.339	0.453	0.574

1.5 Composite Sandwich Beam Load Test-University of New Orleans

In the summer of 2005, researchers from University of New Orleans (UNO, 2005) conducted a series of flexure tests on a set of composite sandwich beams that consisted of laminated skin materials (Ellen Lackey et al., 2000) and balsa wood core of three different densities: S 56, D 100, and S 1415 (Alcan Baltek Corporation). The intent of these tests was to determine the performance of composite sandwich beams with varying beam geometries, core thicknesses, and core densities while maintaining constant skin thickness. Resulting data from these bending tests were used to calculate flexural stiffness and shear modulus.

The following figures were generated using data as reported by researchers from the University of New Orleans (UNO, 2005). Group I tests were performed using a core of D 100 with increasing core thickness. Group II tests were performed using a core thickness of 3" with increasing balsa wood core density. The laminate skin for all tests (Group I & Group II) was held at a constant ¼" thickness and all of the same manufacture. The proprietary SCRIMP method was used to manufacture all specimens. Specimens were manufactured by Siemens Corporation. Appendix I contains detailed calculations for average modulus of elasticity of the skin material. Figure 1 shows experimental strain from Group I-Center Load. Figure 2 shows experimental

deflection from Group I-Center Load. Figure 3 shows experimental strain from Group I-Quarter Load. Figure 4 shows experimental deflection from Group I-Quarter Load. The results for experimental strain from Group I and experimental deflection from Group I are presented in accordance to flexural analysis schedules shown in Table 5, Table 6, and Table 7 of Chapter II.

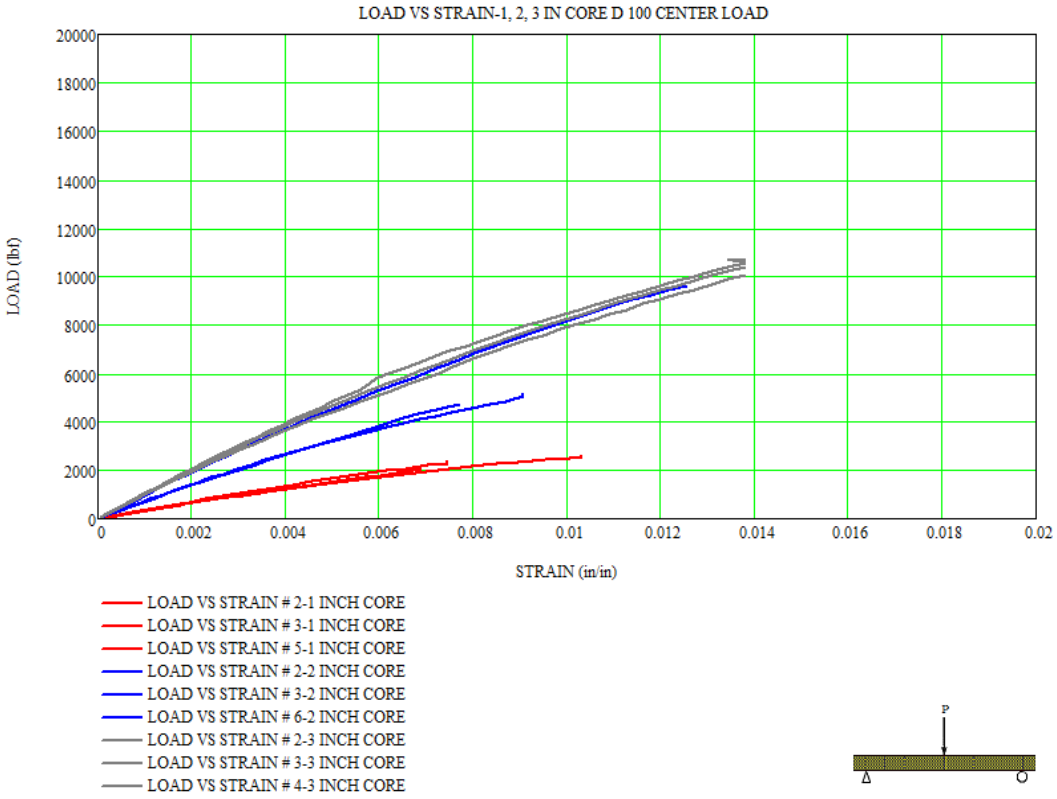

Figure 1. Experimental Load vs. Strain-Group I-Center Load

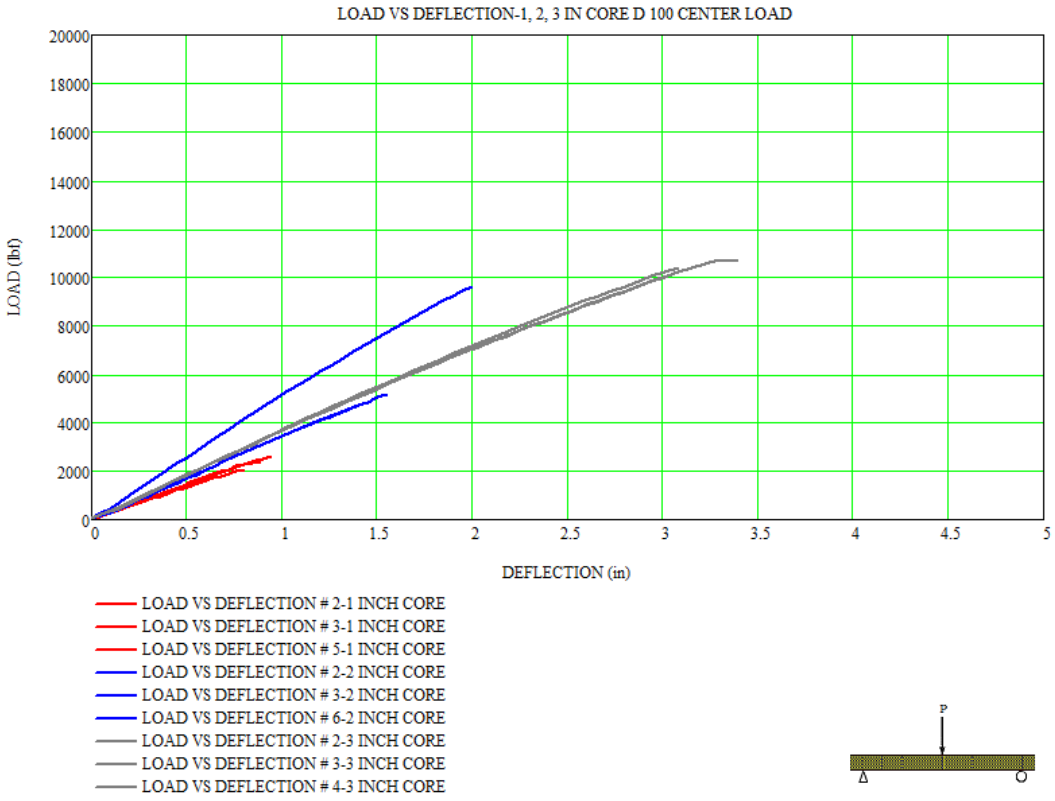

Figure 2. Experimental Load vs. Deflection-Group I-Center Load

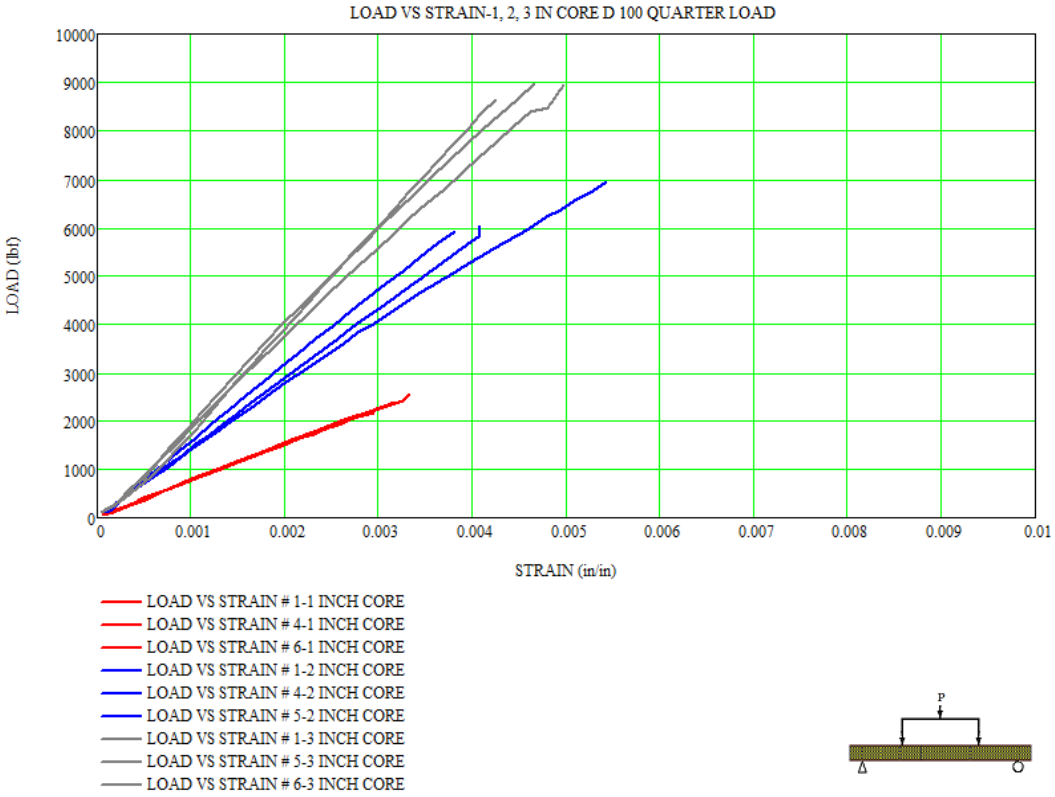

Figure 3. Experimental Load vs. Strain-Group I-Quarter Load

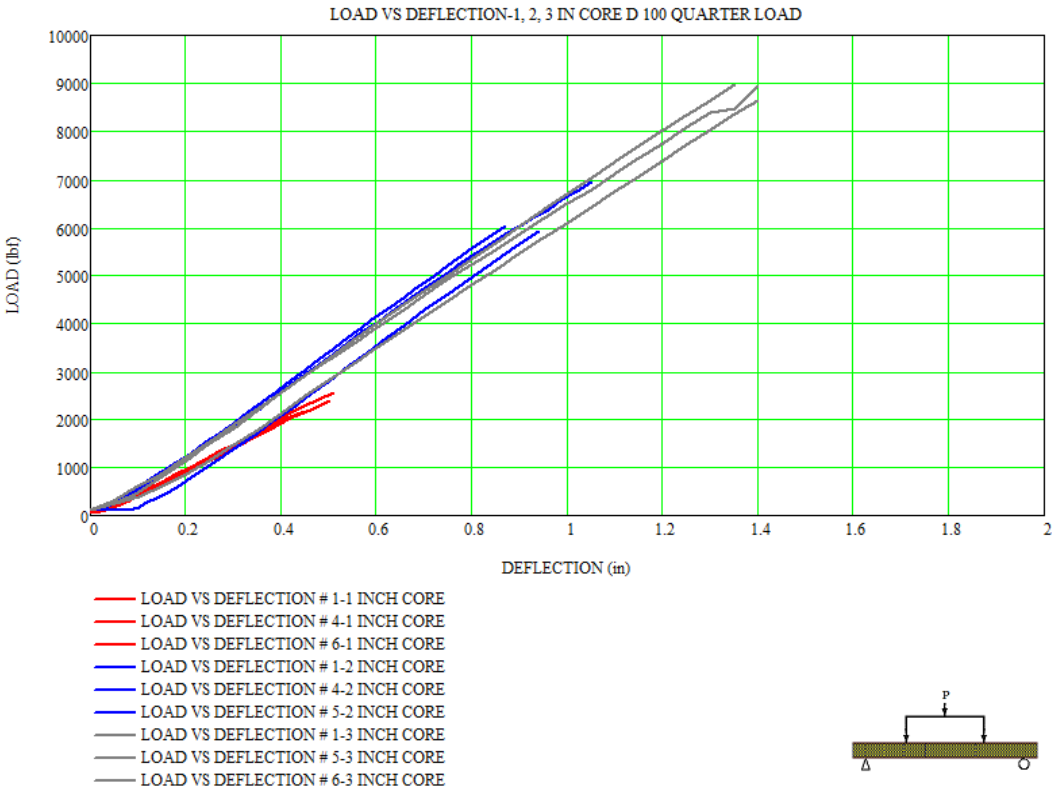

Figure 4. Experimental Load vs. Deflection-Group I-Quarter Load

The following figures were generated using data as reported by researchers from the University of New Orleans (UNO, 2005). Figure 5 shows experimental strain from Group II-Center Load. Figure 6 shows experimental deflection from Group II-Center Load. Figure 7 shows experimental strain from Group II-Quarter Load. Figure 8 shows experimental deflection from Group II-Quarter Load. The results for experimental strain from Group II and experimental deflection from Group II are presented in accordance to flexural analysis schedules shown in Table 8, Table 9, and Table 10 of Chapter II.

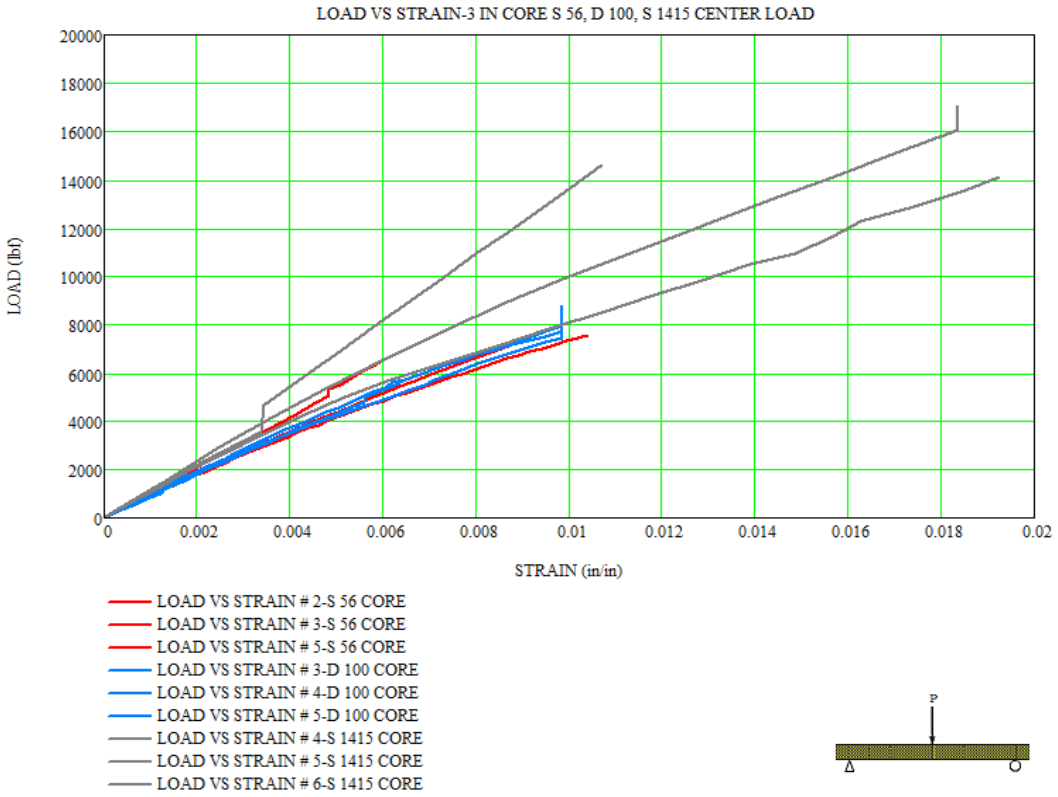

Figure 5. Experimental Load vs. Strain-Group II-Center Load

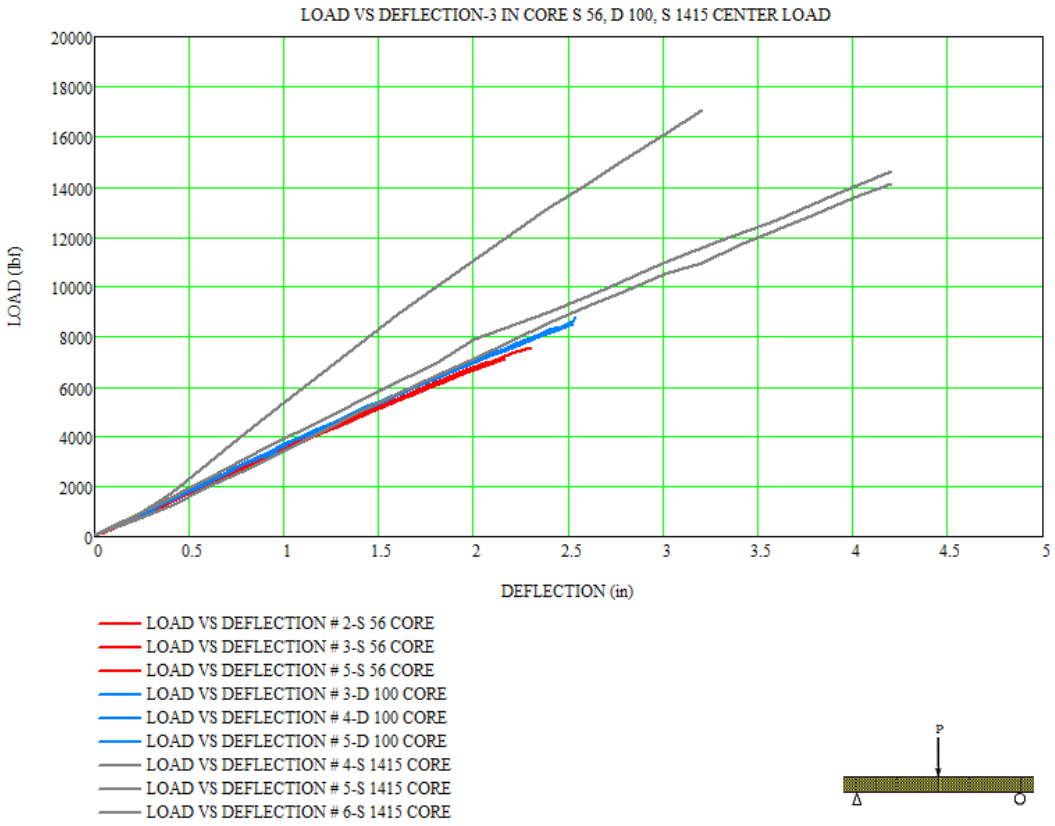

Figure 6. Experimental Load vs. Deflection-Group II-Center Load

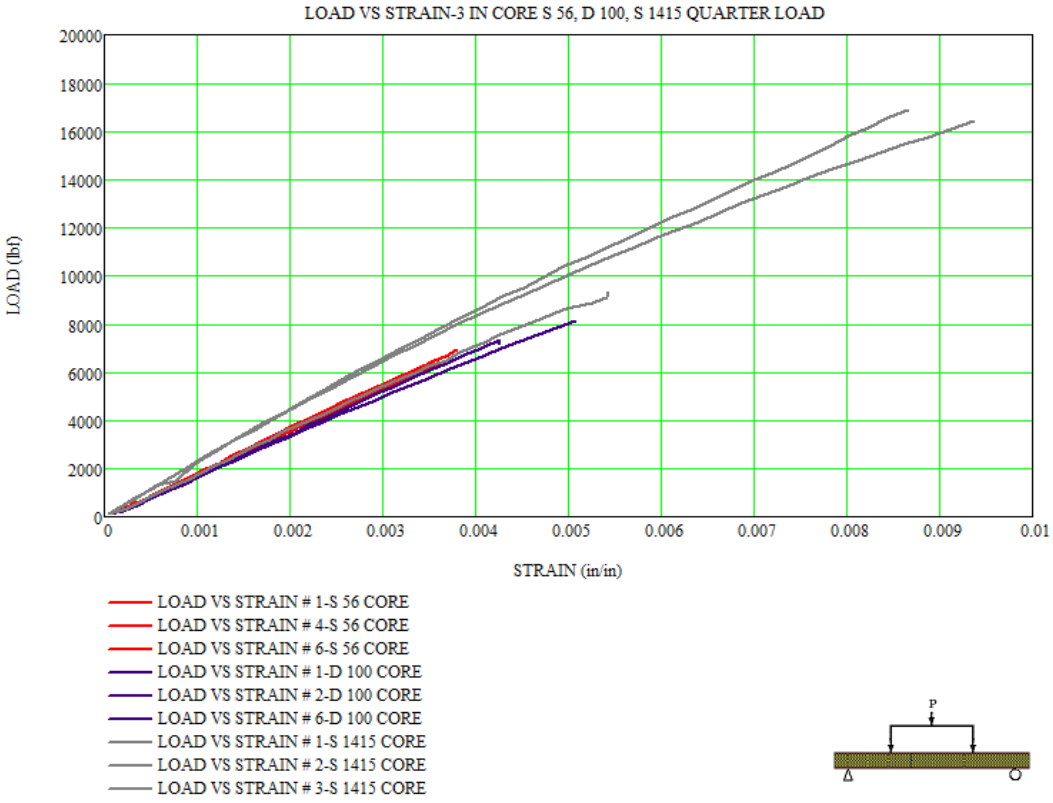

Figure 7. Experimental Load vs. Strain-Group II-Quarter Load

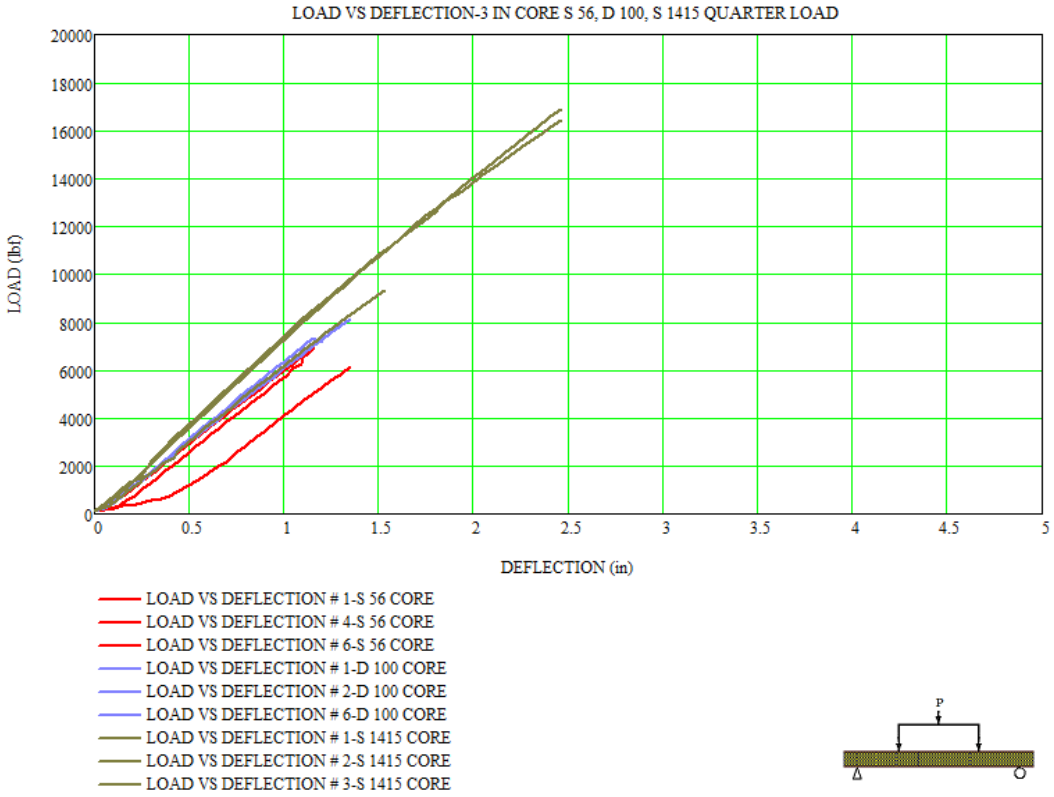

Figure 8. Experimental Load vs. Deflection-Group II-Quarter Load

CHAPTER II

BEAM GEOMETRY AND LOADING CONFIGURATIONS

2.1 Composite Sandwich Beam Geometry

Sandwich construction is of particular interest and widely used, because the concept is very suitable and amenable to the development of lightweight structures with high in-plane and flexural stiffness. Sandwich panels consist typically of two thin face sheets (or facings, or skins) and a lightweight thicker core (E.E. Gdoutos et al., 2008). The composite sandwich concept allows the positioning of different materials to take advantage of their combined properties. In a composite sandwich beam, the beam's bending stiffness is proportional to the core thickness, in the same way an I-beam is stiffer as the distance between the flanges increases. Certainly, steel I-beams are always preferable over laminated composite beams in terms of strength. However, in some cases, adequate structural solutions can be found in laminated composite sandwich with specifically designed load capacity that favors weight reduction and geometric modifications.

In this research, the composite sandwich beams consist of composite vinyl ester outer skins and balsa wood cores that are designed to be narrow and consistently slender in accordance with Euler-Bernoulli beam theory's requirements. In terms of reducing deformation and delaying failure under loading conditions, precise beam geometry and mechanical properties of the constituent materials may enhance the performance of the beams (Leichti, 1989). The typical geometry of a composite sandwich beam is shown in Figure 9 (UNO, 2005).

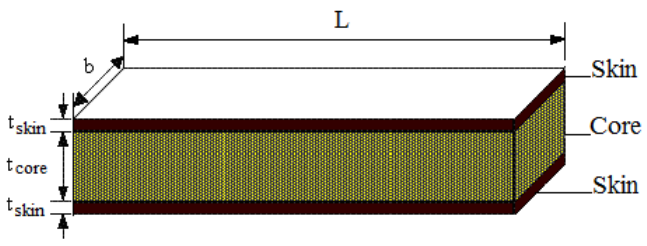

Figure 9. Composite sandwich beam overall geometry.

In order to assess the accuracy of the Euler-Bernoulli beam theory, tests from two groups of composite sandwich beams were used for comparison. In Group I, the overall beam length, span length, beam width, and core thickness for composite sandwich beams varied, while core density and skin thickness were kept constant. Geometric data and core density data for Group I are given in Table 3. Composite sandwich beams geometry for Group I is given in Figure 10 (UNO, 2005).

Table 3. Group I-Geometric data and core density

Core Thickness t_{core} (in)	Skin Thickness t_{skin} (in)	Beam Width b (in)	Beam Length L (in)	Span Under Loading (in)	Core Density (pcf)
1	**0.25**	**3**	**32**	**29.5**	**9.4**
2	**0.25**	**5**	**52.5**	**50.5**	**9.4**
3	**0.25**	**7**	**73.5**	**70**	**9.4**

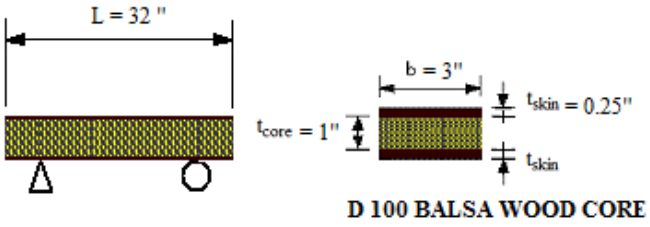

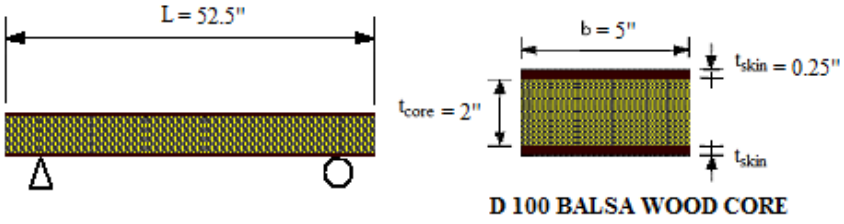

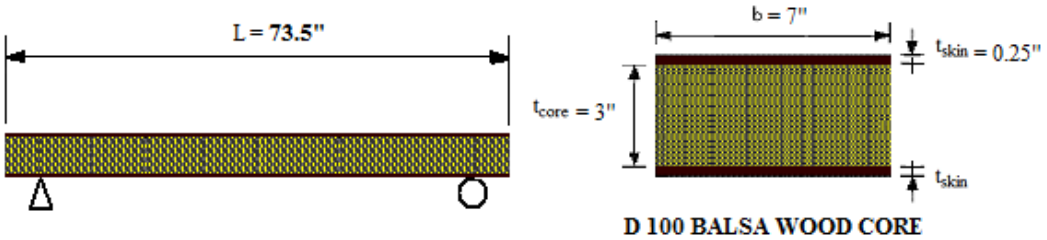

Figure 10. Composite sandwich beams geometry Group I

In Group II, core density varied, while overall length, span length, beam width, skin thickness, and core thickness were kept constant. Geometric data and core density data for Group II are given in Table 4. Composite sandwich beams geometry for Group II is given in Figure 11 (UNO. 2005).

Table 4. Group II-Geometric data and core density

Core Thickness t_{core} (in)	Skin Thickness t_{skin} (in)	Beam Width b (in)	Beam Length L (in)	Span Under Loading (in)	Core Density (pcf)
3	**0.25**	**7**	**73.5**	**70**	**6.07**
3	**0.25**	**7**	**73.5**	**70**	**9.4**
3	**0.25**	**7**	**73.5**	**70**	**15**

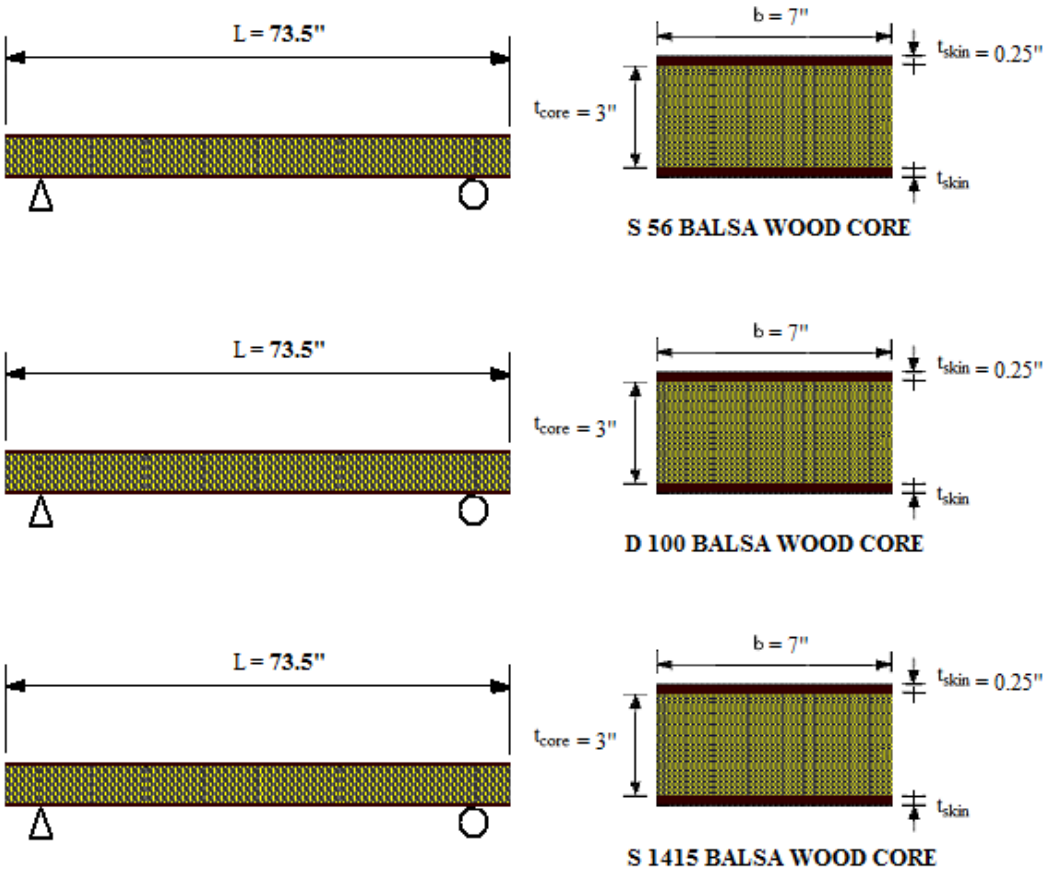

Figure 11. Composite sandwich beams geometry Group II.

2.2 Loading Configurations-ASTM Procedure

Given the structural composition of the composite sandwich beams, ASTM C 393-00 was used, being a suitable testing method for flexural properties of composite sandwich construction that allows the applied transverse loads to produce a curvature across all layers of the composite structure. ASTM C 393-00 is an acceptable testing method for both center-point loading and quarter-point loading, or three-point and four-point load (ASTM Standard C 393-00).

Figure 12 shows center-point loading configuration with beam lengths of L = 32”, 52.5”, and 73.5”, L_{span} = 29.5”, 50.5”, and 70” (UNO. 2005).

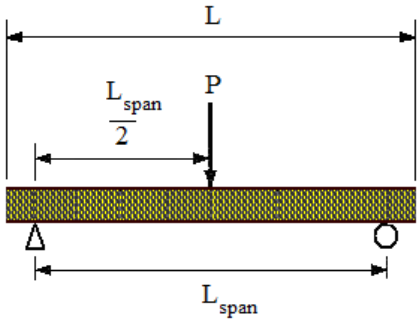

Figure 12. Center-point load configuration

Figure 13 shows quarter-point loading configuration with beam lengths of L = 32”, 52.5”, and 73.5”, L_{span} = 29.5”, 50.5”, and 70” (UNO, 2005).

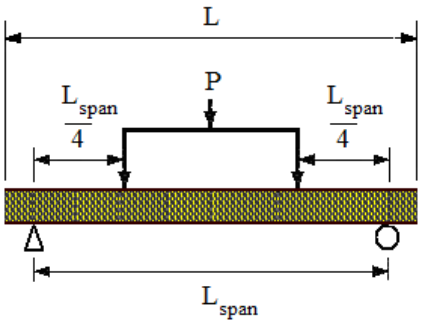

Figure 13. Quarter-point load configuration

The following sections present composite sandwich beam geometry and loading configuration for Group I and Group II (UNO, 2005).

2.2.1 Group I

In Group I, core density and skin thickness are constant, while core thickness, beam width, beam length, span under loading, and loading configurations vary. The objective in Group I is to assess loading capacity in composite sandwich beams with increasing core thickness. There are six identical composite sandwich beams for each given core thickness, with three beams subjected to center loading and three beams subjected to quarter loading configuration. In total, there are 18 composite sandwich beams and 18 loading tests-9 center-point load tests and 9 quarter-point load tests. Table 5, Table 6, and Table 7 list pertinent data for each composite beam in Group I (UNO, 2005).

Table 5. Flexural testing schedule-1 in. core-D 100 core density

Beam #	E=510176 psi Balsawood Core Thickness (in)	E=5154319 psi Laminated Skin Thickness (in)	Beam Width b (in)	Beam Length L (in)	Span Under Loading (in)	D 100 Core Density (pcf)	Loading Configuration
2	**1**	**0.25**	**3**	**32**	**29.5**	**9.4**	**Center**
3	**1**	**0.25**	**3**	**32**	**29.5**	**9.4**	**Center**
5	**1**	**0.25**	**3**	**32**	**29.5**	**9.4**	**Center**
1	**1**	**0.25**	**3**	**32**	**29.5**	**9.4**	**Quarter**
4	**1**	**0.25**	**3**	**32**	**29.5**	**9.4**	**Quarter**
6	**1**	**0.25**	**3**	**32**	**29.5**	**9.4**	**Quarter**

Table 6. Flexural testing schedule-2 in. core-D 100 core density

Beam #	E=510176 psi Balsawood Core Thickness (in)	E=5154319 psi Laminated Skin Thickness (in)	Beam Width b (in)	Beam Length L (in)	Span Under Loading (in)	D 100 Core Density (pcf)	Loading Configuration
2	2	0.25	5	52.5	50.5	9.4	Center
3	2	0.25	5	52.5	50.5	9.4	Center
6	2	0.25	5	52.5	50.5	9.4	Center
1	2	0.25	5	52.5	50.5	9.4	Quarter
4	2	0.25	5	52.5	50.5	9.4	Quarter
5	2	0.25	5	52.5	50.5	9.4	Quarter

Table 7. Flexural testing schedule-3 in. core-D 100 core density

Beam #	E=510176 psi Balsawood Core Thickness (in)	E=5154319 psi Laminated Skin Thickness (in)	Beam Width b (in)	Beam Length L (in)	Span Under Loading (in)	D 100 Core Density (pcf)	Loading Configuration
2	3	0.25	7	73.5	70	9.4	Center
3	3	0.25	7	73.5	70	9.4	Center
4	3	0.25	7	73.5	70	9.4	Center
1	3	0.25	7	73.5	70	9.4	Quarter
5	3	0.25	7	73.5	70	9.4	Quarter
6	3	0.25	7	73.5	70	9.4	Quarter

2.2.2 Group II

In Group II, core densities and loading configurations vary, while core thickness, beam width, beam length, and span under loading remain constant. The objective in Group II is to assess loading capacity in composite sandwich beams with varying core densities. There are six identical composite sandwich beams for each given core density, with three beams subjected to center loading and three beams subjected to quarter loading configuration. In total, there are 18 composite sandwich beams and 18 loading tests-9 center-point load tests and 9 quarter-point load tests. Table 8, Table 9, and Table 10 list pertinent data for each composite beam in Group II (UNO, 2005).

Table 8. Flexural testing schedule 3 in. core-S 56 core density

Panel #	E=329443 psi Balsawood Core Thickness (in)	E=5154319 psi Laminated Skin Thickness (in)	Beam Width b (in)	Beam Length L (in)	Span Under Loading (in)	S 56 Core Density (pcf)	Loading Configuration
2	3	0.25	7	73.5	70	6.07	Center
3	3	0.25	7	73.5	70	6.07	Center
5	3	0.25	7	73.5	70	6.07	Center
1	3	0.25	7	73.5	70	6.07	Quarter
4	3	0.25	7	73.5	70	6.07	Quarter
6	3	0.25	7	73.5	70	6.07	Quarter

Table 9. Flexural testing schedule 3 in. core-D 100 core density

Panel #	E=510176 psi Balsawood Core Thickness (in)	E=5154319 psi Laminated Skin Thickness (in)	Beam Width b (in)	Beam Length L (in)	Span Under Loading (in)	D 100 Core Density (pcf)	Loading Configuration
3	3	0.25	7	73.5	70	9.4	Center
4	3	0.25	7	73.5	70	9.4	Center
5	3	0.25	7	73.5	70	9.4	Center
1	3	0.25	7	73.5	70	9.4	Quarter
2	3	0.25	7	73.5	70	9.4	Quarter
6	3	0.25	7	73.5	70	9.4	Quarter

Table 10. Flexural testing schedule 3 in. core-S 1415 core density

Panel #	E=814110 psi Balsawood Core Thickness (in)	E=5154319 psi Laminated Skin Thickness (in)	Beam Width b (in)	Beam Length L (in)	Span Under Loading (in)	S 1415 Core Density (pcf)	Loading Configuration
4	3	0.25	7	73.5	70	15	Center
5	3	0.25	7	73.5	70	15	Center
6	3	0.25	7	73.5	70	15	Center
1	3	0.25	7	73.5	70	15	Quarter
2	3	0.25	7	73.5	70	15	Quarter
3	3	0.25	7	73.5	70	15	Quarter

CHAPTER III

ALGORITHM DEVELOPMENT AND ASSESSMENT

3.1 Algorithm Development Overview

In this chapter, the first two sections present required criteria for employing Euler-Bernoulli beam theory and equivalent area transformations for predicting stress-strain behavior of composite sandwich beams. In subsequent sections, detailed development and application of the Euler-Bernoulli's based algorithm are presented.

3.2 Theoretical Relevance

The Euler-Bernoulli beam theory is the gold standard used in the determination of stress field or deflections of a homogeneous elastic beam (Stefano Cutrona et al., 2013). The Euler-Bernoulli beam theory can be adapted to assess the flexural behavior of laminated sandwich beams (Tanveer, 2013). One of the primary advantages of employing the Euler-Bernoulli beam theory is its simplicity in modeling load carrying capacity of composite sandwich structures. This development condenses the complex three-dimensional structural response of the slender beams in bending, torsion, and so on, and casts this into a manageable mathematical format. These models are indispensable in all fields of structural engineering and the advantage of the dimensional reduction is condensation of the three-dimensional response and the related mechanical insight into typical ‘engineering phenomena’, like stretching, transverse shear deformation, bending, or twisting (M. Bischoff et al., 2004). According to Haukaas (Terje Haukaas, 2002), the Euler Bernoulli beam theory assumptions are:

1. The material is linear elastic according to Hooke’s law.
2. Beam material is homogeneous and isotropic.
3. Plane sections remain plane and perpendicular to the neutral axis.
4. The beam must be straight with constant cross-section.
5. The beam has an axis of symmetry in the plane of bending.

6. The loads must be perpendicular to the longitudinal axis of the beam.

The following sections outline significant assumptions and subsequent algorithmic development, based on the Euler-Bernoulli beam theory, for calculating strain and deflection analysis in composite sandwich beams.

3.3 Fundamental Assumptions

In this research, the aim is to assess the accuracy of the Euler-Bernoulli beam theory as computational bases to model the strain and deflection characteristics of two groups of composite sandwich beam subjected to three-point and four-point bending tests, for the linearly elastic portion of the loading. As mentioned previously, the Euler-Bernoulli beam theory can be used to predict theoretical values of strain and deflection, among other quantities (Tanveer, 2013). The Euler-Bernoulli beam theory can be adapted to facilitate analysis of composite sandwich beams. A key piece in this approach is based on the assumption that the relationship between bending moment and beam curvature exists in a composite sandwich beam under loading conditions. For a prismatic member, possessing a plane of symmetry, subjected to transverse loads, internal reactions are assumed to take place in any vertical cross-section perpendicular to the longitudinal axis. Therefore, for a beam experiencing bending, initially straight cross sections remain straight throughout deformation (M. Bischoff et al., 2004). Due to applied loads, internal compressive stress forces form a couple or moment equal in magnitude and opposite in direction to minimize deflection. Within the elastic range, the longitudinal fibers above the neutral surface shortened, and the longitudinal fibers below the neutral surface lengthened thereby resulting in longitudinal strain. Gradually, the process of bending stops, when every cross-section sets up full resistance to the bending moment. The internal forces shown in Figure 14 are results of applied transverse loads. In using the Euler-Bernoulli formulation for sandwich panel bending, the bond at the interface between the skin and core must remain intact throughout the duration of the loading.

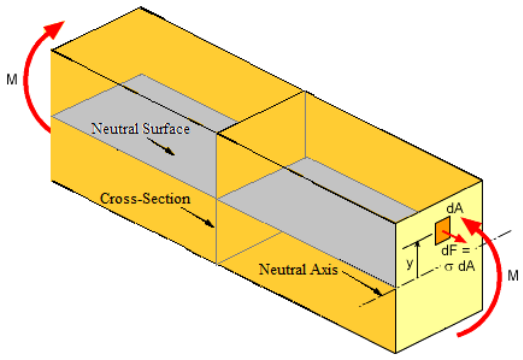

Figure 14. Internal forces due to transverse loads

Under transverse loading, the deflection is usually expressed in terms of vertical deflection from its original unloaded position. Figure 15 shows deflection of a beam, also known as the elastic curve of the beam.

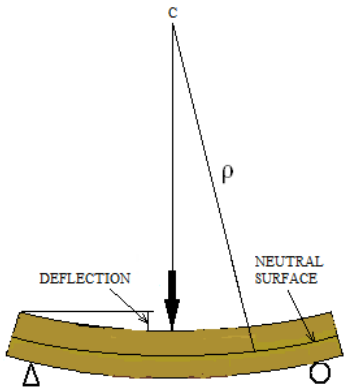

Figure 15. Simply supported beam in bending.

3.4 Formulation

In flexural analysis, the deformation of a composite member may be determined by using the transformed-section method (Beer et al., 1992). The transformed-section method, also known as equivalent area method, provides the critical function of convergent mediation for eventual application of the Euler-Bernoulli beam theory. As a result of employing the equivalent area method, the cross-section of a composite sandwich beam is transformed to resemble an I-beam cross-section, which satisfies conditions 1, 2, 3 and 4. Figure 16 shows the original cross-section

and the transformed cross-section of a composite sandwich beam. Under simulated transverse loads, the virtually transformed composite sandwich beam is assumed to exhibit loading characteristics similar to that of an I-beam. That is, the transformed beam forms an elastic curve with center C and radius of curvature ρ, and internal forces are assumed to take place uniformly in any vertical cross section perpendicular to the longitudinal axis as presented in Figure 14 and Figure 15. Thus, with conditions 4 and 5 satisfied, application of the Euler-Bernoulli beam theory is justified and the proposed algorithm based on Euler-Bernoulli beam theory is now fully enabled for further derivation.

The following sections present the development of the Euler-Bernoulli based algorithm with the incorporation of the equivalent area method, which will enable subsequent application to generate predicted flexural stress-strain and deflection of composite sandwich beams under loading conditions. To facilitate consistency, algorithm development is arranged in an orderly manner along with appropriate illustrations.

3.4.1 Transformed-Section Method or Equivalent Area Method

The equivalent area method, also known as transformed-section method, provides the necessary logical bridge in solving composite beam problems involving transverse loading. By imposing a strain compatibility condition, materials making up the cross section are transformed into a fictitious homogeneous material. This is accomplished by adjusting the geometry of each material by a ratio of its elastic modulus to that of the base material modulus, creating a fictionalized shape of homogeneous material. The resulting single material cross section may then be analyzed in the traditional manner. As long as the relationship between strain and the loads is linear and the geometry of the member would not undergo significant change when the loads are applied, the principle of superposition can be used (Hamilton et al., 2001).

The base material is usually the most dominant material within the cross section. In this case, the dominant material is balsa wood. The area of the laminated outer skins is then adjusted laterally to emulate the base material's elastic characteristics. As a result, the newly transformed

cross-section is assumed to be made completely from the base material-balsa wood. The transformation begins with the ratio of moduli of elasticity as defined as,

$$n = \frac{E_{skin}}{E_{core}} \quad \text{..... (Eq. 1)}$$

where the different moduli are E_{skin} = modulus of elasticity-skin material and E_{core} = modulus of elasticity-core material, with $E_{skin} > E_{core}$.

With the moduli ratio n established, the next step is to transform the laminated composite cross-section by multiplying the width b of the skin by n.

$$b_{transformed} = n \cdot b \quad \text{..... (Eq. 2)}$$

where b = skin width, n*b = effective laminated skin width.

The virtual geometric modifications made to the laminated skin layers are shown in Figure 16. The location of the neutral axis coincides with the neutral surface or the centroidal plane. In addition, the transformed skin layers retain their original thickness, maintain symmetry about the core's vertical axis and horizontal axis, and resemble flanges on a common I-beam.

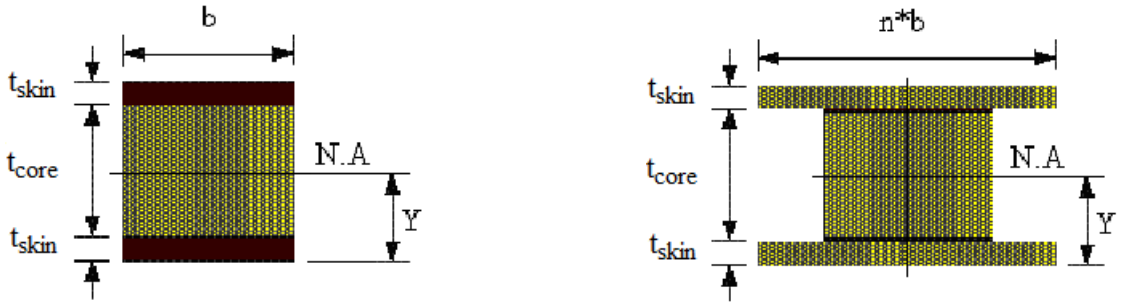

(a) Composite sandwich beam cross-section (b) Transformed cross-section

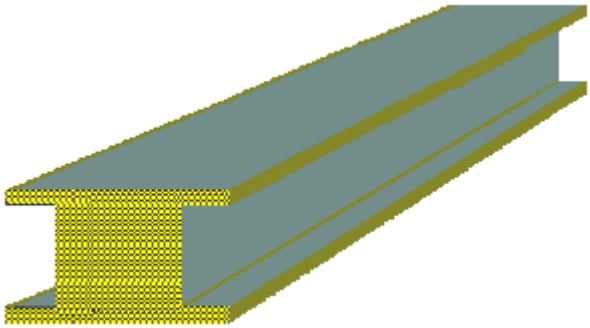

(c) Transformed composite sandwich beam

Figure 16. Composite sandwich beam geometric modifications

3.4.2 Equivalent Flexural Rigidity

From this point forward, the Euler-Bernoulli beam theory is applied for calculation of relevant beam parameters, normal strain, and beam deflection. All measurements and calculations are in direct reference to the transformed composite sandwich beam and transformed cross-section presented in Figure 16. The centroidal plane or the neutral axis of the transformed cross-section is given as,

$$Y = \frac{\Sigma y \cdot A}{\Sigma A} \quad \text{..... (Eq. 3)}$$

which equals

$$Y = \frac{\left(b_{transformed} \cdot t_{skin}\right) \cdot \left(\frac{t_{skin}}{2}\right) + \left(b \cdot t_{core}\right) \cdot \left(t_{skin} + \frac{t_{core}}{2}\right) + \left(b_{transformed} \cdot t_{skin}\right) \cdot \left(t_{skin} + t_{core} + \frac{t_{skin}}{2}\right)}{2 \cdot \left(b_{transformed} \cdot t_{skin}\right) + \left(b \cdot t_{core}\right)}$$

where b = original composite beam width, $b_{transformed}$ = effective laminated skin width, t_{core} = core thickness, and t_{skin} = skin thickness.

With the location of the neutral axis identified, the moment of inertia of the transformed composite sandwich beam cross-section is given by,

$$I = \Sigma\left(I_{centroid} + A \cdot d^2\right) \quad \text{..... (Eq. 4)}$$

which equals

$$I = \frac{b \cdot t_{core}^{\ 3}}{12} + 2 \cdot \left[\frac{n \cdot b \cdot t_{skin}^{\ 3}}{12} + n \cdot b \cdot t_{skin} \cdot \left(\frac{t_{core}}{2} + \frac{t_{skin}}{2}\right)^2\right]$$

As mentioned, the equivalent area method provides a logical way to address the multiple modulus of elasticity issue by introducing n, the ratio of moduli of elasticity. This value allows the original composite sandwich beam with two elasticity values, E_{skin} and E_{core}, to be transformed into an I-beam with elasticity value of balsa wood-E_{core}. Subsequently, flexural assessment for the transformed composite sandwich beam requires an equivalent flexural rigidity- EI_{eq}-value to be defined. Computational procedure for equivalent flexural rigidity is as follows,

$$EI_{eq} = E_{core} \cdot \left[\frac{b \cdot t_{core}^{\ 3}}{12} + 2 \cdot \left[\frac{n \cdot b \cdot t_{skin}^{\ 3}}{12} + n \cdot b \cdot t_{skin} \cdot \left(\frac{t_{core}}{2} + \frac{t_{skin}}{2}\right)^2\right]\right] \quad \text{..... (Eq. 5)}$$

where EI_{eq} = equivalent flexural rigidity, and E_{core} = modulus of elasticity of the core material.

3.4.3 Bending Moment

For both center-point load and quarter-point load configurations, bending moment values are given by,

$$M_{center} = \frac{P \cdot L_{span}}{4} \quad \text{..... (Eq. 6)}$$

and

$$M_{quarter} = \frac{P}{2} \cdot \frac{L_{span}}{4} \quad \text{..... (Eq. 7)}$$

where P = applied loads, L_{span} = length of composite beam under support as shown in Figure 12 and Figure 13. For three-point loading, the maximum bending moment occurs only at the center of the beam. For four-point loading, the bending moment is uniformly maximum between the loading points.

3.4.4 Normal Strain

For positive bending moment, normal strain varies linearly with y from the neutral axis and is assumed active at mid-beam. At the top of the beam, the fiber elements are in compression, those below the neutral axis are in tension, and at the neutral axis normal strain is zero. Under tension induced transverse loads, the corresponding strain is called tensile strain; as normal strain, it is positive. The ratio of the elongation of any isolated partial length of the bar over the initial partial length is constant over the entire bar (Beer et al., 1992). Using the bending moment calculated previously, tensile strain at outermost fiber of skin layers for laminated beams can be calculated as follows,

$$\varepsilon_m = \frac{c}{\rho} \quad \text{..... (Eq. 8)}$$

with the radius of curvature defined as

$$\frac{1}{\rho} = \frac{M}{EI_{eq}} \Rightarrow \rho = \frac{EI_{eq}}{M} \quad \text{..... (Eq. 9)}$$

Therefore, as long as the relationship between stress and strain remains $E = \frac{\sigma}{\varepsilon}$ the maximum normal strain at distance c from the neutral surface of the transformed composite sandwich beam is given as (Beer et al., 1992),

$$\varepsilon_m = \frac{c}{\rho} = \frac{c}{\frac{EI_{eq}}{M}} \Rightarrow \varepsilon_m = \frac{M \cdot c}{EI_{eq}}$$

which equals

$$\varepsilon_{center} = \frac{M_{center} \cdot c}{EI_{eq}} \quad \text{..... (Eq. 10)}$$

$$\varepsilon_{quarter} = \frac{M_{quarter} \cdot c}{EI_{eq}} \quad \text{..... (Eq. 11)}$$

where ε_{center} and $\varepsilon_{quarter}$ are tensile strain due to center-point and quarter-point loads, bending moment M_{center} and $M_{quarter}$ = bending moments due to load P, $c = \frac{t_{skin} + t_{core}}{2}$ distance from neutral surface to outer fiber, ρ = radius of curvature, and EI_{eq} = equivalent flexural rigidity.

3.4.5 Deflection

The deflection of a beam depends on its length, its cross-sectional shape, the material, how the beam is supported, and loading configuration. Therefore, deflection assumed to take place at mid-beam can be different for the same beam under varying loading configurations. The equations given here are appropriate for transformed composite sandwich beams. The total deflection of a simply supported beam under center-point and quarter-point loading conditions given as (Beer et al., 1992),

$$D_{center} = \frac{P \cdot L_{span}^{3}}{48 \cdot EI_{eq}} \quad \text{..... (Eq. 12)}$$

and

$$D_{quarter} = \frac{\frac{-L_{span}}{4} \cdot \left[\left[4 \left(\frac{L_{span}}{4} \right)^{2} - 3 \cdot L_{span}^{2} \right] \frac{P}{2} \right]}{24 \cdot EI_{eq}} \quad \text{..... (Eq. 13)}$$

where D_{center} = center load displacement, $D_{quarter}$ = quarter load displacement, L_{span} = length of composite beam under support, EI_{eq} = equivalent flexural rigidity, and P = applied load. In the quasi-static case, the amount of deflection and stresses are assumed not to change over time.

3.5 Algorithm Assessment-Verification Cases

The introduction of the equivalent area method transforms and allows composite sandwich beams to be evaluated as typical isotropic and homogenous I-beams. Equation 3 calculates the position of the neutral axis, which permits calculations for the moment of inertia I of the transformed cross-section using Equation 4. Within the elastic range, the assumption is that there is no change in the length of the neutral axis or any lateral distortion in the cross-sections of the composite sandwich beam (Beer et al., 1992). Therefore, the second moment of the transformed cross-sectional area about the neutral axis is constant under bending. For composite sandwich beams of three layers, two skin layers of the same thickness and a core, the location of the neutral axis is typically unchanged post transformation.

The validity of the proposed algorithm is based on the assumption that there is a relationship between bending moment M and beam curvature in a composite sandwich beam under flexural (Beer et al., 1992). As bending moment M values increase in response to additional loads, the radius of curvature becomes smaller, while normal strain increases in the outer fiber of the bottom skin layer. As shown in Equation 9, the radius of curvature of the

composite sandwich beam under loading is equal to the ratio of equivalent flexural rigidity EI_{eq} to bending moment M and is an exponentially decreasing function with M as an independent variable. This fact serves to verify that in practice when bending moment M is nonexistent; the radius of curvature ρ is at infinity (Morten Dæhlen et al., 2008).

In either loading configuration, center-point load or quarter-point load, the distance from each point on the beam to the center of curvature is called the radius of curvature and is designated as ρ. The maximum strain ε_{center} and $\varepsilon_{quarter}$ Equation 10 and 11, as functions of bending moment values M, are assumed to occur at mid-beam and at a distance **c** from the neutral surface of the transformed composite sandwich beam (Issac M. Daniel et al., 2000). Typically, normal strain **ε** is in a linear relationship with bending moment M that terminates in beam failure at maximum bending moment (Tessler A, 2007).

In order to verify the applicability and validity of the Euler-Bernoulli beam theory, direct computation that results in analytical data has been performed. The process begins with generating bending moment values M_{center} and $M_{quarter}$ as presented in Equation 6 and 7. Next, these bending moment values M are applied accordingly to calculate normal strain ε_{center} and $\varepsilon_{quarter}$ using Equation 10 and Equation 11, and deflection values D_{center} and $D_{quarter}$ using Equation 12 and Equation 13.

Typically, dependent variable is plotted on the y axis. Throughout this thesis, analytical load-deflection and load-strain will be plotted with the independent variable (applied load) on the vertical axis. In engineering mechanics, load and stress are typically plotted on the vertical axis, with deflection and strain typically plotted horizontally. Note: The Euler-Bernoulli equation does not predict failure. Figures 9-41 graphs predicted strain and deflections calculated using applied (experimental) load values. Each plot ends at the actual failure load is. In the following sections, analytical strain and defection results for each composite sandwich beam subjected to three-point and four-point bending tests are presented.

3.6 Flexural Analysis Schedules for Composite Sandwich Beams-Group I

In Group I, core density and skin thickness are constant, while core thickness, beam width, span under loading, and loading configurations vary. As a result of incorporating the equivalent area method in order to verify the applicability and validity of the Euler-Bernoulli beam theory, the EI_{eq} = equivalent flexural rigidity of 3,188,000 lbf*in^2 will be used to generate the predicted load versus strain and load versus deflection.

3.7 Assessment of Analytical Strain Data-Group I

The following sections show graphical results in accordance with Group I specimens with strain equations determined earlier in this chapter. Both center and quarter loading conditions are presented for the proposed Euler-Bernoulli beam theory so that the predicted strain behavior can be compared to the strain behavior found experimentally.

3.7.1 Analytical Strain Data-Group I Center Load

In the following load versus strain graphs Figures 17, 18, and 19 the x-axis represents analytical results for normal strain, ε_{center} (Eq. 10), and the y-axis represents increasing applied loads, P, with increasing core thickness (UNO, 2005).

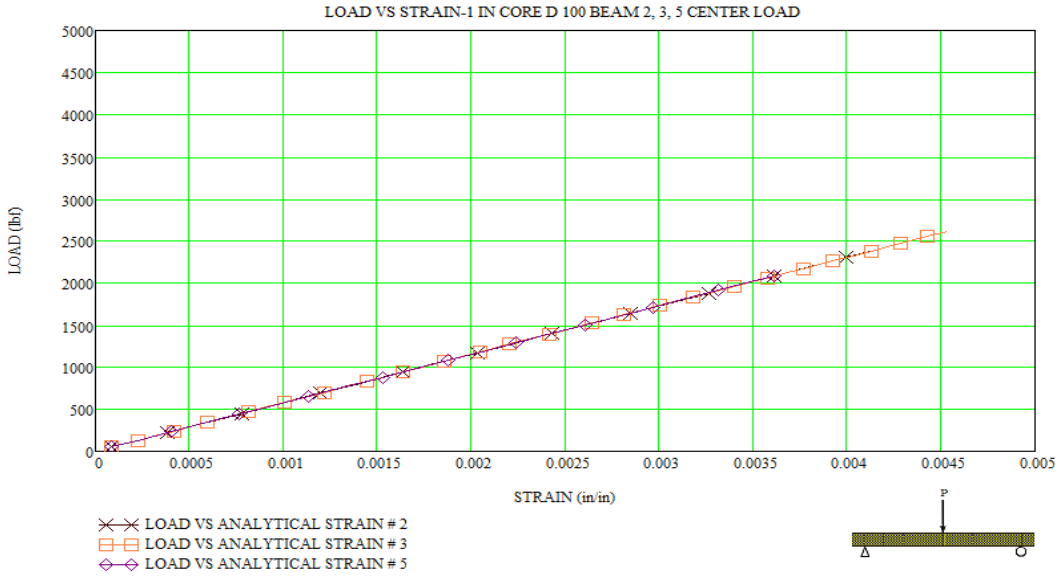

Figure 17. Load vs. Strain-1 in. core-D 100-center load Beam # 2, 3, 5

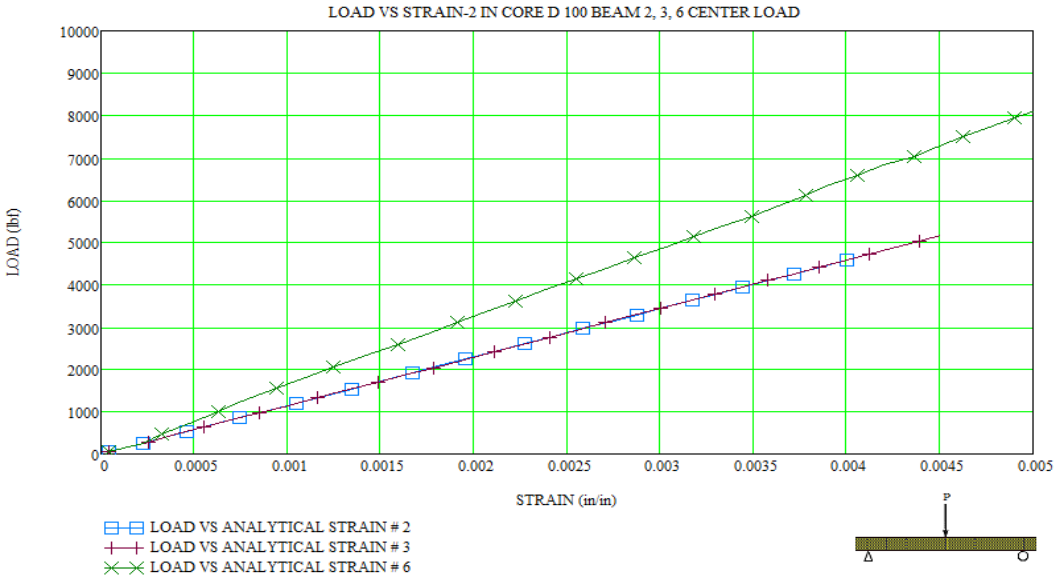

Figure 18. Load vs. Strain-2 in. core-D 100-center load Beam # 2, 3, 6

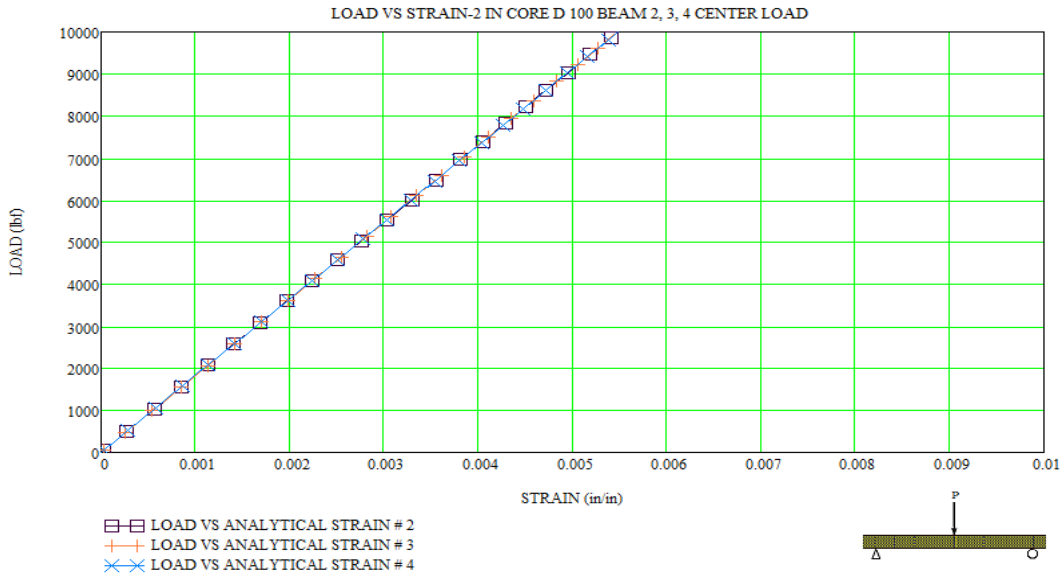

Figure 19. Load vs. Strain-3 in. core-D 100-center load Beam # 2, 3, 4

The tabulation in Table 11 is intended to present changes in center loading capacity with increasing core thickness.

Table 11. Summary of maximum applied center load and corresponding calculated strain

Core Density & Modulus of Elasticity	Balsawood Core Thickness (in)	E=5154319 psi Laminated Skin Thickness (in)	Beam Width b (in)	Span Under Loading (in)	Beam Number	Maximum Applied Load P (lbf)	Maximum Strain ε_{center} (in/in)
D 100 9.5 pcf E=510176 psi	1	0.25	3	29.5	2	2391	0.0041
					3	2611	0.0045
					5	2081	0.0036
D 100 9.5 pcf E=510176 psi	2	0.25	5	50.5	2	4721	0.0041
					3	5161	0.0045
					6	6831	0.0059
D 100 9.5 pcf E=510176 psi	3	0.25	7	70	2	10071	0.0055
					3	10411	0.0057
					4	10741	0.0058

Figure 20 presents a combined view that demonstrates the relationship between t_{core} = core thickness, b = composite beam width, L_{span} = length of composite beam under support, center load capacity, and corresponding longitudinal strain. For each composite sandwich beam

from Table 11, the x-axis represents analytical results for maximum strain, ε_{center} (Eq. 10), and the y-axis represents increasing applied loads, P, with increasing core thickness (UNO, 2005).

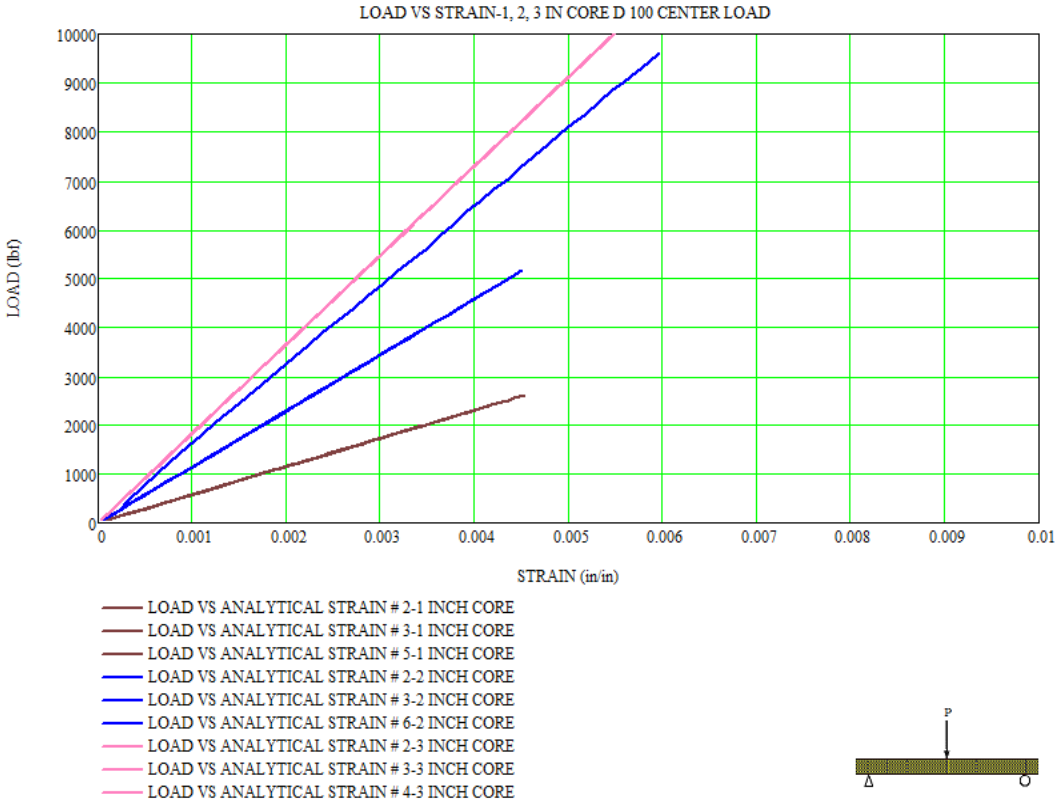

Figure 20. Analytical Strain Data-Group I Center Load

3.7.2 Analytical Strain Data-Group I Quarter Load

In the following load versus strain graphs Figures 21, 22, and 23 the x-axis represents analytical results for normal strain, $\varepsilon_{quarter}$ (Eq. 11), and the y-axis represents increasing applied loads, P, with increasing core thickness (UNO, 2005).

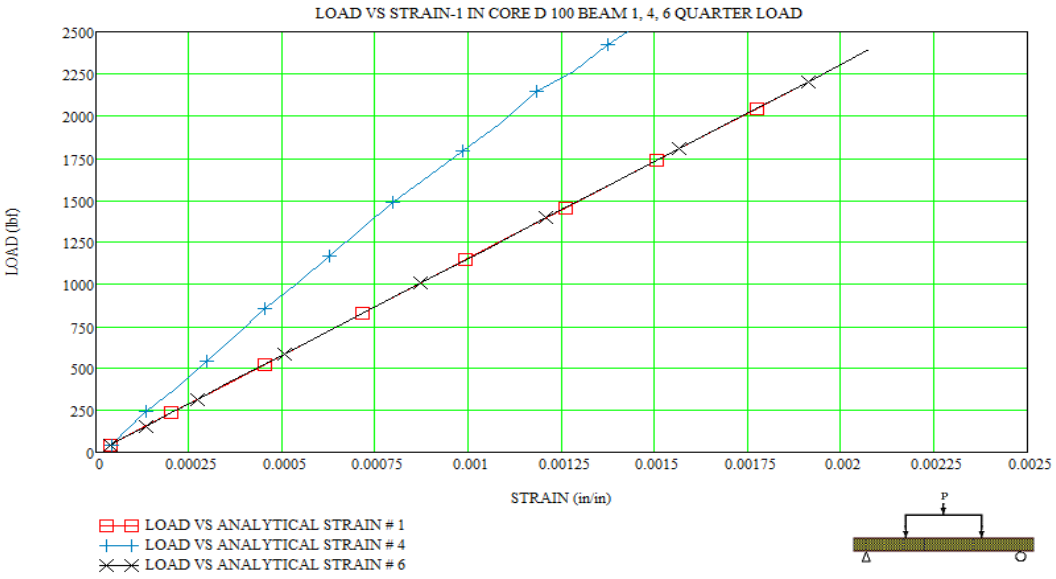

Figure 21. Load vs. Strain-1 in. core-D 100-quarter load Beam # 1, 4, 6

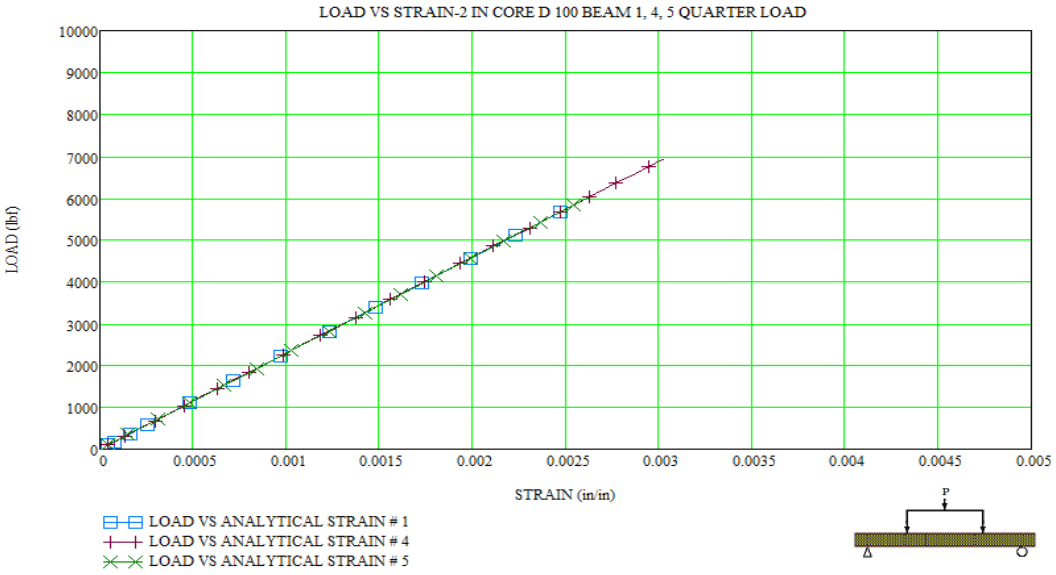

Figure 22. Load vs. Strain-2 in. core-D 100-quarter load Beam # 1, 4, 5

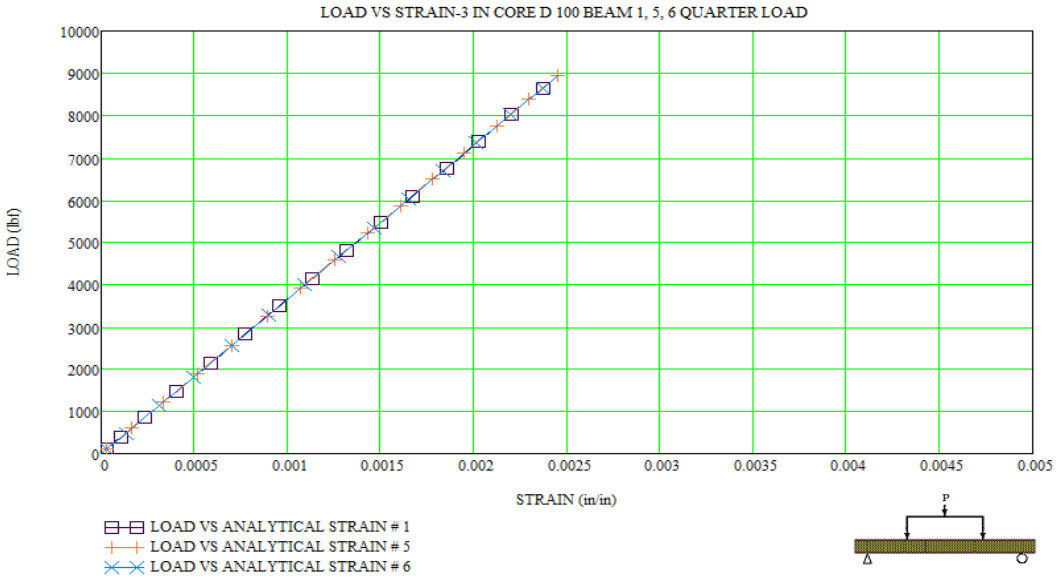

Figure 23. Load vs. Strain- 3 in. core-D 100-quarter load Beam # 1, 5, 6

The tabulation in Table 12 is intended to present changes in quarter loading capacity in parallel with increasing core thickness.

Table 12. Summary of maximum applied quarter load and corresponding calculated strain

Core Density & Modulus of Elasticity	Balsawood Core Thickness (in)	E=5154319 psi Laminated Skin Thickness (in)	Beam Width b (in)	Span Under Loading (in)	Beam Number	Maximum Applied Load P (lbf)	Maximum Strain $\varepsilon_{quarter}$ (in/in)
D 100 9.5 pcf E=510176 psi	1	0.25	3	29.5	1	2173	0.0018
					4	2563	0.0022
					6	2393	0.002
D 100 9.5 pcf E=510176 psi	2	0.25	5	50.5	1	5909	0.0025
					4	6949	0.003
					5	6019	0.0026
D 100 9.5 pcf E=510176 psi	3	0.25	7	70	1	8649	0.0023
					5	8949	0.0024
					6	8969	0.0024

Figure 24 presents a combined view that demonstrates the relationship between t_{core} = core thickness, b = composite beam width, L_{span} = length of composite beam under support, center load capacity, and corresponding longitudinal strain. For each composite sandwich beam from Table 12, the x-axis represents analytical results for maximum strain, $\varepsilon_{quarter}$ (Eq. 11), and the y-axis represents increasing applied loads, P, with increasing core thickness (UNO, 2005).

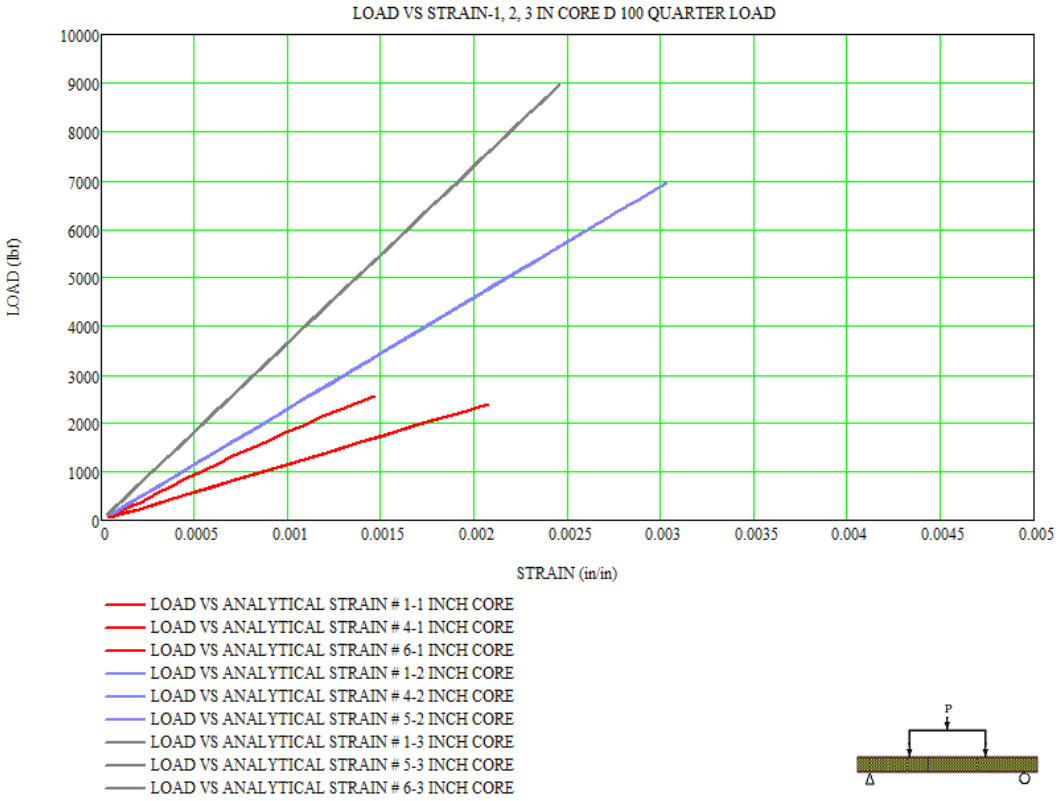

Figure 24. Analytical Strain Data-Group I Quarter Load

3.8 Assessment of Analytical Deflection Data-Group I

The following sections show graphical results in accordance with Group I specimens with deflection equations determined earlier in this chapter. Both center and quarter loading conditions are presented for the proposed Euler-Bernoulli beam theory so that the predicted deflection behavior can be compared to the deflection behavior found experimentally.

3.8.1 Analytical Deflection Data-Group I Center Load

In the following load versus deflection graphs Figures 25, 26, and 27 the x-axis represents analytical results for deflection, D_{center} (Eq. 12), and the y-axis represents increasing applied loads, P, with increasing core thickness (UNO, 2005).

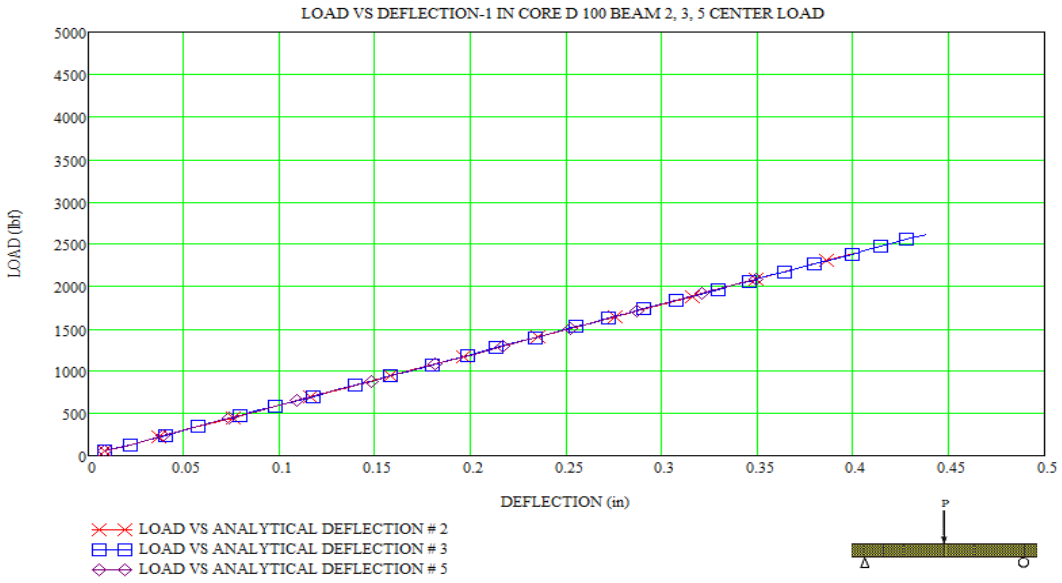

Figure 25. Load vs. Deflection-1 in. core-D 100-center load Beam # 2, 3, 5

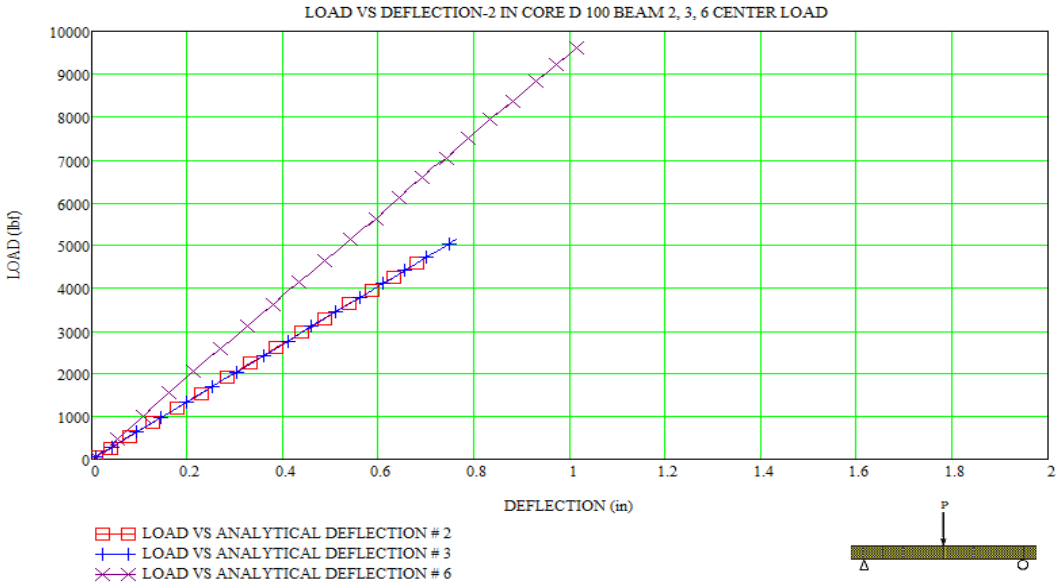

Figure 26. Load vs. Deflection-2 in. core-D 100-center load Beam # 2, 3, 6

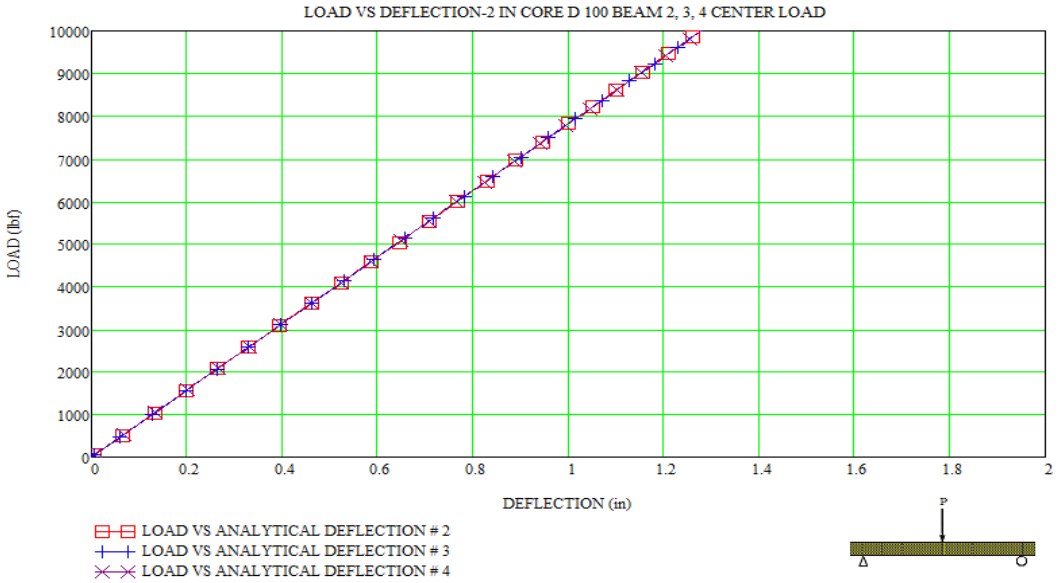

Figure 27. Load vs. Deflection-3 in. core-D 100-center load Beam # 2, 3, 4

The tabulation in Table 13 is intended to present changes in center loading capacity with increasing core thickness.

Table 13. Summary of maximum applied center load and corresponding calculated deflection

Core Density & Modulus of Elasticity	Balsawood Core Thickness (in)	E=5154319 psi Laminated Skin Thickness (in)	Beam Width b (in)	Span Under Loading (in)	Beam Number	Maximum Applied Load P (lbf)	Maximum Deflection D_{center} (in)
D 100 9.5 pcf E=510176 psi	1	0.25	3	29.5	2	2391	0.401
					3	2611	0.438
					5	2081	0.349
D 100 9.5 pcf E=510176 psi	2	0.25	5	50.5	2	4721	0.7
					3	5161	0.766
					6	6831	0.101
D 100 9.5 pcf E=510176 psi	3	0.25	7	70	2	10071	1.28
					3	10411	1.33
					4	10741	1.37

Figure 28 presents a combined view that demonstrates the relationship between t_{core} = core thickness, b = composite beam width, L_{span} = length of composite beam under support, center load capacity, and corresponding deflection. For each composite sandwich beam from Table 13, the x-axis represents analytical results for deflection, D_{center} (Eq. 12), and the y-axis represents increasing applied loads, P, with increasing core thickness (UNO, 2005).

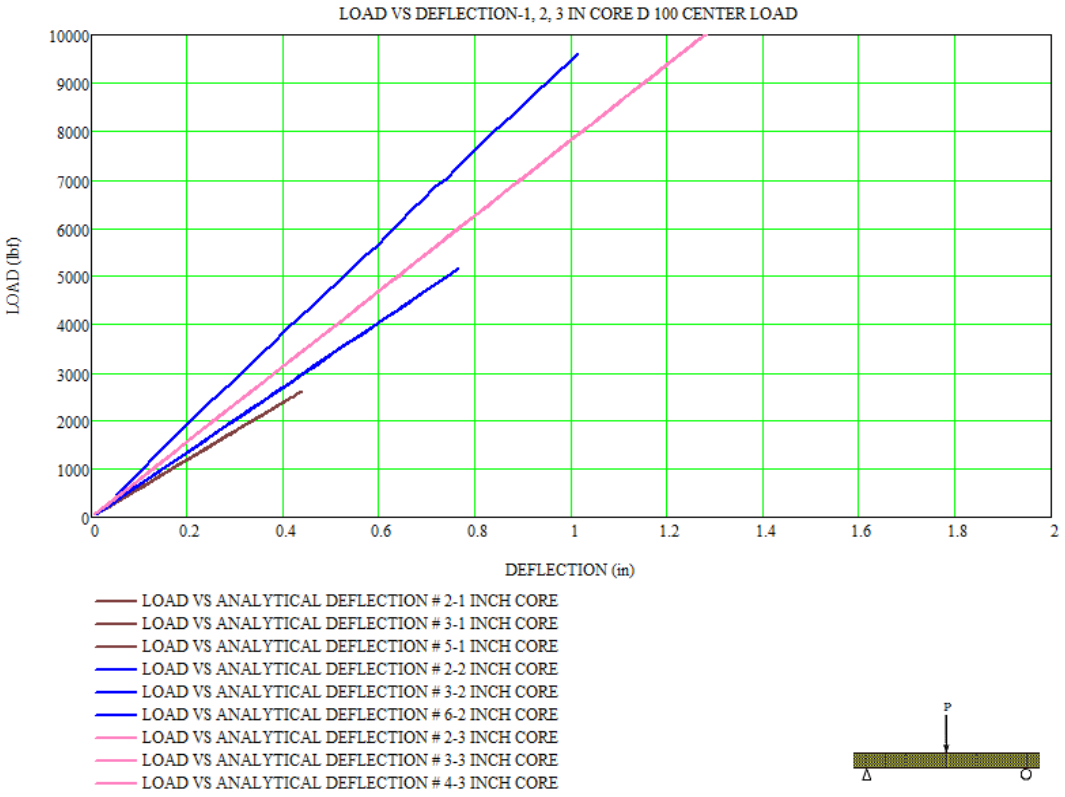

Figure 28. Analytical Deflection Data-Group I Center Load

3.8.2 Analytical Deflection Data-Group I Quarter Load

In the load versus deflection graphs Figures 29, 30, and 31 the x-axis represents analytical results for deflection, $D_{quarter}$ (Eq. 13), and the y-axis represents increasing applied loads, P, with increasing core thickness (UNO, 2005).

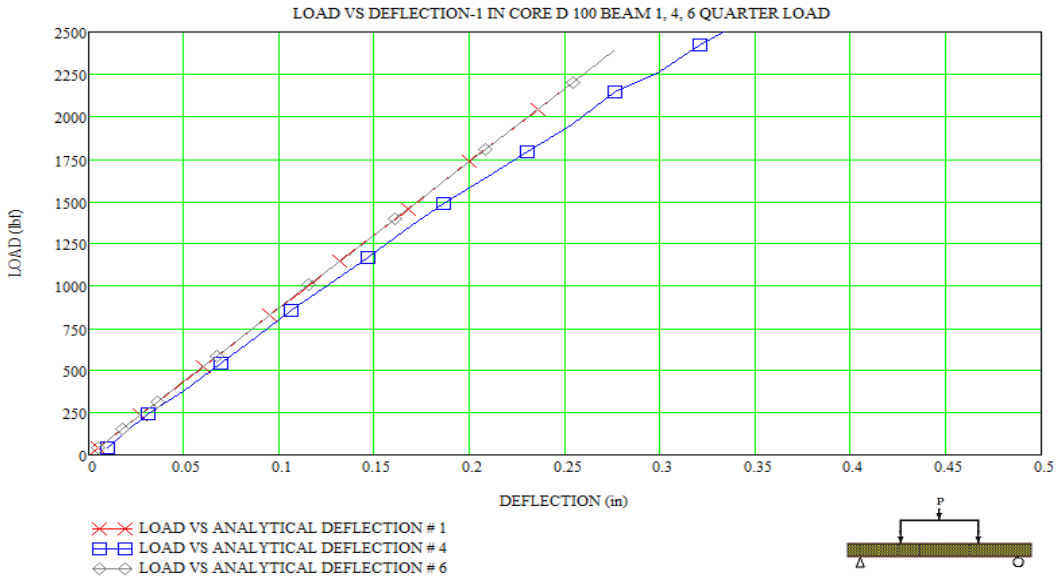

Figure 29. Load vs. Deflection-1 in. core-D 100-quarter load Beam # 1, 4, 6

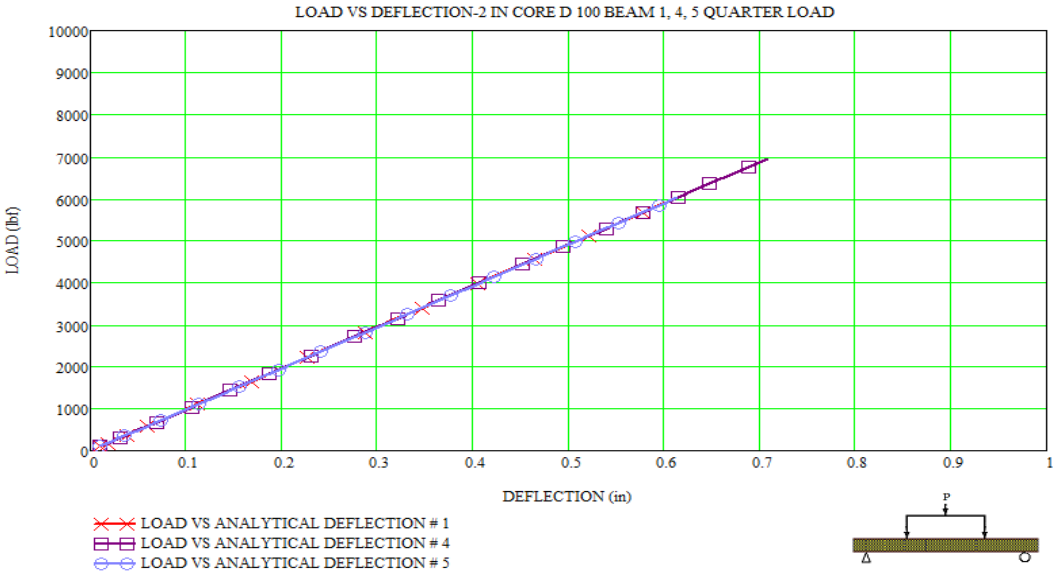

Figure 30. Load vs. Deflection-2 in. core-D 100-quarter load Beam # 1, 4, 5

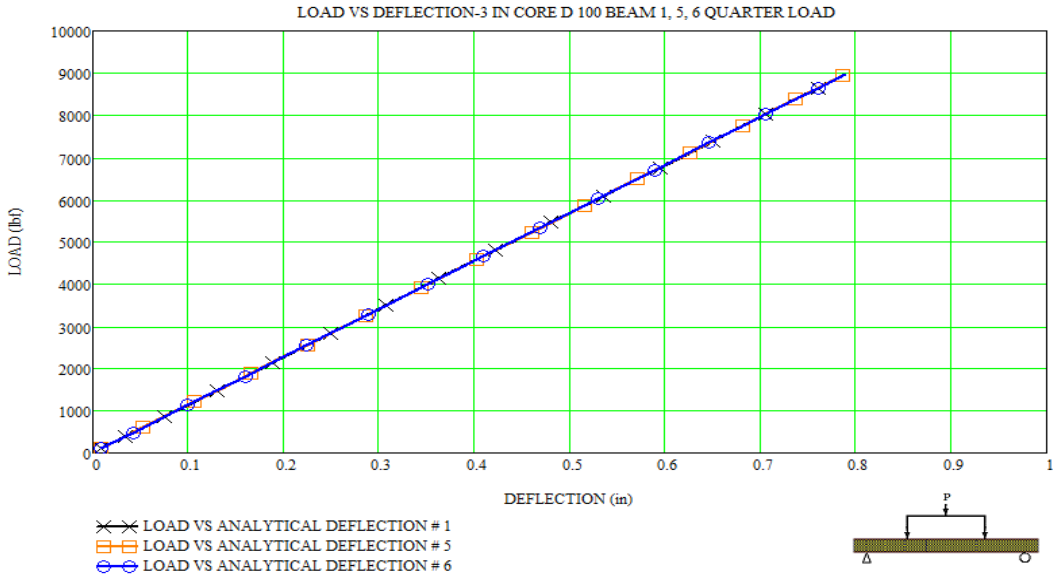

Figure 31. Load vs. Deflection-3 in. core-D 100-quarter load Beam # 1, 5, 6

The tabulation in Table 14 is intended to present changes in quarter loading capacity with increasing core thickness.

Table 14. Summary of maximum applied quarter load and corresponding calculated deflection

Core Density & Modulus of Elasticity	Balsawood Core Thickness (in)	E=5154319 psi Laminated Skin Thickness (in)	Beam Width b (in)	Span Under Loading (in)	Beam Number	Maximum Applied Load P (lbf)	Maximum Deflection $D_{quarter}$ (in)
D 100 9.5 pcf E=510176 psi	1	0.25	3	32	1	2173	0.25
				29.5	4	2563	0.295
					6	2393	0.276
D 100 9.5 pcf E=510176 psi	2	0.25	5	52.5	1	5909	0.602
				50.5	4	6949	0.708
					5	6019	0.613
D 100 9.5 pcf E=510176 psi	3	0.25	7	73.5	1	8649	0.76
				70	5	8949	0.786
					6	8969	0.788

Figure 32 presents a combined view that demonstrates the relationship between t_{core} = core thickness, b = composite beam width, L_{span} = length of composite beam under support, quarter load capacity, and corresponding deflection. For each composite sandwich beam from Table 14, the x-axis represents analytical results for deflection, $D_{quarter}$ (Eq. 13), and the y-axis represents increasing applied loads, P, with increasing core thickness (UNO, 2005).

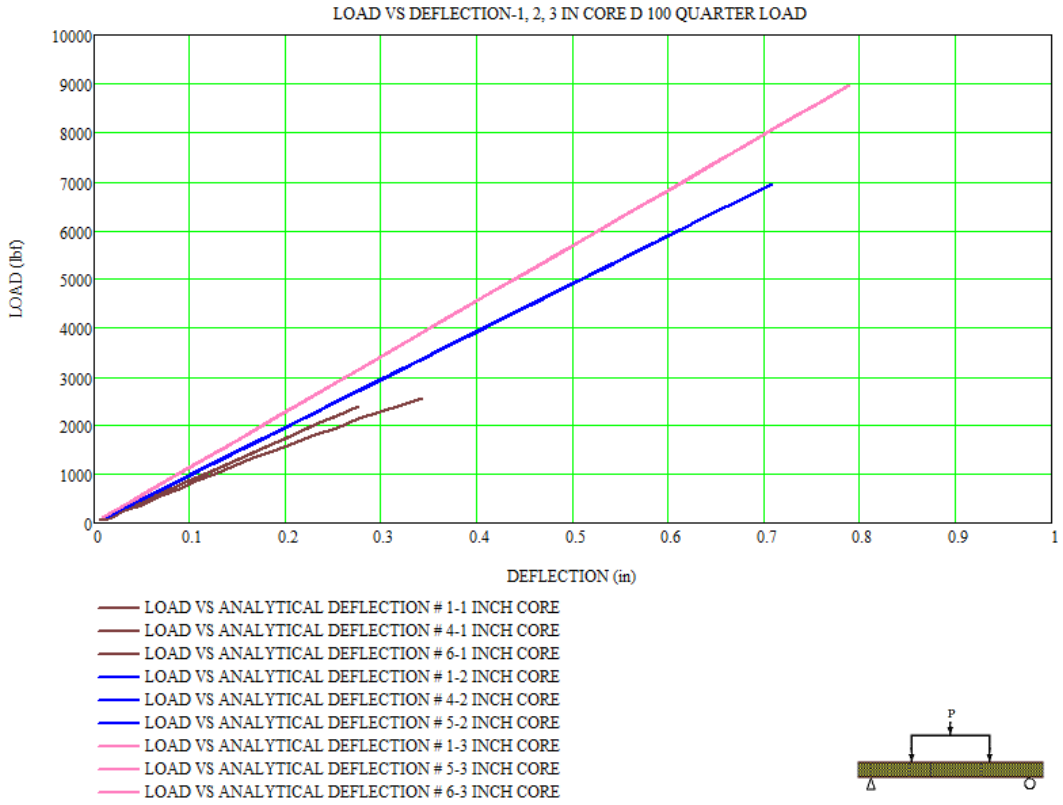

Figure 32. Analytical Deflection Data-Group I Quarter Load

3.9 Flexural Analysis for Composite Sandwich Beams-Group II

In Group II, core thickness, skin thickness, beam width, and span under loading are constant, while core density and loading configurations vary. As a result of incorporating the equivalent area method in order to verify the applicability and validity of the Euler-Bernoulli beam theory, the EI_{eq} = equivalent flexural rigidity of 3,188,000 lbf*in^2 will be used to generate the predicted load versus strain and load versus deflection.

3.10 Assessment of Analytical Strain Data-Group II

The following sections show graphical results in accordance with Group II specimens with strain equations determined earlier in this chapter. Both center and quarter loading conditions are presented for the proposed Euler-Bernoulli beam theory so that the predicted strain behavior can be compared to the strain behavior found experimentally.

3.10.1 Analytical Strain Data-Group II Center Load

In the following load versus strain graphs Figures 33, 34, and 35 the x-axis represents analytical results for normal strain, ε_{center} (Eq. 10), and the y-axis represents increasing applied loads, P, with increasing core density (UNO, 2005).

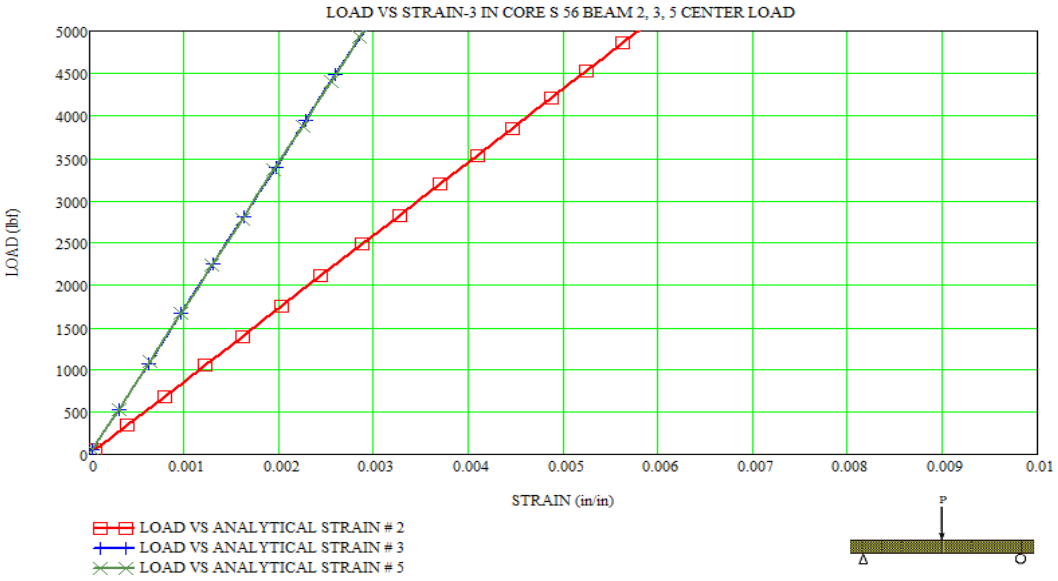

Figure 33. Load vs. Strain-3 in. core-S 56-center load Beam # 2, 3, 5

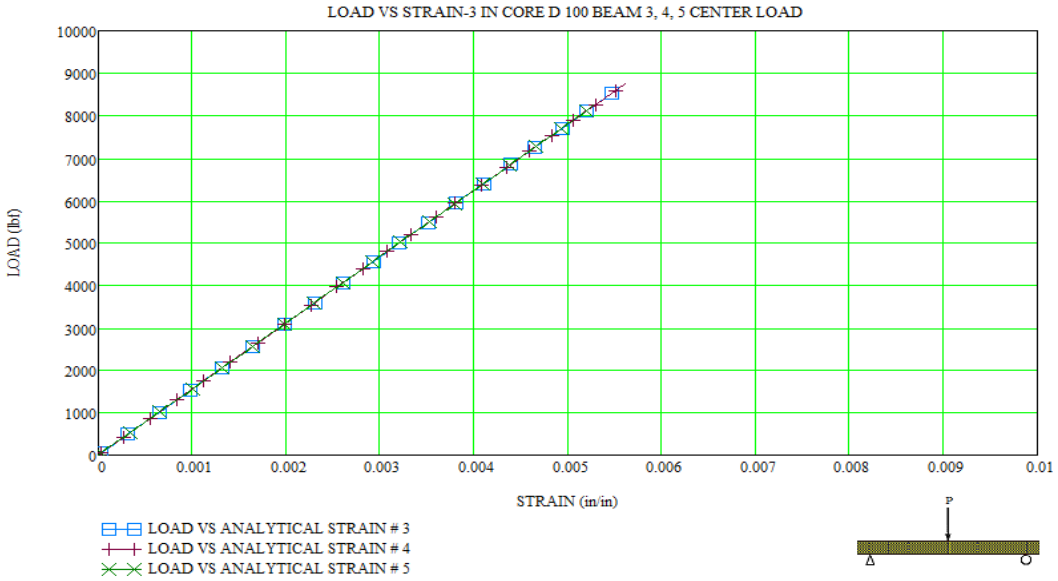

Figure 34. Load vs. Strain-3 in. core-D 100-center load Beam # 3, 4, 5

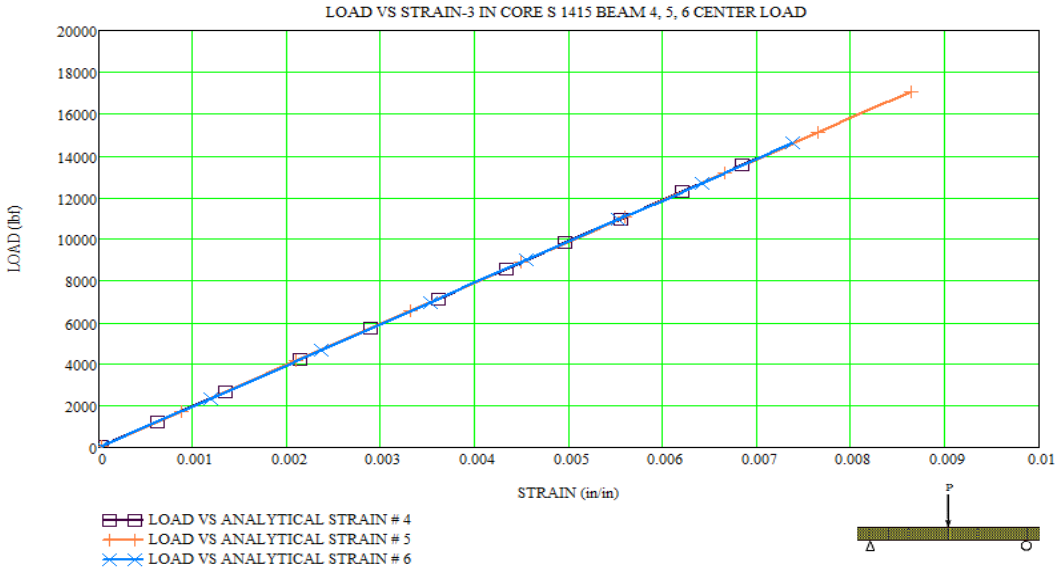

Figure 35. Load vs. Strain-3 in. core-S 1415-center load Beam # 4, 5, 6

The tabulation in Table 15 is intended to present changes in center loading capacity with increasing core density.

Table 15. Summary of maximum applied center load and corresponding calculated strain

Core Density & Modulus of Elasticity	Balsawood Core Thickness (in)	E=5154319 psi Laminated Skin Thickness (in)	Beam Width b (in)	Span Under Loading (in)	Beam Number	Maximum Applied Load P (lbf)	Maximum Strain ε_{center} (in/in)
S 56 5.6 pcf E=329443 psi	3	0.25	7	70	2	7581	0.0087
					3	6991	0.0040
					5	7131	0.0041
D 100 9.5 pcf E=510176 psi	3	0.25	7	70	3	8521	0.0054
					4	8771	0.0056
					5	8101	0.0051
S 1415 14.15 pcf E=814110 psi	3	0.25	7	70	4	14121	0.0071
					5	17081	0.0086
					6	14601	0.0073

Figure 36 presents a combined view that demonstrates the relationship between different core density, center load capacity and corresponding longitudinal strain. For each composite sandwich beam from Table 15, the x-axis represents analytical results for normal strain, ε_{center} (Eq. 10), and the y-axis represents applied loads, P, with increasing core density (UNO, 2005).

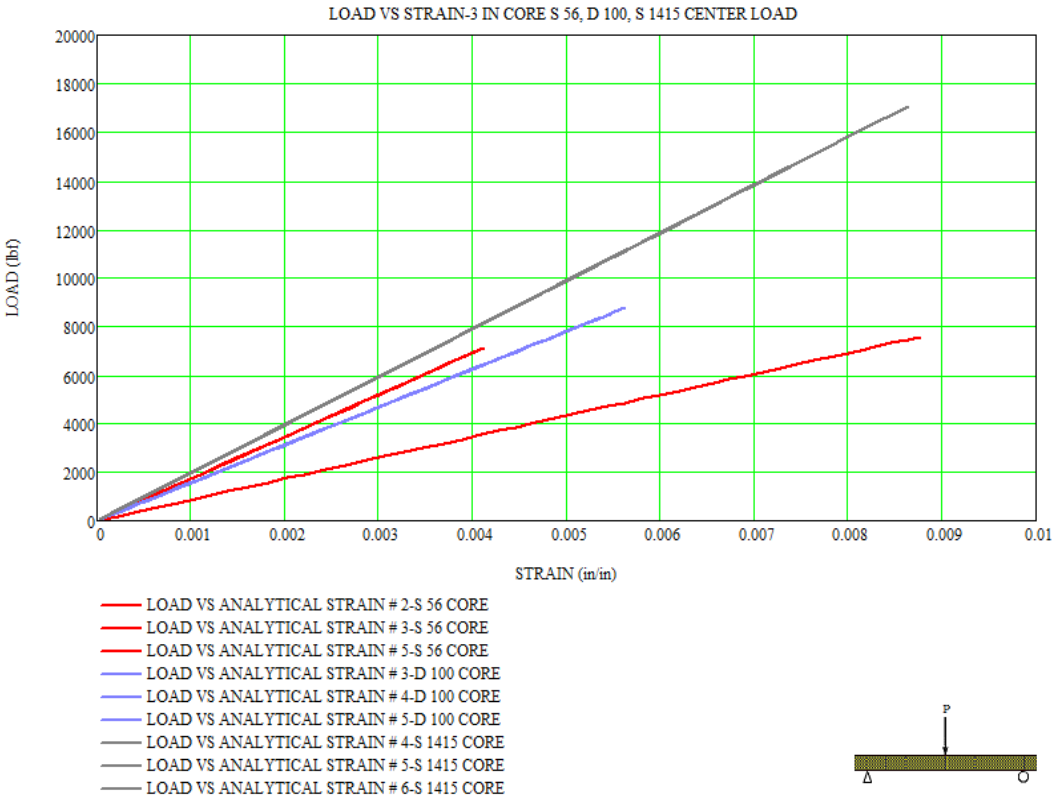

Figure 36. Analytical Strain Data-Group II Center Load

3.10.2 Analytical Strain Data-Group II Quarter Load

In the following load versus strain graphs Figures 37, 38, and 39 the x-axis represents analytical results for normal strain, $\varepsilon_{quarter}$ (Eq. 11), and the y-axis represents increasing applied loads, P, with increasing core density (UNO, 2005).

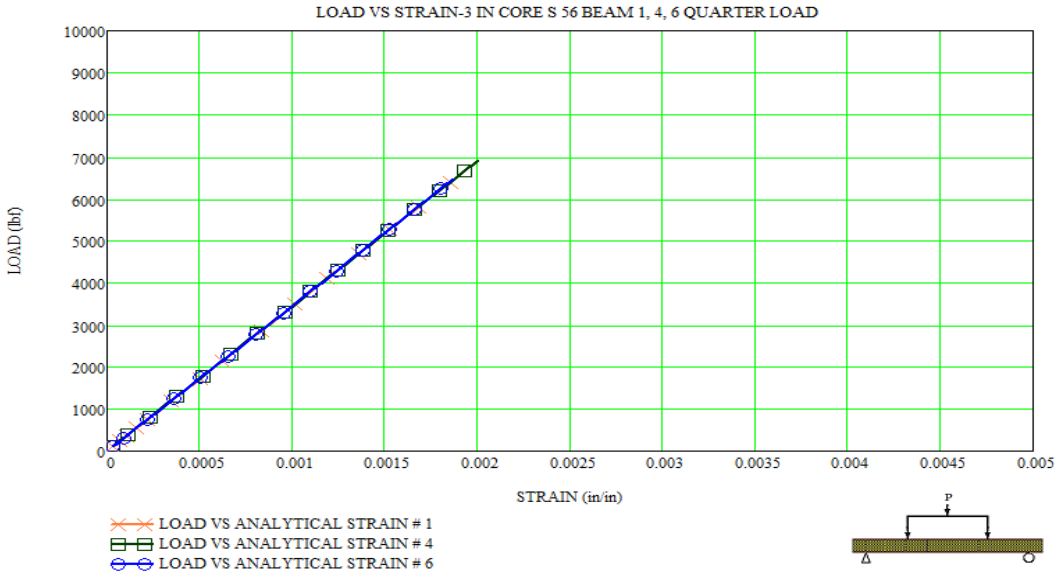

Figure 37. Load vs. Strain-3 in. core-S 56-quarter load Beam # 1, 4, 6

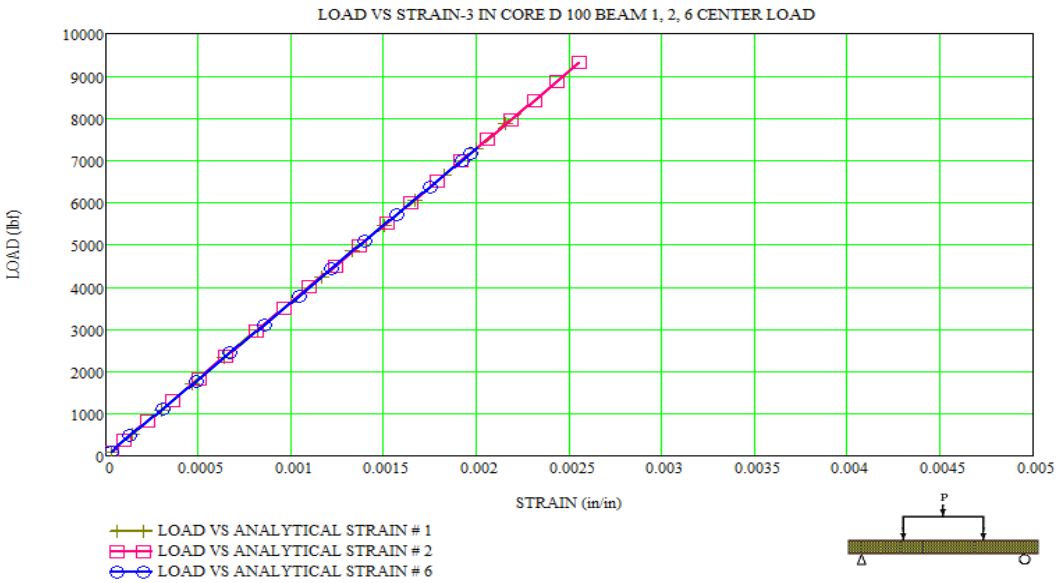

Figure 38. Load vs. Strain-3 in. core-D 100-quarter load Beam # 1, 2, 6

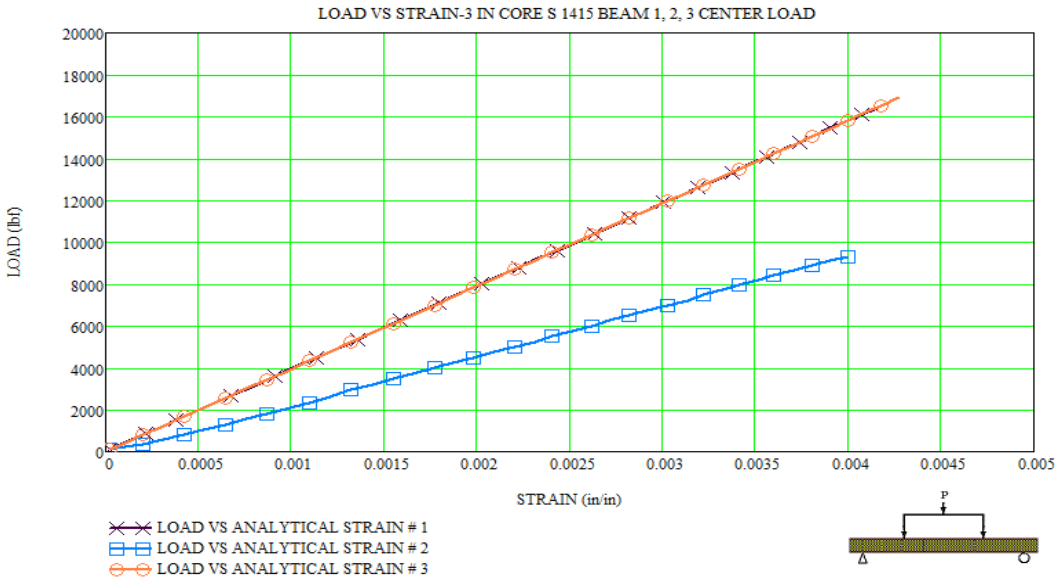

Figure 39. Load vs. Strain-3 in. core-S 1415-quarter load Beam # 1, 2, 3

The tabulation in Table 16 is intended to present changes in quarter loading capacity with increasing core density.

Table 16. Summary of maximum applied quarter load and corresponding calculated strain

Core Density & Modulus of Elasticity	Balsawood Core Thickness (in)	E=5154319 psi Laminated Skin Thickness (in)	Beam Width b (in)	Span Under Loading (in)	Beam Number	Maximum Applied Load P (lbf)	Maximum Strain $\varepsilon_{quarter}$ (in/in)
S 56 5.6 pcf E=329443 psi	3	0.25	7	70	1	6399	0.0018
					4	6929	0.002
					6	6459	0.001
D 100 9.5 pcf E=510176 psi	3	0.25	7	70	1	8139	0.002
					2	9309	0.0025
					6	7309	0.002
S 1415 14.15 pcf E=814110 psi	3	0.25	7	70	1	16419	0.0041
					2	16619	0.004
					3	16889	0.004

Figure 40 presents a combined view that demonstrates the relationship between different core density, quarter load capacity and corresponding longitudinal strain. For each composite sandwich beam from Table 16, the x-axis represents analytical results for normal strain, $\varepsilon_{quarter}$ (Eq. 11), and the y-axis represents applied loads-P (UNO. 2005). Figure 40 shows changes in quarter loading capacity with increasing core density.

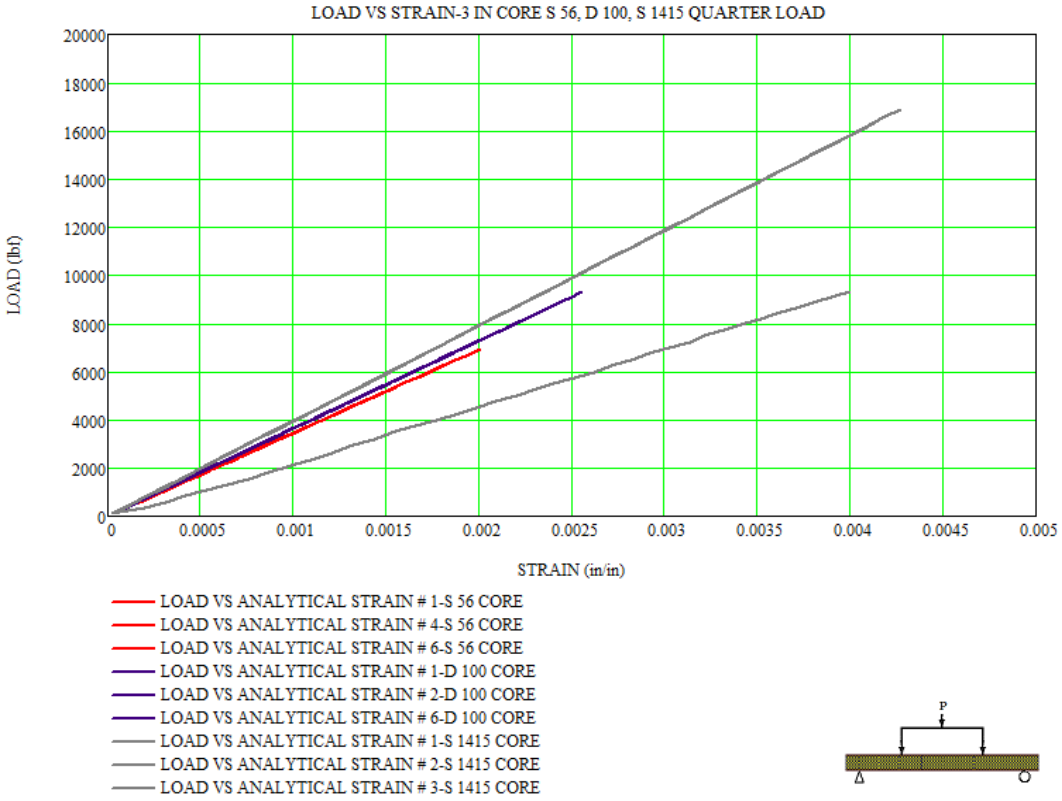

Figure 40. Analytical Strain Data-Group II Quarter Load

3.11 Assessment of Analytical Deflection Data-Group II

The following sections show graphical results in accordance with Group II specimens with deflection equations determined earlier in this chapter. Both center and quarter loading conditions are presented for the proposed Euler-Bernoulli beam theory so that the predicted deflection behavior can be compared to the deflection behavior found experimentally.

3.11.1 Analytical Deflection Data-Group II Center Load

In the following load versus deflection graphs Figures 41, 42, and 43 the x-axis represents analytical results for deflection, D_{center} (Eq. 12), and the y-axis represents increasing applied loads, P, with increasing core density (UNO, 2005).

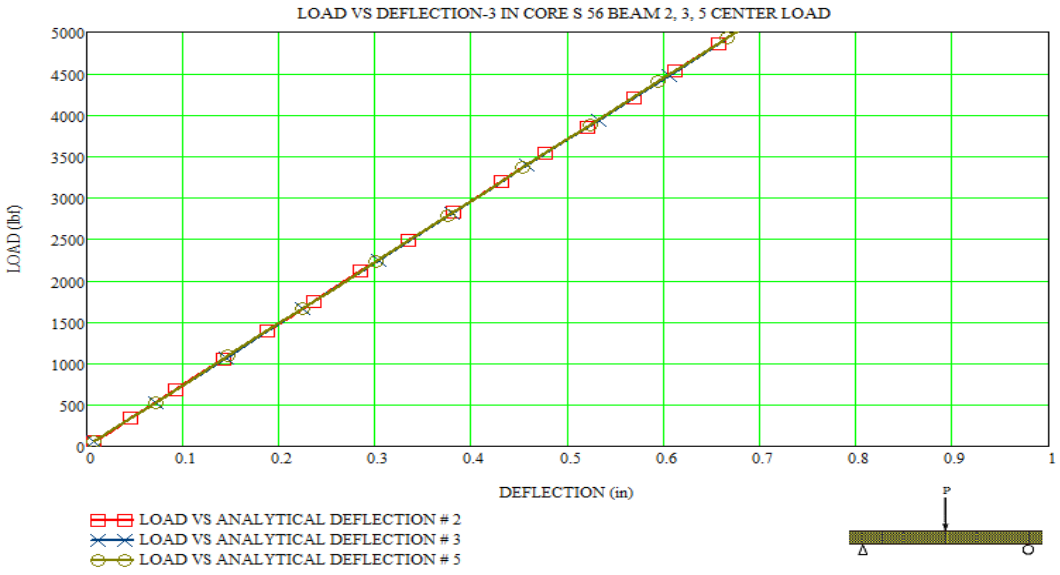

Figure 41. Load vs. Deflection-3 in. core-S 56-center load Beam # 2, 3, 5

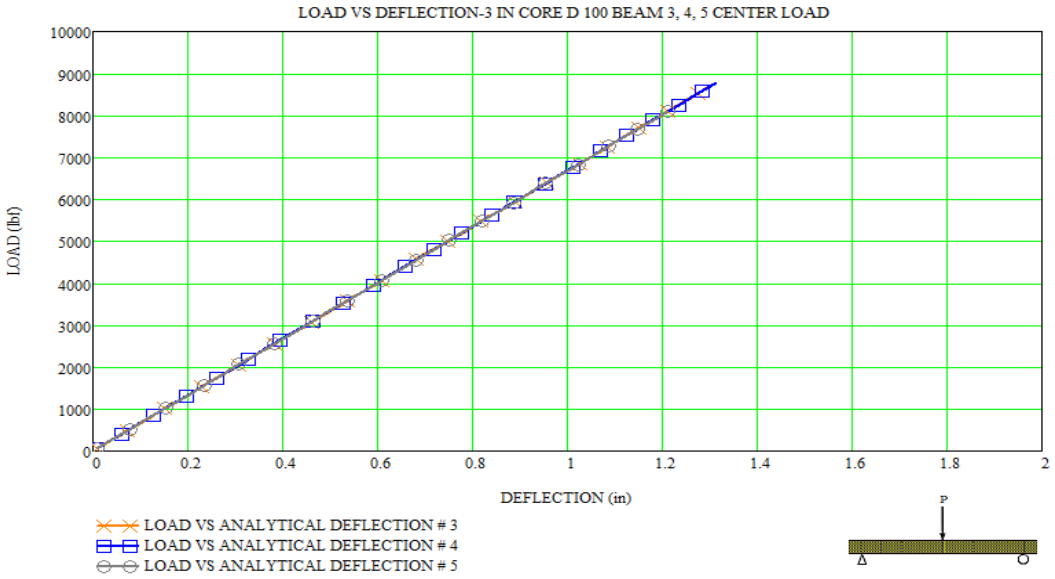

Figure 42. Load vs. Deflection-3 in. core-D 100-center load Beam # 3, 4, 5

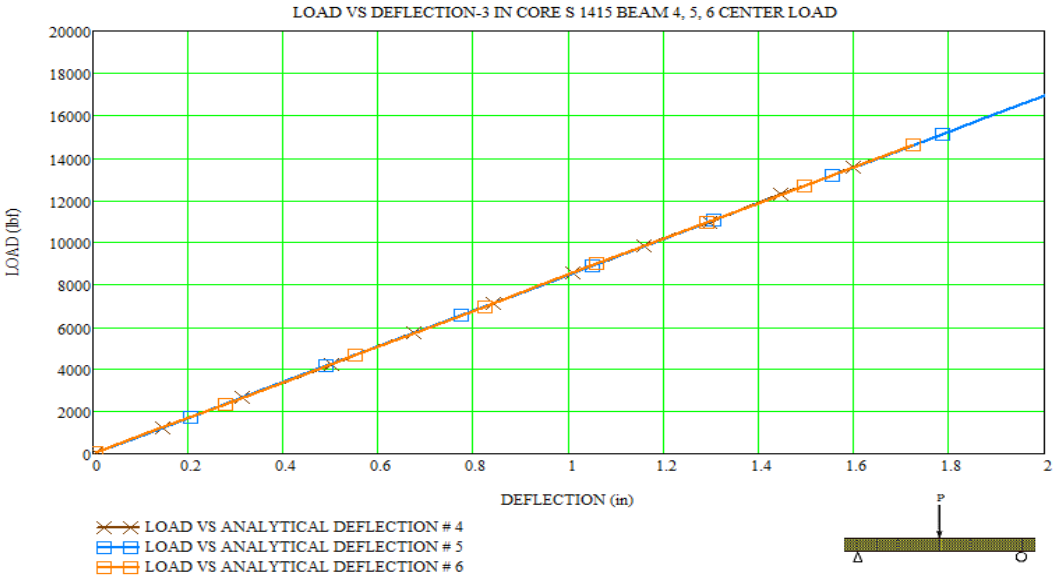

Figure 43. Load vs. Deflection-3 in. core-S 1415-center load Beam # 4, 5, 6

The tabulation in Table 17 is intended to present changes in center loading capacity with increasing core density.

Table 17. Summary of maximum applied center load and corresponding calculated deflection

Core Density & Modulus of Elasticity	Balsawood Core Thickness (in)	E=5154319 psi Laminated Skin Thickness (in)	Beam Width b (in)	Span Under Loading (in)	Beam Number	Maximum Applied Load P (lbf)	Maximum Deflection D_{center} (in)
S 56 5.6 pcf E=329443 psi	3	0.25	7	70	2	7581	1.023
					3	6991	0.944
					5	7131	0.962
D 100 9.5 pcf E=510176 psi	3	0.25	7	70	3	8521	1.274
					4	8771	1.312
					5	8101	1.212
S 1415 14.15 pcf E=814110 psi	3	0.25	7	70	4	14121	1.666
					5	17081	2.015
					6	14601	1.723

Figure 44 presents a combined view that demonstrates the relationship between different core density, center load capacity and corresponding deflection. For each composite sandwich beam in Table 17, the x-axis represents analytical results for deflection, D_{center} (Eq. 12), and the y-axis represents increasing applied loads, P, with increasing core density (UNO, 2005).

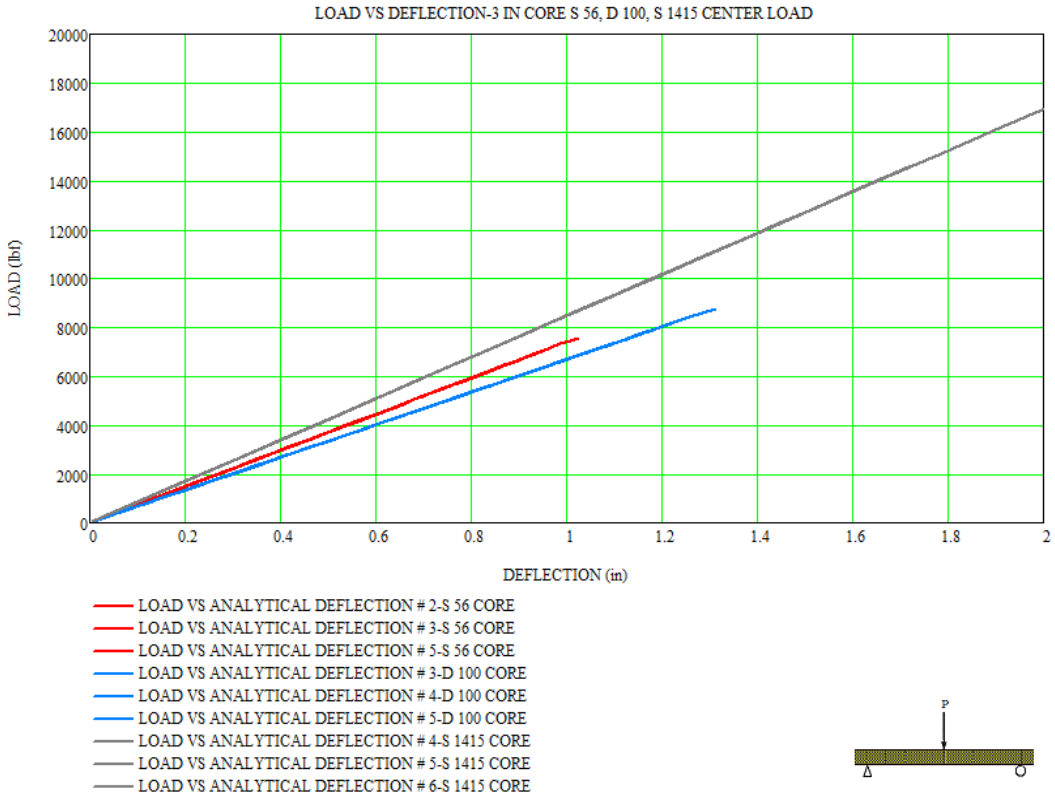

Figure 44. Analytical Deflection Data-Group II Center Load

3.11.2 Analytical Deflection Data-Group II Quarter Load

In the load versus deflection graphs Figures 45, 46, and 47 the x-axis represents analytical results for deflection, $D_{quarter}$ (Eq. 13), and the y-axis represents increasing applied loads, P, with increasing core density (UNO, 2005).

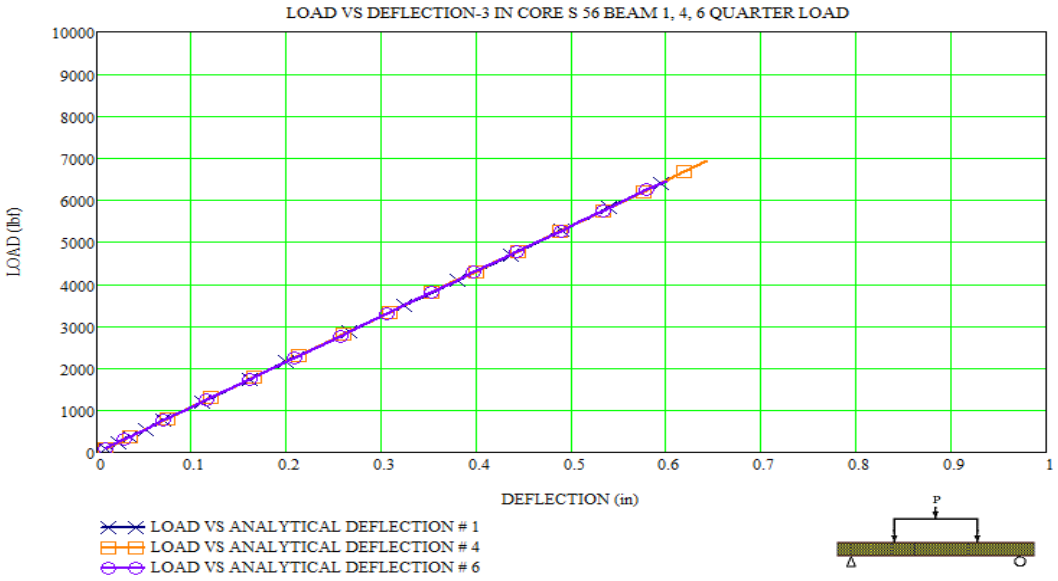

Figure 45. Load vs. Deflection-3 in. core-S 56-quarter load Beam # 1, 4, 6

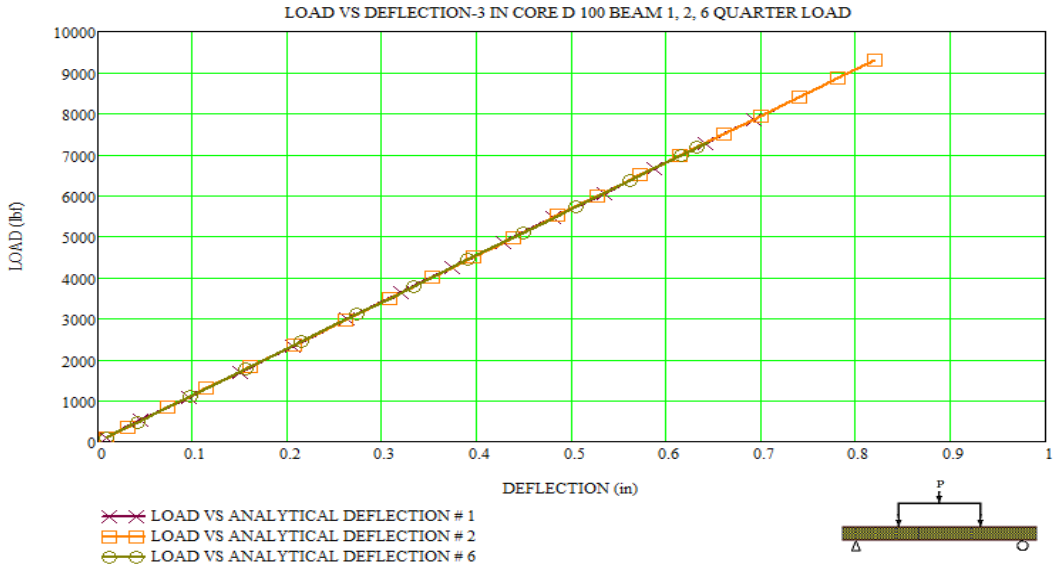

Figure 46. Load vs. Deflection-3 in. core-D 100-quarter load Beam # 1, 2, 6

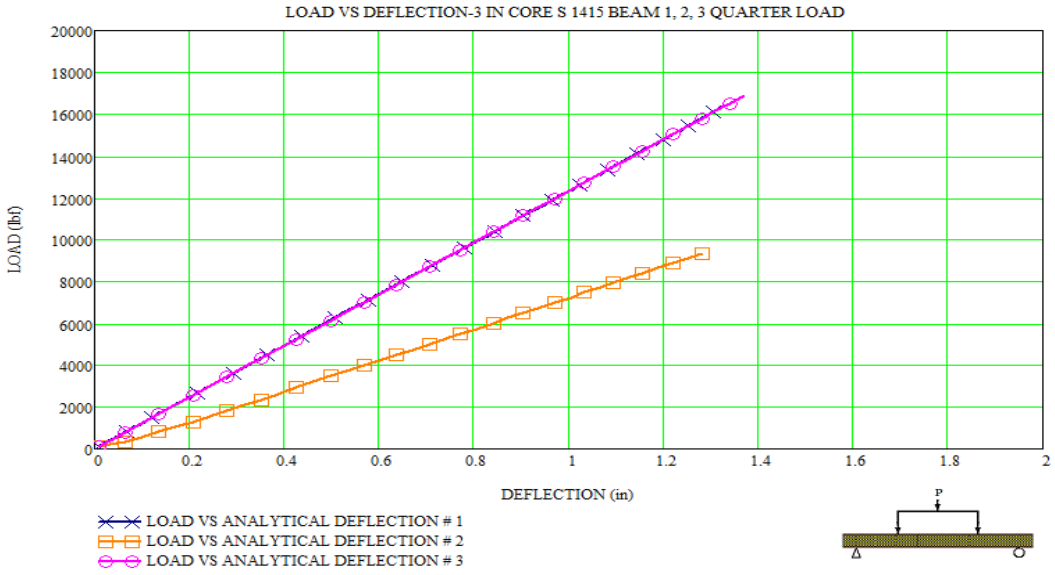

Figure 47. Load vs. Deflection-3 in. core-S 1415-quarter load Beam # 1, 2, 3

The tabulation in Table 18 is intended to present changes in quarter loading capacity with increasing core density.

Table 18. Summary of maximum applied quarter load and corresponding calculated deflection

Core Density & Modulus of Elasticity	Balsawood Core Thickness (in)	E=5154319 psi Laminated Skin Thickness (in)	Beam Width b (in)	Span Under Loading (in)	Beam Number	Maximum Applied Load P (lbf)	Maximum Deflection $D_{quarter}$ (in)
S 56 5.6 pcf E=329443 psi	3	0.25	7	70	1	6399	0.594
					4	6929	0.643
					6	6459	0.599
D 100 9.5 pcf E=510176 psi	3	0.25	7	70	1	8139	0.717
					2	9309	0.820
					6	7309	0.643
S 1415 14.15 pcf E=814110 psi	3	0.25	7	70	1	16419	1.332
					2	16619	1.348
					3	16889	1.370

Figure 48 presents a combined view that demonstrates the relationship between different core density, quarter load capacity and corresponding deflection. For each composite sandwich beam in Table 18, the x-axis represents analytical results for maximum deflection, $D_{quarter}$ (Eq. 13), and the y-axis represents increasing applied loads, P, with increasing core density (UNO, 2005).

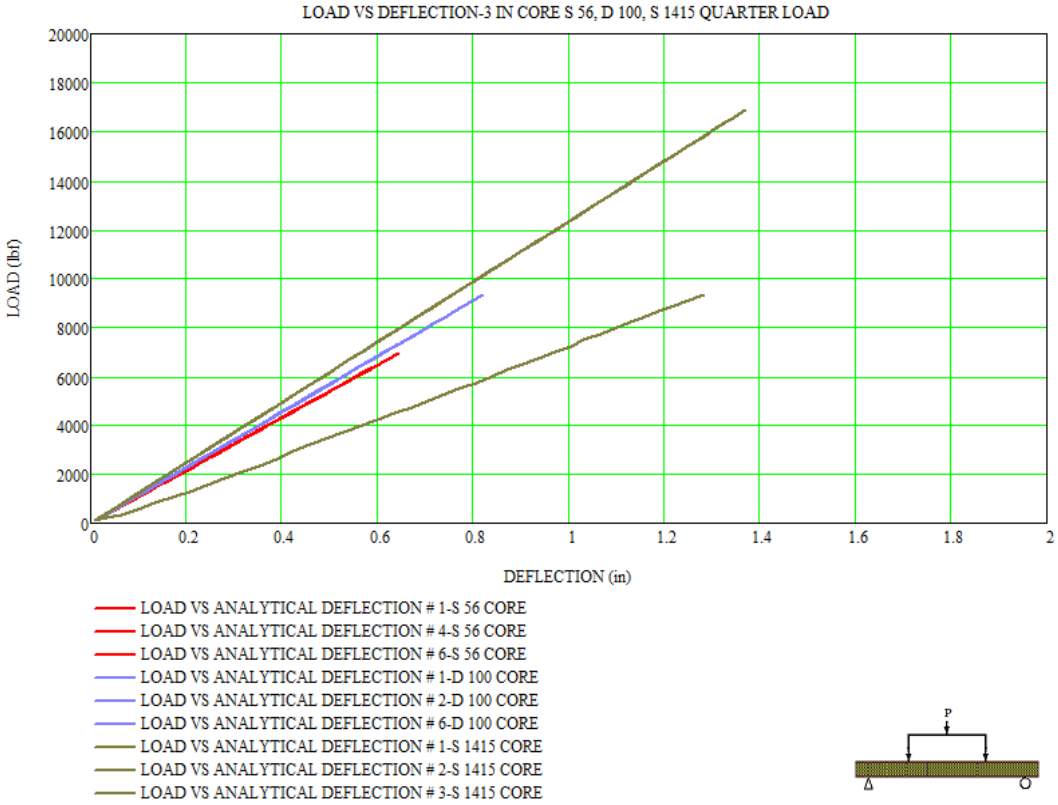

Figure 48. Analytical Deflection Data-Group II Quarter Load

CHAPTER IV

COMPARISON OF ANALYTICAL AND EXPERIMENTAL DATA

4.1 Overview

The following sections focus on assessing the differences between analytical and experimental data (UNO, 2005). For each composite sandwich beam, analytical and experimental data are presented side-by-side for comparison purposes. Summaries of relevant data necessary for discussion are presented in Table 19 and Table 20.

Table 19. Group I

Core Density & Modulus of Elasticity	Balsawood Core Thickness (in.)	E=5154319 psi Laminated Skin Thickness (in.)	Beam Width b (in.)	Beam Length L (in.)	Span Under Loading (in.)	Moment of Inertia Transformed Com/San/Beam (in^4)	Equivalent Flexural Rigidity EI_{eq} ($lbf*in^2$)
D 100 9.4 pcf E=510176 psi	1	0.25	3	32	29.5	6.25	3188000
D 100 9.4 pcf E=510176 psi	2	0.25	5	52.5	50.5	35.4	18080000
D 100 9.4 pcf E=510176 psi	3	0.25	7	73.5	70	109.3	55770000

Table 20. Group II

Core Density & Modulus of Elasticity	Balsawood Core Thickness (in.)	E=5154319 psi Laminated Skin Thickness (in.)	Beam Width b (in.)	Beam Length L (in.)	Span Under Loading (in.)	Moment of Inertia Transformed Com/San/Beam (in^4)	Equivalent Flexural Rigidity EI_{eq} ($lbf*in^2$)
S 56 6.07 pcf E=329443 psi	3	0.25	7	73.5	70	160.6	52920000
D 100 9.4 pcf E=510176 psi	3	0.25	7	73.5	70	109.3	55770000
S 1415 15 pcf E=814110 psi	3	0.25	7	73.5	70	74.4	60550000

4.2 Assessment of Analytical vs. Experimental Strain Data-Group I

In Group I, the focus is to assess loading characteristics for composite sandwich beams with increasing core thickness, while the core density remains constant. Representative illustrations for center-point and quarter-point load configurations are provided in Chapter II. As described in the equations for normal strain ε_{center} (Eq. 10) and $\varepsilon_{quarter}$ (Eq. 11) in Chapter III, the analytical results are linear in contrast to the slight nonlinearity observed in experimental strain (UNO, 2005). For these flexure tests, the maximum strain is assumed to be at mid-span of the loaded composite beams.

The following sections compare analytical strain to experimental strain (UNO, 2005). The results are presented in accordance to flexural testing schedules shown in Table 5, Table 6, and Table 7 of Chapter II.

4.2.1 Analytical vs. Experimental Strain Data-Group I Center-Point Load

Figure 49 compares analytical strain to experimental strain for composite beam # 2 with core thickness equal 1 inch and core density D 100, under increasing applied load. Experimental strain data is in blue, and red represents strain data obtained analytically. Comparison graphs for composite beams # 3 and # 5 with core thickness equal 1 inch and core density D 100 are presented in Appendix II.

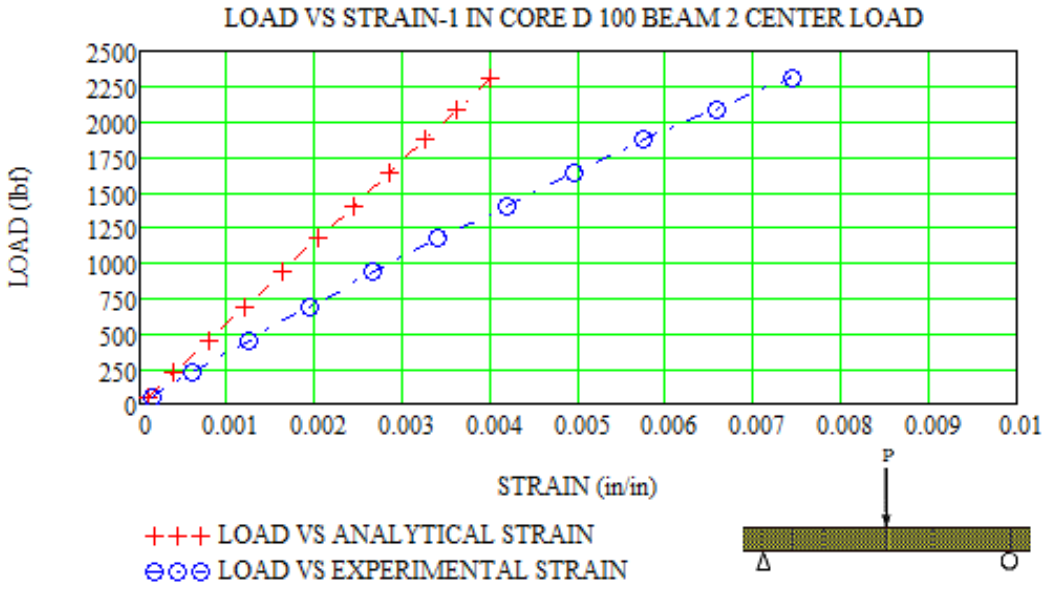

Figure 49. Load vs. Strain-1 in. core-D 100-center load Beam # 2

Figure 50 compares analytical strain to experimental strain for composite beam # 2 with core thickness equal 2 inch and core density D 100, under increasing applied load. Experimental strain data is in blue, and red represents strain data obtained analytically. Comparison graphs for composite beams # 3 and # 6 with core thickness equal 2 inch and core density D 100 are presented in Appendix II.

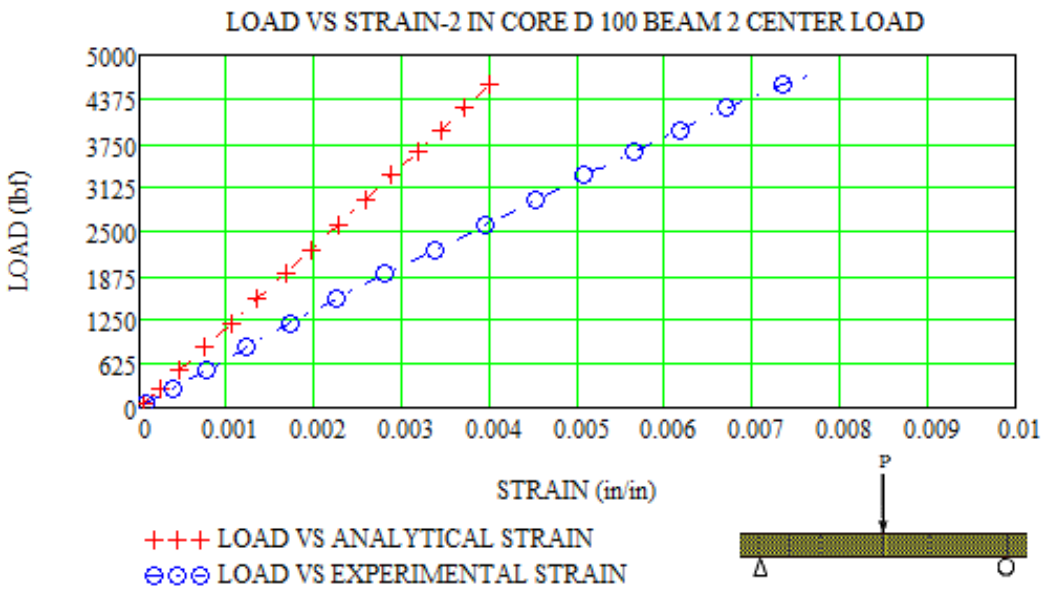

Figure 50. Load vs. Strain-2 in. core-D 100-center load Beam # 2

Figure 51 compares analytical strain to experimental strain for composite beam # 2 with core thickness equal 3 inch and core density D 100, under increasing applied load. Experimental strain data is in blue, and red represents strain data obtained analytically. Comparison graphs for composite beams # 3 and # 4 with core thickness equal 3 inch and core density D 100 are presented in Appendix II.

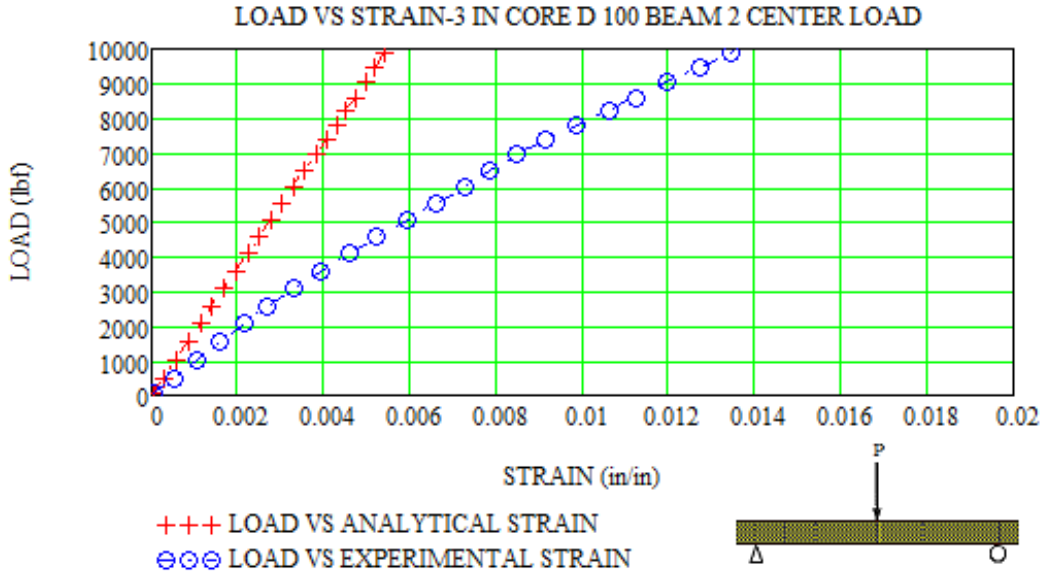

Figure 51. Load vs. Strain-3 in. core-D 100-center load Beam # 2

4.2.2 Analytical vs. Experimental Strain Data-Group I Quarter-Point Load

Figure 52 compares analytical strain to experimental strain for composite beam # 1 with core thickness equal 1 inch and core density D 100, under increasing applied load. Experimental strain data is in blue, and red represents strain data obtained analytically. Comparison graphs for composite beams # 4 and # 6 with core thickness equal 1 inch and core density D 100 are presented in Appendix II.

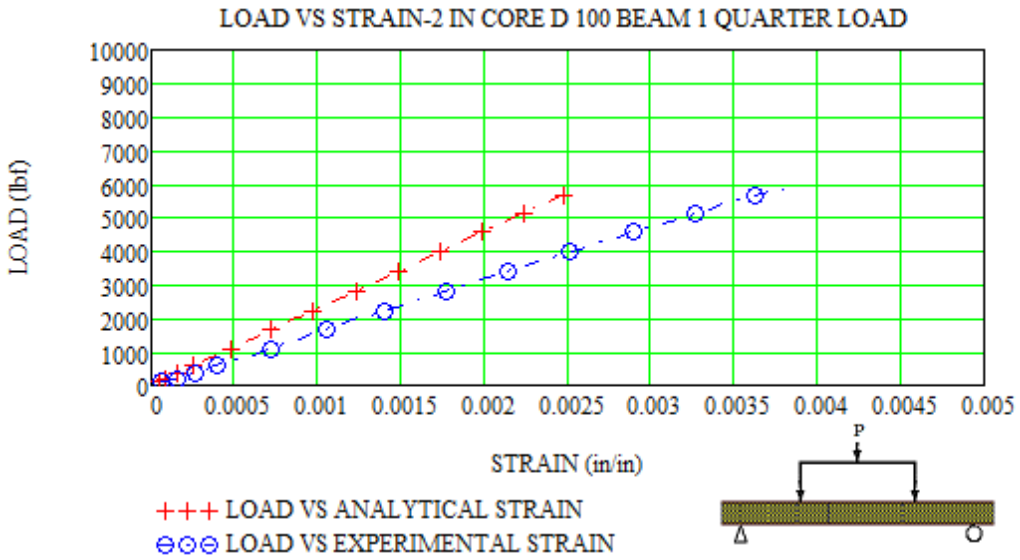

Figure 52. Load vs. Strain-1 in. core-D 100-quarter load Beam # 1

Figure 53 compares analytical strain to experimental strain for composite beam # 1 with core thickness equal 2 inch and core density D 100, under increasing applied load. Experimental strain data is in blue, and red represents strain data obtained analytically. Comparison graphs for composite beams # 4 and # 5 with core thickness equal 2 inch and core density D 100 are presented in Appendix II.

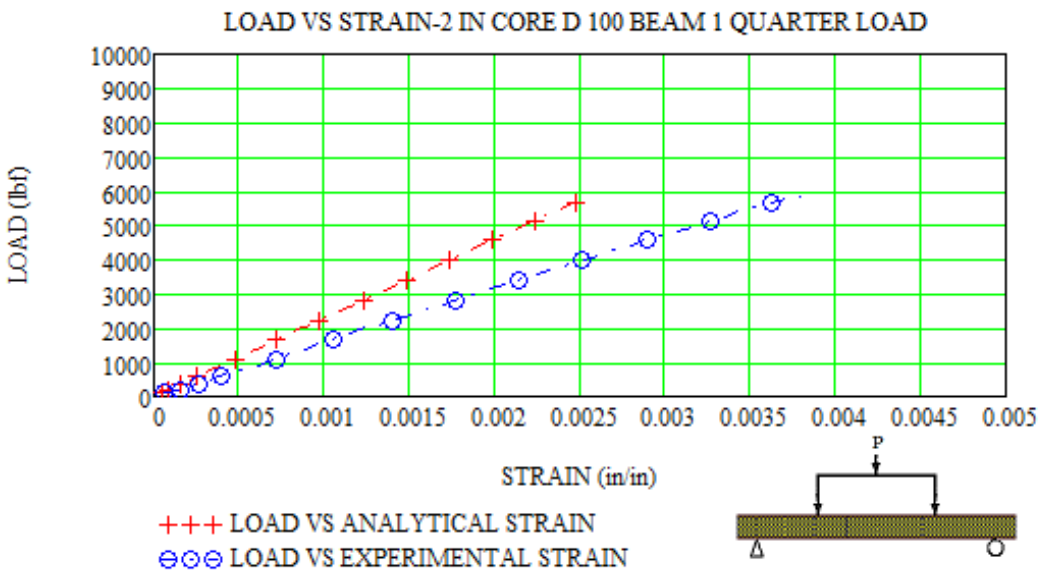

Figure 53. Load vs. Strain-2 in. core-D 100-quarter load Beam # 1

Figure 54 compares analytical strain to experimental strain for composite beam # 1 with core thickness equal 3 inch and core density D 100, under increasing applied load. Experimental strain data is in blue, and red represents strain data obtained analytically. Comparison graphs for composite beams # 5 and # 6 with core thickness equal 3 inch and core density D 100 are presented in Appendix II.

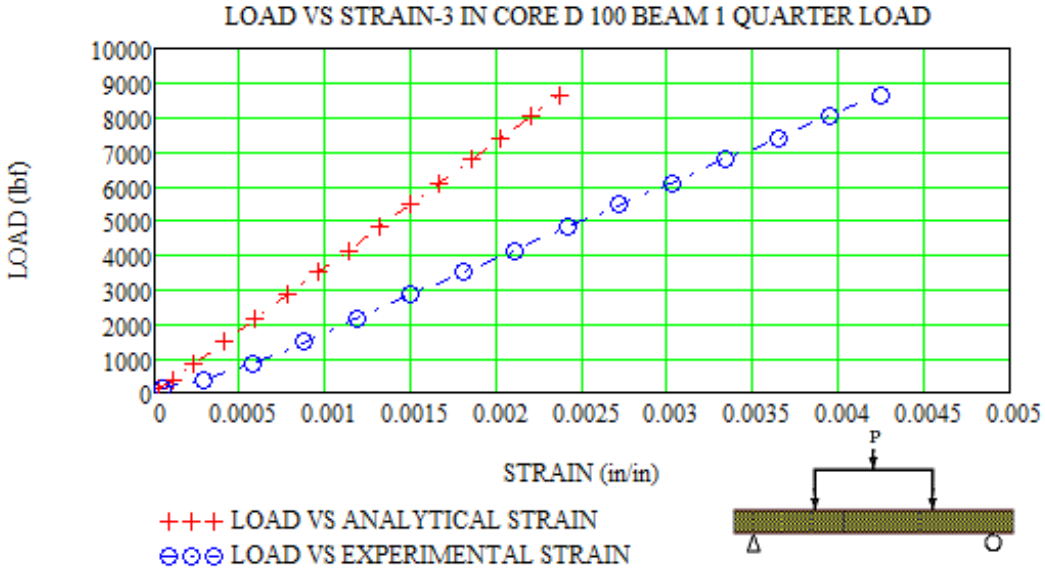

Figure 54. Load vs. Strain-3 in. core-D 100-quarter load Beam # 1

4.3 Assessment of Analytical vs. Experimental Deflection Data-Group I

In Group I, the focus is to assess loading characteristics for composite sandwich beams with increasing core thickness, while the core density remains constant. Representative illustrations for center-point and quarter-point load configurations are provided in Chapter II. As described in the equations for deflection D_{center} (Eq. 12) and $D_{quarter}$ (Eq. 13) in Chapter III, the analytical results are linear in contrast to the slight nonlinearity observed in experimental deflection (UNO, 2005). For these flexure tests, the maximum deflection is assumed to be at mid-span of the loaded composite beams.

The following sections compare analytical deflection to experimental deflection data (UNO, 2005). The results are presented in accordance to flexural testing schedules shown in Table 5, Table 6, and Table 7 of Chapter II.

4.3.1 Analytical vs. Experimental Deflection Data-Group I Center-Point Load

Figure 55 compares analytical deflections to experimental deflections for composite beam # 2 with core thickness equal 1 inch and core density D 100, under increasing applied load. Experimental deflection data is in blue, and red represents deflection data obtained analytically. Comparison graphs for composite beams # 3 and # 5 with core thickness equal 1 inch and core density D 100 are presented in Appendix II.

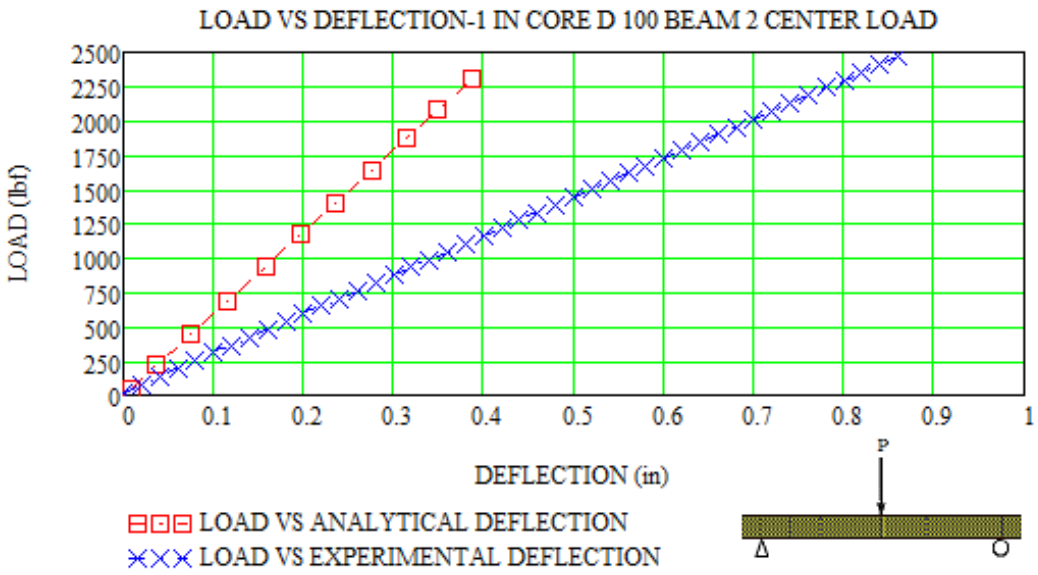

Figure 55. Load vs. Deflection-1 in. core-D 100-center load Beam # 2

Figure 56 compares analytical deflections to experimental deflections for composite beam # 2 with core thickness equal 2 inch and core density D 100, under increasing applied load. Experimental deflection data is in blue, and red represents deflection data obtained analytically. Comparison graphs for composite beams # 3 and # 6 with core thickness equal 2 inch and core density D 100 are presented in Appendix II.

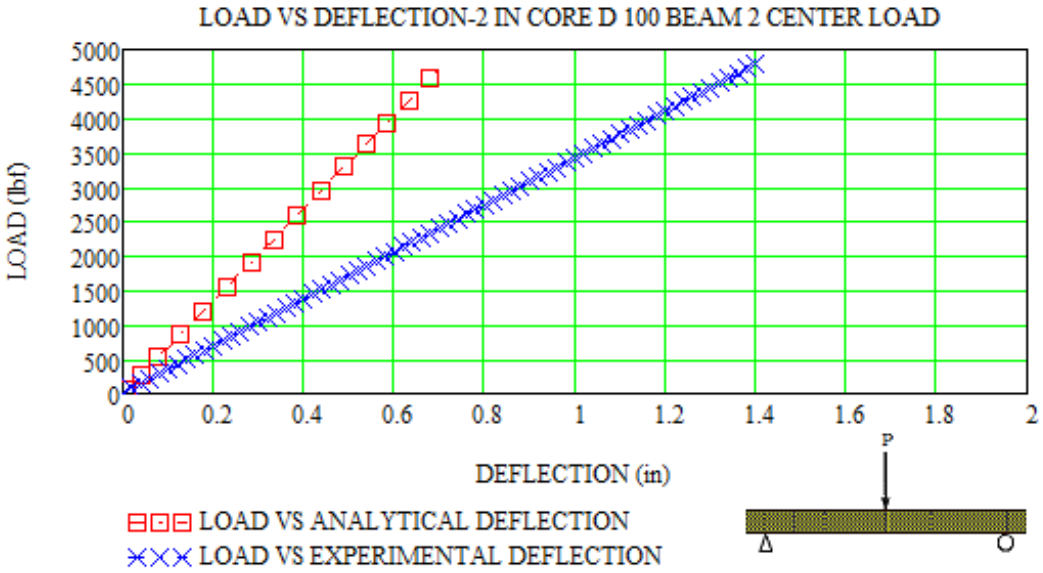

Figure 56. Load vs. Deflection-2 in. core-D 100-center load Beam # 2

Figure 57 compares analytical deflections to experimental deflections for composite beam # 2 with core thickness equal 3 inch and core density D 100, under increasing applied load. Experimental deflection data is in blue, and red represents deflection data obtained analytically. Comparison graphs for composite beams # 3 and # 4 with core thickness equal 3 inch and core density D 100 are presented in Appendix II.

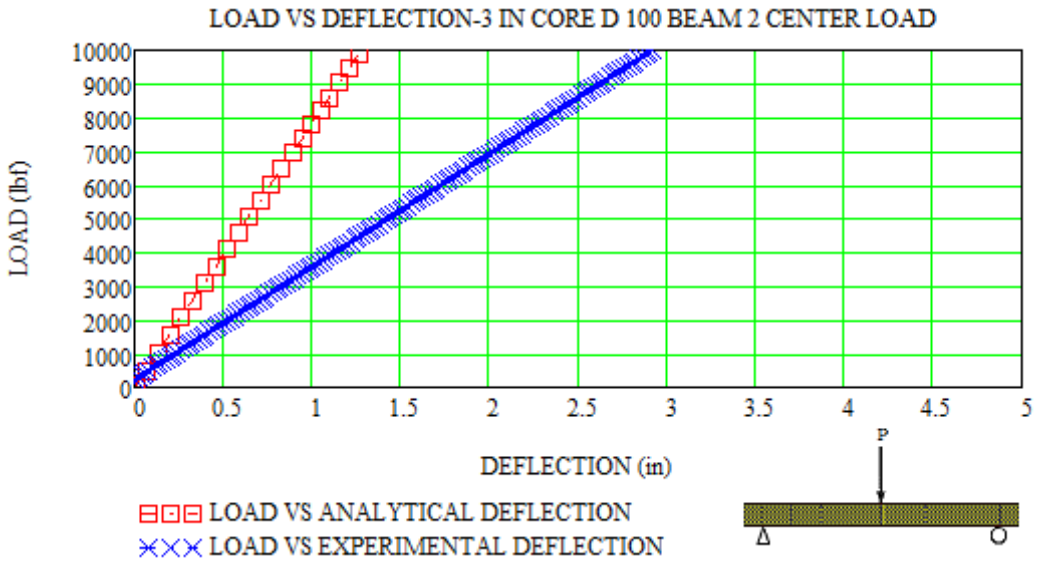

Figure 57. Load vs. Deflection-3 in. core-D 100-center load Beam # 2

4.3.2 Analytical vs. Experimental Deflection Data-Group I Quarter-Point Load

Figure 58 compares analytical deflections to experimental deflections for composite beam # 1 with core thickness equal 1 inch and core density D 100, under increasing applied load. Experimental deflection data is in blue, and red represents deflection data obtained analytically. Comparison graphs for composite beams # 4 and # 6 with core thickness equal 1 inch and core density D 100 are presented in Appendix II.

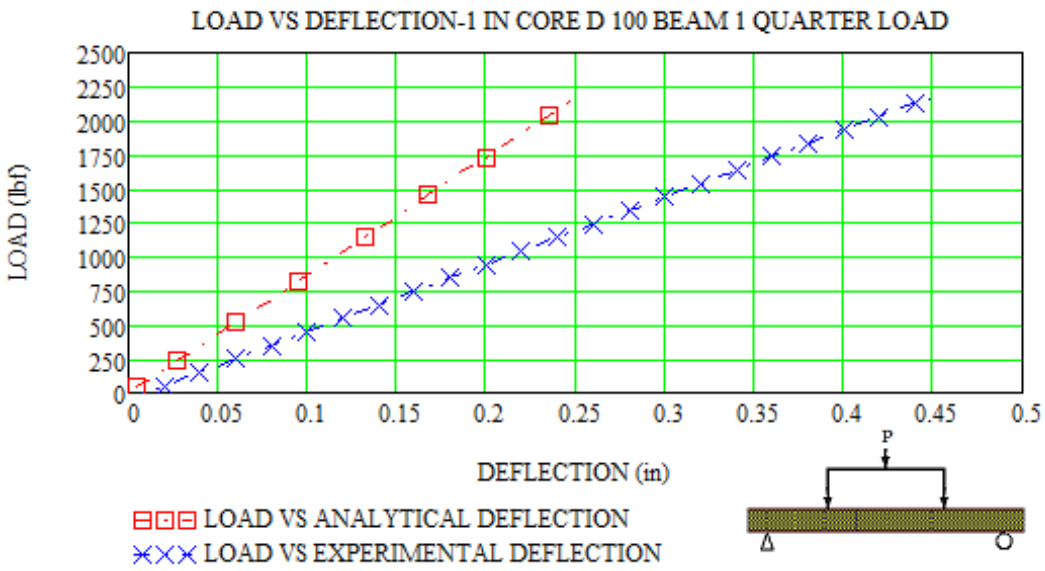

Figure 58. Load vs. Deflection-1 in. core-D 100-quarter load Beam # 1

Figure 59 compares analytical deflections to experimental deflections for composite beam # 1 with core thickness equal 2 inch and core density D 100, under increasing applied load. Experimental deflection data is in blue, and red represents deflection data obtained analytically. Comparison graphs for composite beams # 4 and # 5 with core thickness equal 2 inch and core density D 100 are presented in Appendix II.

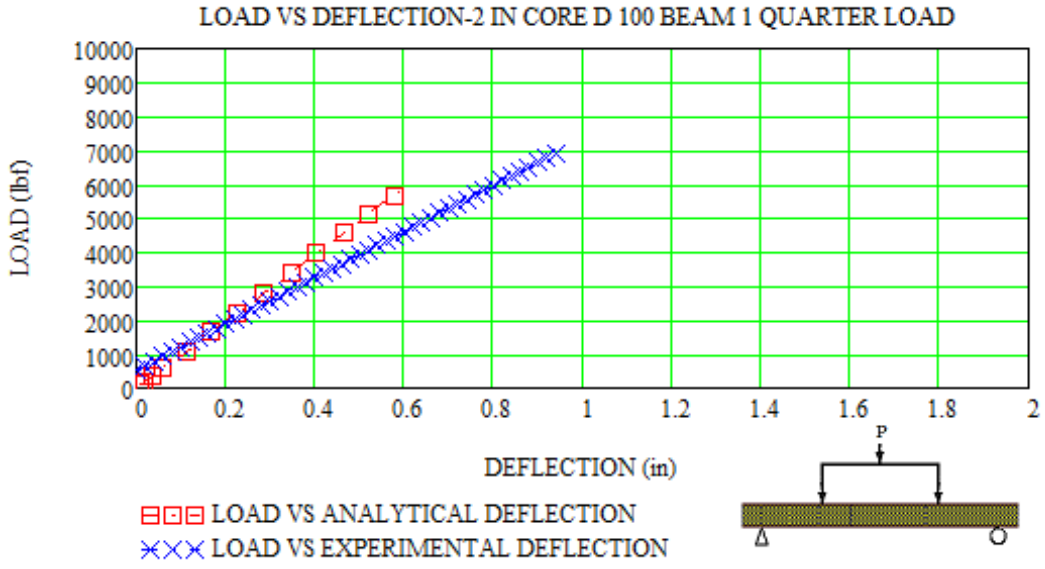

Figure 59. Load vs. Deflection-2 in. core-D 100-quarter load Beam # 1

Figure 60 compares analytical deflections to experimental deflections for composite beam # 1 with core thickness equal 3 inch and core density D 100, under increasing applied load. Experimental deflection data is in blue, and red represents deflection data obtained analytically. Comparison graphs for composite beams # 5 and # 6 with core thickness equal 3 inch and core density D 100 are presented in Appendix II.

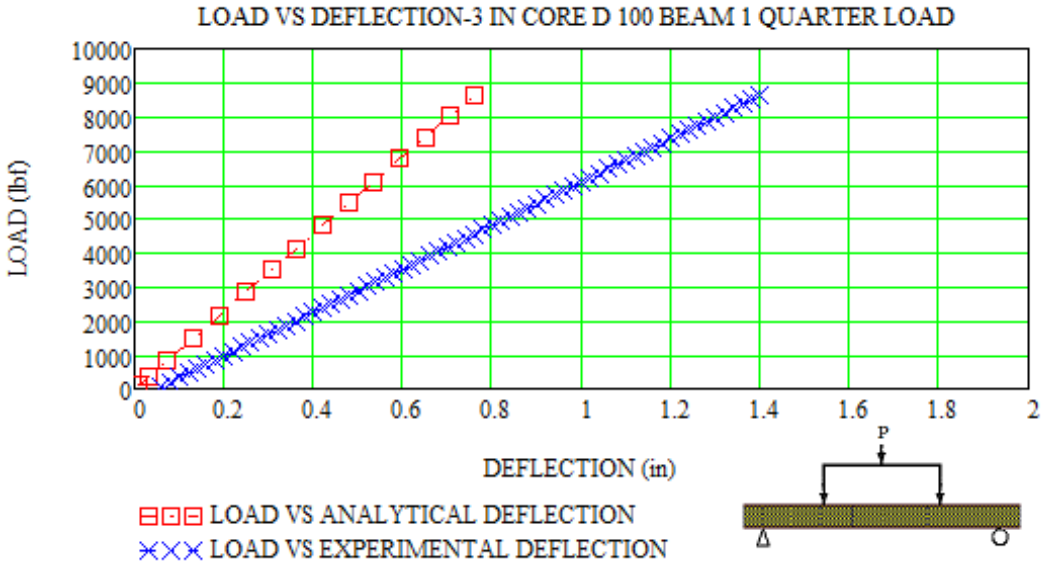

Figure 60. Load vs. Deflection-3 in. core-D 100-quarter load Beam # 1

4.4 Assessment of Analytical vs. Experimental Strain Data-Group II

In Group II, the focus shifts to assessing loading characteristics for composite sandwich beams with increasing core densities, while the core thickness remains constant. Representative illustrations for center-point and quarter-point load configurations are provided in Chapter II. As described in the equations for normal strain ε_{center} (Eq. 10) and $\varepsilon_{quarter}$ (Eq. 11) in Chapter III, the analytical results are linear in contrast to the slight nonlinearity observed in experimental strain (UNO, 2005). For these flexure tests, the maximum strain is assumed to be at mid-span of the loaded composite beams.

The following sections compare analytical strain to experimental strain (UNO, 2005). The results are presented in accordance with flexural testing schedules shown in Table 8, Table 9, and Table 10 in Chapter II.

4.4.1 Analytical vs. Experimental Strain Data-Group II Center-Point Load

Figure 61 compares analytical strain to experimental strain for composite beam # 2 with core thickness equal 3 inch and core density S 56, under increasing applied load. Experimental strain data is in blue, and red represents strain data obtained analytically. Comparison graphs for composite beams # 3 and # 5 with core thickness equal 3 inch and core density S 56 are presented in Appendix II.

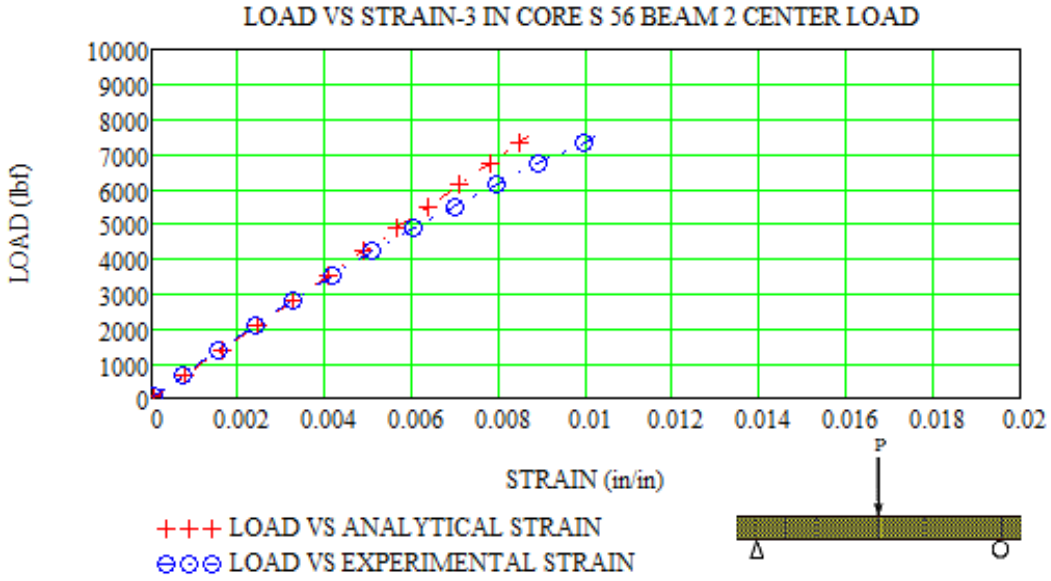

Figure 61. Load vs. Strain-3 in. core-S 56-center load Beam # 2

Figure 62 compares analytical strain to experimental strain for composite beam # 3 with core thickness equal 3 inch and core density D 100, under increasing applied load. Experimental strain data is in blue, and red represents strain data obtained analytically. Comparison graphs for composite beams # 4 and # 5 with core thickness equal 3 inch and core density D 100 are presented in Appendix II.

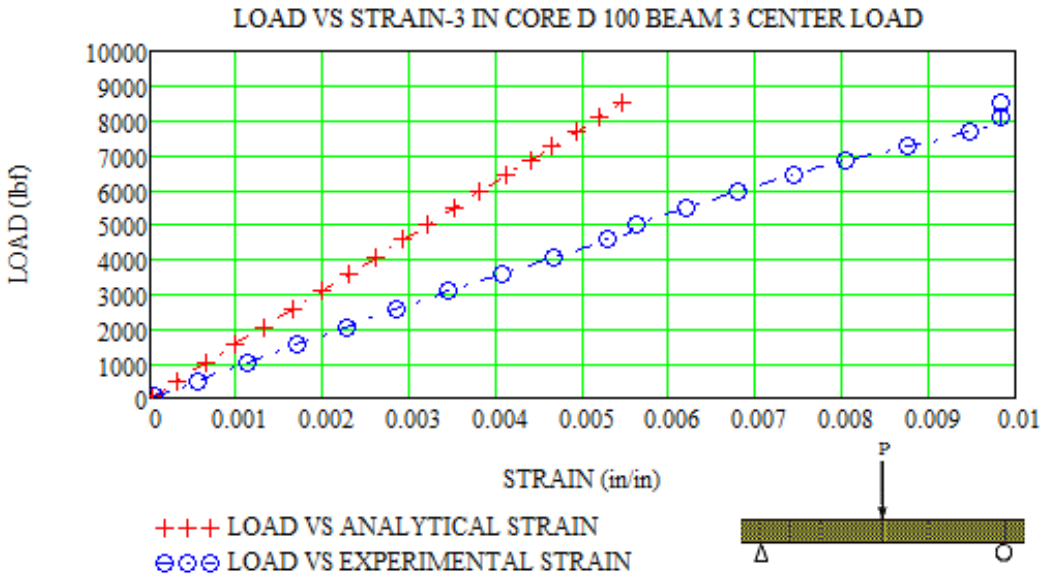

Figure 62. Load vs. Strain-3 in. core-D 100-center load Beam # 3

Figure 63 compares analytical strain to experimental strain for composite beam # 4 with core thickness equal 3 inch and core density S 1415, under increasing applied load. Experimental strain data is in blue, and red represents strain data obtained analytically. Comparison graphs for composite beams # 5 and # 6 with core thickness equal 3 inch and core density S 1415 are presented in Appendix II.

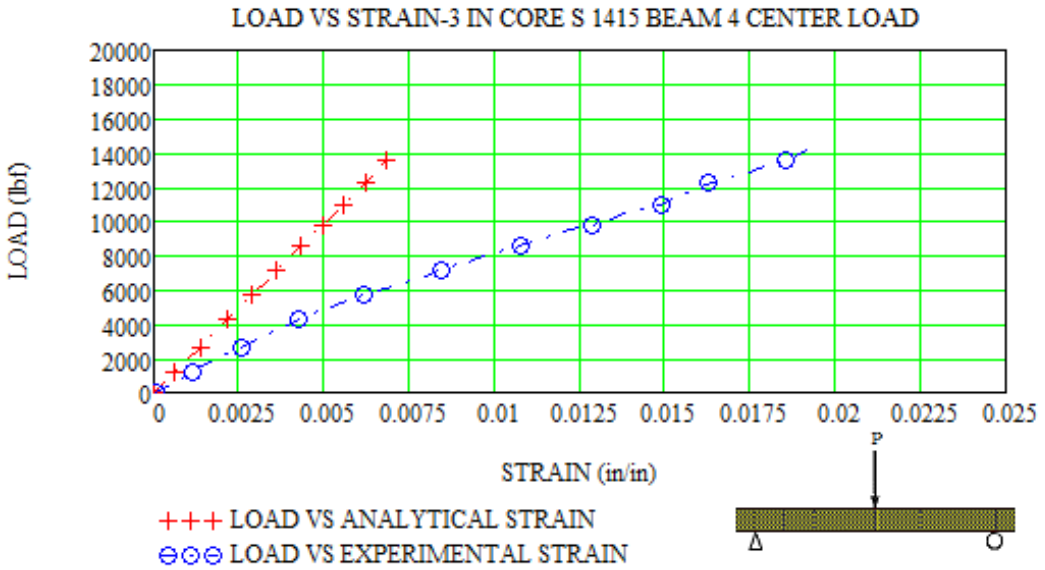

Figure 63. Load vs. Strain-3 in. core-S 1415-center load Beam # 4

4.4.2 Analytical vs. Experimental Strain Data-Group II Quarter-Point Load

Figure 64 compares analytical strain to experimental strain for composite beam # 1 with core thickness equal 3 inch and core density S 56, under increasing applied load. Experimental strain data is in blue, and red represents strain data obtained analytically. Comparison graphs for composite beams # 4 and # 6 with core thickness equal 3 inch and core density S 56 are presented in Appendix II.

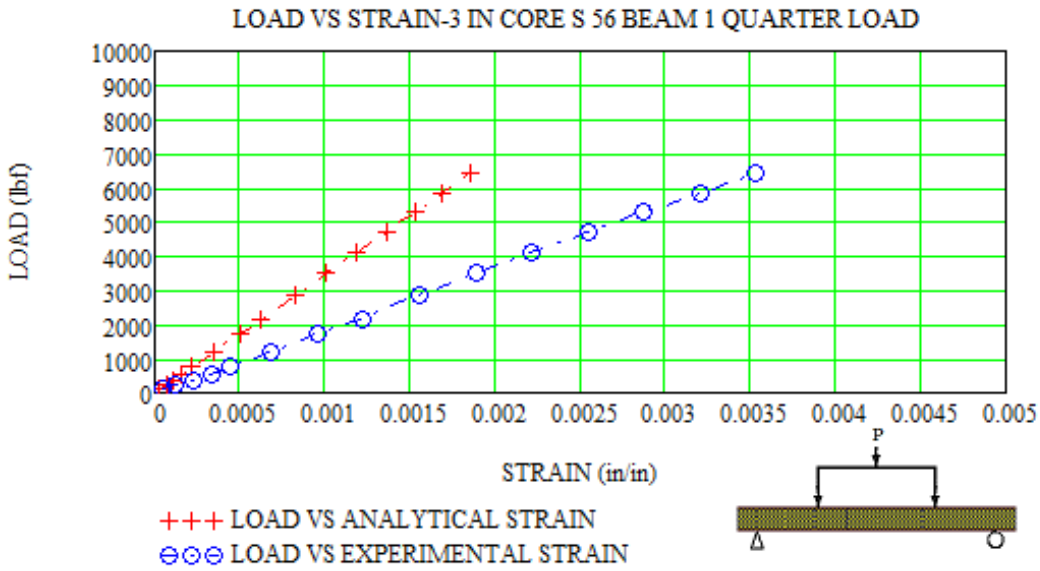

Figure 64. Load vs. Strain-3 in. core-S 56-quarter load Beam # 1

Figure 65 compares analytical strain to experimental strain for composite beam # 1 with core thickness equal 3 inch and core density D 100, under increasing applied load. Experimental strain data is in blue, and red represents strain data obtained analytically. Comparison graphs for composite beams # 2 and # 6 with core thickness equal 3 inch and core density D 100 are presented in Appendix II.

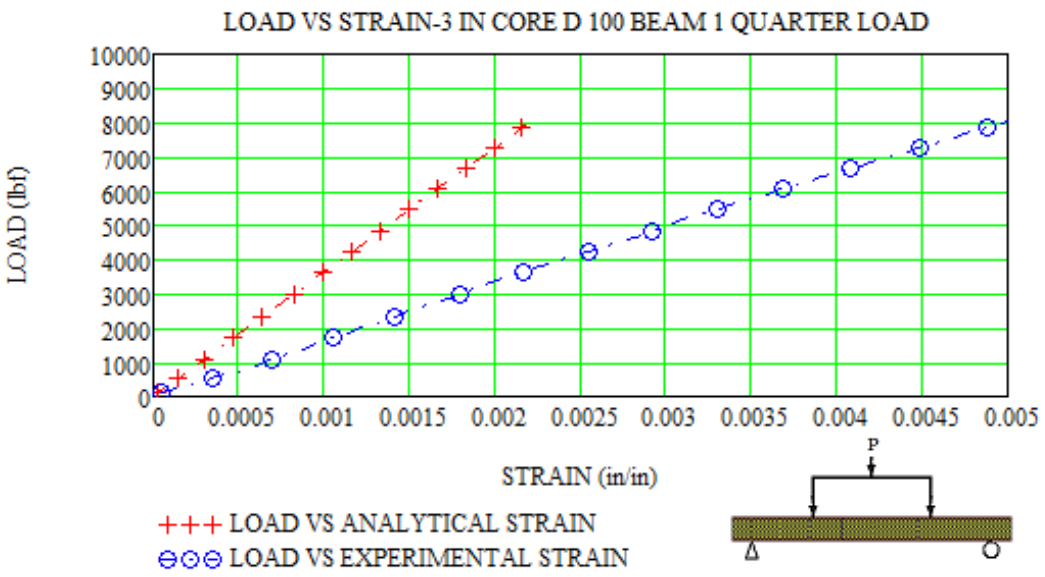

Figure 65. Load vs. Strain-3 in. core-D 100-quarter load Beam # 1

Figure 66 compares analytical strain to experimental strain for composite beam # 1 with core thickness equal 3 inch and core density S 1415, under increasing applied load. Experimental strain data is in blue, and red represents strain data obtained analytically. Comparison graphs for composite beams # 2 and # 3 with core thickness equal 3 inch and core density S 1415 are presented in Appendix II.

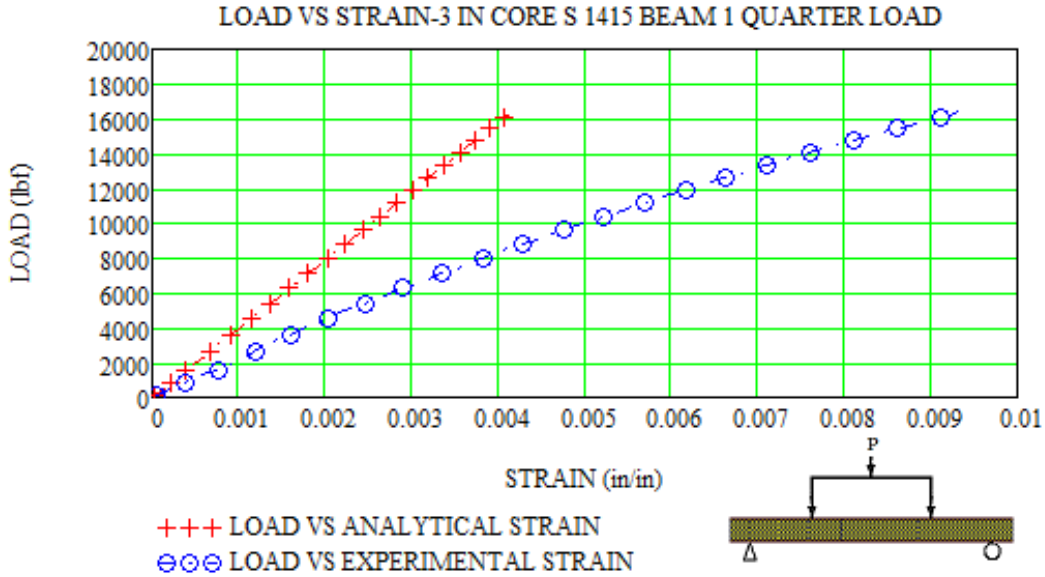

Figure 66. Load vs. Strain-3 in. core-S 1415-quarter load Beam # 1

4.5 Assessment of Analytical vs. Experimental Deflection Data-Group II

In Group II, the focus shifts to assessing loading characteristics for composite sandwich beams with increasing core densities, while the core thickness remains constant. Representative illustrations for center-point and quarter-point load configurations are provided in Chapter II. As described in the equations for deflection D_{center} (Eq. 12) and $D_{quarter}$ (Eq. 13) in Chapter III, the analytical results are linear in contrast to the slight nonlinearity observed in experimental deflection (UNO, 2005). For these flexure tests, the maximum deflection is assumed to be at mid-span of the loaded composite beams.

The following sections compare analytical deflection to experimental deflection data (UNO, 2005). The results are presented in accordance with flexural analysis schedules shown in Table 8, Table 9, and Table 10 in Chapter II.

4.5.1 Analytical vs. Experimental Deflection Data-Group II Center-Point Load

Figure 67 compares analytical deflections to experimental deflections for composite beam # 2 with core thickness equal 3 inch and core density S 56, under increasing applied load. Experimental deflection data is in blue, and red represents deflection data obtained analytically. Comparison graphs for composite beams # 3 and # 5 with core thickness equal 3 inch and core density S 56 are presented in Appendix II.

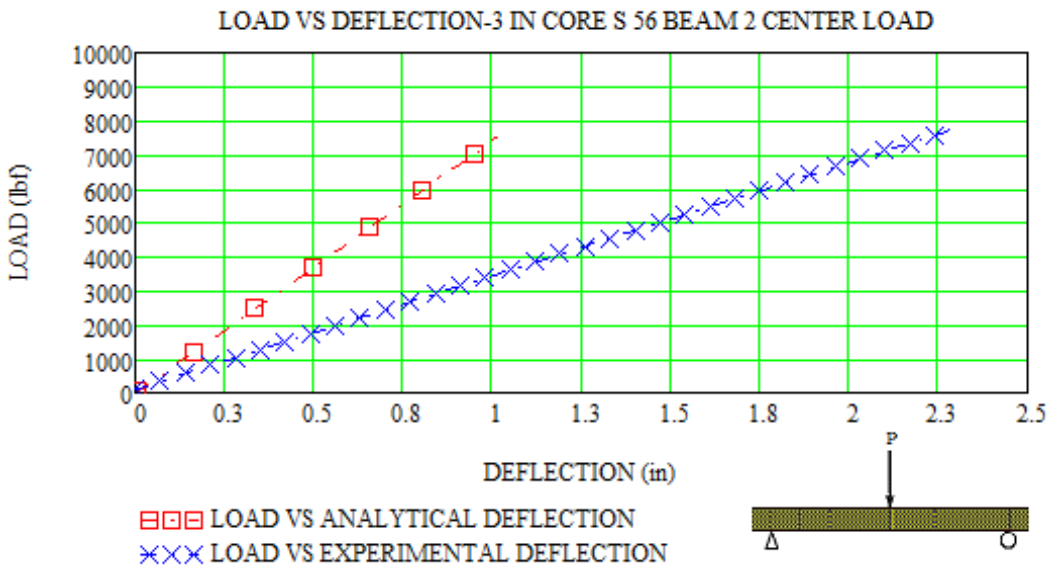

Figure 67. Load vs. Deflection-3 in. core-S 56-center load Beam # 2

Figure 68 compares analytical deflections to experimental deflections for composite beam # 3 with core thickness equal 3 inch and core density D 100, under increasing applied load. Experimental deflection data is in blue, and red represents deflection data obtained analytically. Comparison graphs for composite beams # 4 and # 5 with core thickness equal 3 inch and core density D 100 are presented in Appendix II.

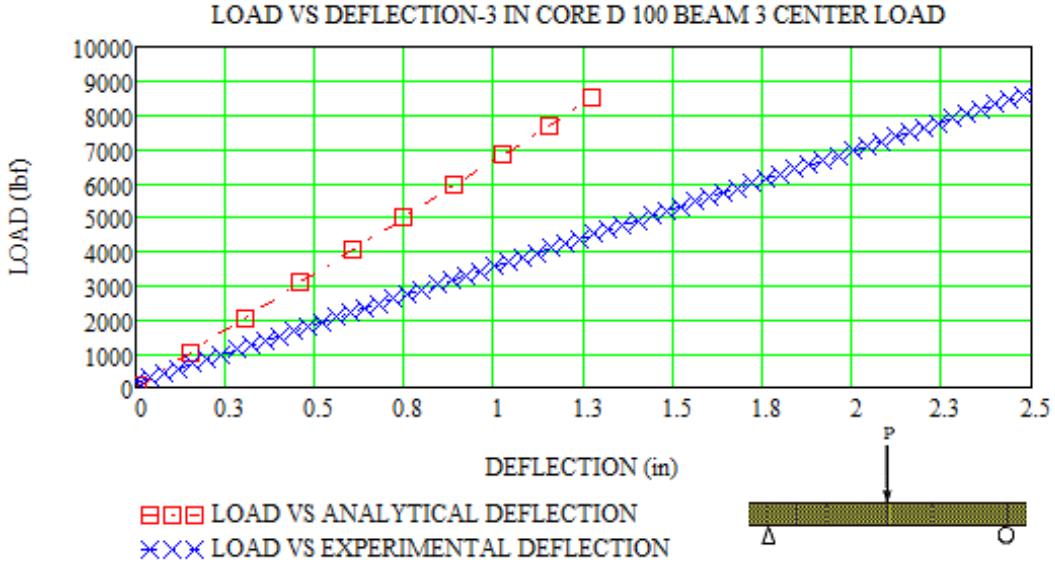

Figure 68. Load vs. Deflection-3 in. core-D 100-center load Beam # 3

Figure 69 compares analytical deflections to experimental deflections for composite beam # 4 with core thickness equal 3 inch and core density S 1415, under increasing applied load. Experimental deflection data is in blue, and red represents deflection data obtained analytically. Comparison graphs for composite beams # 5 and # 6 with core thickness equal 3 inch and core density S 1415 are presented in Appendix II.

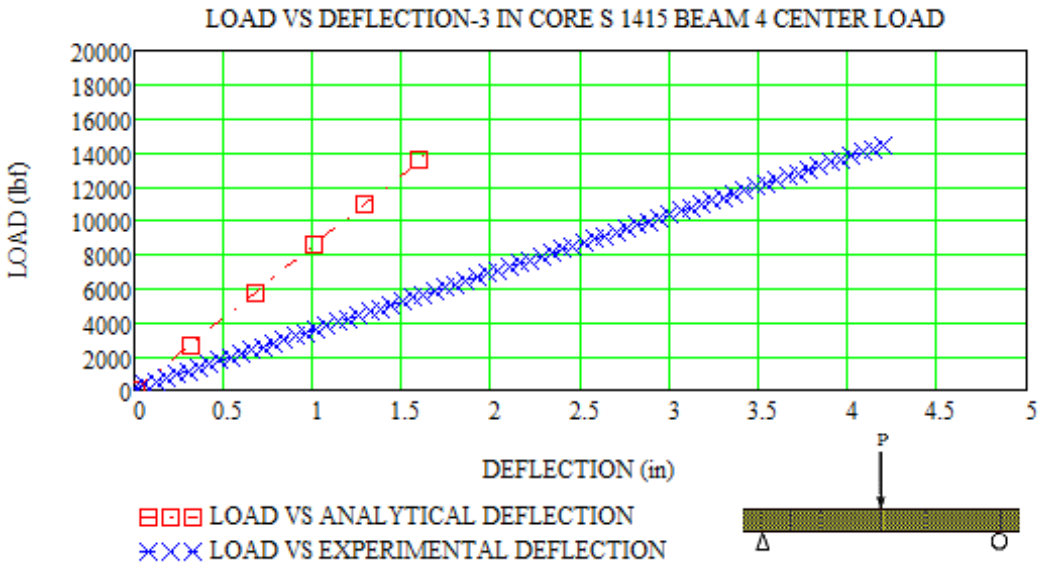

Figure 69. Load vs. Deflection-3 in. core-S 1415-center load Beam # 4

4.5.2 Analytical vs. Experimental Deflection Data-Group II Quarter-Point Load

Figure 70 compares analytical deflections to experimental deflections for composite beam # 1 with core thickness equal 3 inch and core density S 56, under increasing applied load. Experimental deflection data is in blue, and red represents deflection data obtained analytically. Comparison graphs for composite beams # 4 and # 6 with core thickness equal 3 inch and core density S 56 are presented in Appendix II.

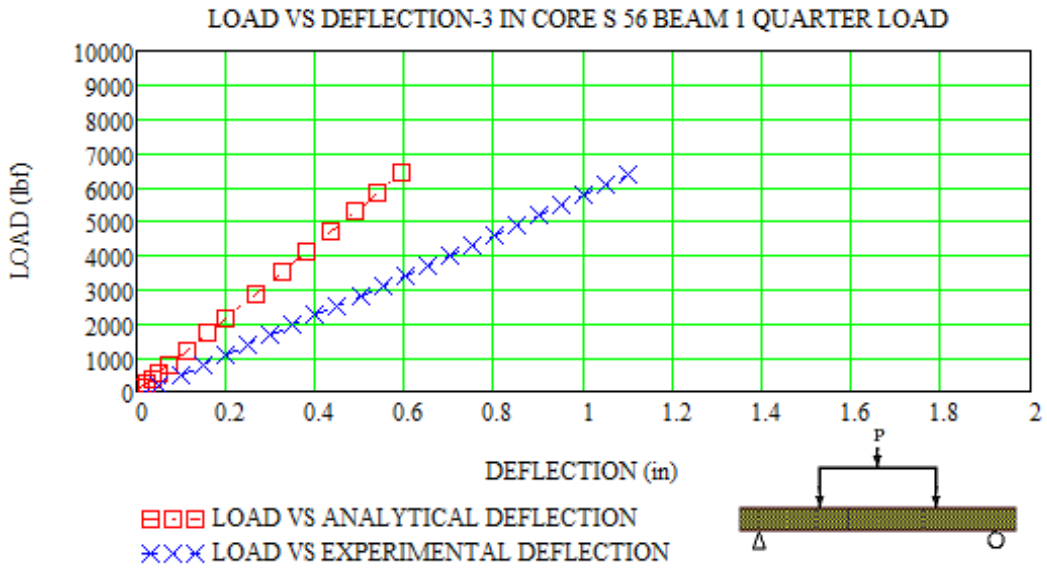

Figure 70. Load vs. Deflection-3 in. core-S 56-quarter load Beam # 1

Figure 71 compares analytical deflections to experimental deflections for composite beam # 1 with core thickness equal 3 inch and core density D 100, under increasing applied load. Experimental deflection data is in blue, and red represents deflection data obtained analytically. Comparison graphs for composite beams # 2 and # 6 with core thickness equal 3 inch and core density D 100 are presented in Appendix II.

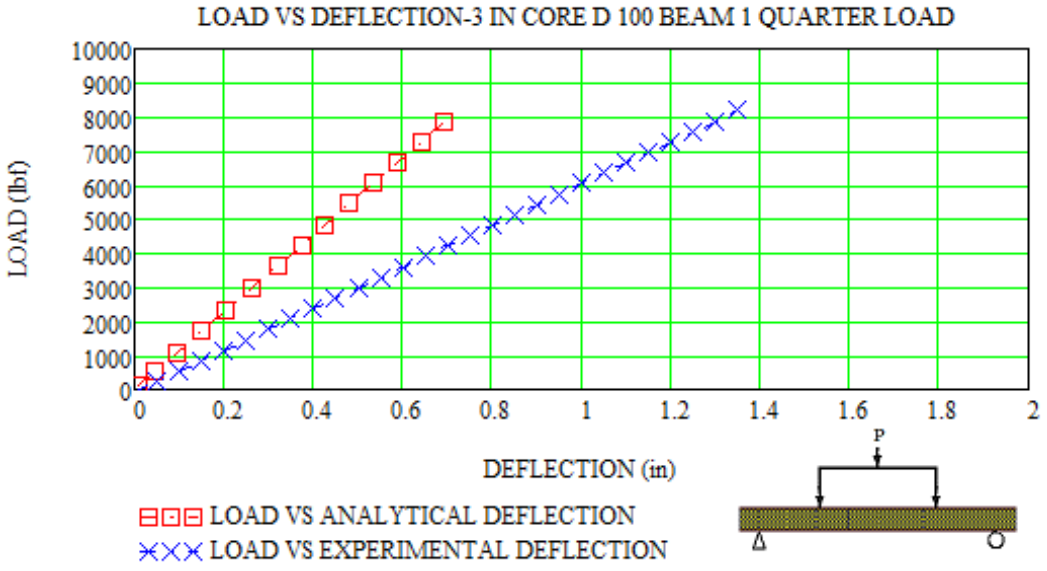

Figure 71. Load vs. Deflection-3 in. core-D 100-quarter load Beam # 1

Figure 72 compares analytical deflections to experimental deflections for composite beam # 1 with core thickness equal 3 inch and core density S 1415, under increasing applied load. Experimental deflection data is in blue, and red represents deflection data obtained analytically. Comparison graphs for composite beams # 2 and # 3 with core thickness equal 3 inch and core density S 1415 are presented in Appendix II.

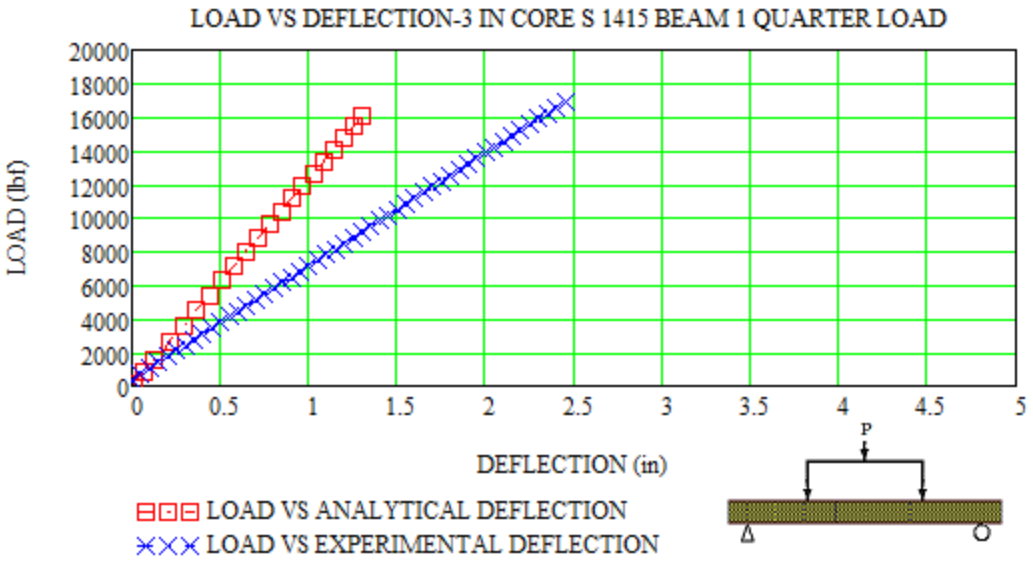

Figure 72. Load vs. Deflection-3 in. core-S 1415-quarter load Beam # 1

4.6 Summary of Analytical vs. Experimental Data

As presented, the relative simplicity and rapid solution time of the Euler-Bernoulli beam theory underestimates typical transverse responses of composite sandwich beams under flexural loads. For most cases, analytical strain and deflection results are significantly less than experimental strain and deflection results. In general, agreement between experimental data and analytical data has been minimal.

CHAPTER V

RECOMMENDATIONS AND CONCLUSIONS

The purpose of the present study has been to make a new analytical contribution to issues related to flexural strain and displacement behavior of composite sandwich beams using Euler-Bernoulli simple beam theory. With this in mind, the specific objective in this study was to use the Euler-Bernoulli beam theory to perform normal strain and deflection calculations on composite sandwich beams with mechanical properties and geometry as described in Chapter I, Chapter II, and Chapter III. As presented in Chapter IV, the analytical values for strain and deflection generated using the Euler-Bernoulli beam theory were compared to experimental values provided by researchers from the University of New Orleans (UNO, 2005). The results reveal that agreement between experimental values and analytical values is minimal. The Euler-Bernoulli based equations normal strain and deflection underestimate flexure responses for most composite beams in both Group I and Group II.

In this case, the most effective remedy is to introduce uniform convergence in the form of standard curve-fitting methods or a correction factor –a mathematical adjustment made to account for deviations in either the sample or the method of measurement. The incorporation of a correction factor, $c_r = 0.5$, into existing normal strain and deflection equations, as shown in Table 21, will produce adequate agreement between experimental values and analytical values. The correction factor $c_r = 0.5$ is based on the average of all deviations between experimental values and analytical values seen in Chapter IV.

Table 21. Equations with Correction Factor $c_r = 0.5$

	Current	Correction Factor $c_r = 0.5$
Normal Strain (in/in) Center load-Eq. 10	$\varepsilon_{center} = \frac{M_{center} \cdot c}{EI_{eq}}$	$\varepsilon_{center} = \frac{M_{center} \cdot c}{0.5EI_{eq}}$
Normal Strain (in/in) Quarter load-Eq. 11	$\varepsilon_{quarter} = \frac{M_{quarter} \cdot c}{EI_{eq}}$	$\varepsilon_{quarter} = \frac{M_{quarter} \cdot c}{0.5EI_{eq}}$
Deflection (in) Center load-Eq. 12	$D_{center} = \frac{P \cdot L_{span}^{3}}{48 \cdot EI_{eq}}$	$D_{center} = \frac{P L_{span}^{3}}{0.5 \cdot 48 \cdot EI_{eq}}$
Deflection (in) Quarter load-Eq. 13	$D_{quarter} = \frac{\frac{-L_{span}}{4} \cdot \left[\left[4\left(\frac{L_{span}}{4}\right)^{2} - 3 \cdot L_{span}^{2} \right] \frac{P}{2} \right]}{24 \cdot EI_{eq}}$	$D_{quarter} = \frac{\frac{-L_{span}}{4} \cdot \left[\left[4\left(\frac{L_{pan}}{4}\right)^{2} - 3 \cdot L_{pan}^{2} \right] \frac{P}{2} \right]}{0.5 \cdot 24 \cdot EI_{eq}}$

For demonstration purposes, the following graphs show current and corrected strain and deflection results for composite beam # 2 with core thickness equal 2 inch and core density D 100 from Group I, and beam # 4 with core thickness equal 3 inch and core density S 56 from Group II. For each of the following graphs, experimental data is in blue, and red represents data obtained analytically.

Figure 73 and Figure 74 show current comparison between experimental data and analytical data to for composite beam # 2 with core thickness equal 2 inch and core density D 100.

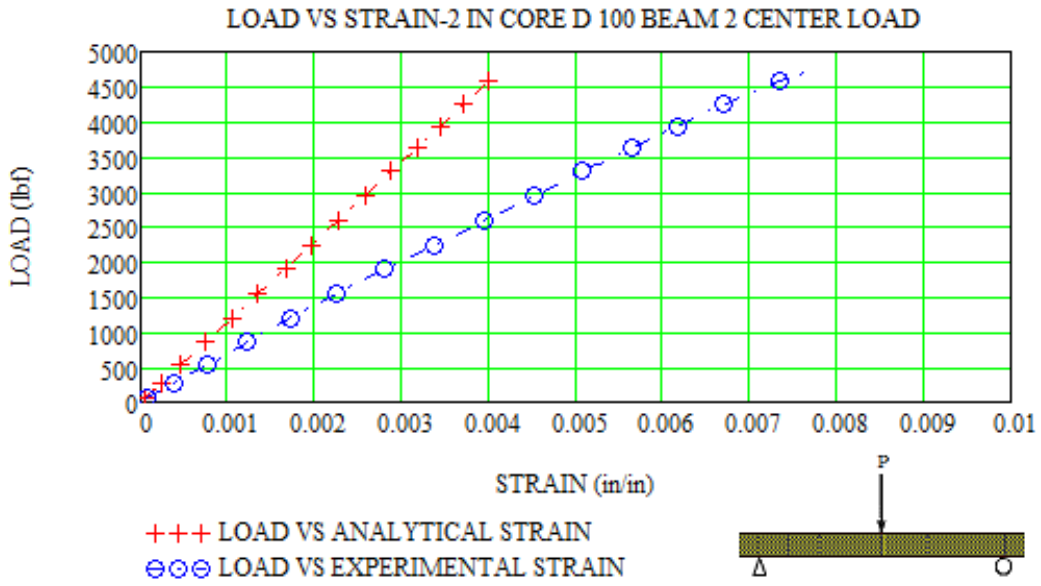

Figure 73. Load vs. Strain-2 in. core-D 100-center load Beam # 2

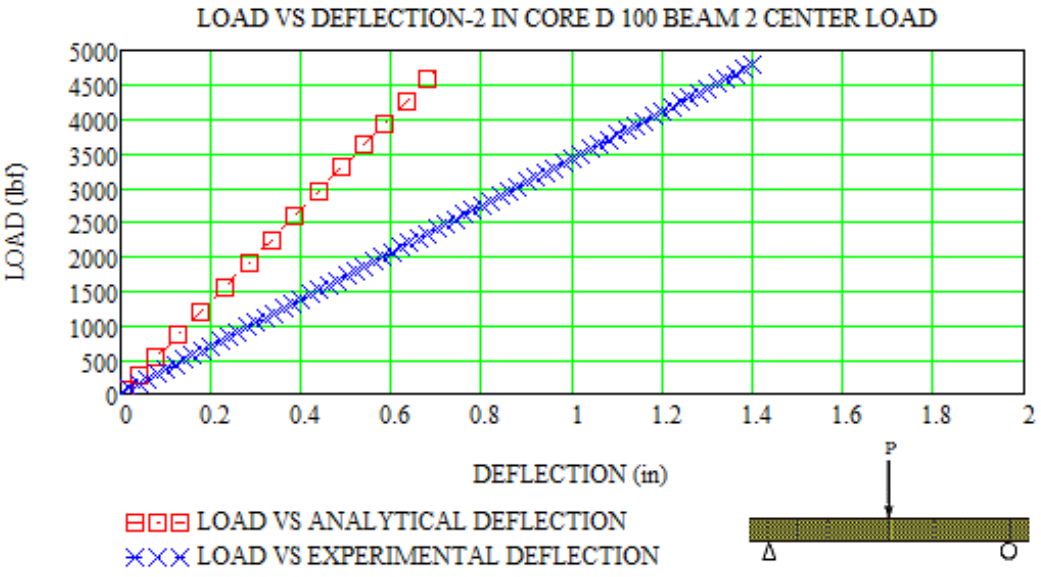

Figure 74. Load vs. Deflection-2 in. core-D 100-center load Beam # 2

Figure 75 and Figure 76 show comparison between experimental data and corrected analytical data to for composite beam # 2 with core thickness equal 2 inch and core density D 100.

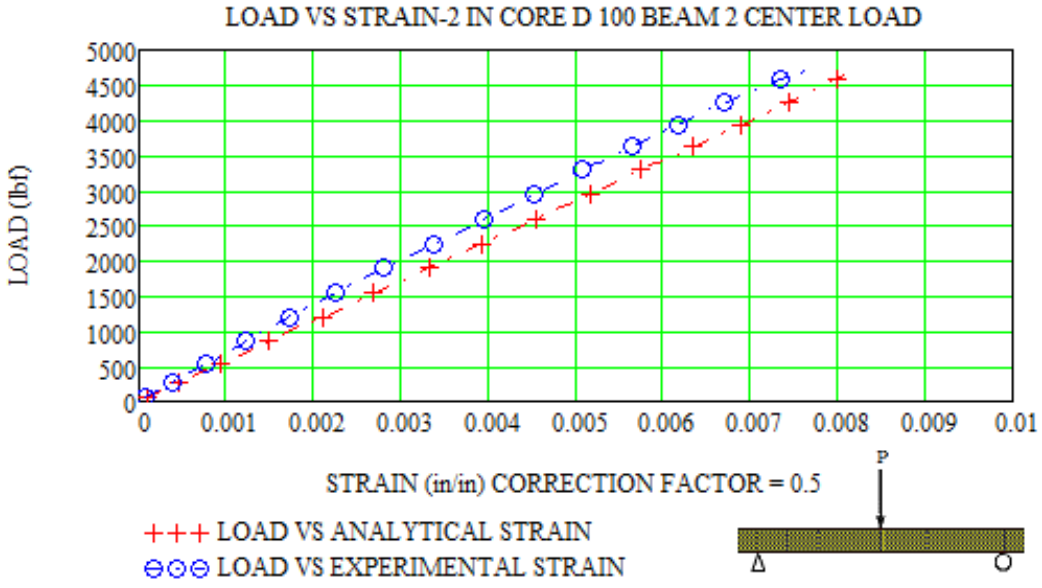

Figure 75. Load vs. Strain-2 in. core-D 100-center load Beam # 2-with $c_r = 0.5$

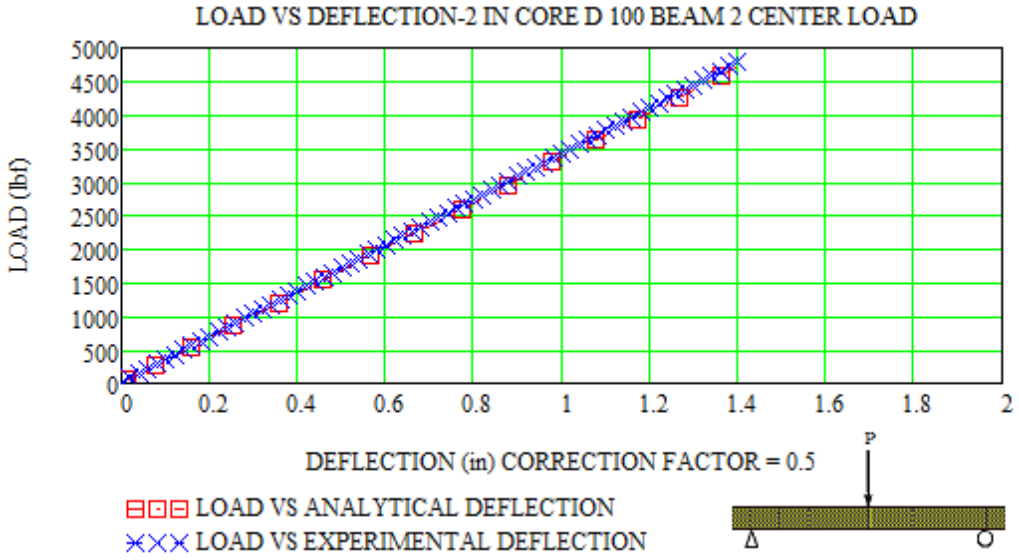

Figure 76. Load vs. Deflection-2 in. core-D 100-center load Beam # 2-with $c_r = 0.5$

Figure 77 and Figure 78 show current comparison between experimental data and analytical data to for composite beam # 4 with core thickness equal 3 inch and core density S 56.

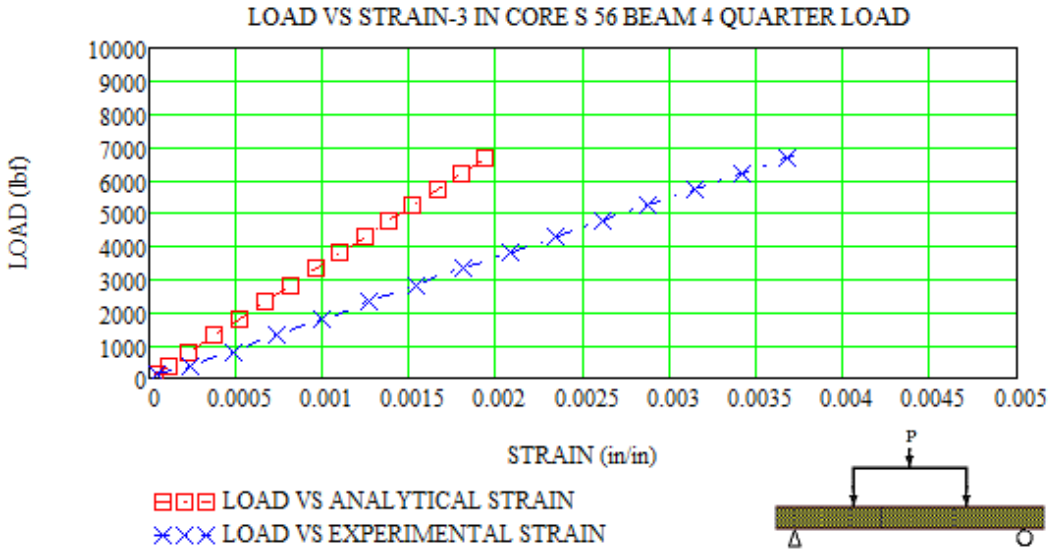

Figure 77. Load vs. Strain-3 in. core-S 56-quarter load Beam # 4

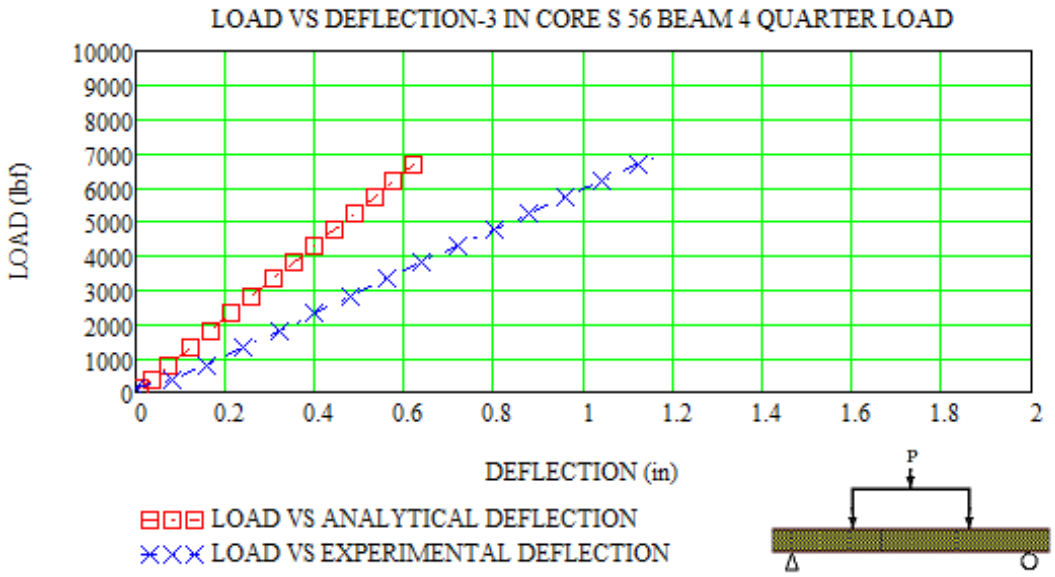

Figure 78. Load vs. Deflection-3 in. core-S 56-quarter load Beam # 4

Figure 79 and Figure 80 show comparison between experimental data and corrected analytical data to for composite beam # 4 with core thickness equal 3 inch and core density S 56.

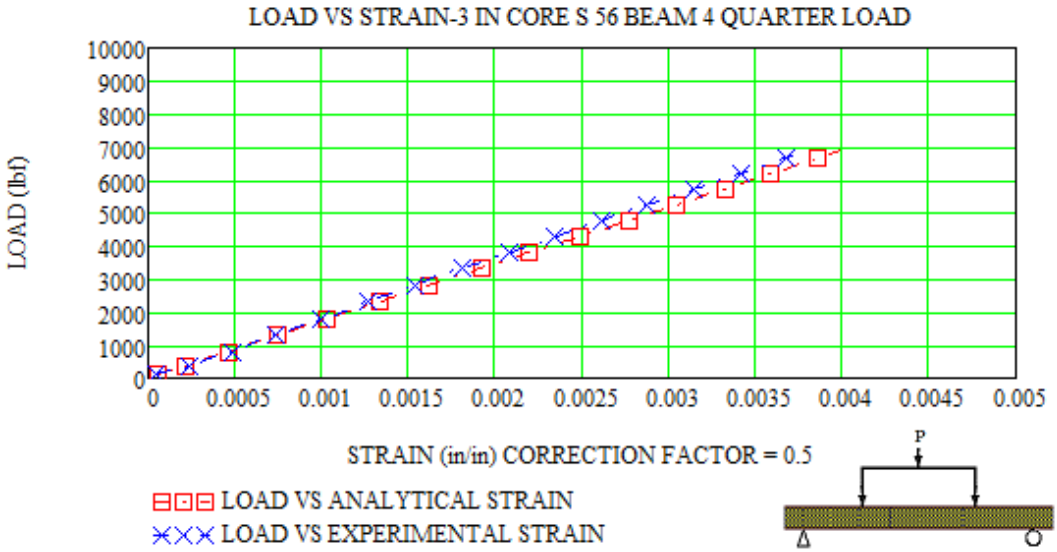

Figure 79. Load vs. Strain-3 in. core-S 56-quarter load Beam # 4-with $c_r = 0.5$

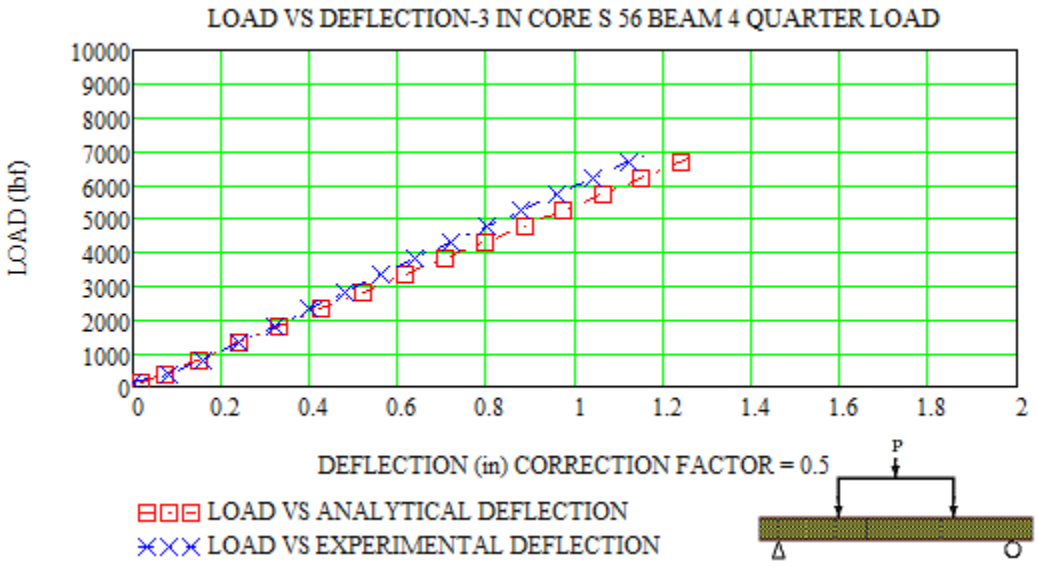

Figure 80. Load vs. Deflection-3 in. core-S 56-quarter load Beam # 4-with $c_r = 0.5$

As shown, relative agreement between experimental data and analytical data was achieved with the introduction of correction factor $c_r = 0.5$. From the results, the addition of a correction factor of 0.5 has provided a significant adjustment to the predicted deflection and strain. There is now good agreement between the experimental deflection and strain and analytical deflection and strain as the applied load increases. The correlation between experimental data and adjusted analytical data suggests that the Euler-Bernoulli beam theory can be used to predict the theoretical values of deflection and normal strain for composite sandwich beams in flexure in this study. Appendix III contains additional comparison graphs for Group I and Group II.

In conclusion, the simplified Euler-Bernoulli equation relating moment over rigidity to curvature, used in conjunction with the equivalent area method, to predict flexural behavior of a sandwich composite panel in flexure is not accurate without the use of a correction factor.

REFERENCES

Alcan Baltek Corporation "Baltek SL 56 Structural End-Grain Balsa." "Baltek SB 100 Structural End-Grain Balsa." Baltek SB 1415 Structural End-Grain Balsa."

Alexander Tessler; Marco Di Sciuva; Marco Gherlone. "Refinement of Timoshenko Beam Theory for Composite and Sandwich Beams Using Zigzag Kinematics" NASA/TP-2007-215086.

Alexander Tessler, A.; Spangler, J. L. "A Variational Principle for Reconstruction of Elastic Deformation in Shear Deformable Plates and Shells." NASA/TM-2003-212445.2003

Ambartsumian S. A. On the problem of calculation of laminated anisotropic shells. Translated by Armenian SSR Acad. 1953.

André Teófilo Becka; Cláudio R.A. da Silva Jr. "Timoshenko versus Euler beam theory: Pitfalls of a deterministic approach." Department of Structural Engineering, EESC, University of São Paulo, Brazil. May 2010.

Ashland Composite Polymers. "Composite Polymers Fabricating Tips." 2005.

ASTM C393-00, Standard Test Method for Flexural Properties of Sandwich Constructions, ASTM International, West Conshohocken, PA, 2000.

ASTM D790-10, Standard Test Methods for Flexural Properties of Unreinforced and Reinforced Plastics and Electrical Insulating Materials, ASTM International, West Conshohocken, PA, 2010.

Beer, Ferdinand. P.; Johnston, E. Russell, Jr. Mechanics of Materials. McGraw-Hill. New York, NY. Second Edition. 1992.

Dan Zenkert. The Handbook of Sandwich Construction. Engineering Materials Advisory Services Ltd. (EMAS), 1997.

Ellen Lackey; James Vaughan. "Experimental Determination of GIIC for Secondary SCRIMP Fabrication Laminates Using the End Notch Flexural Test." University of Mississippi. 3 November 2000.

Eugenio Oñate. Structural Analysis with the Finite Element Method. Linear Statics. Springer. Volume 2. 2009

E.E. Gdoutos; I.M. Daniel. "Nonlinearities in the Deformation of Composite Sandwich Beams." School of Engineering, Democritus University of Thrace. Robert McCormick School of Engineering and Applied Sciences Northwestern University. June 2008.

Francisco Arias; Paul J.A. Kenis; Bing Xu; Tao Deng; Olivier J.A. Schueller; George M. Whitesidesa. "Fabrication and characterization of micro-scale sandwich beams." Harvard University. November 2000.

Hamilton Robert; Stephen Tennyson; Wayne Hamilton. "Analysis by the Transformed-Section Method" Boise State University/Boise State University/University of Maine at Orono.

Isaac M. Daniel; Jandro L. Abot. "Fabrication, testing and analysis of composite sandwich beams." Robert McCormick School of Engineering and Applied Sciences Northwestern University. Jan 2000.

John F. Hunt; Houjiang Zhang; Jang Huang. "Analysis of Cantilever-Beam Bending Stress Relaxation Properties of Thin Wood Composites." USDA Forest Products Laboratory. 2015.

M. Bischoff; W.A. Wall; K.-U.Bletzinger; E.Ramm. “Encyclopedia of Computational Mechanics. Volume 2: Solids, Structures and Coupled Problems.” John Wiley % Sons, Ltd. 2004.

University of New Orleans. “Effect of Composite Sandwich Beam Mechanical Properties and Geometry on Flexural Performance.” University of New Orleans. 2005.

U.S. Department of Defense (USDOD). “Composite Materials Handbook. Volume 2: Polymer Matrix Composites Materials Properties.” Publication Number MIL-HDBK-17-2F. June 2002.

Wim Van Paepegem. “Composite Engineering Materials.” Ghent University. November 2004.

APPENDIX I

AVERAGE MODULUS OF ELASTICITY FOR SKIN MATERIAL

In November 2000, Ellen Lackey and James Vaughan, researchers from the University of Mississippi conducted flexural testing on laminated panels composed of 24 oz. woven fabric with Dow Derakane 510A vinyl ester resin. The overall geometry for laminated skin specimens are: length L_{skin} = 5 in., width w = 1 in., and thickness t_{skin} = 0.25 in. An illustration for the tested laminated skin geometry is shown here.

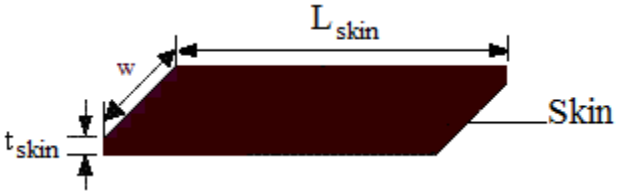

Laminated skin geometry

These laminated skin panels, from Ingalls Shipbuilding, were subjected to 3-point bending tests and environmental conditioning-room temperature and humidity to ensure bonding and proper strength post cure. There are four load versus displacement graphs, one for each tested specimen of identical measurements. The graph below shows load versus displacement results for the laminated skin panels, subjected to flexural loads.

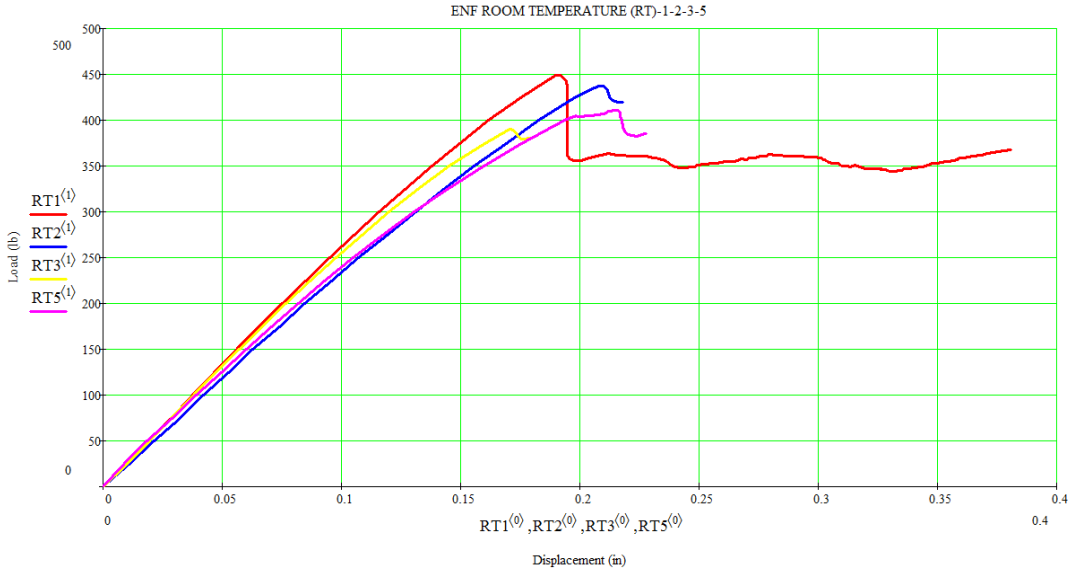

Load vs. Displacement-RT1, RT2, RT3, and RT5

The flexural modulus E derived from each load versus displacement is,

$$E = \frac{P \cdot L_{skin}^{3}}{4 \cdot w \cdot t_{skin}^{3} \cdot y}$$

where P = applied load, L_{skin} = length of laminated skin, w = width, t_{skin} = skin thickness, and y = vertical displacement at load point. The equation for flexural modulus $E_{average}$ is taken from ASTM D790-10 "Standard Test Methods for Flexural Properties of Unreinforced and Reinforced Plastics and Electrical Insulating Materials".

For this research, only the average modulus of elasticity, $E_{average}$, for the laminated skin material is to be used in assessing the accuracy of the Euler-Bernoulli beam theory. The average modulus of elasticity value for the laminated skin is as follows,

$$E_{average} = \frac{E_{RT1} + E_{RT2} + E_{RT3} + E_{RT5}}{4}$$

where E_{RT1}, E_{RT2}, E_{RT3}, and E_{RT5} are flexural modulus for each laminated skin panel. The individual modulus of elasticity value and average modulus of elasticity value to be used in this analysis are given here.

Flexural Moduli and Average Flexural Modulus

LAMINATED PANEL #	ELASTICITY
	(psi)
RT 1	E_{RT1} = 5479452
RT 2	E_{RT2} = 4854369
RT 3	E_{RT3} = 5405405
RT 5	E_{RT5} = 4878048
	$E_{average}$= 5154319

APPENDIX II

Analytical vs. Experimental Strain Data-Group I Center-Point Load

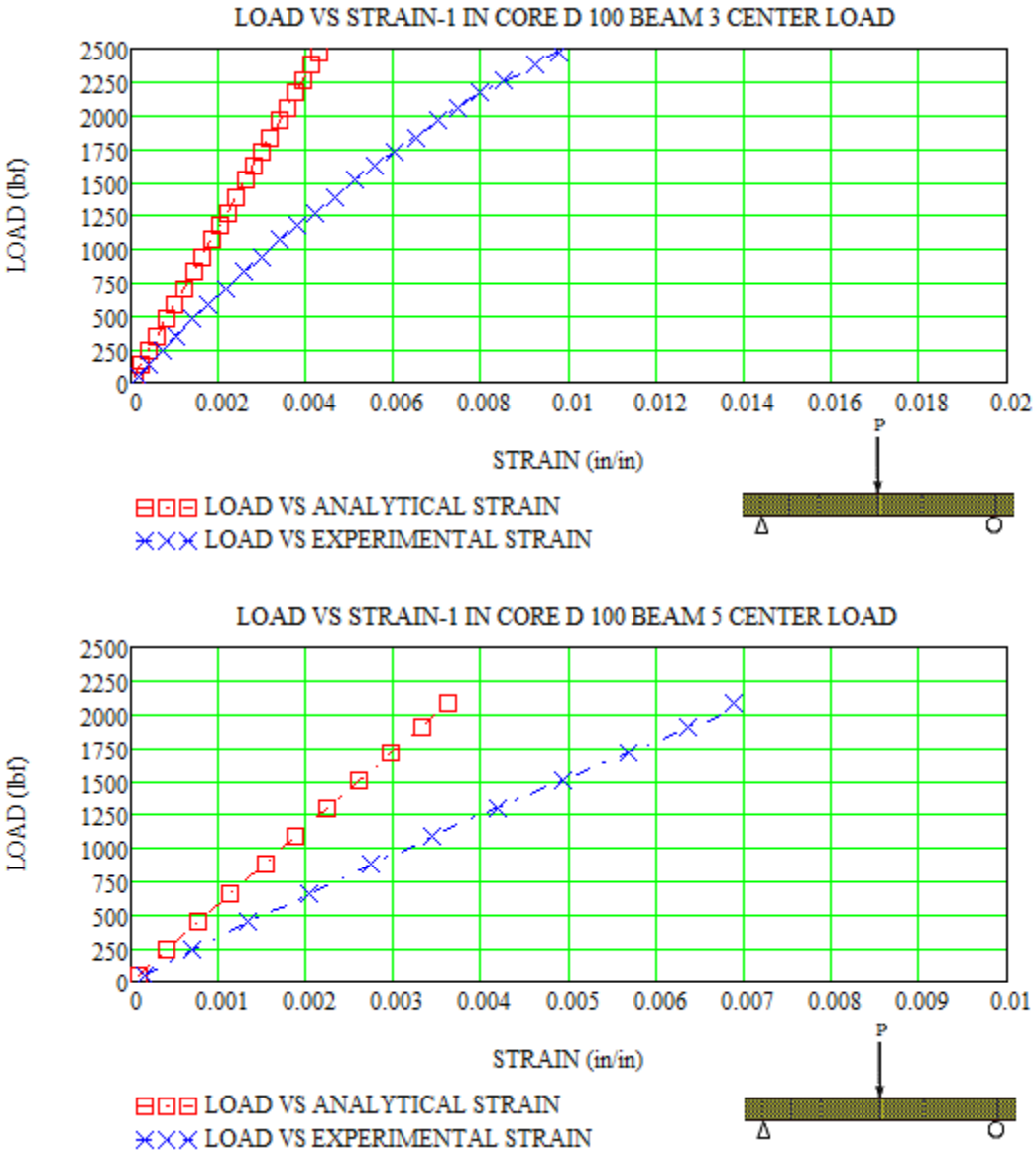

Load vs. Strain-1 in. core-D 100-center load Beam # 3, 5

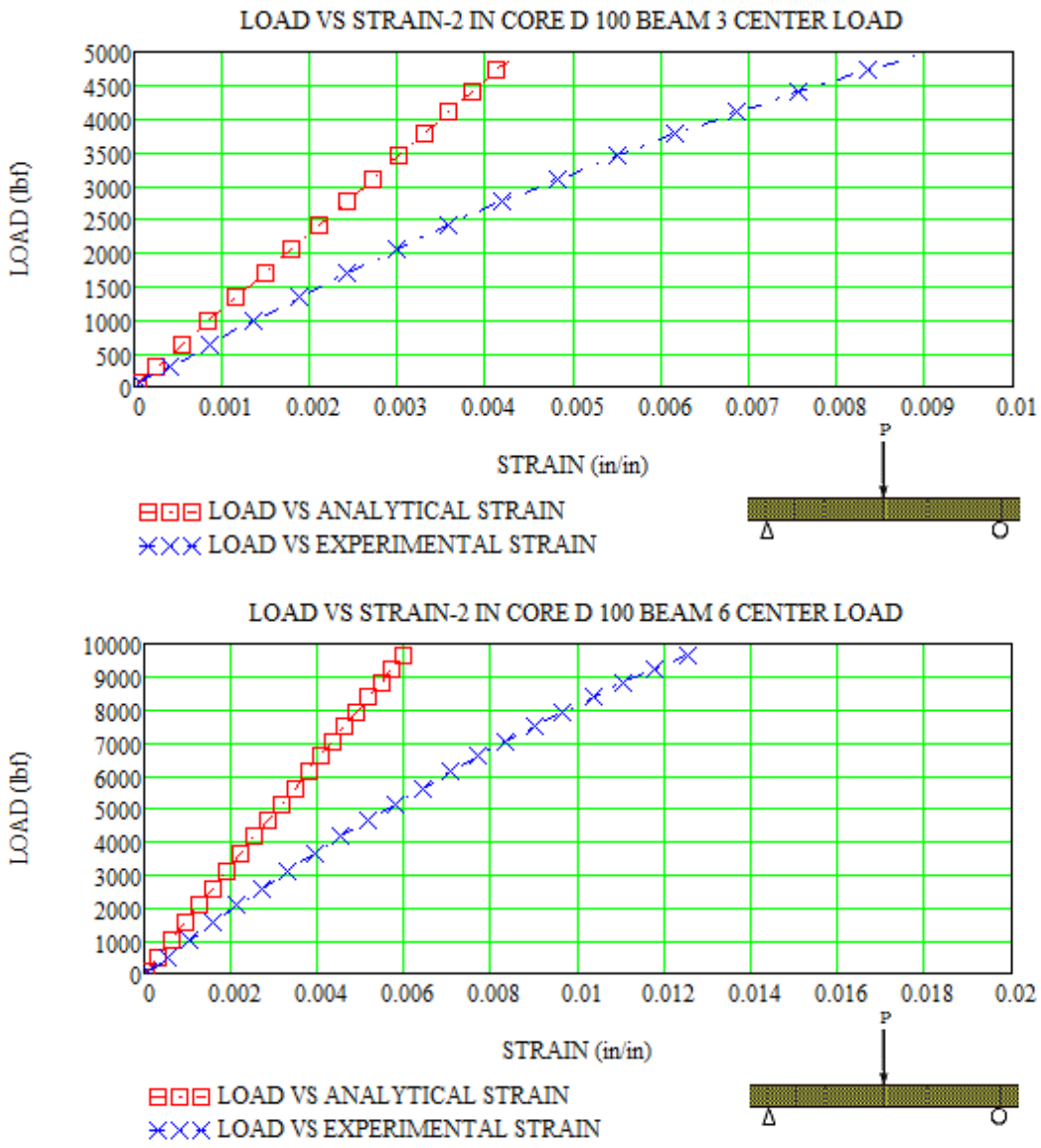

Load vs. Strain-2 in. core-D 100-center load Beam # 3, 6

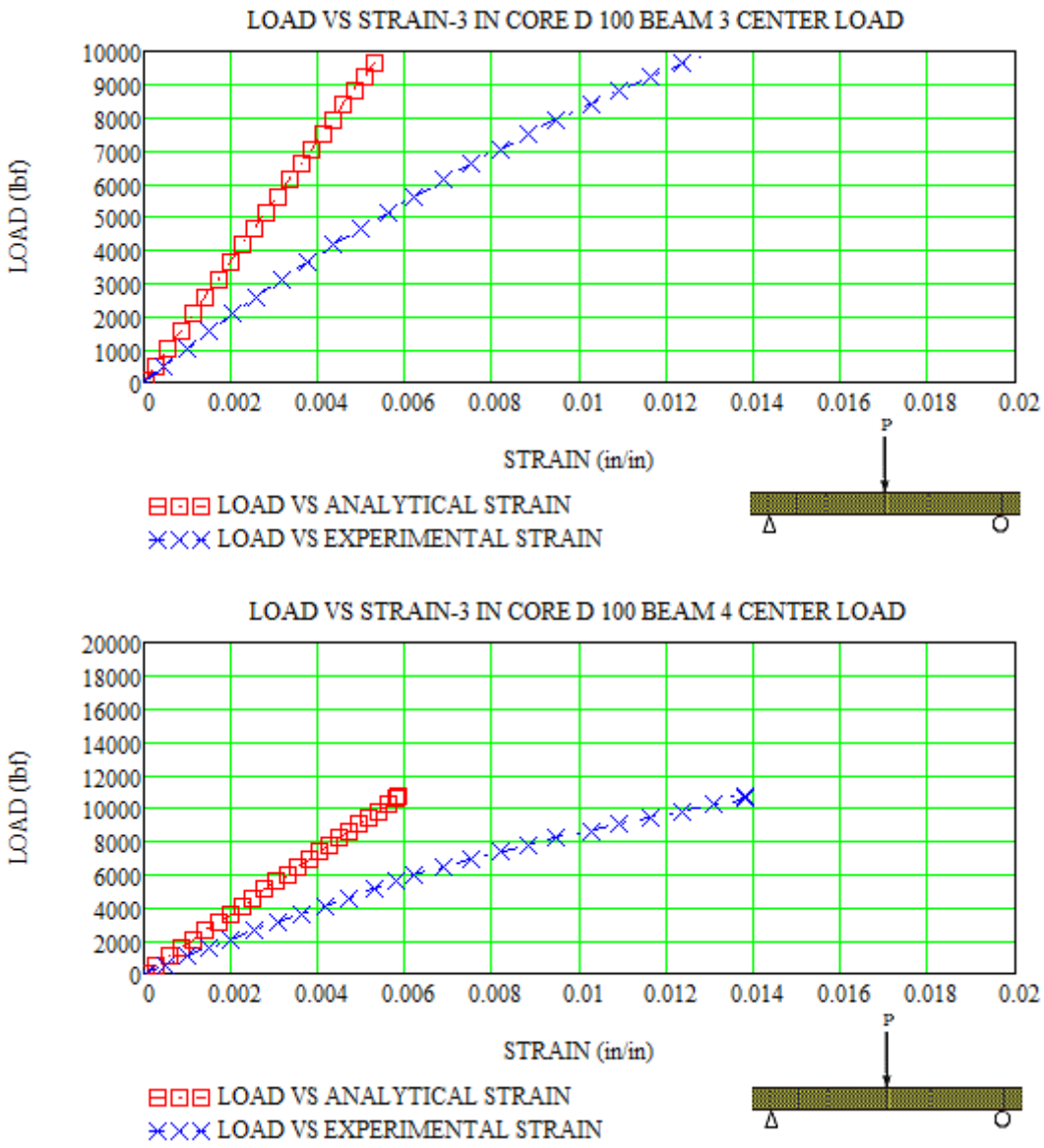

Load vs. Strain-3 in. core-D 100-center load Beam # 3, 4

Analytical vs. Experimental Strain Data-Group I Quarter-Point Load

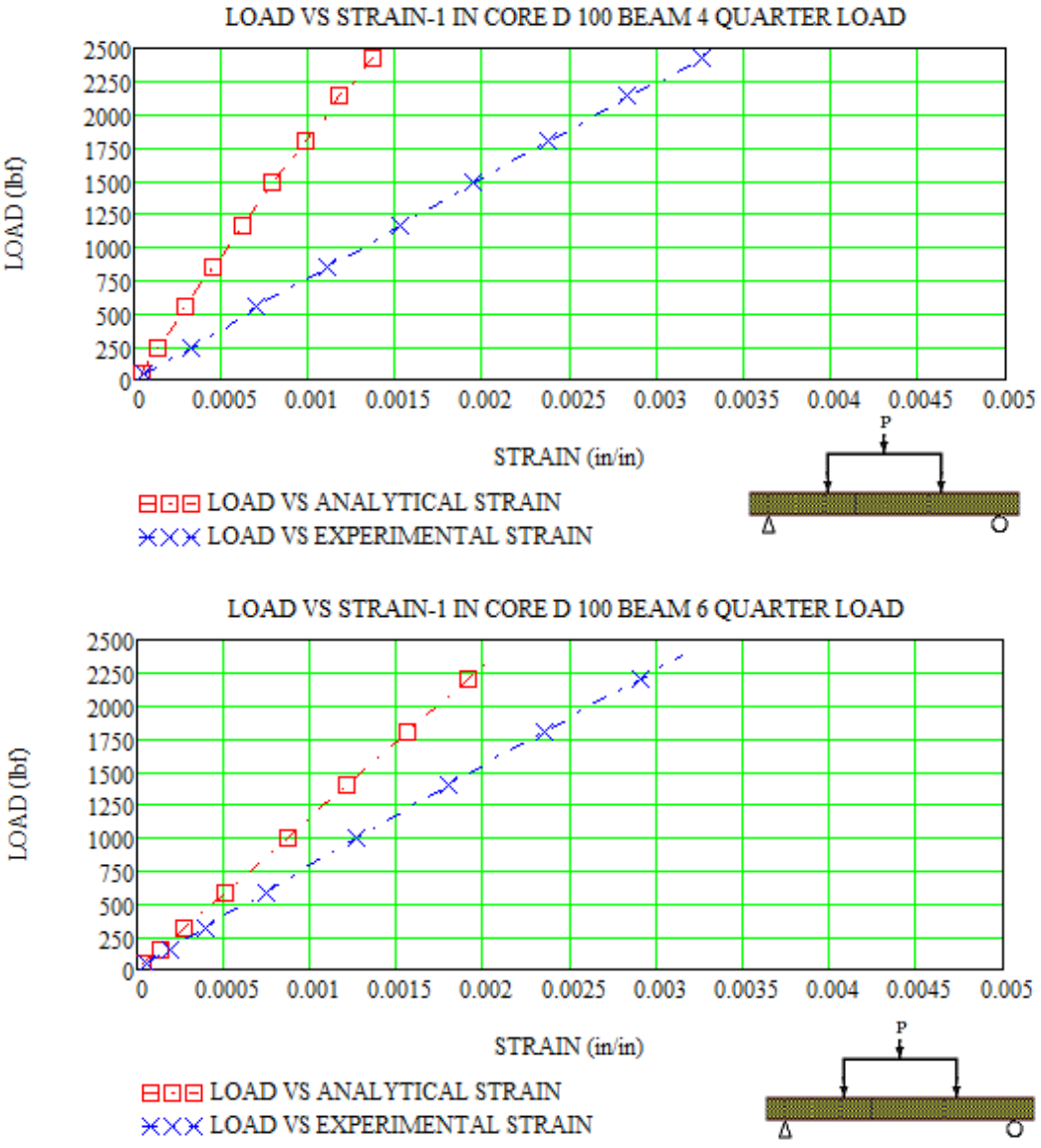

Load vs. Strain-1 in. core-D 100-quarter load Beam # 4, 6

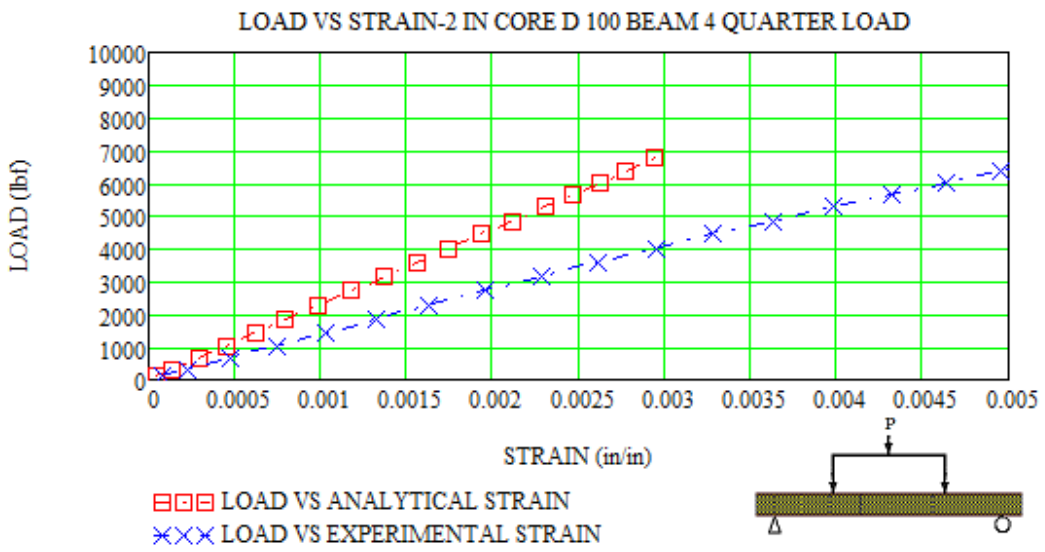

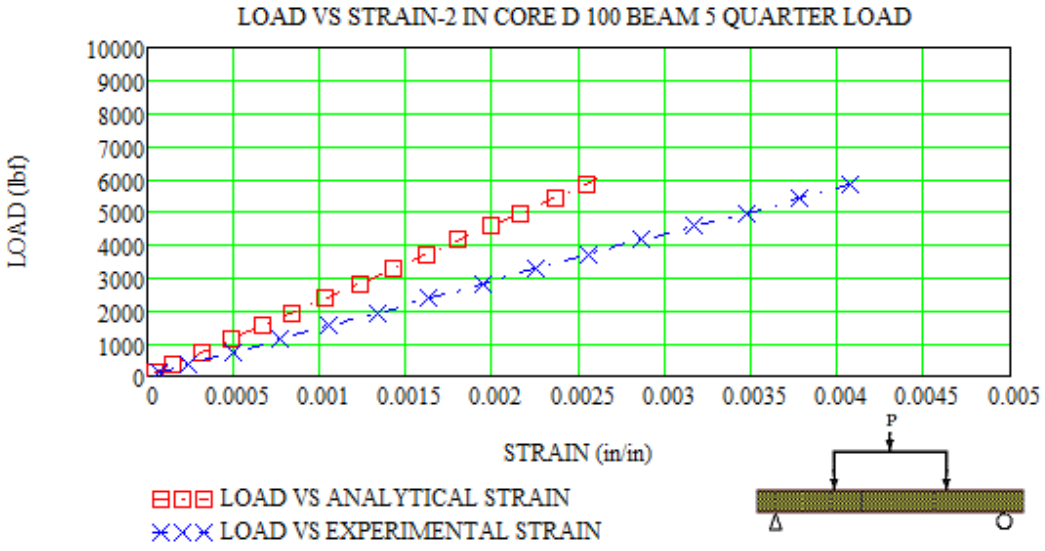

Load vs. Strain-2 in. core-D 100-quarter load Beam # 4, 5

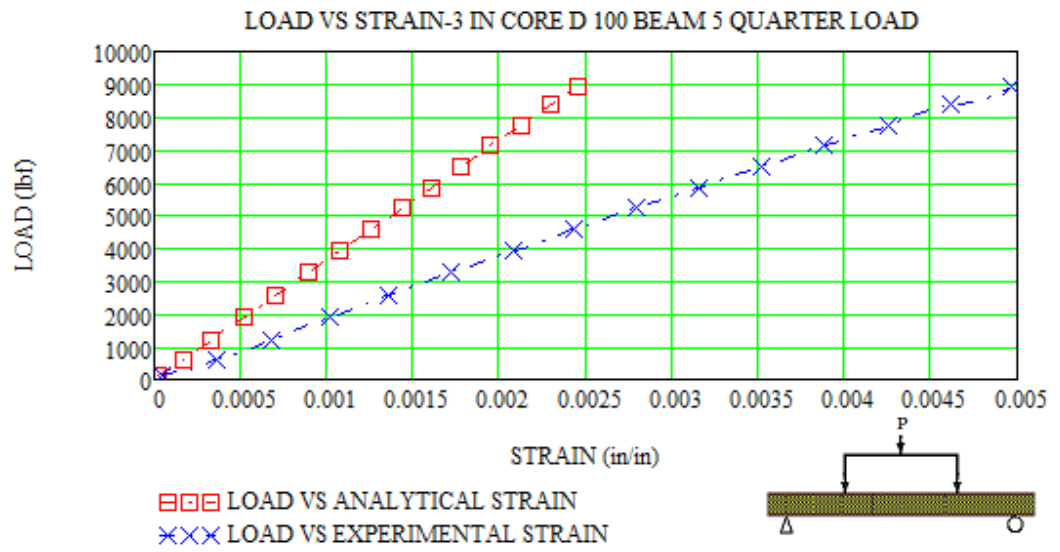

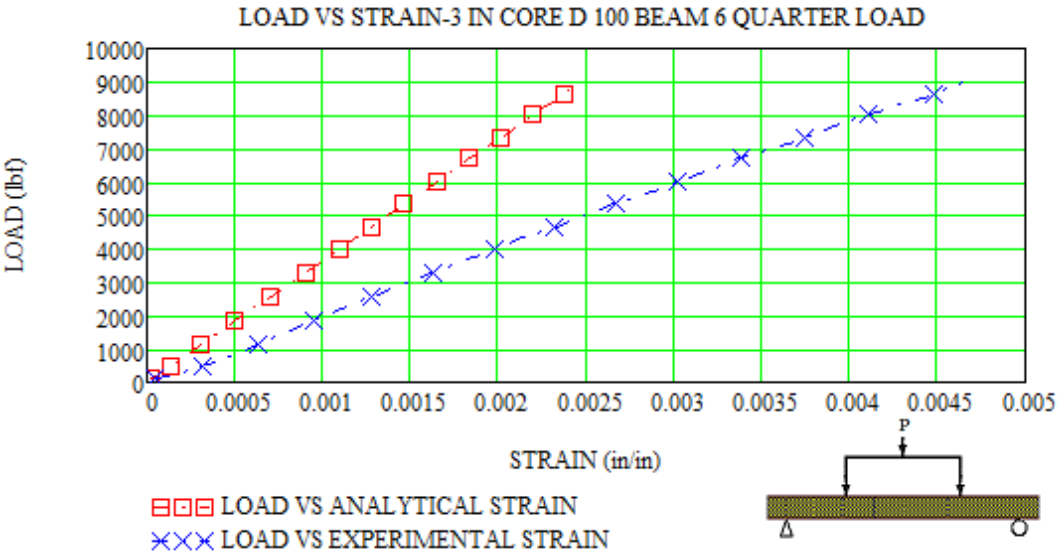

Load vs. Strain-3 in. core-D 100-quarter load Beam # 5, 6

Analytical vs. Experimental Deflection Data-Group I Center-Point Load

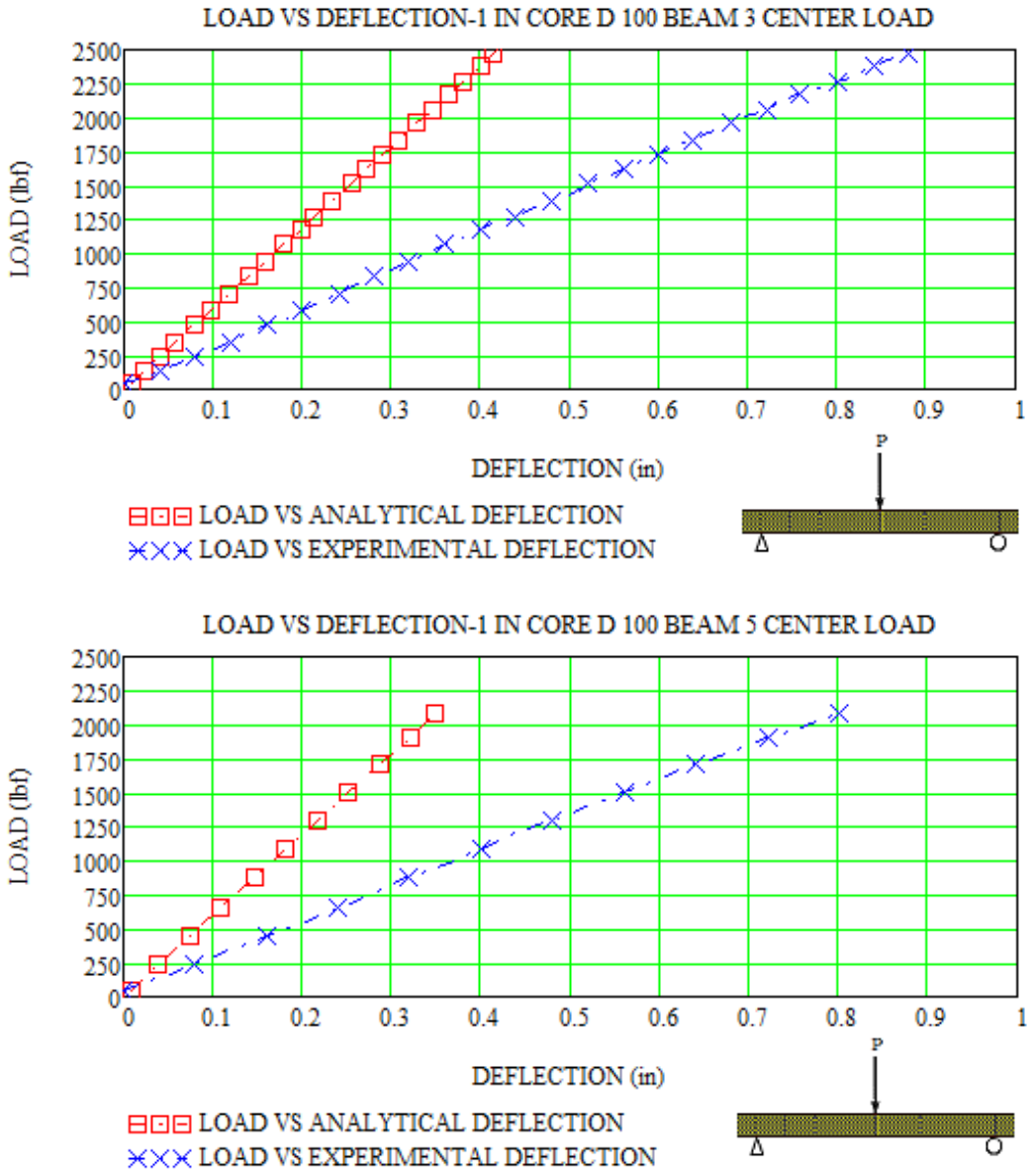

Load vs. Deflection-1 in. core-D 100-center load Beam # 3, 5

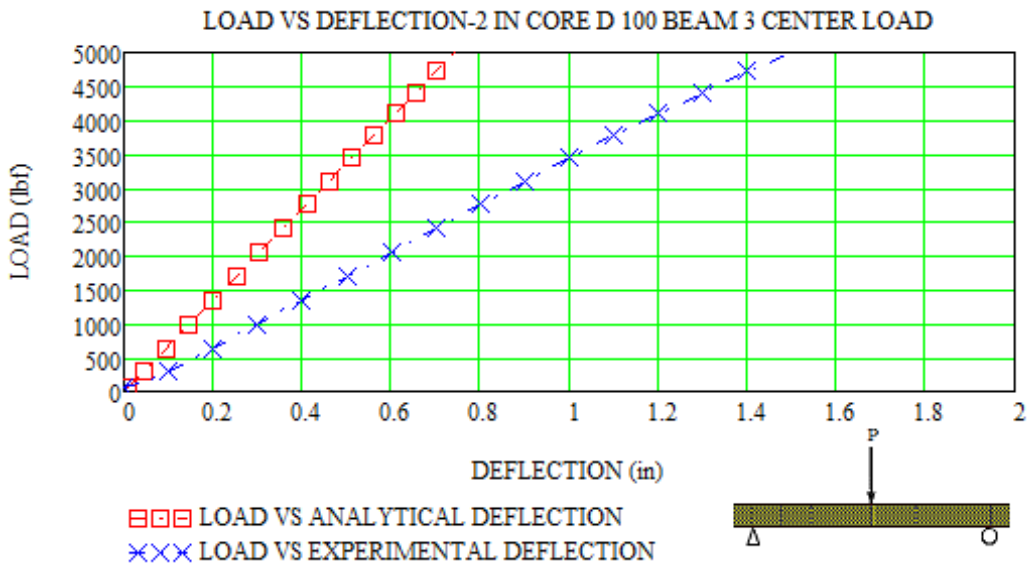

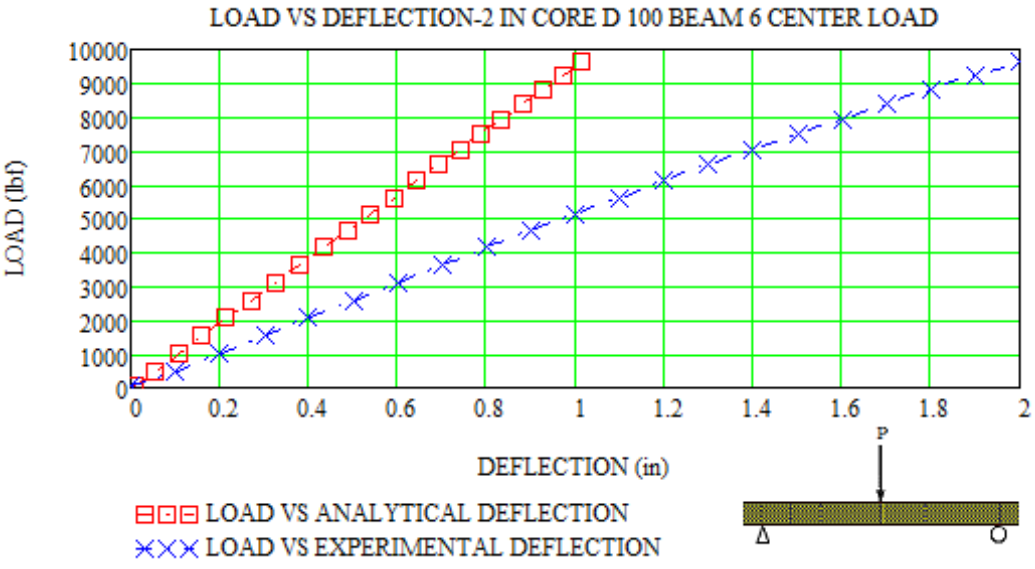

Load vs. Deflection-2 in. core-D 100-center load Beam # 3, 6

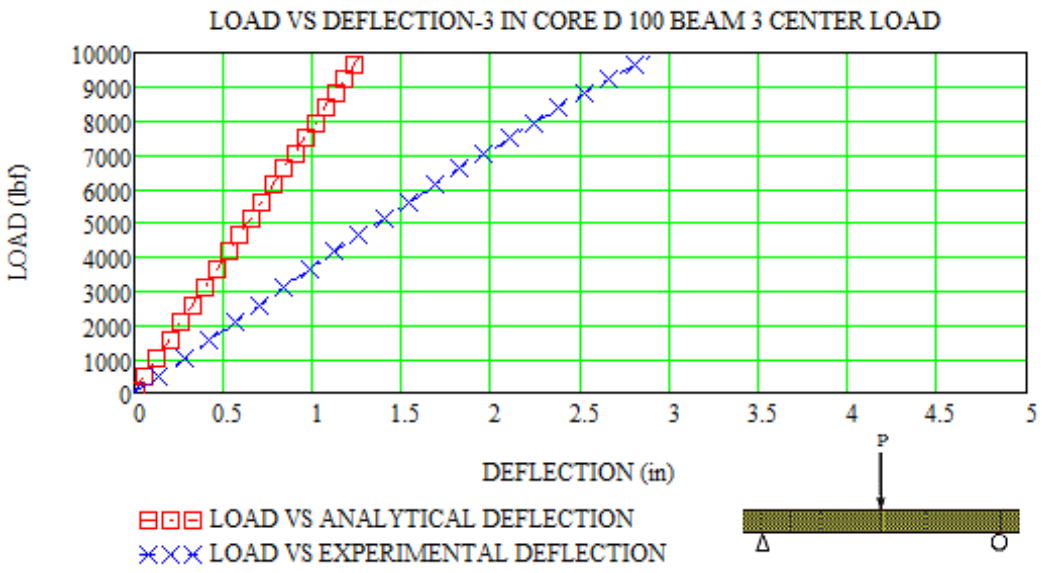

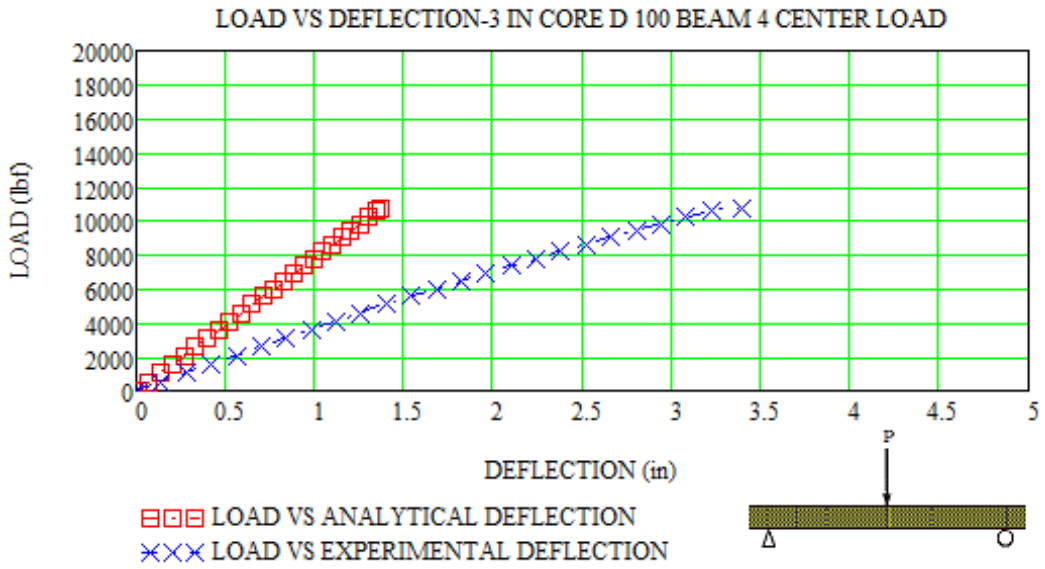

Load vs. Deflection-3 in. core-D 100-center load Beam # 3, 4

Analytical vs. Experimental Deflection Data-Group I Quarter-Point Load

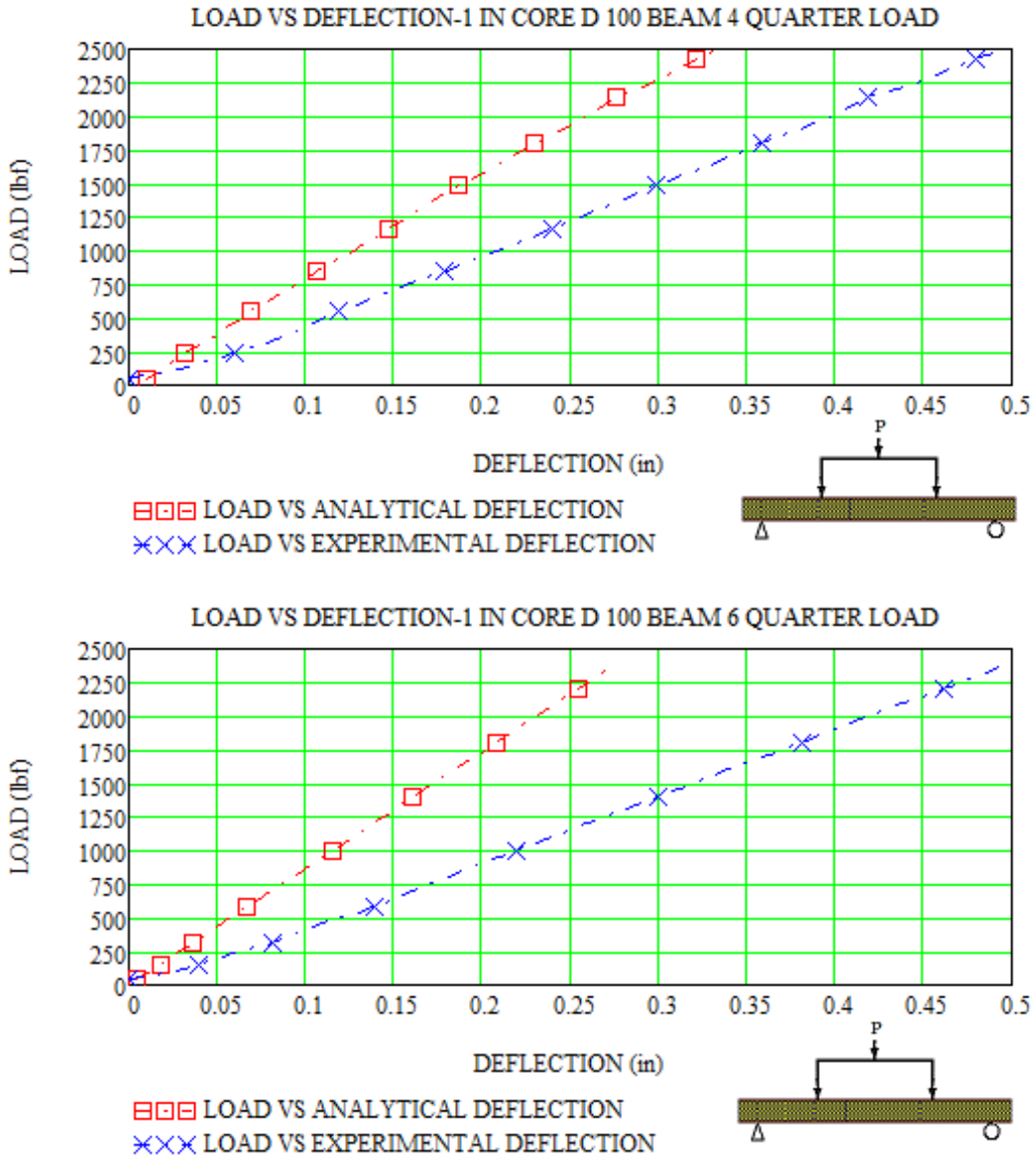

Load vs. Deflection-1 in. core-D 100-quarter load Beam # 4, 6

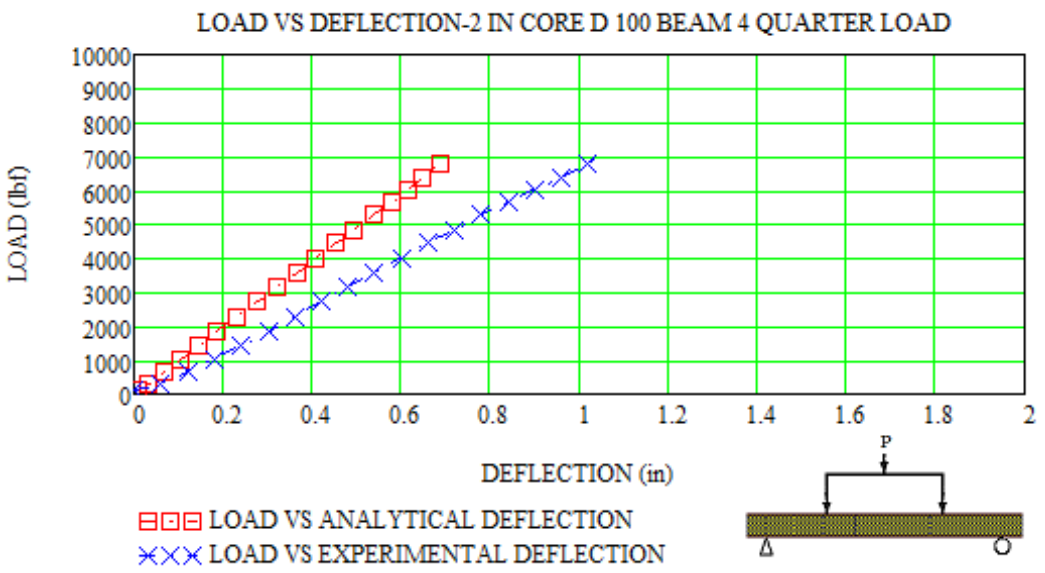

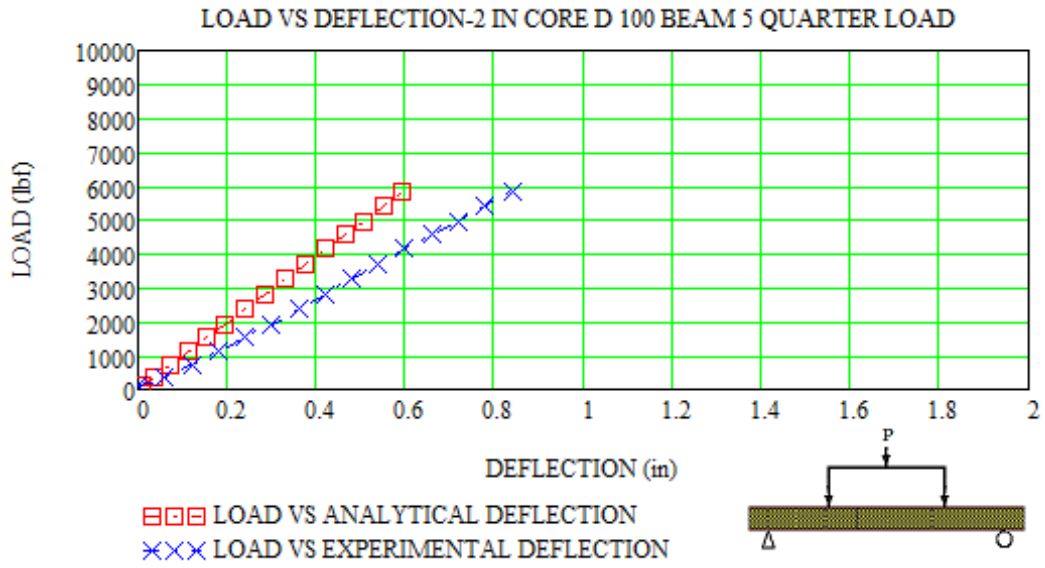

Load vs. Deflection-2 in. core-D 100-quarter load Beam # 4, 5

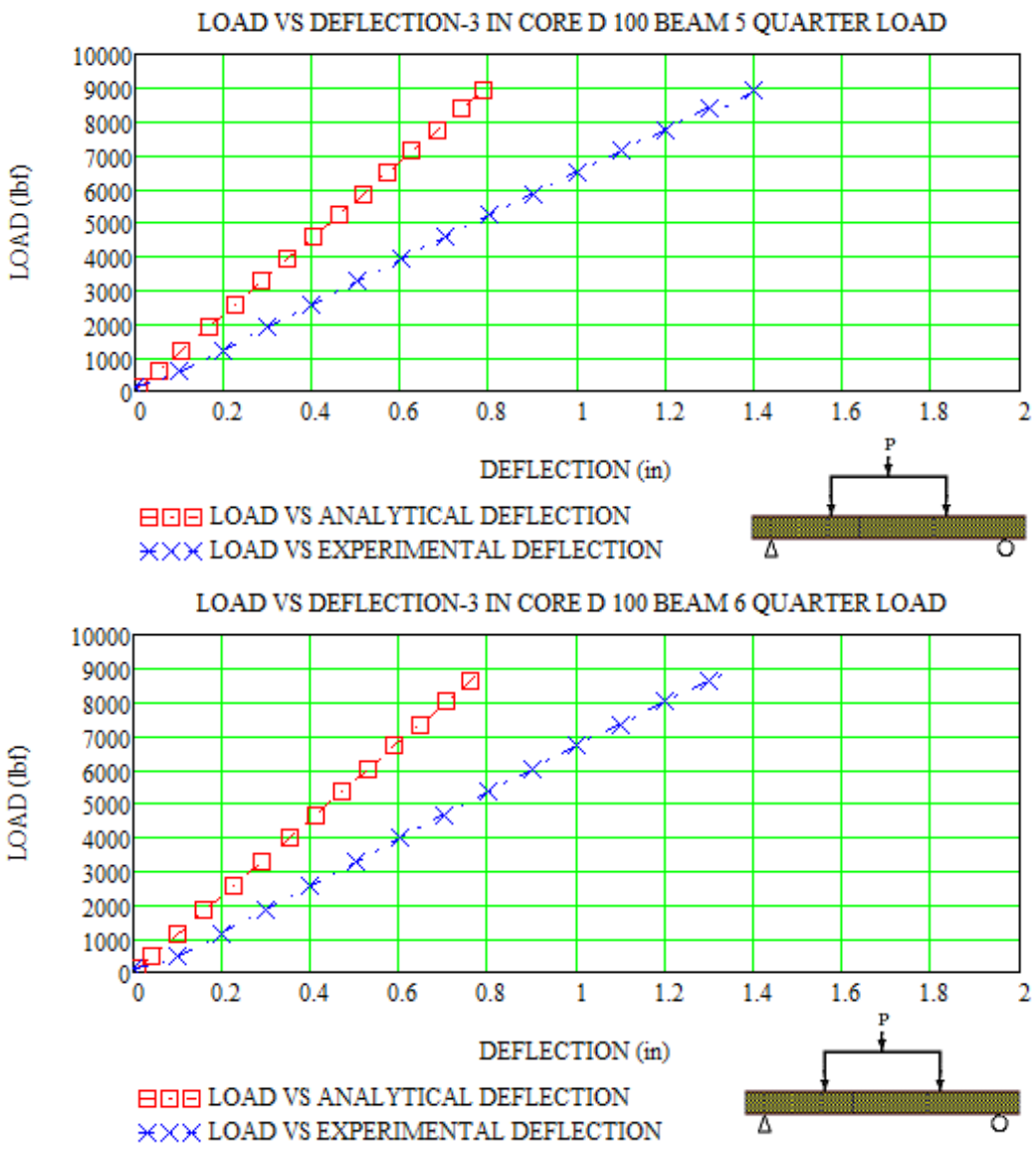

Load vs. Deflection-3 in. core-D 100-quarter load Beam # 5, 6

Analytical vs. Experimental Strain Data-Group II Center-Point Load

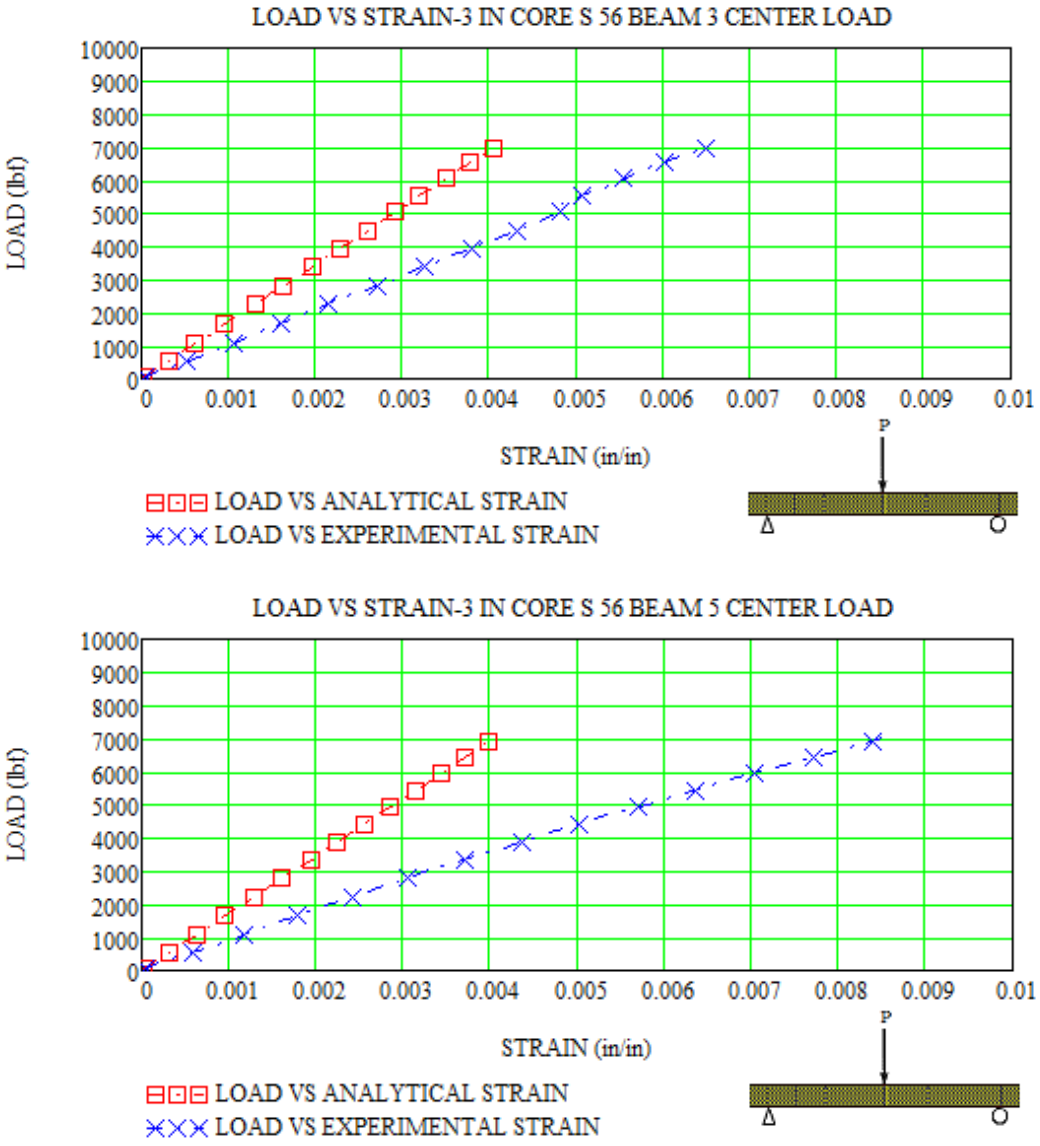

Load vs. Strain-3 in. core-S 56-center load Beam # 3, 5

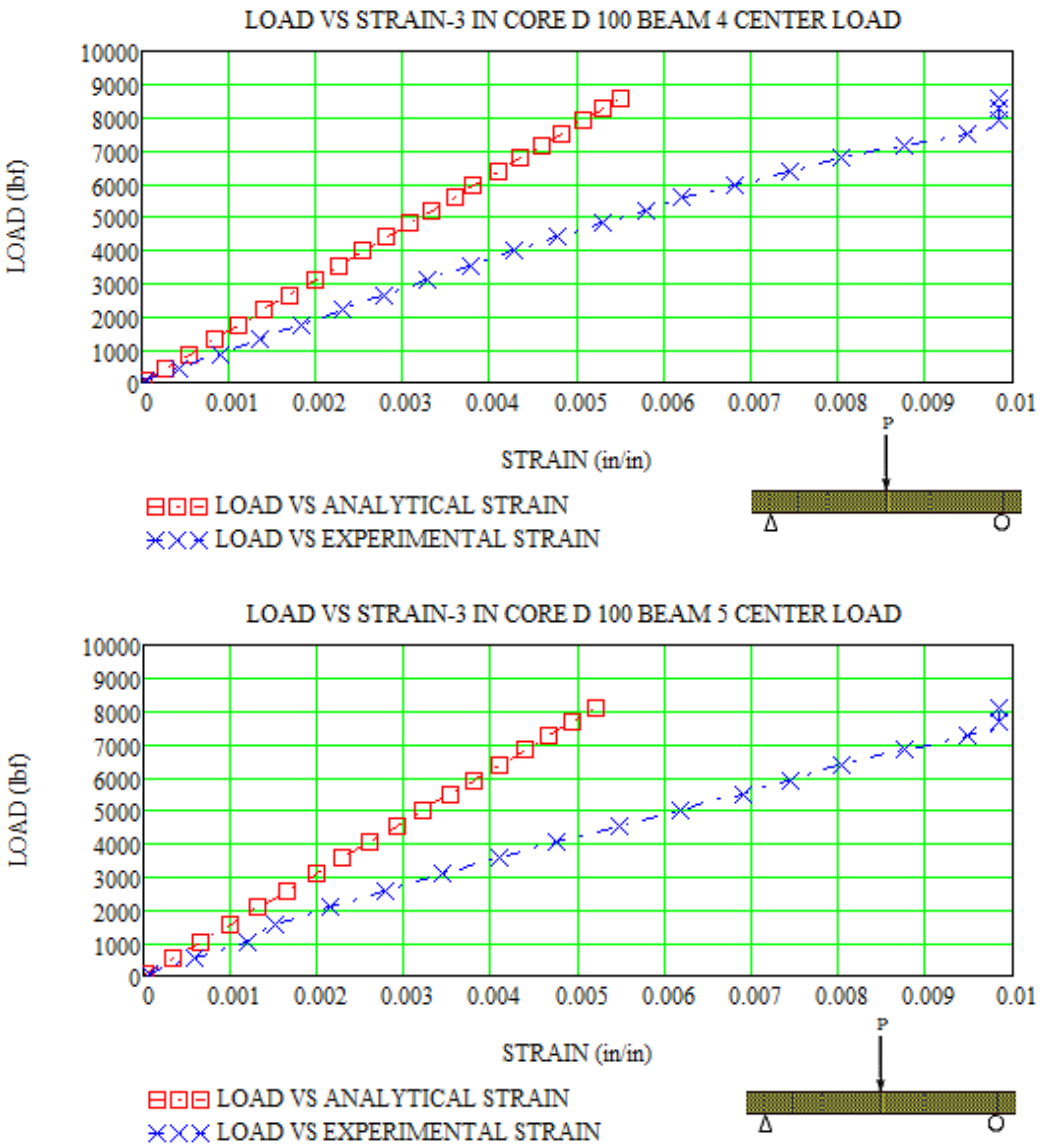

Load vs. Strain-3 in. core-D 100-center load Beam # 4, 5

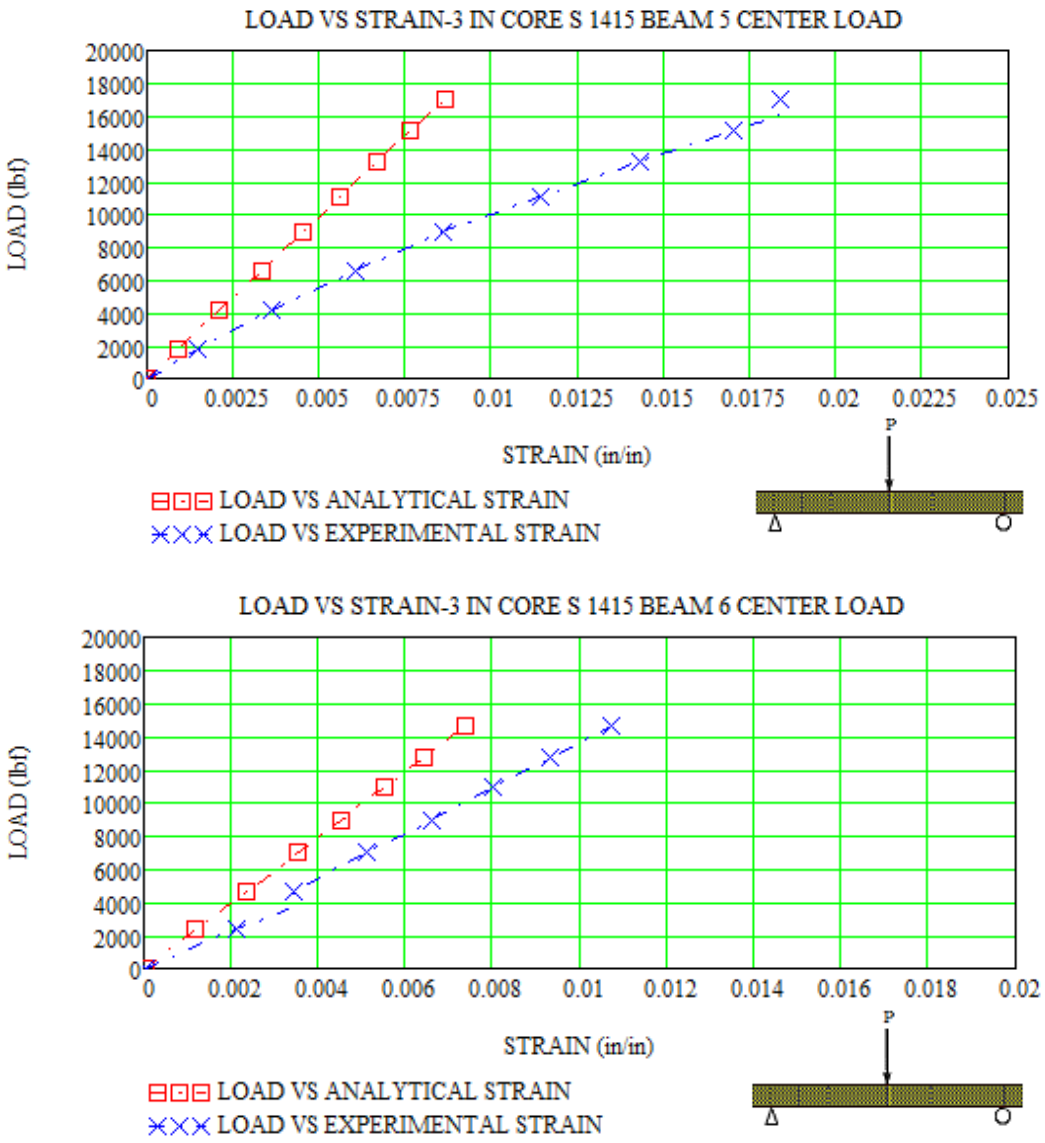

Load vs. Strain-3 in. core-S 1415-center load Beam # 5, 6

Analytical vs. Experimental Strain Data-Group II Quarter-Point Load

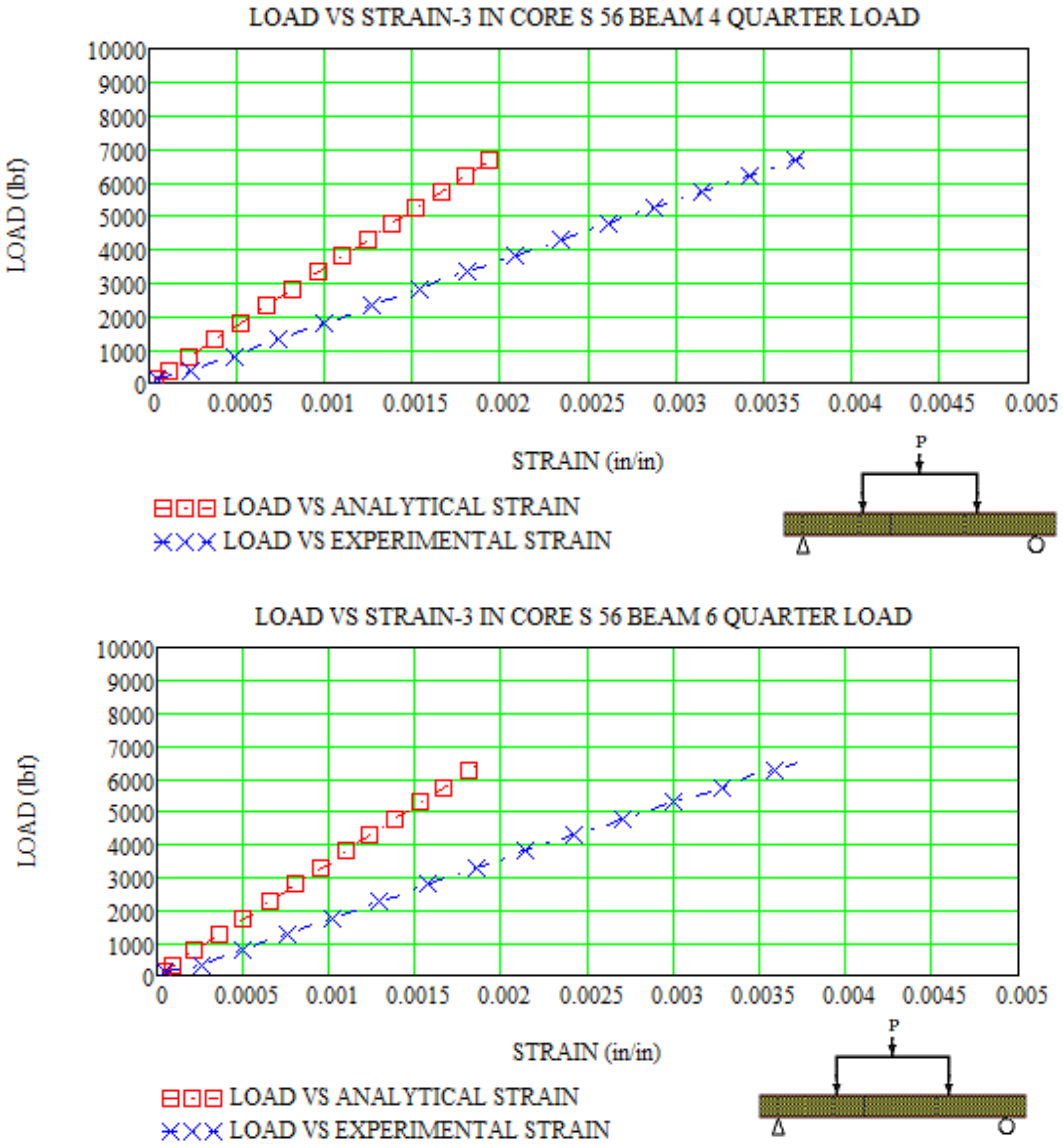

Load vs. Strain-3 in. core-S 56-quarter load Beam # 4, 6

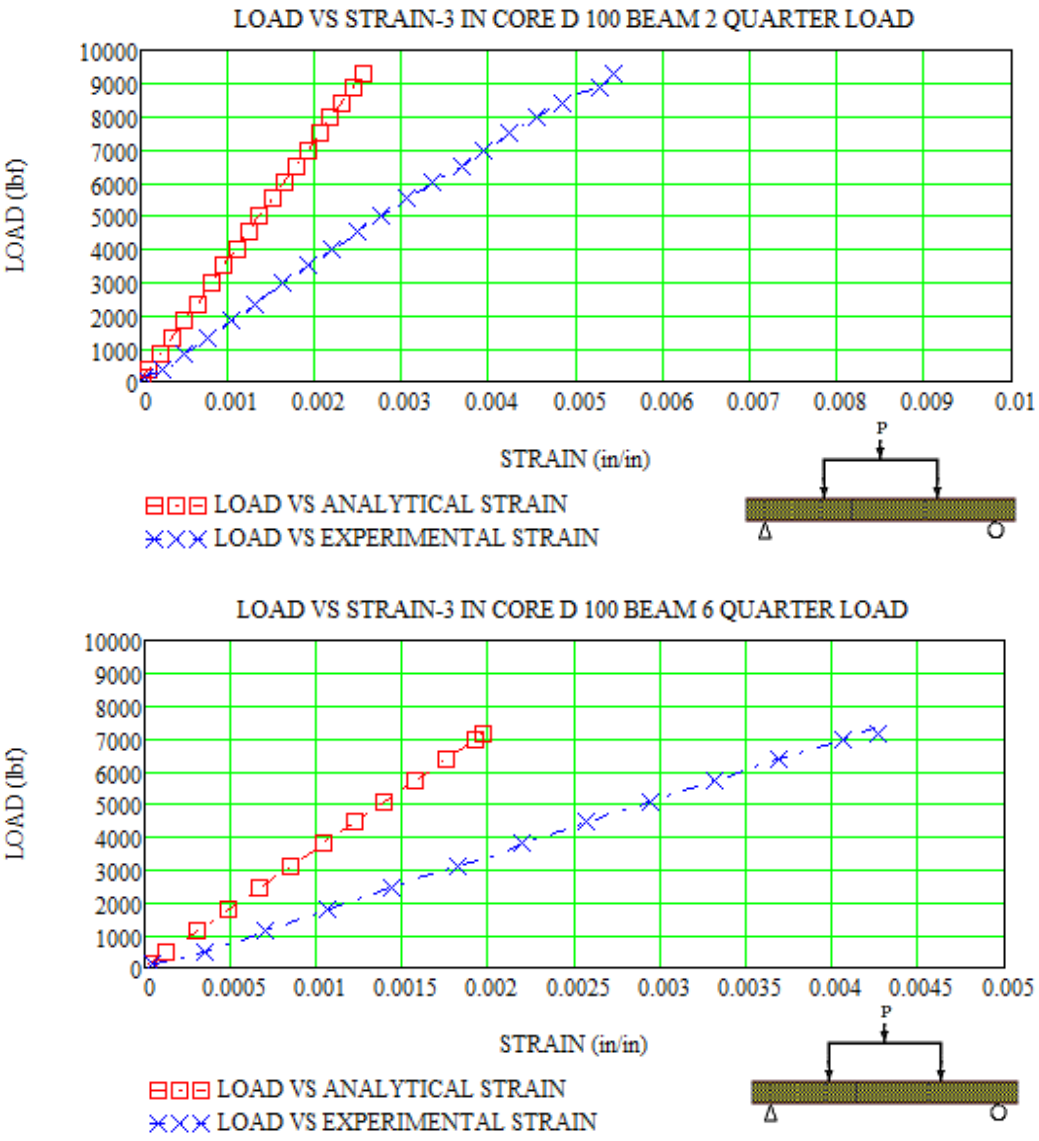

Load vs. Strain-3 in. core-D 100-quarter load Beam # 2, 6

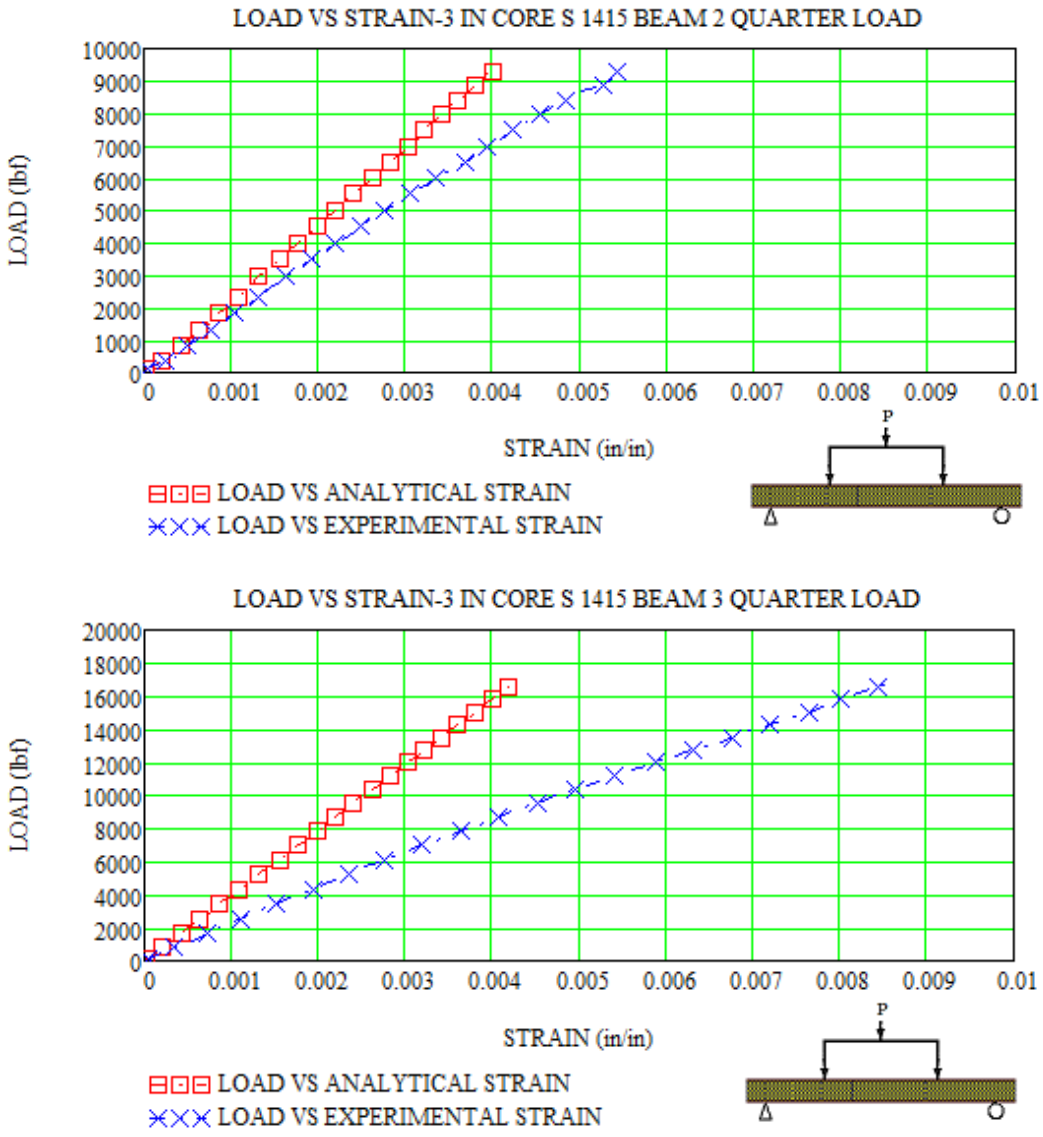

Load vs. Strain-3 in. core-S 1415-quarter load Beam # 2, 3

Analytical vs. Experimental Deflection Data-Group II Center-Point Load

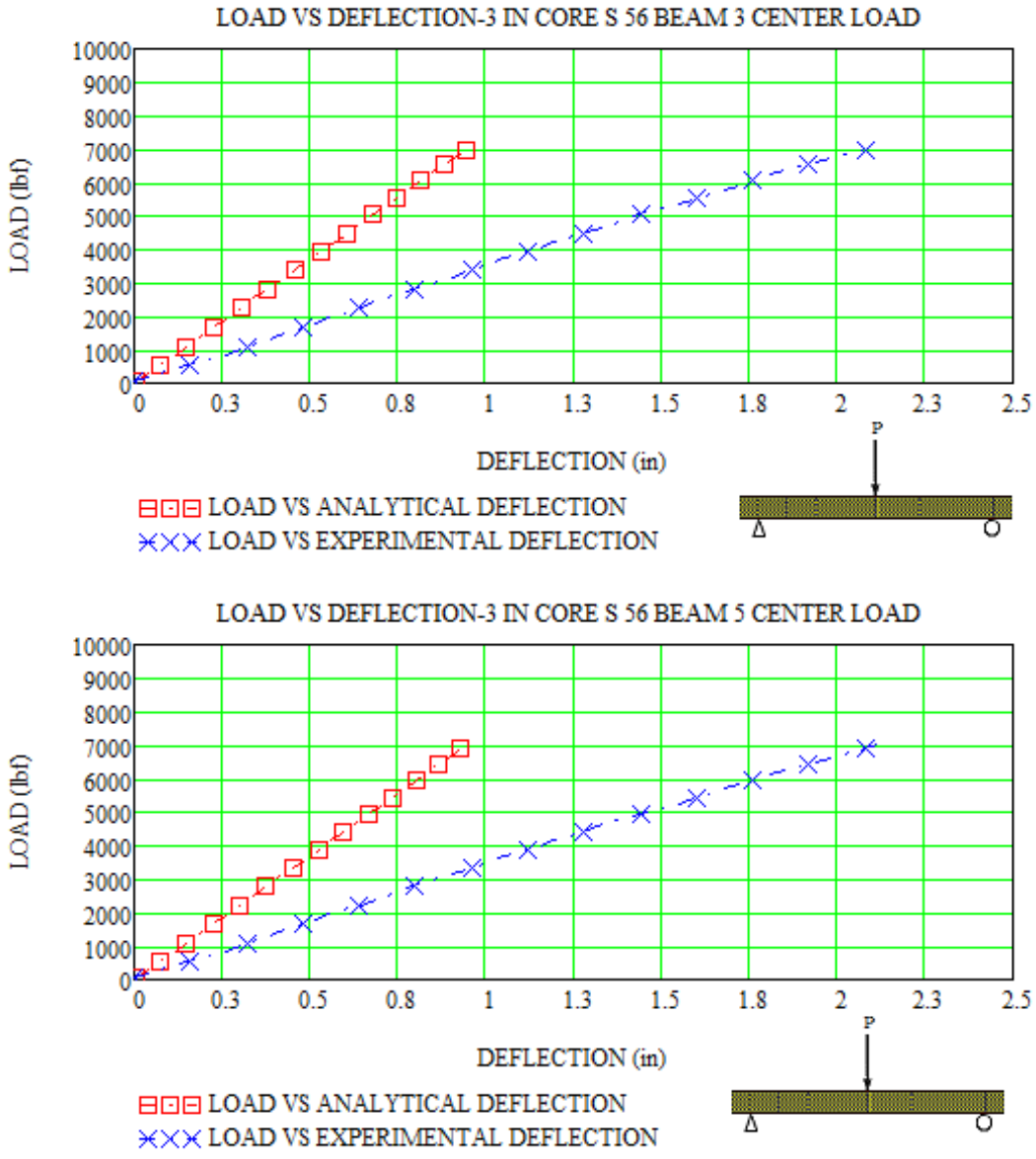

Load vs. Deflection-3 in. core-S 56-center load Beam 3, 5

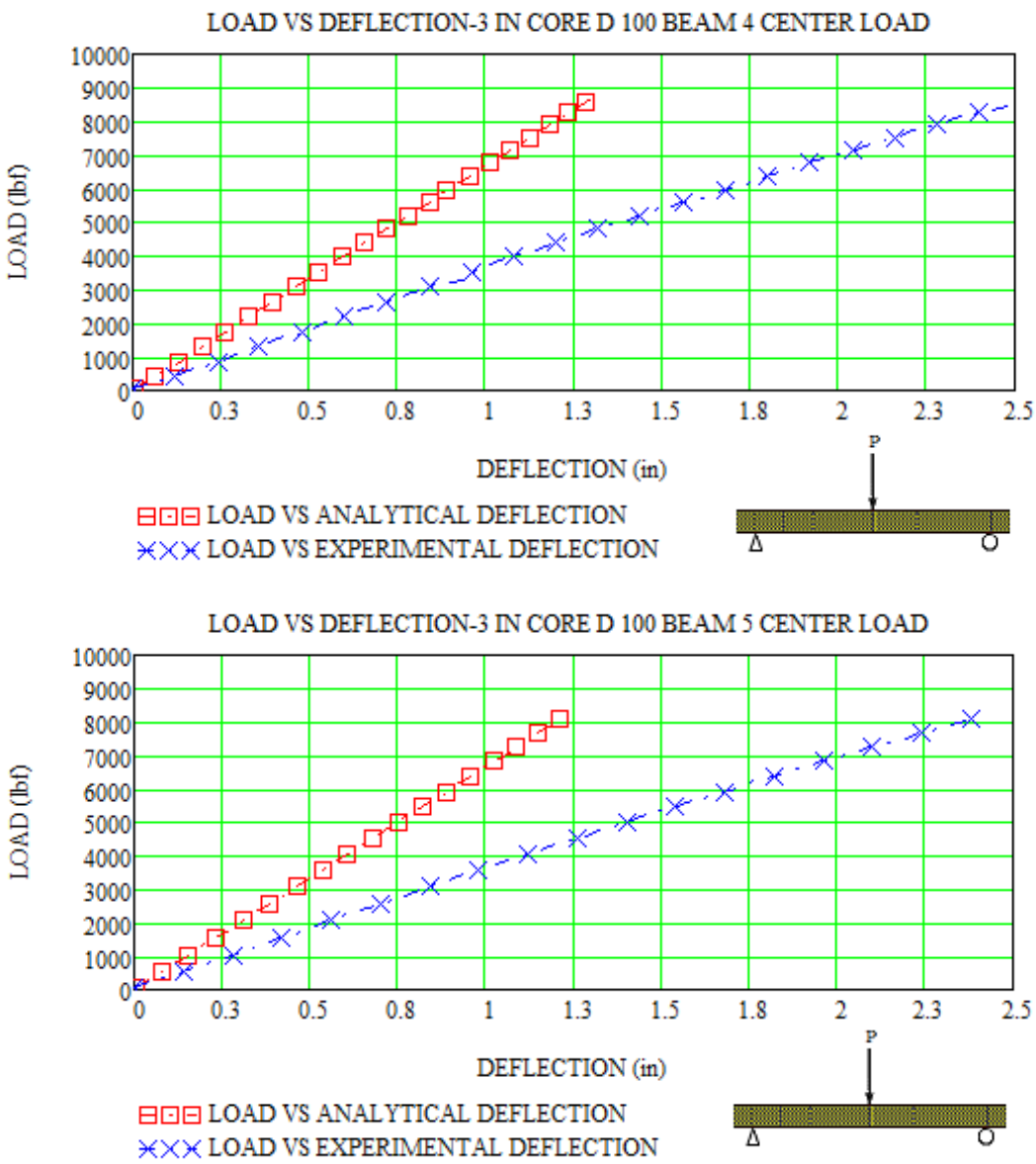

Load vs. Deflection-3 in. core-D 100-center load Beam # 4, 5

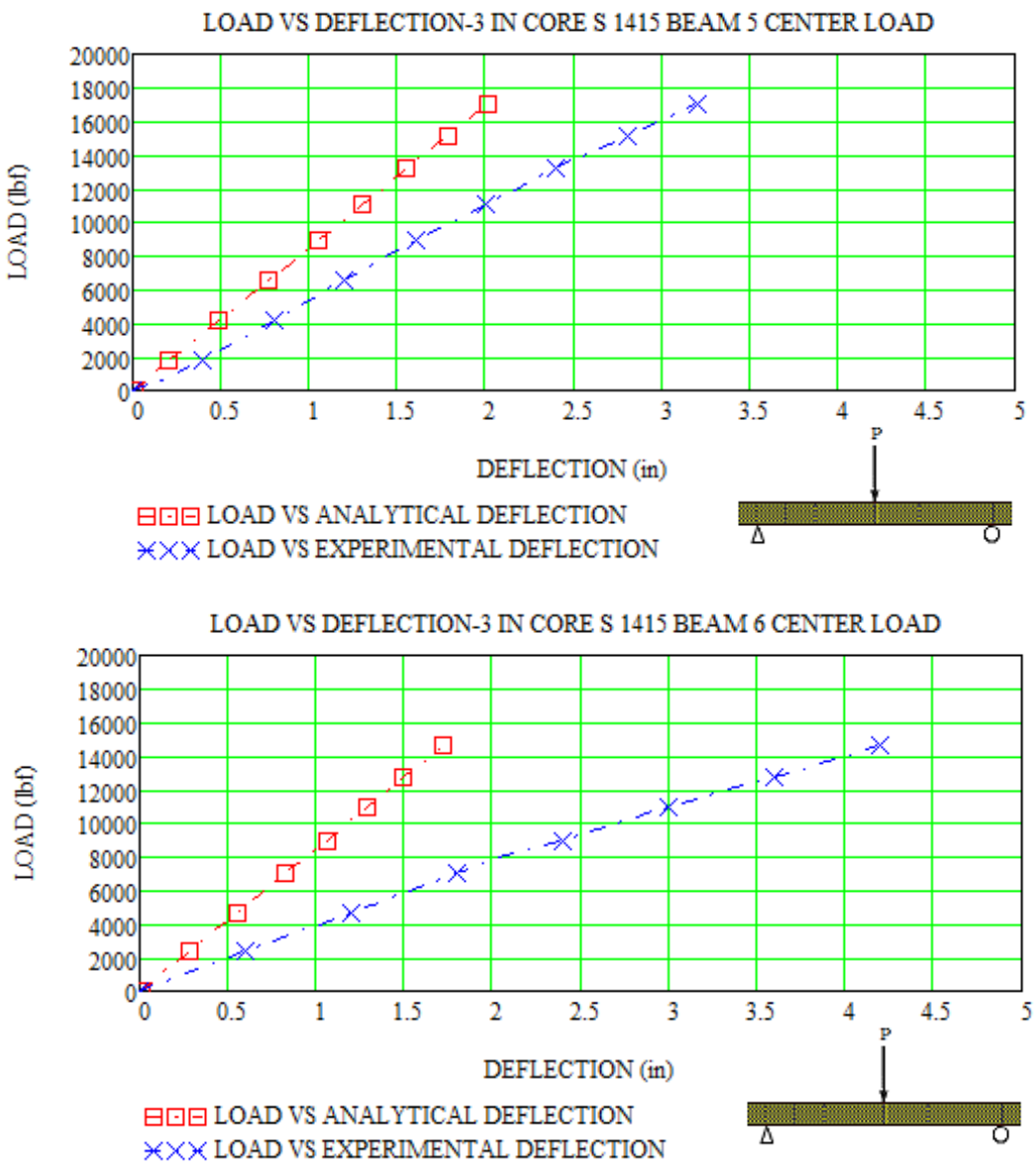

Load vs. Deflection-3 in. core-S 1415-center load Beam # 5, 6

Analytical vs. Experimental Deflection Data-Group II Quarter-Point Load

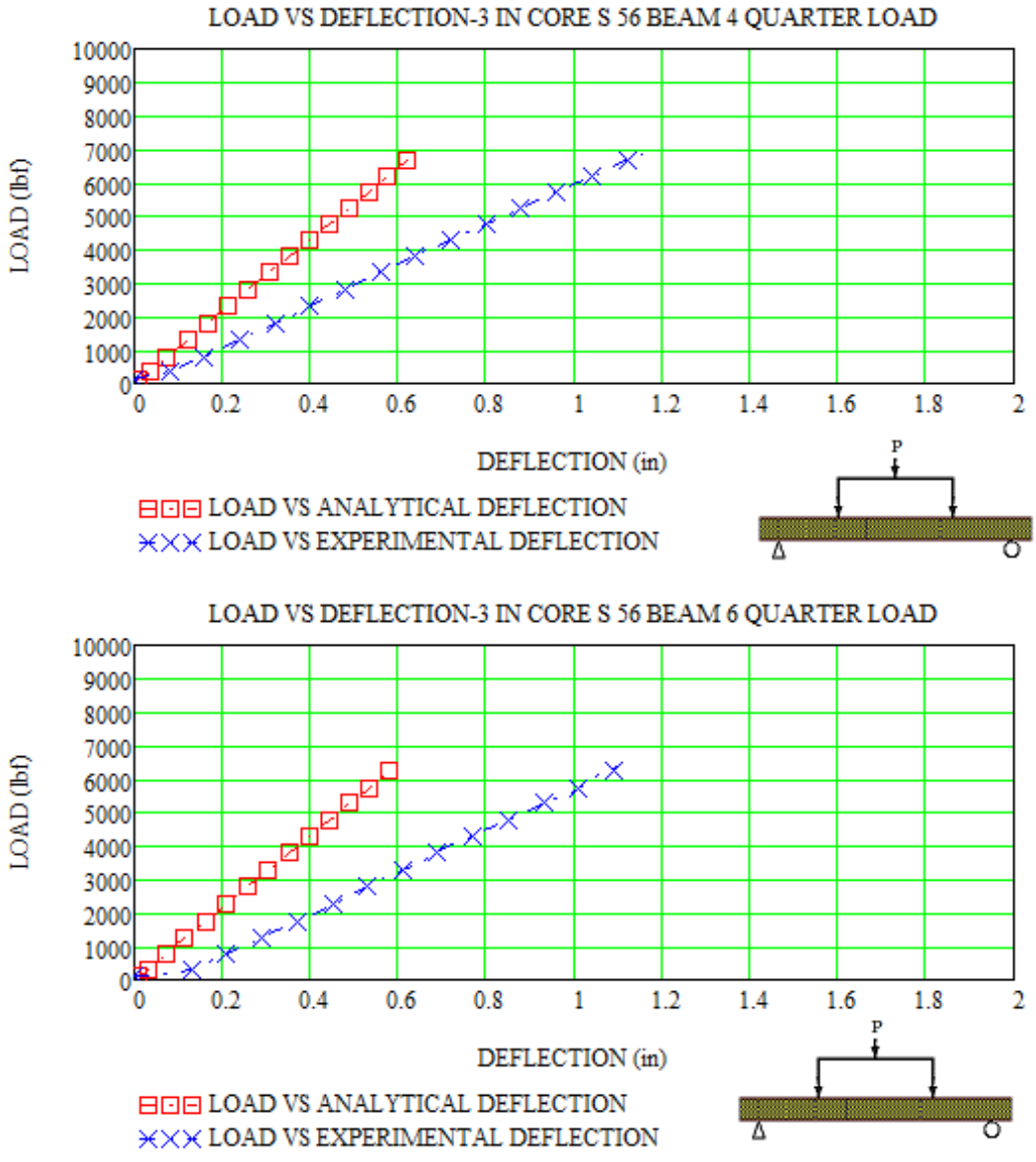

Load vs. Deflection-3 in. core-S 56-quarter load Beam # 4, 6

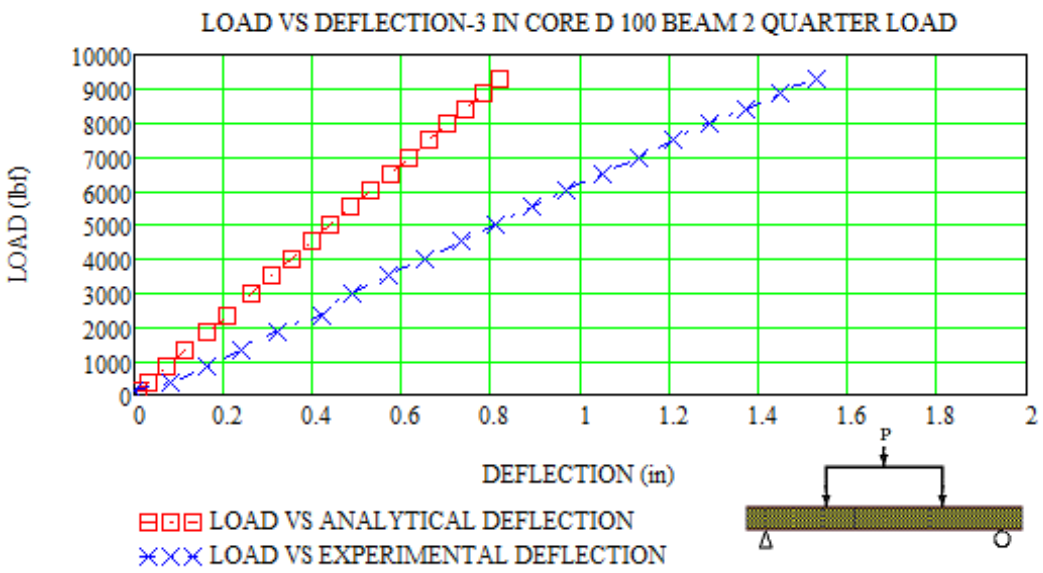

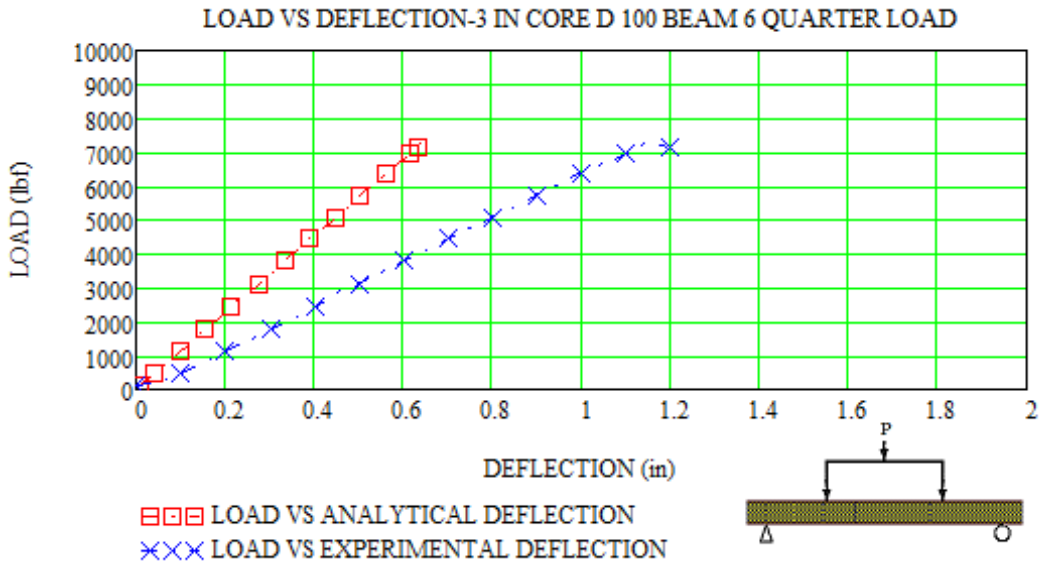

Load vs. Deflection-3 in. core-D 100-quarter load Beam # 2, 6

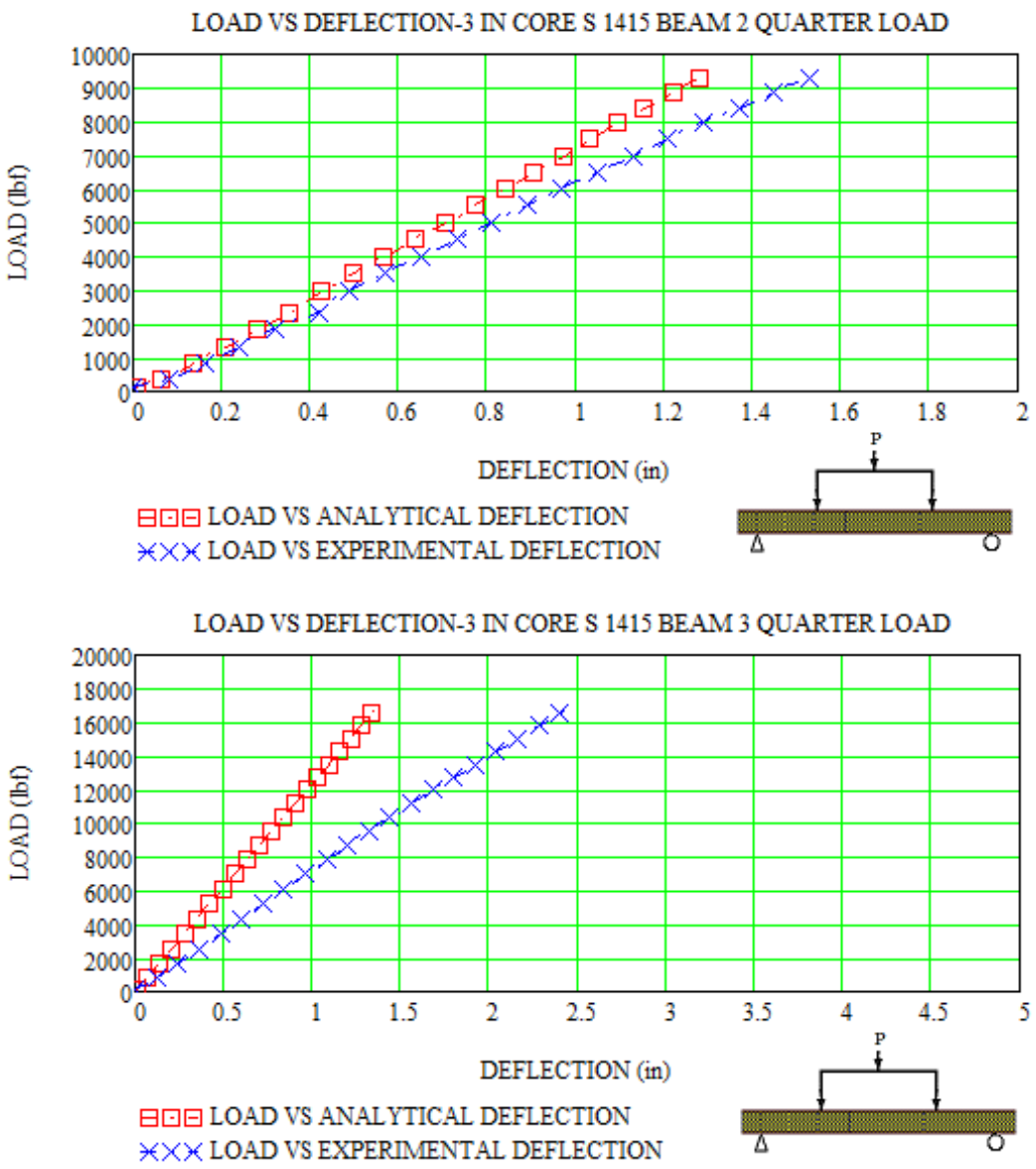

Load vs. Deflection-3 in. core-S 1415-quarter load Beam # 2, 3

APPENDIX III

CORRECTION FACTOR c_r = 0.5

Analytical vs. Experimental Strain Data-Group I Center-Point Load

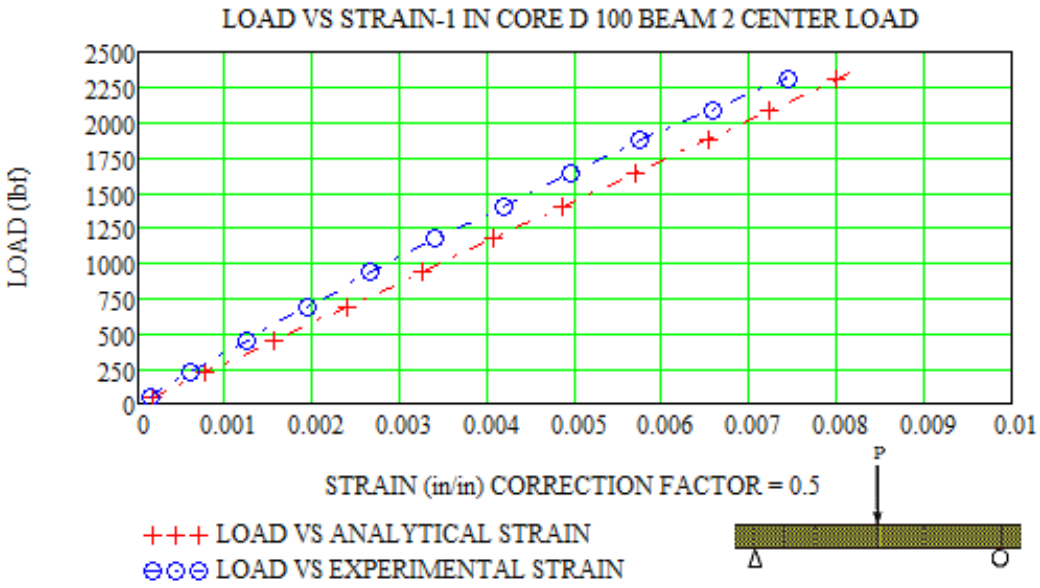

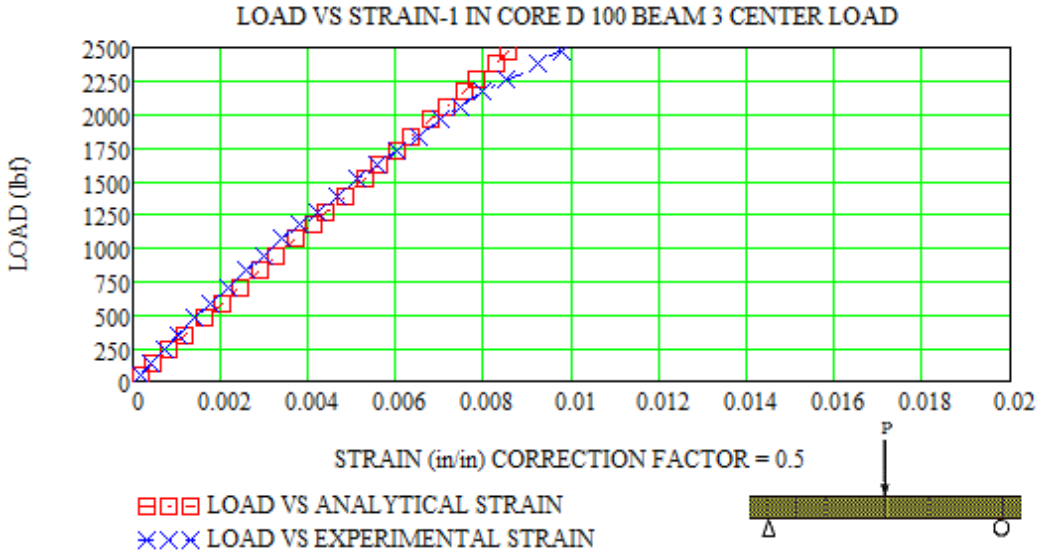

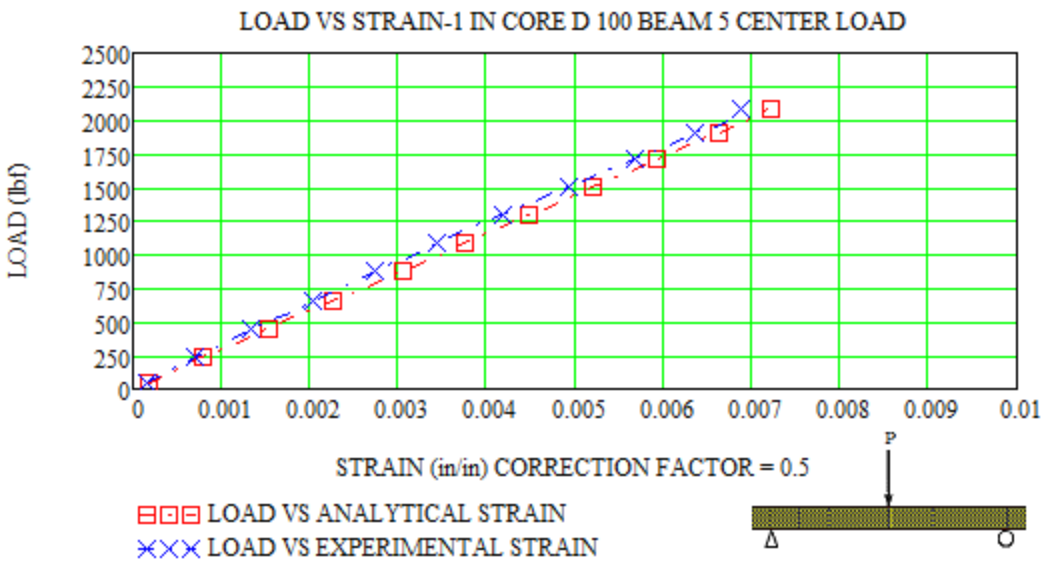

Load vs. Strain-1 in. core-D 100-center load Beam # 2, 3, 5-with $c_r = 0.5$

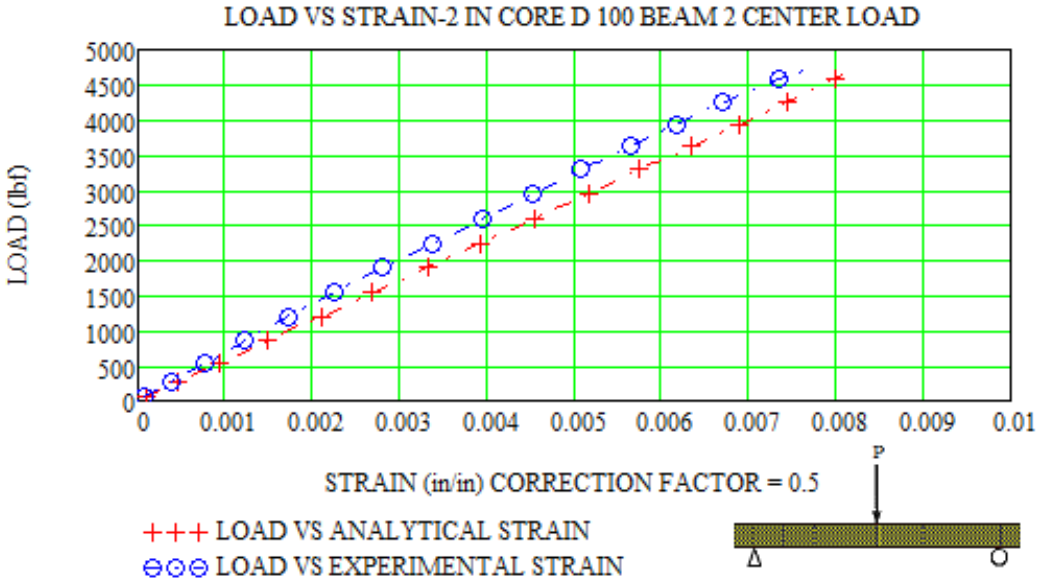

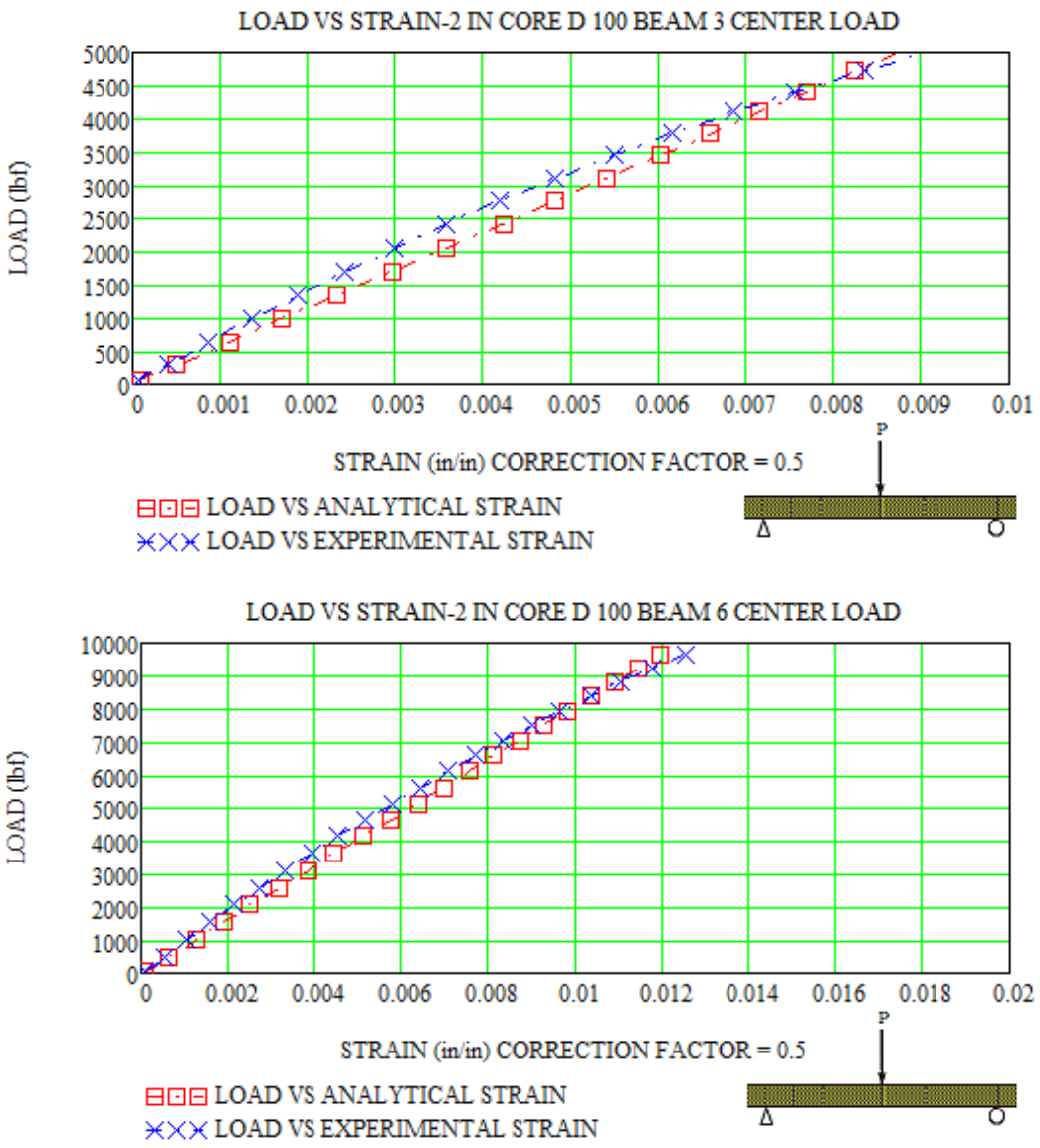

Load vs. Strain-2 in. core-D 100-center load Beam # 2, 3, 6

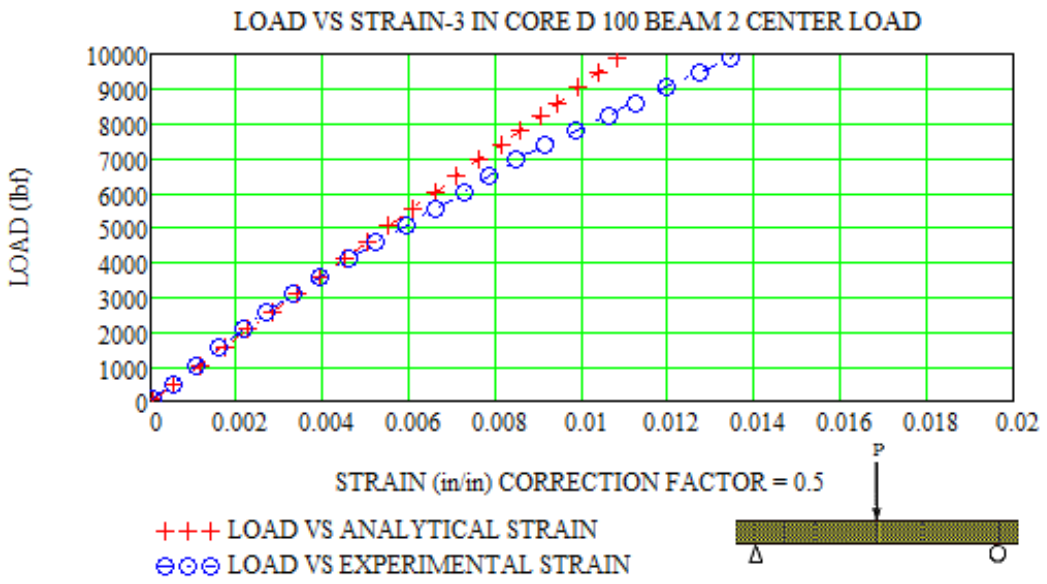
LOAD VS STRAIN-3 IN CORE D 100 BEAM 2 CENTER LOAD
LOAD (lbf)
10000
9000
8000
7000
6000
5000
4000
3000
2000
1000
0
0
0.002
0.004
0.006
0.008
0.01
0.012
0.014
0.016
0.018
0.02
STRAIN (in/in) CORRECTION FACTOR = 0.5
P
LOAD VS ANALYTICAL STRAIN
LOAD VS EXPERIMENTAL STRAIN

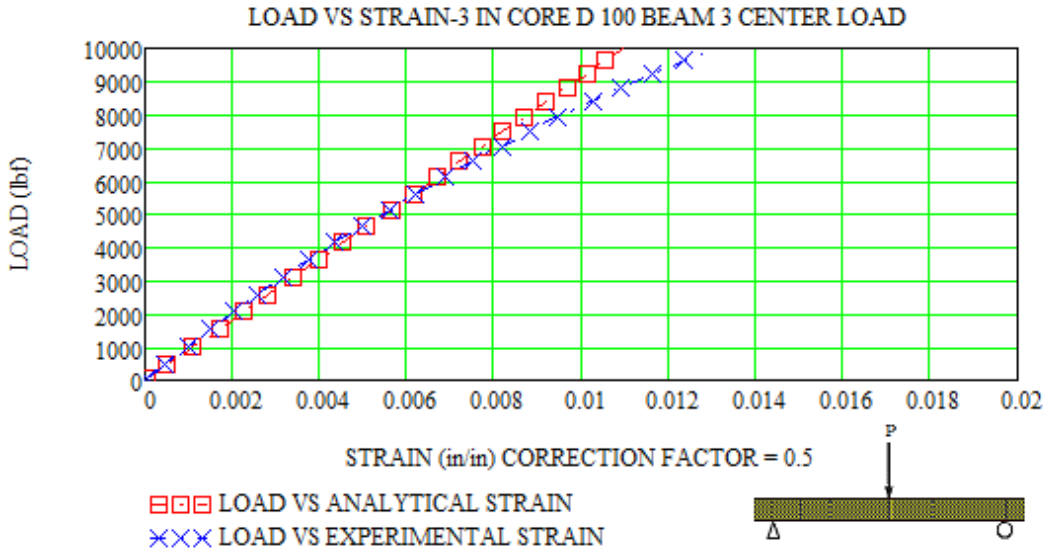
LOAD VS STRAIN-3 IN CORE D 100 BEAM 3 CENTER LOAD
LOAD (lbf)
10000
9000
8000
7000
6000
5000
4000
3000
2000
1000
0
0
0.002
0.004
0.006
0.008
0.01
0.012
0.014
0.016
0.018
0.02
STRAIN (in/in) CORRECTION FACTOR = 0.5
P
LOAD VS ANALYTICAL STRAIN
LOAD VS EXPERIMENTAL STRAIN

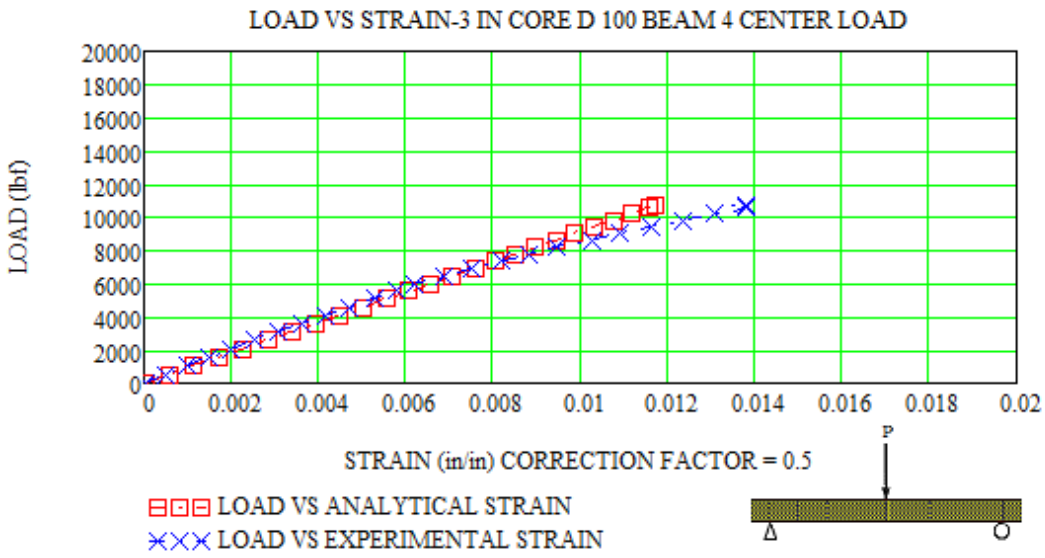

Load vs. Strain-3 in. core-D 100-center load Beam # 2, 3, 4

Analytical vs. Experimental Strain Data-Group I Quarter-Point Load

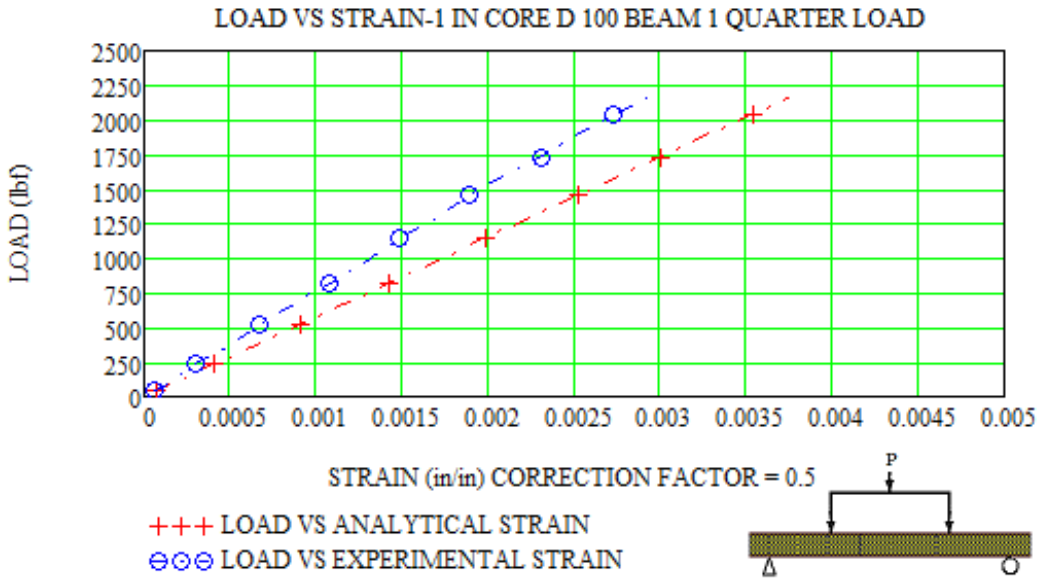

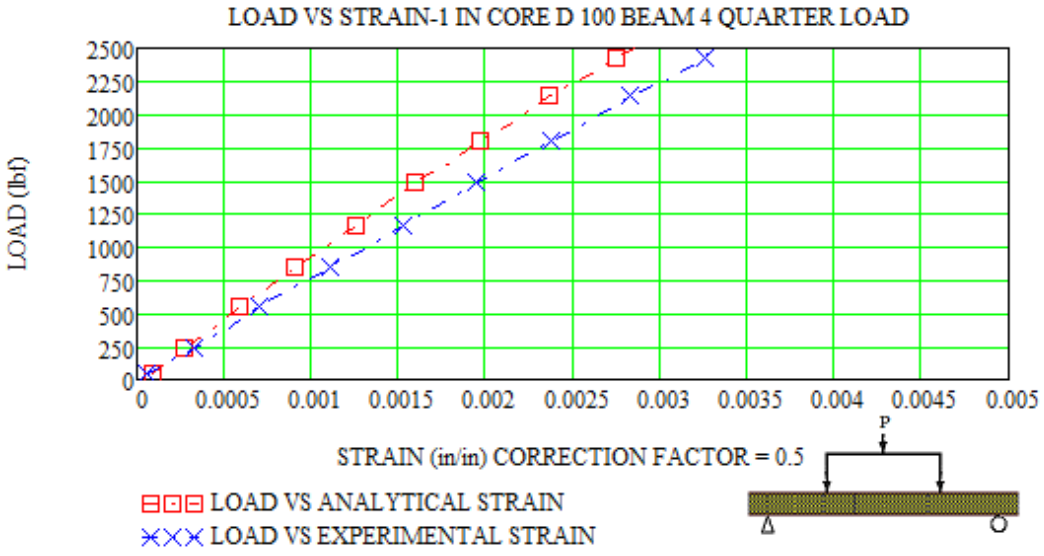

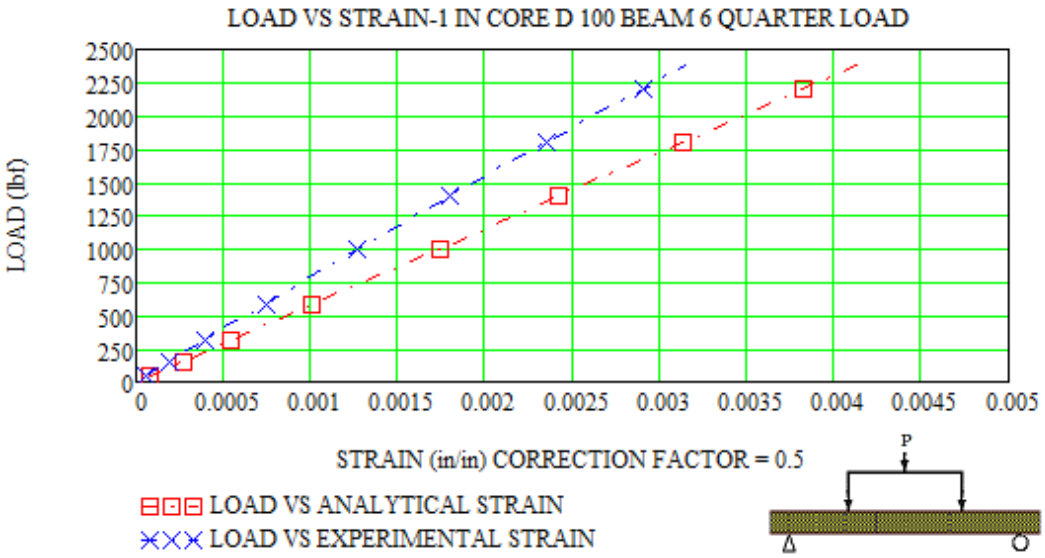

Load vs. Strain-1 in. core-D 100-quarter load Beam # 1, 4, 6

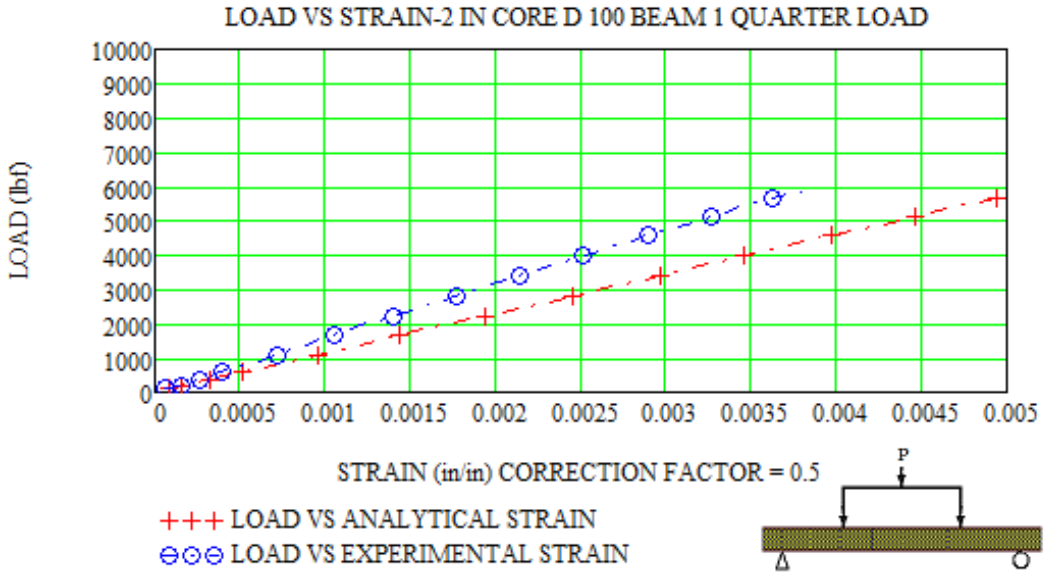

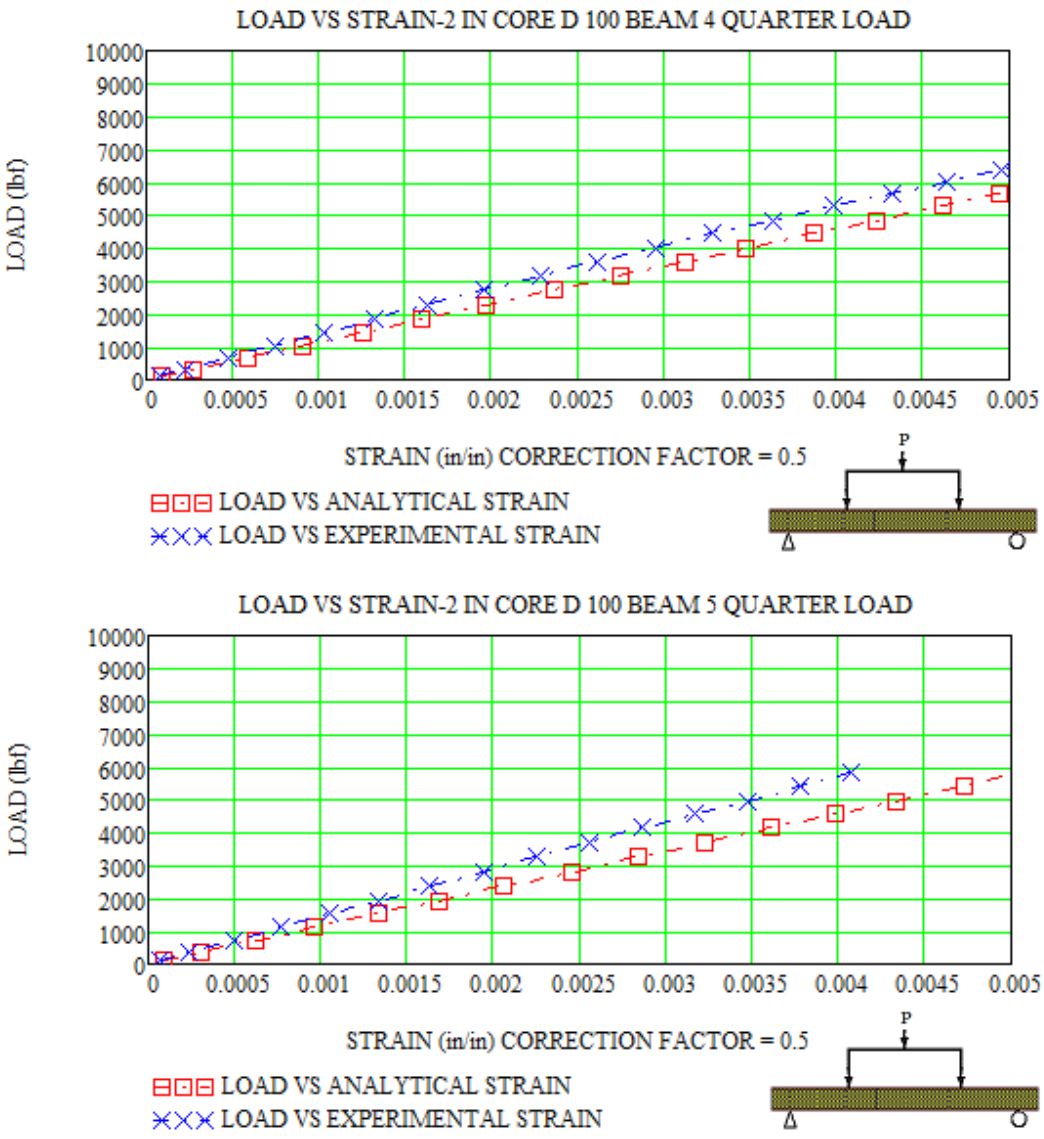

Load vs. Strain-2 in. core-D 100-quarter load Beam # 1, 4, 5

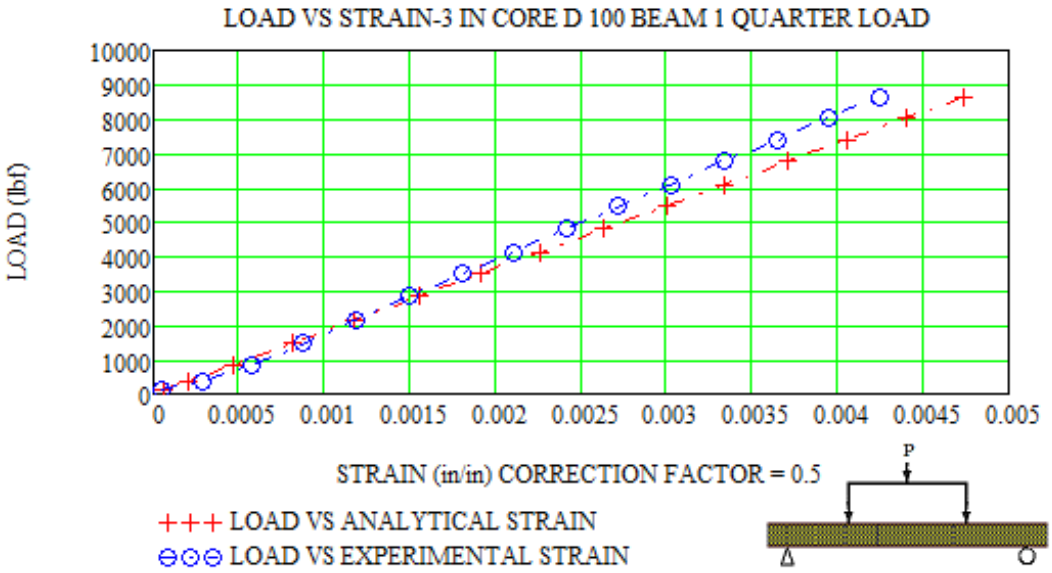
LOAD VS STRAIN-3 IN CORE D 100 BEAM 1 QUARTER LOAD
LOAD (lbf)
10000
9000
8000
7000
6000
5000
4000
3000
2000
1000
0
0
0.0005
0.001
0.0015
0.002
0.0025
0.003
0.0035
0.004
0.0045
0.005
STRAIN (in/in) CORRECTION FACTOR = 0.5
LOAD VS ANALYTICAL STRAIN
LOAD VS EXPERIMENTAL STRAIN
P

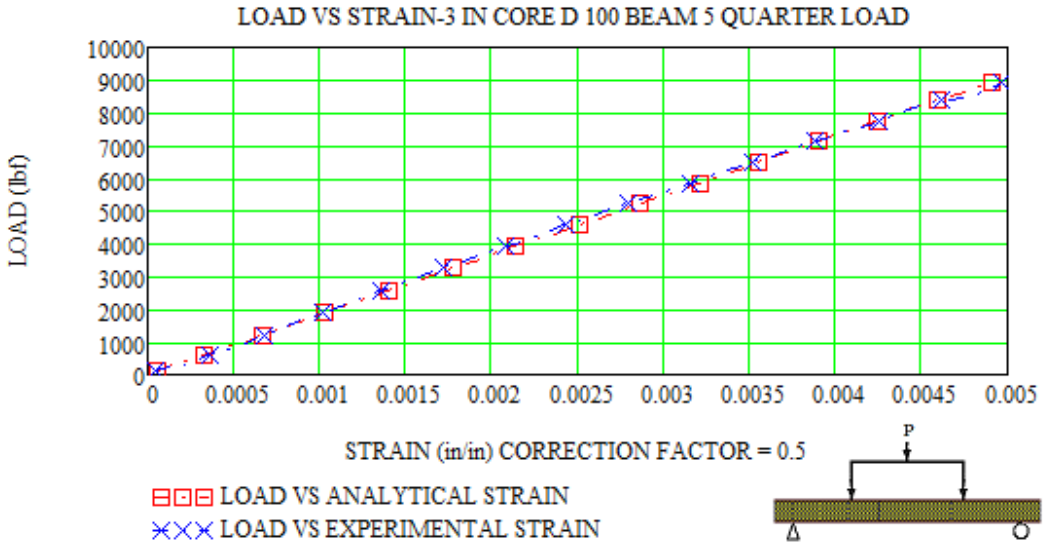
LOAD VS STRAIN-3 IN CORE D 100 BEAM 5 QUARTER LOAD
LOAD (lbf)
10000
9000
8000
7000
6000
5000
4000
3000
2000
1000
0
0
0.0005
0.001
0.0015
0.002
0.0025
0.003
0.0035
0.004
0.0045
0.005
STRAIN (in/in) CORRECTION FACTOR = 0.5
LOAD VS ANALYTICAL STRAIN
LOAD VS EXPERIMENTAL STRAIN
P

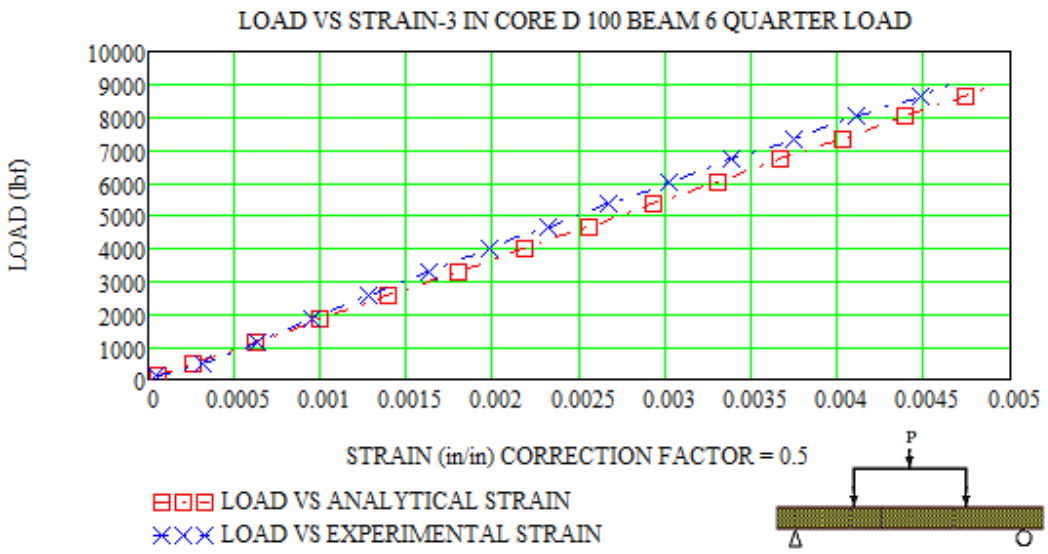

Load vs. Strain-3 in. core-D 100-quarter load Beam # 1, 5, 6

Analytical vs. Experimental Deflection Data-Group I Center-Point Load

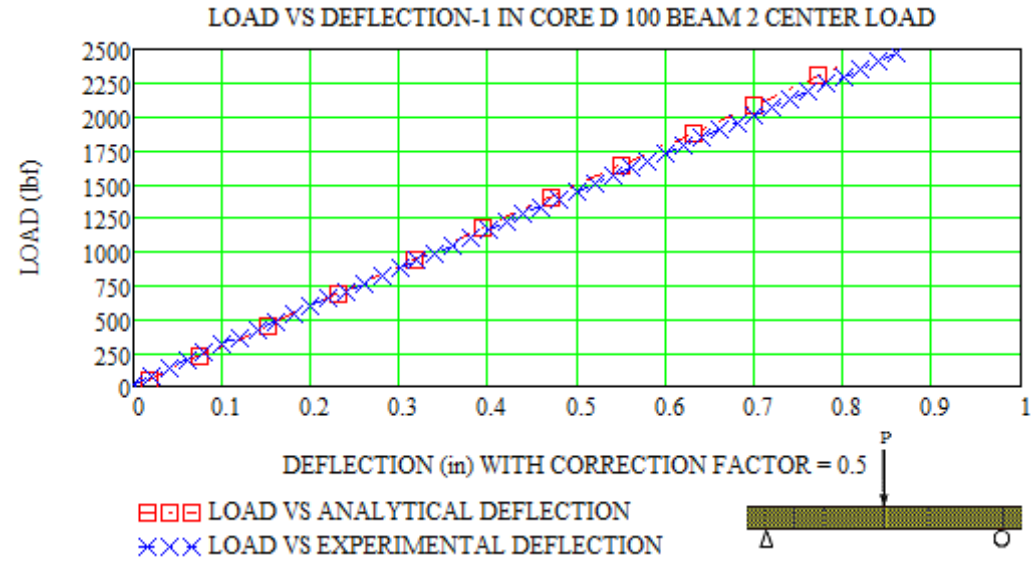

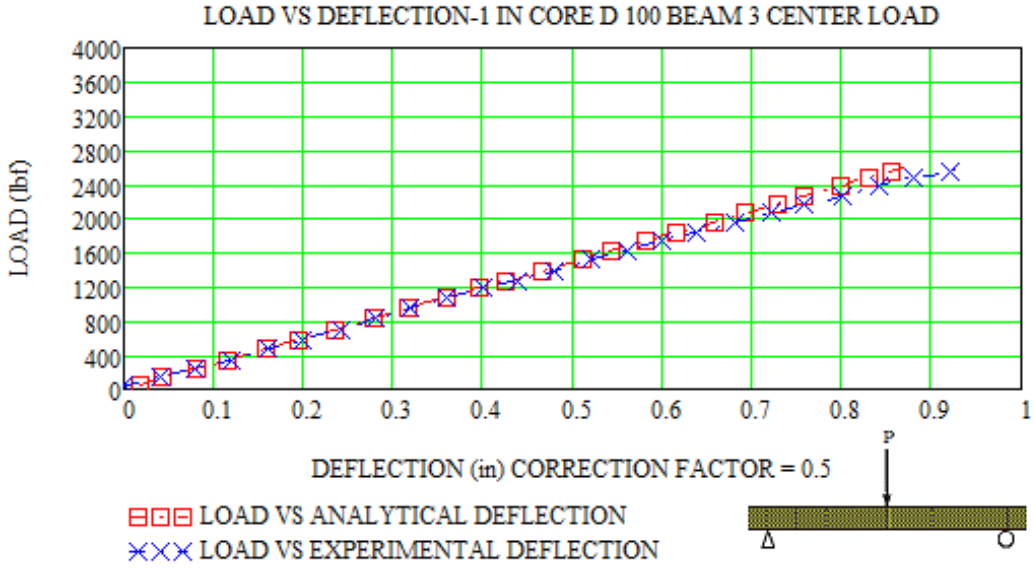

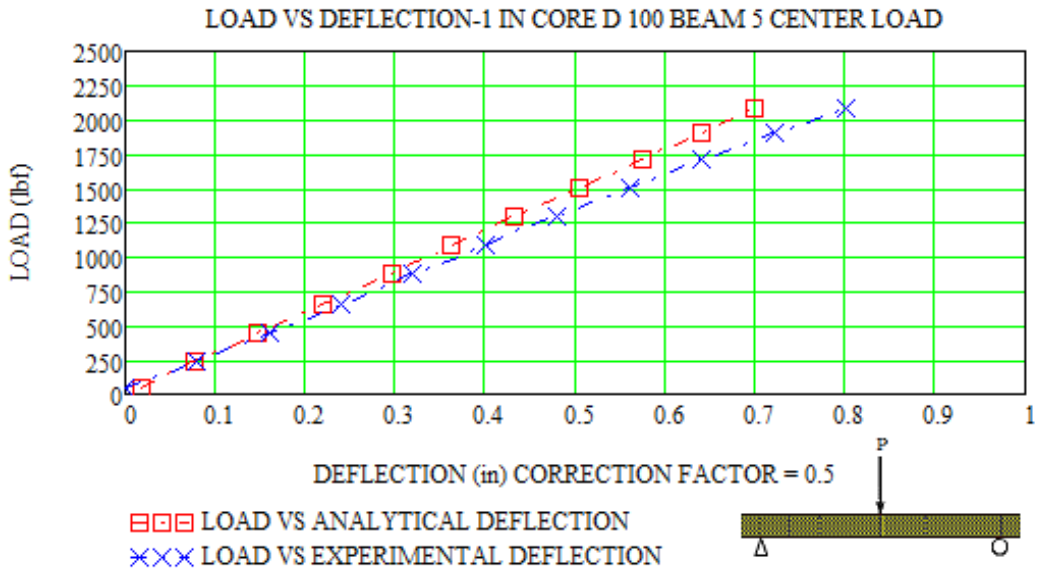

Load vs. Deflection-1 in. core-D 100-center load Beam # 2, 3, 5

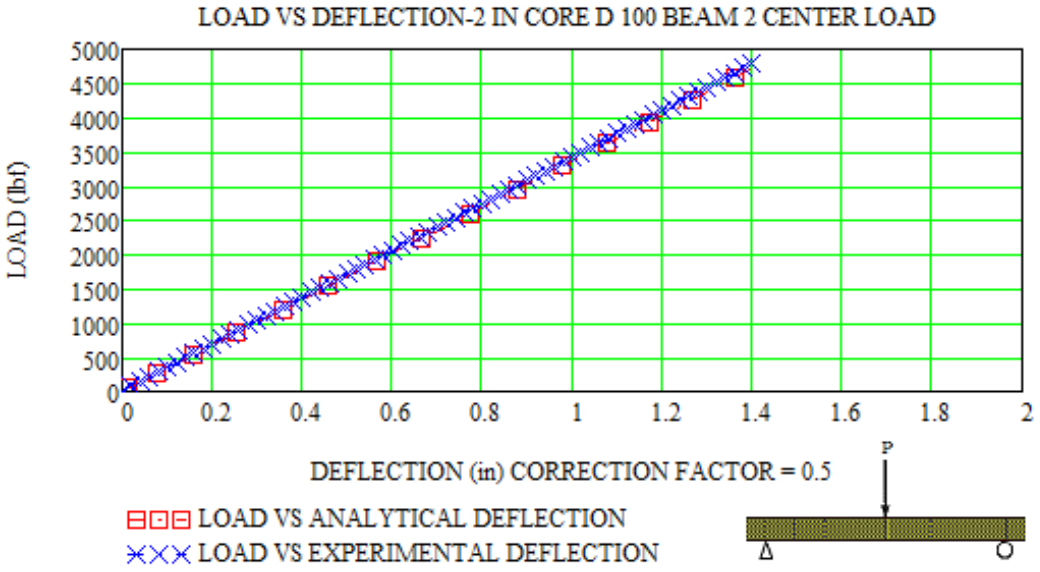

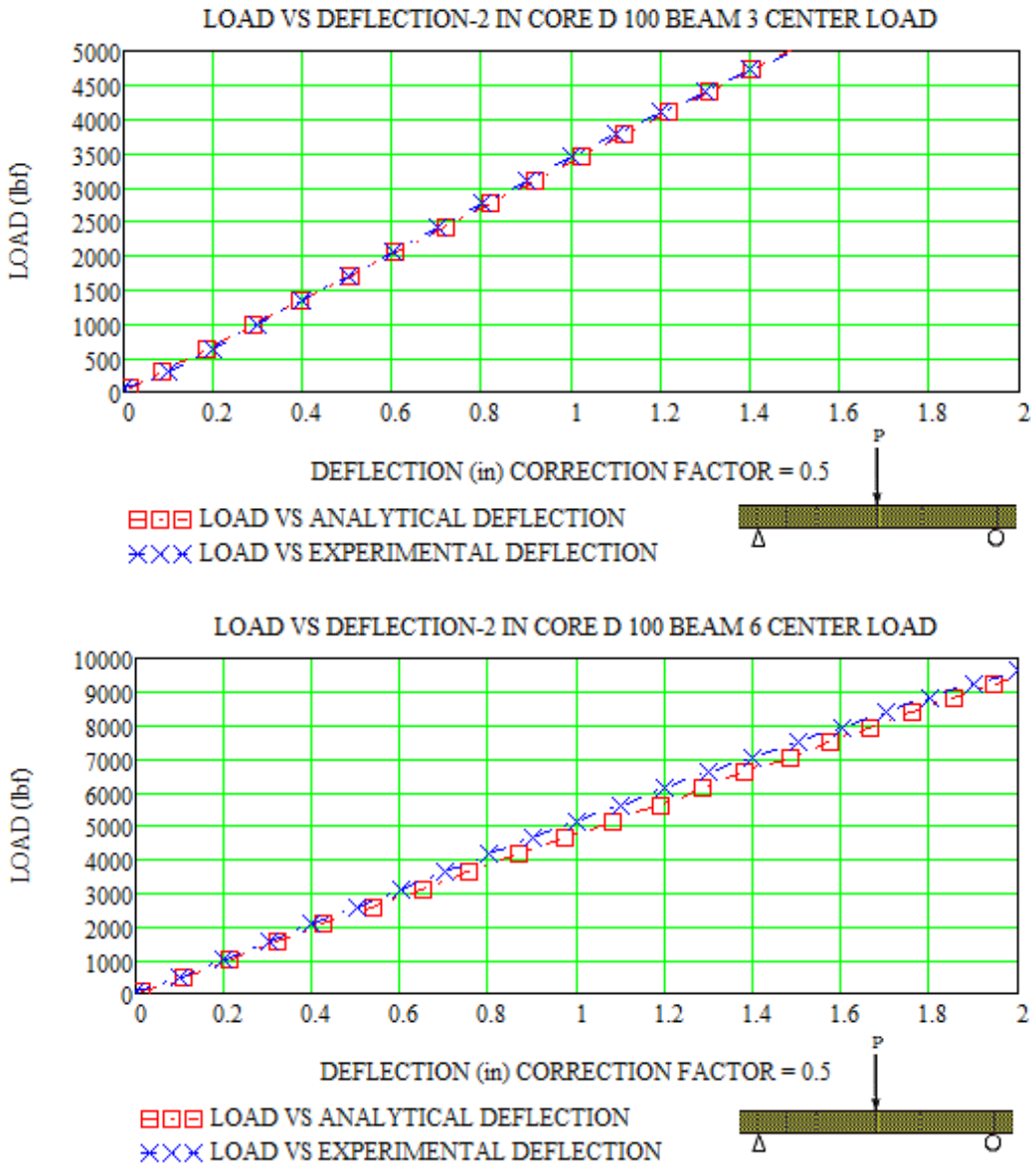

Load vs. Deflection-2 in. core-D 100-center load Beam # 2, 3, 6

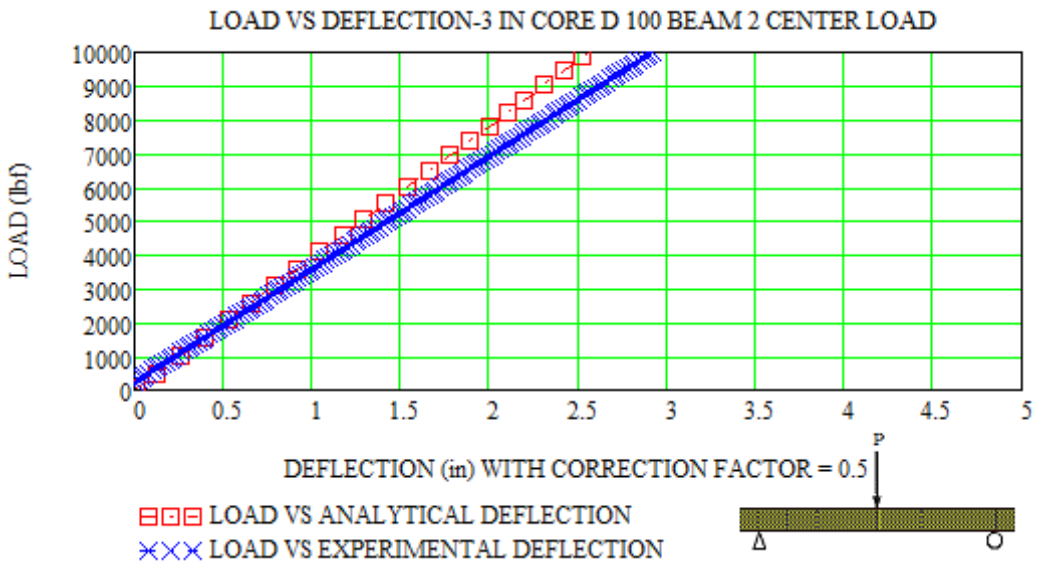
LOAD VS DEFLECTION-3 IN CORE D 100 BEAM 2 CENTER LOAD
LOAD (lbf)
10000
9000
8000
7000
6000
5000
4000
3000
2000
1000
0
0
0.5
1
1.5
2
2.5
3
3.5
4
4.5
5
DEFLECTION (in) WITH CORRECTION FACTOR = 0.5
P
LOAD VS ANALYTICAL DEFLECTION
LOAD VS EXPERIMENTAL DEFLECTION

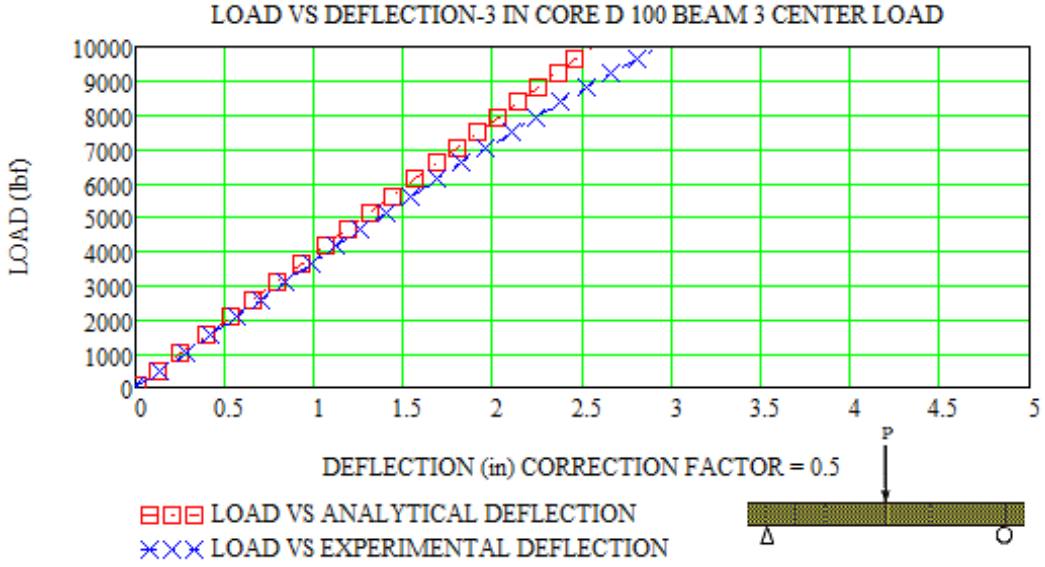
LOAD VS DEFLECTION-3 IN CORE D 100 BEAM 3 CENTER LOAD
LOAD (lbf)
10000
9000
8000
7000
6000
5000
4000
3000
2000
1000
0
0
0.5
1
1.5
2
2.5
3
3.5
4
4.5
5
DEFLECTION (in) CORRECTION FACTOR = 0.5
P
LOAD VS ANALYTICAL DEFLECTION
LOAD VS EXPERIMENTAL DEFLECTION

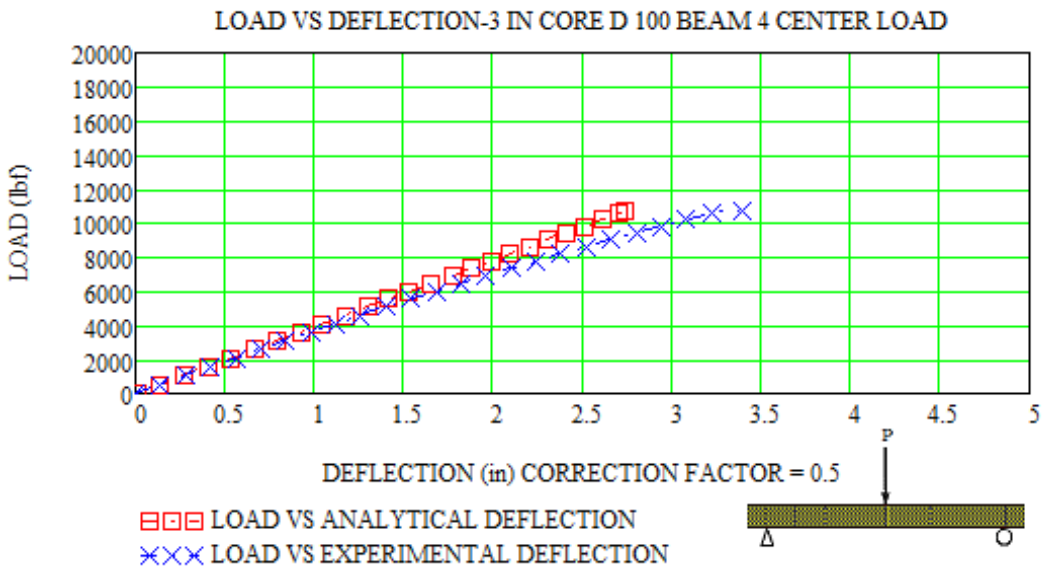

Load vs. Deflection-3 in. core-D 100-center load Beam # 2, 3, 4

Analytical vs. Experimental Deflection Data-Group I Quarter-Point Load

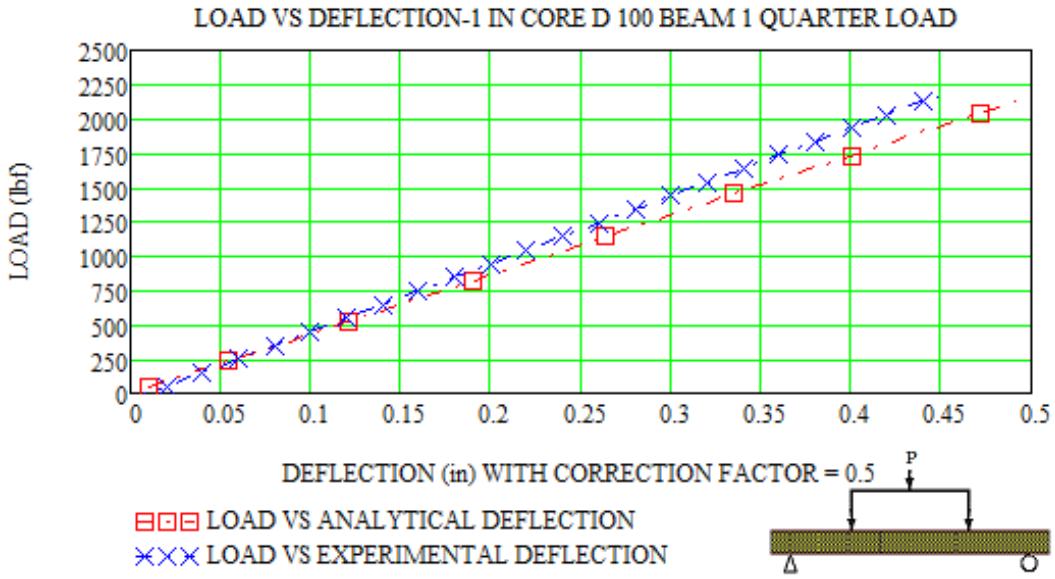

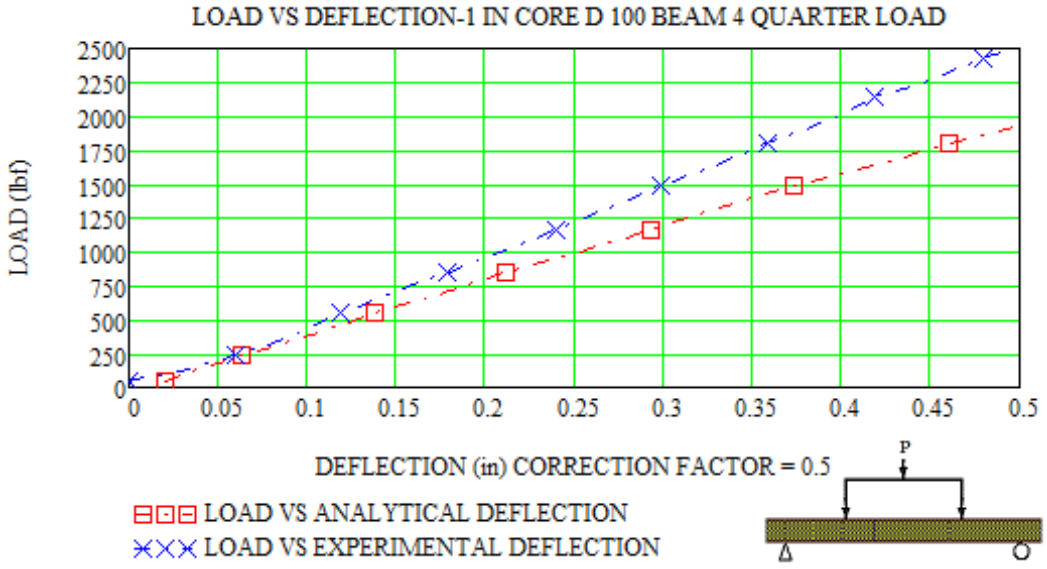

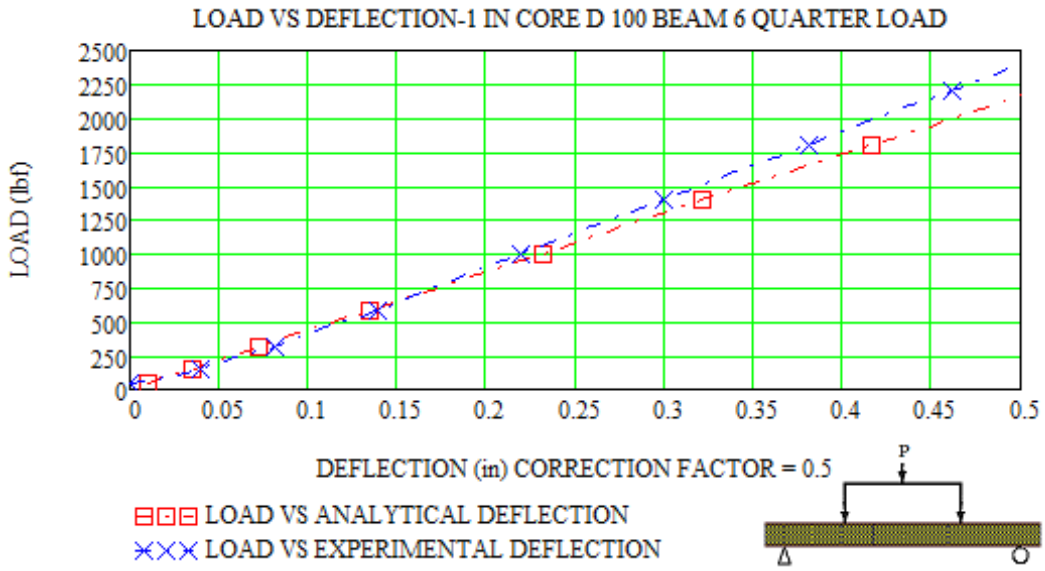

Load vs. Deflection-1 in. core-D 100-quarter load Beam # 1, 4, 6

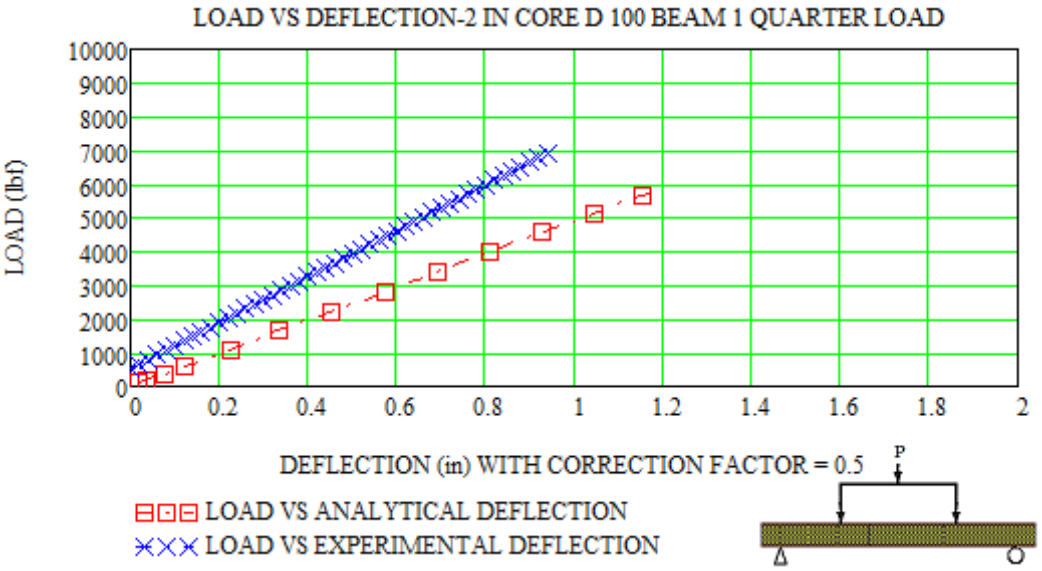

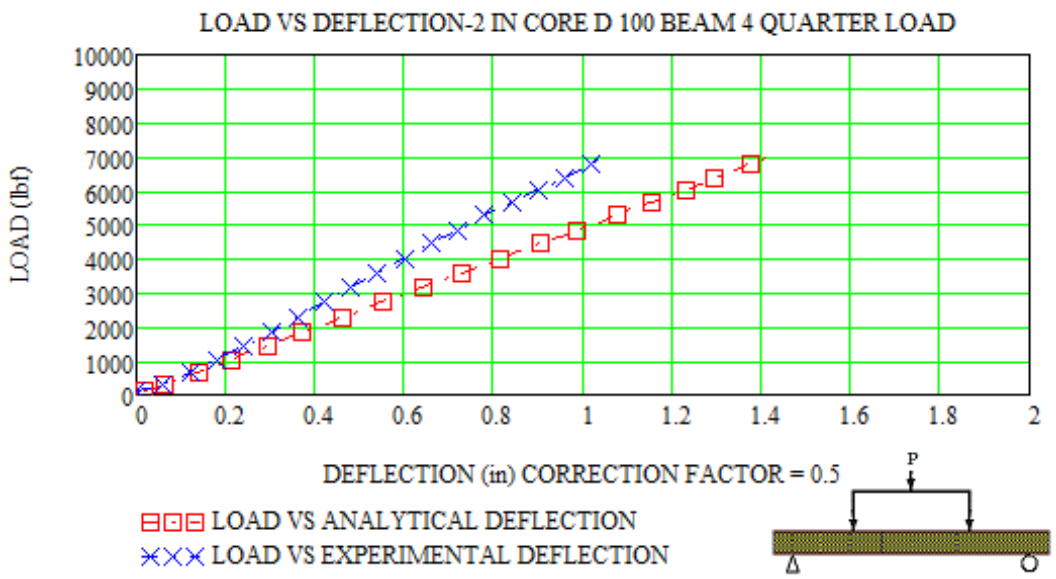

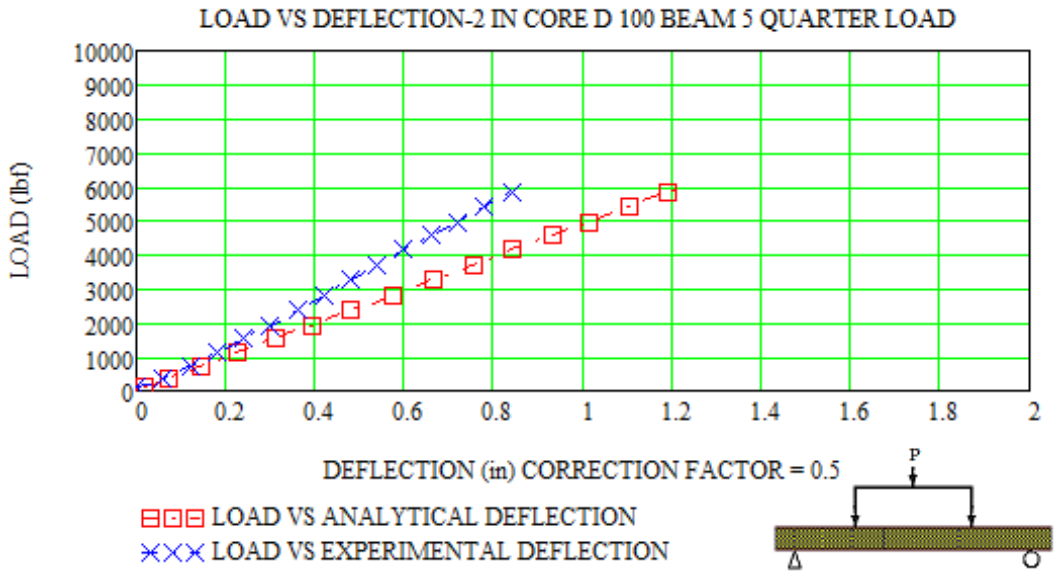

Load vs. Deflection-2 in. core-D 100-quarter load Beam # 1, 4, 5

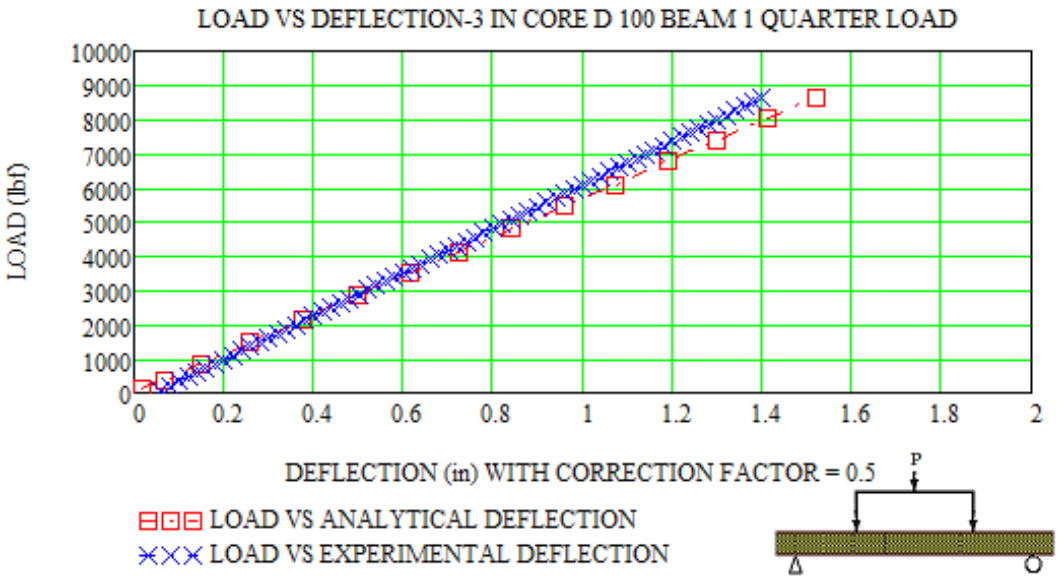
LOAD VS DEFLECTION-3 IN CORE D 100 BEAM 1 QUARTER LOAD
LOAD (lbf)
10000
9000
8000
7000
6000
5000
4000
3000
2000
1000
0
0
0.2
0.4
0.6
0.8
1
1.2
1.4
1.6
1.8
2
DEFLECTION (in) WITH CORRECTION FACTOR = 0.5
LOAD VS ANALYTICAL DEFLECTION
LOAD VS EXPERIMENTAL DEFLECTION
P

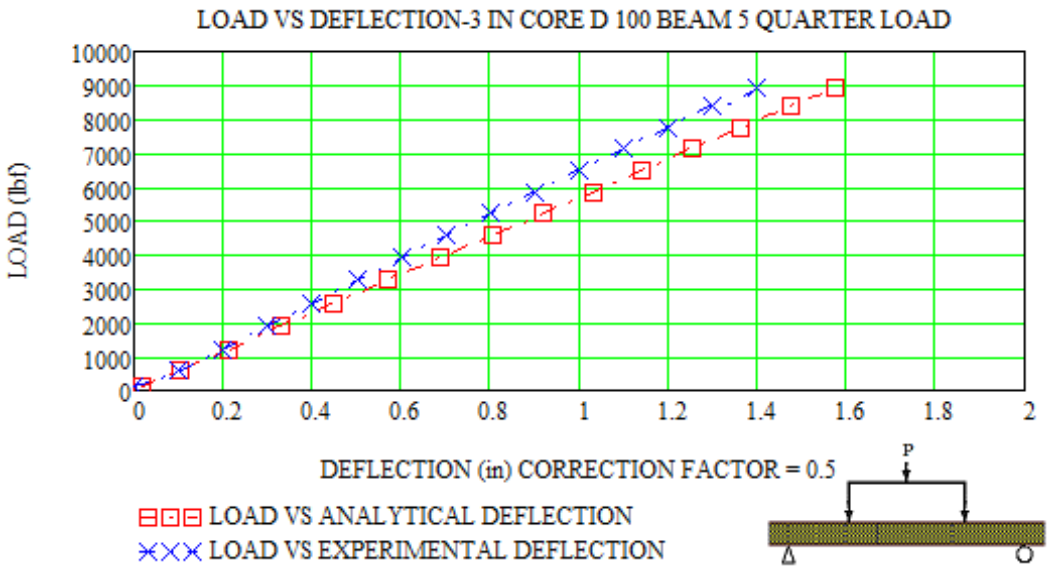
LOAD VS DEFLECTION-3 IN CORE D 100 BEAM 5 QUARTER LOAD
LOAD (lbf)
10000
9000
8000
7000
6000
5000
4000
3000
2000
1000
0
0
0.2
0.4
0.6
0.8
1
1.2
1.4
1.6
1.8
2
DEFLECTION (in) CORRECTION FACTOR = 0.5
LOAD VS ANALYTICAL DEFLECTION
LOAD VS EXPERIMENTAL DEFLECTION
P

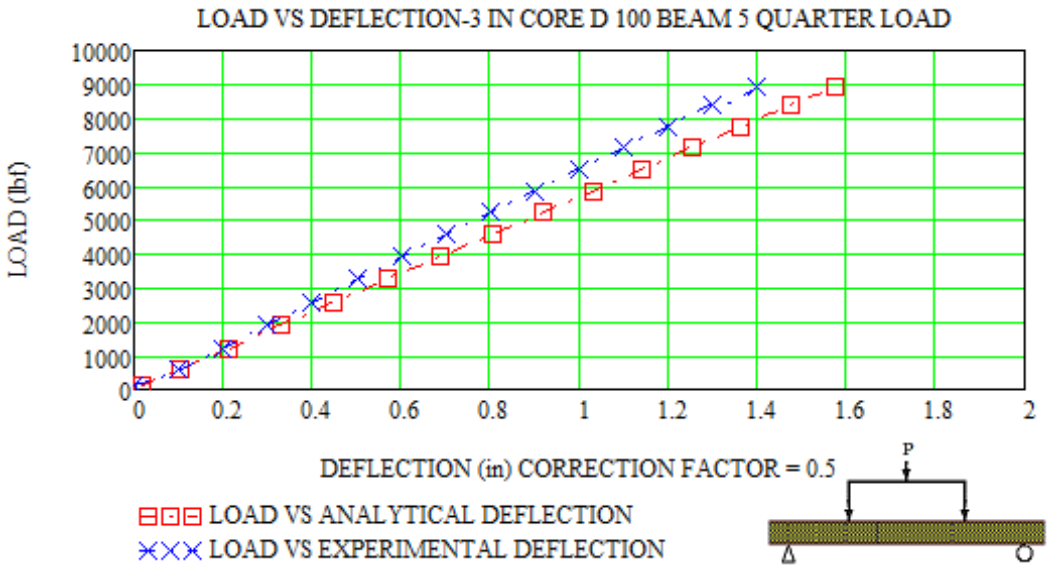

Load vs. Deflection-3 in. core-D 100-quarter load Beam # 1, 5, 6

Analytical vs. Experimental Strain Data-Group II Center-Point Load

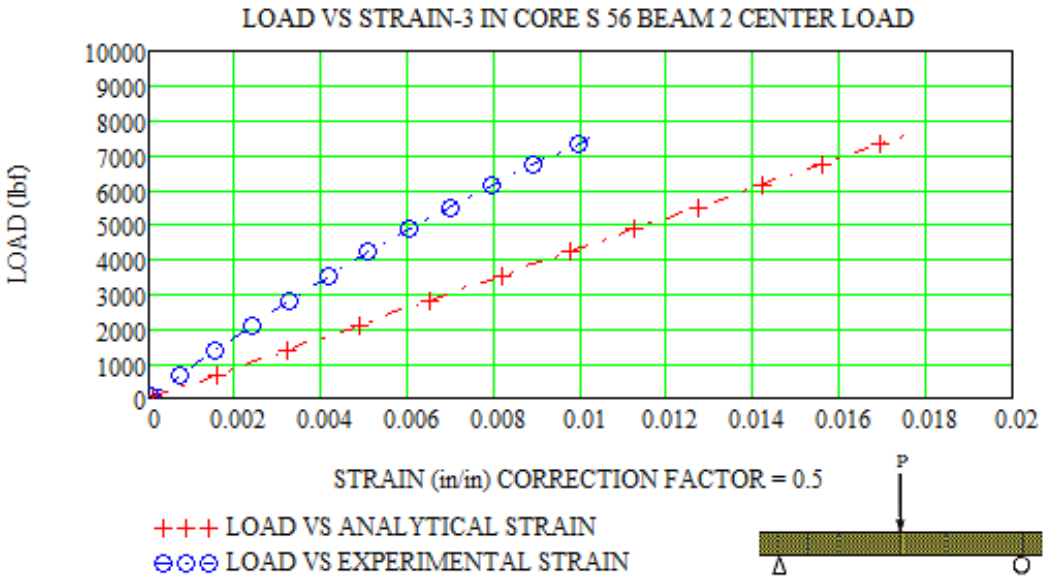

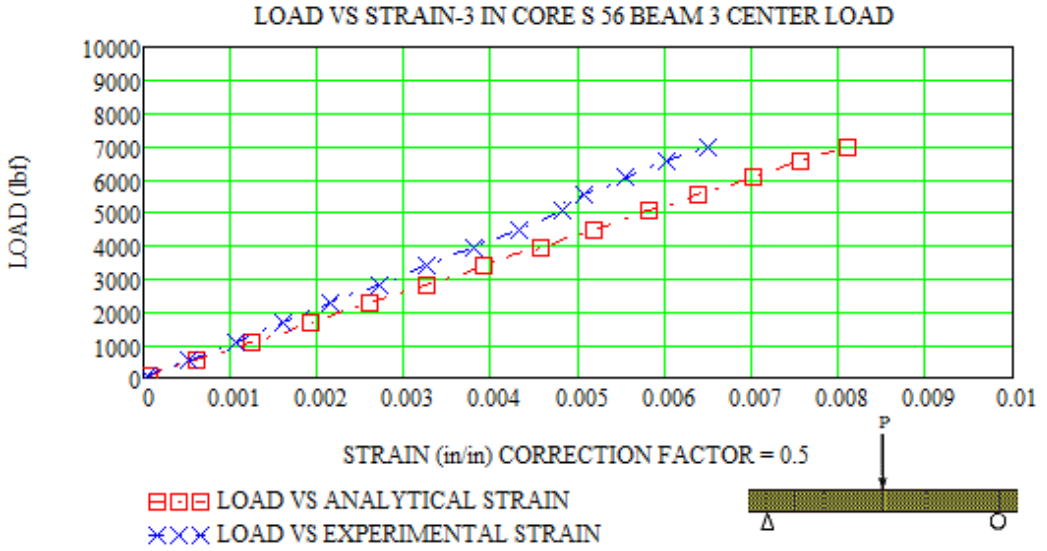

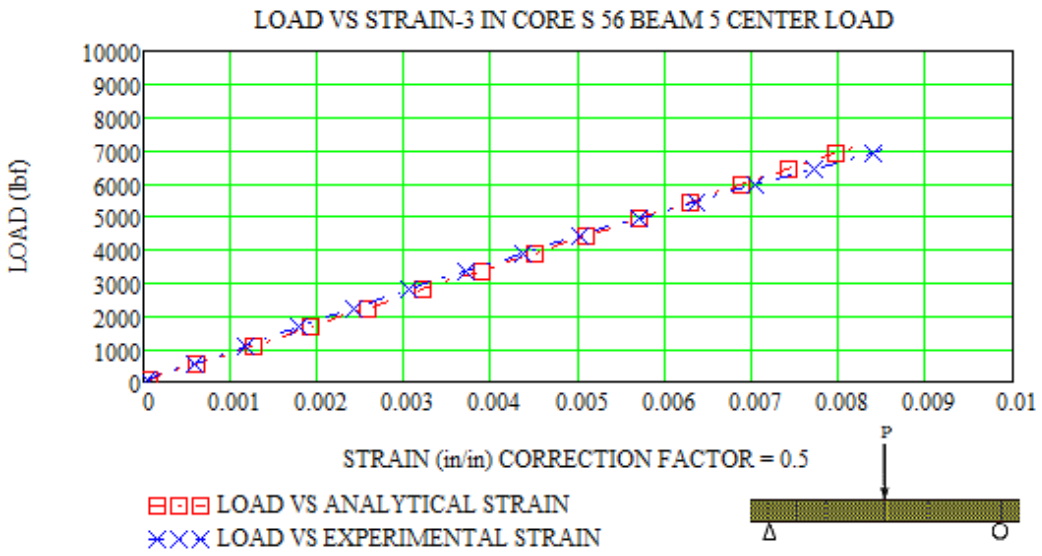

Load vs. Strain-3 in. core-S 56-center load Beam # 2, 3, 5

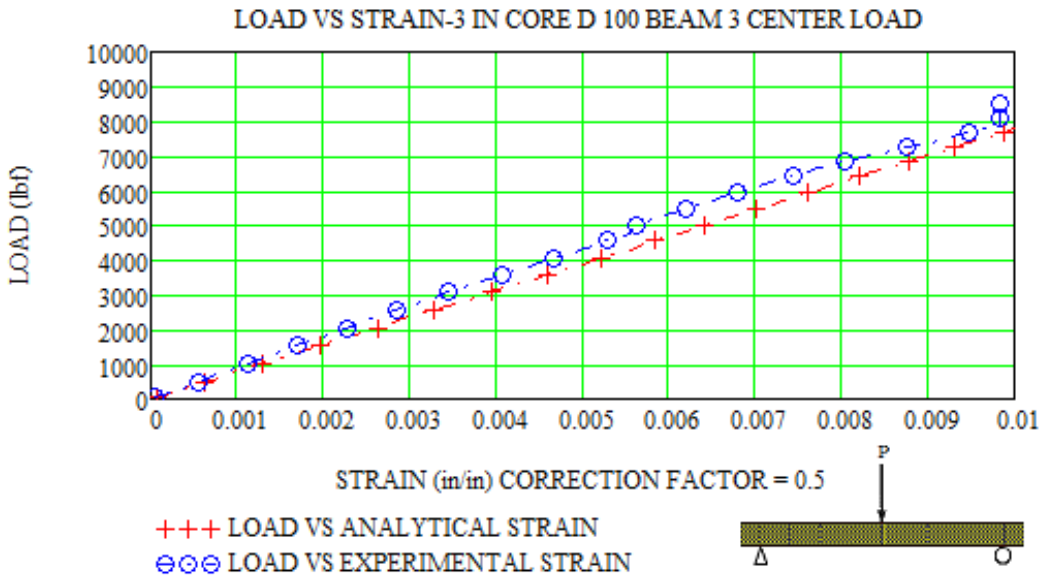

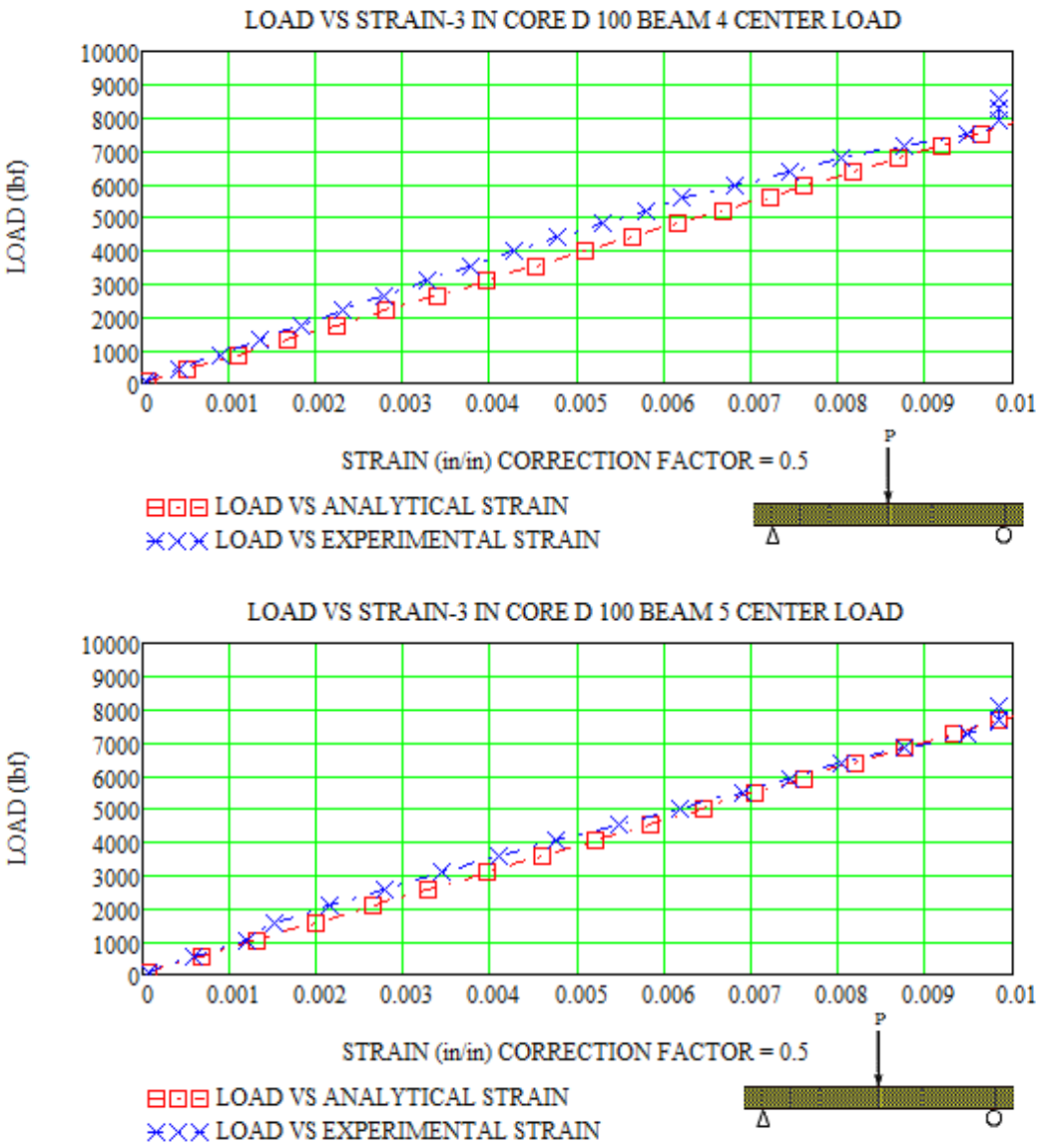

Load vs. Strain-3 in. core-D 100-center load Beam # 3, 4, 5

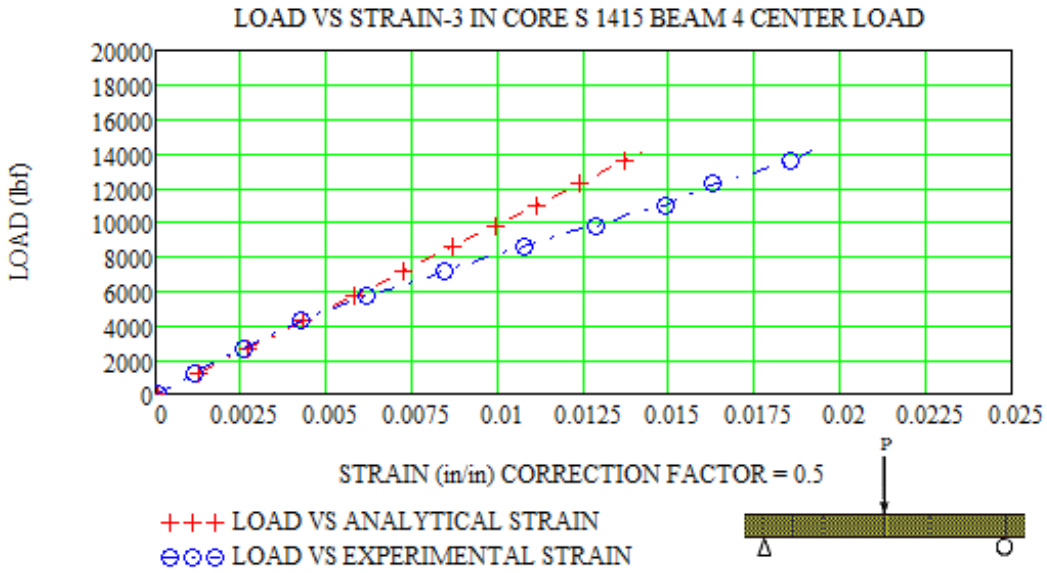
LOAD VS STRAIN-3 IN CORE S 1415 BEAM 4 CENTER LOAD
LOAD (lbf)
20000
18000
16000
14000
12000
10000
8000
6000
4000
2000
0
0
0.0025
0.005
0.0075
0.01
0.0125
0.015
0.0175
0.02
0.0225
0.025
STRAIN (in/in) CORRECTION FACTOR = 0.5
P
LOAD VS ANALYTICAL STRAIN
LOAD VS EXPERIMENTAL STRAIN

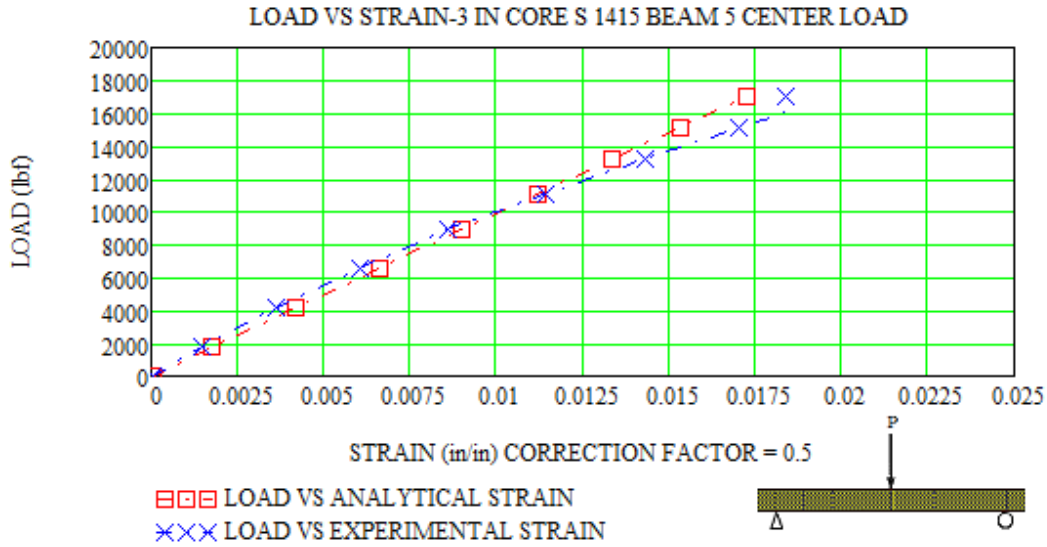
LOAD VS STRAIN-3 IN CORE S 1415 BEAM 5 CENTER LOAD
LOAD (lbf)
20000
18000
16000
14000
12000
10000
8000
6000
4000
2000
0
0
0.0025
0.005
0.0075
0.01
0.0125
0.015
0.0175
0.02
0.0225
0.025
STRAIN (in/in) CORRECTION FACTOR = 0.5
P
LOAD VS ANALYTICAL STRAIN
LOAD VS EXPERIMENTAL STRAIN

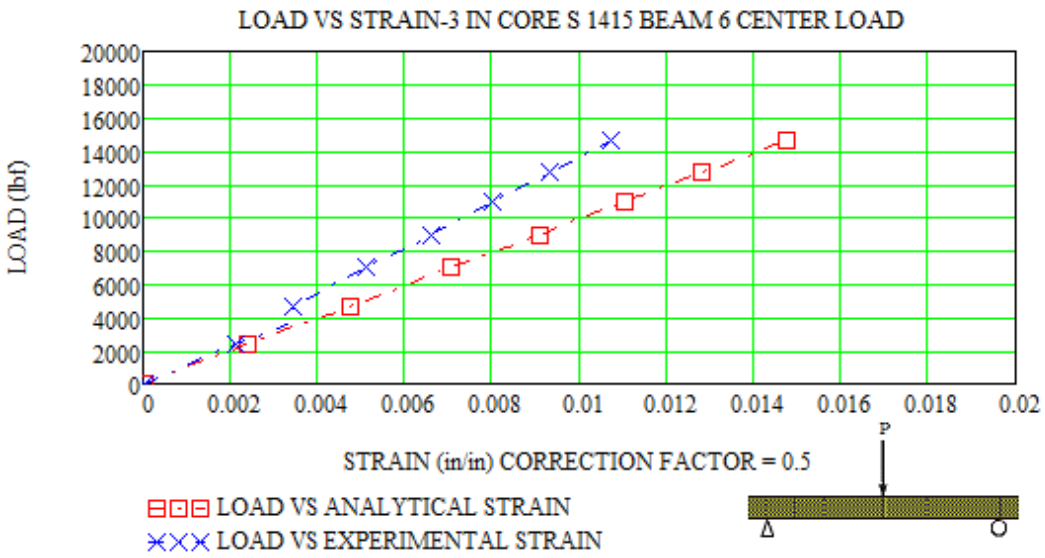

Load vs. Strain-3 in. core-S 1415-center load Beam # 4, 5, 6

Analytical vs. Experimental Strain Data-Group II Quarter-Point Load

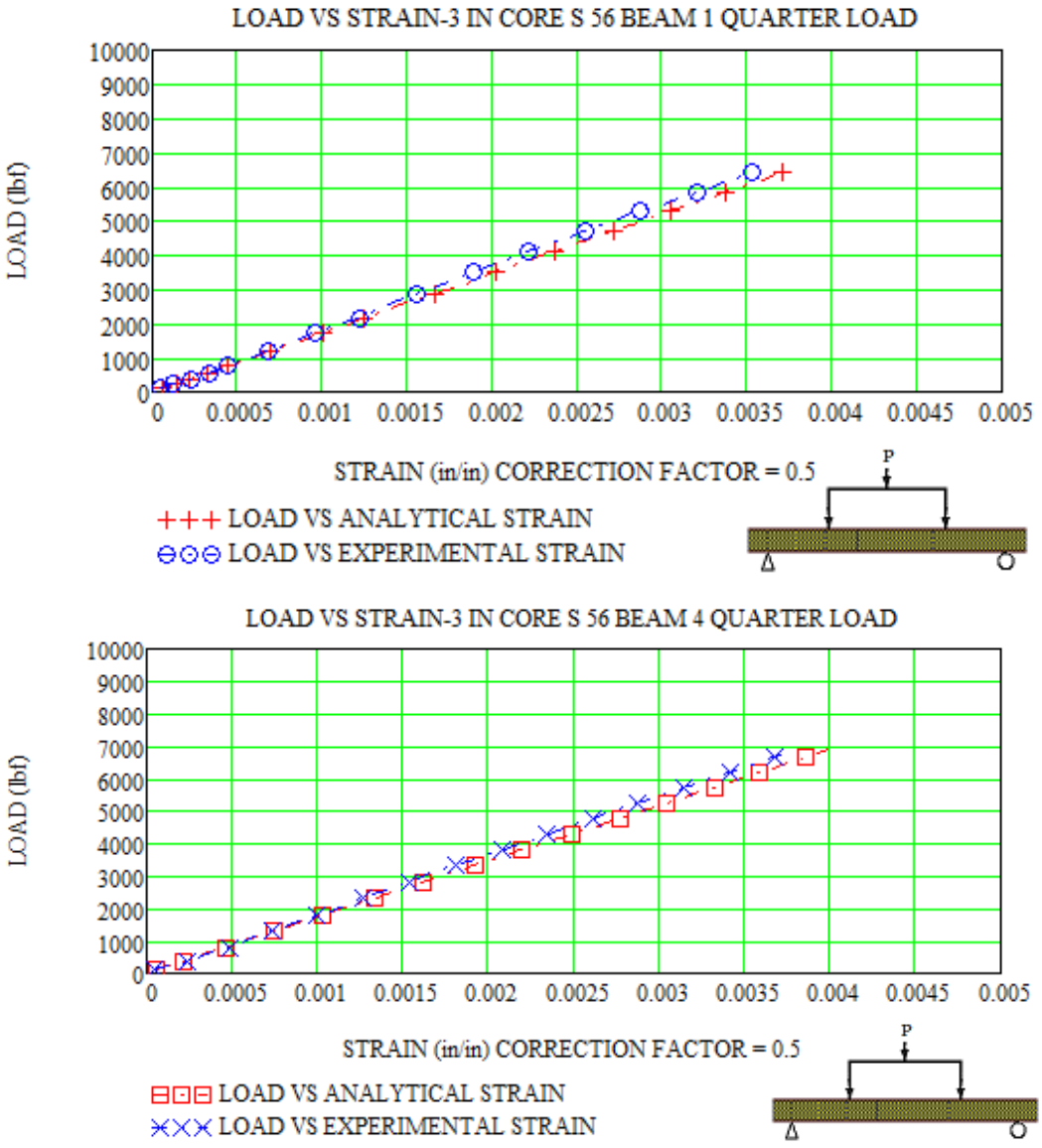

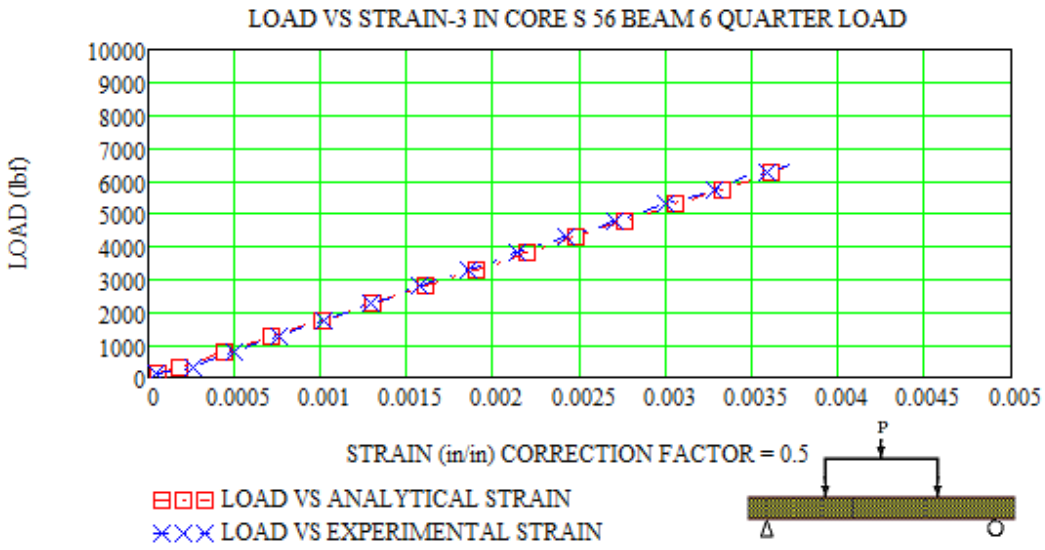

Load vs. Strain-3 in. core-S 56-quarter load Beam # 1, 4, 6

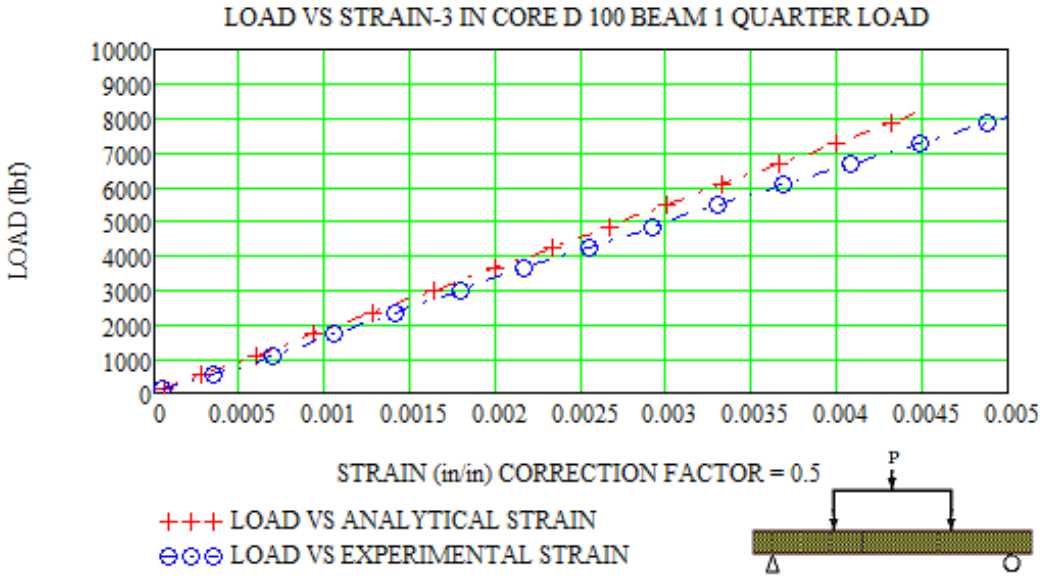

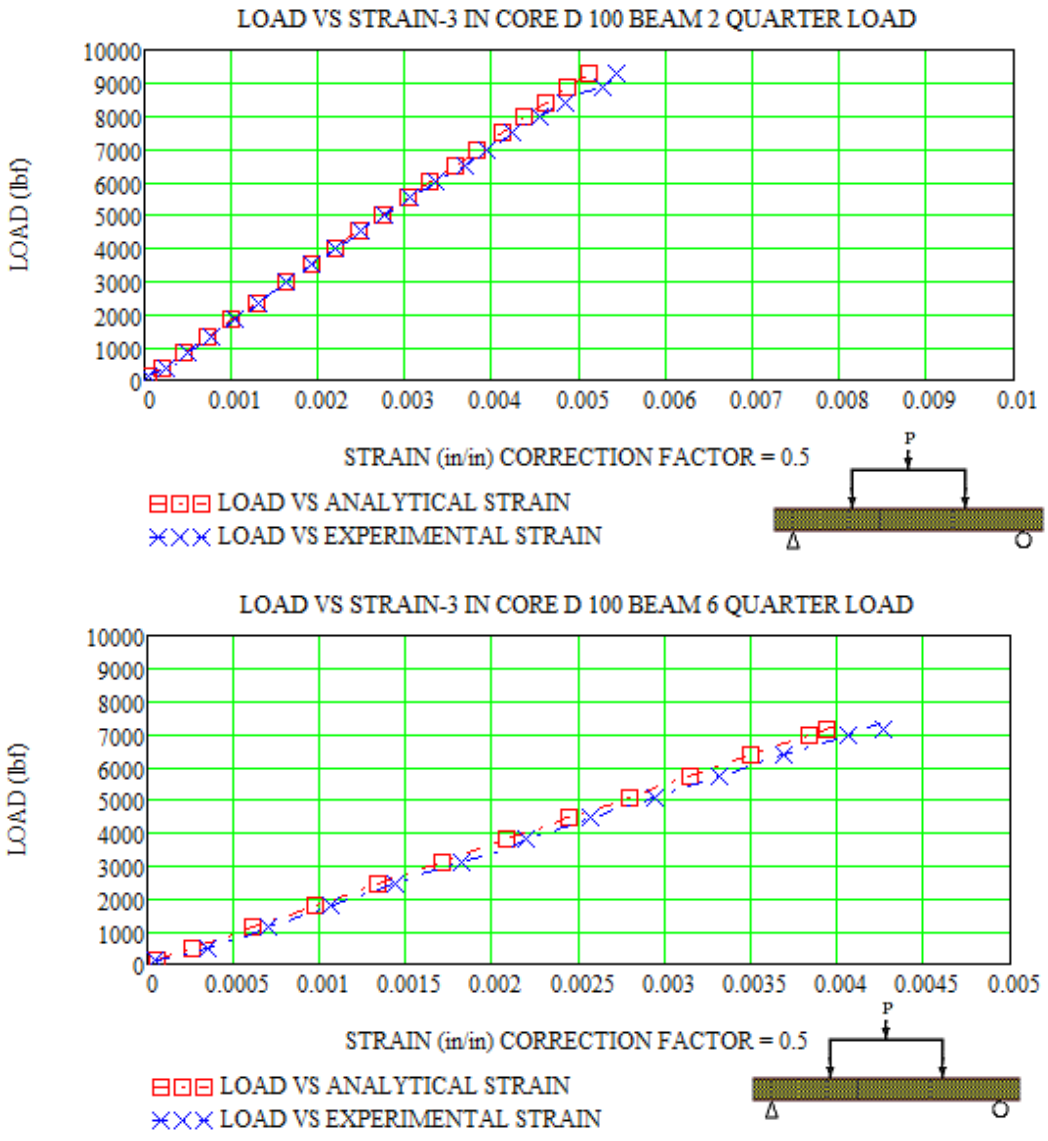

Load vs. Strain-3 in. core-D 100-quarter load Beam # 1, 2, 6

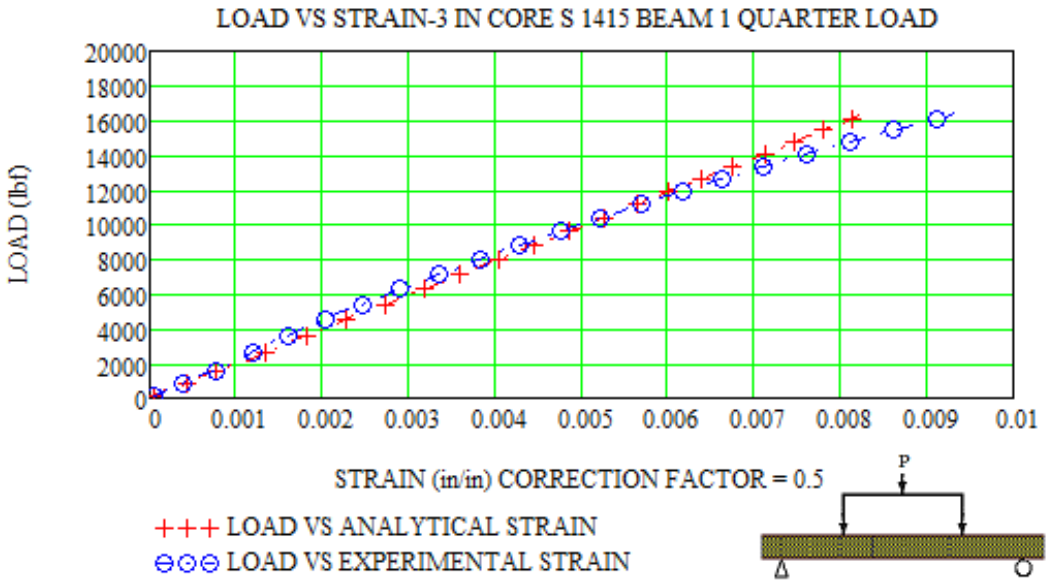
LOAD VS STRAIN-3 IN CORE S 1415 BEAM 1 QUARTER LOAD
LOAD (lbf)
20000
18000
16000
14000
12000
10000
8000
6000
4000
2000
0
0
0.001
0.002
0.003
0.004
0.005
0.006
0.007
0.008
0.009
0.01
STRAIN (in/in) CORRECTION FACTOR = 0.5
LOAD VS ANALYTICAL STRAIN
LOAD VS EXPERIMENTAL STRAIN
P

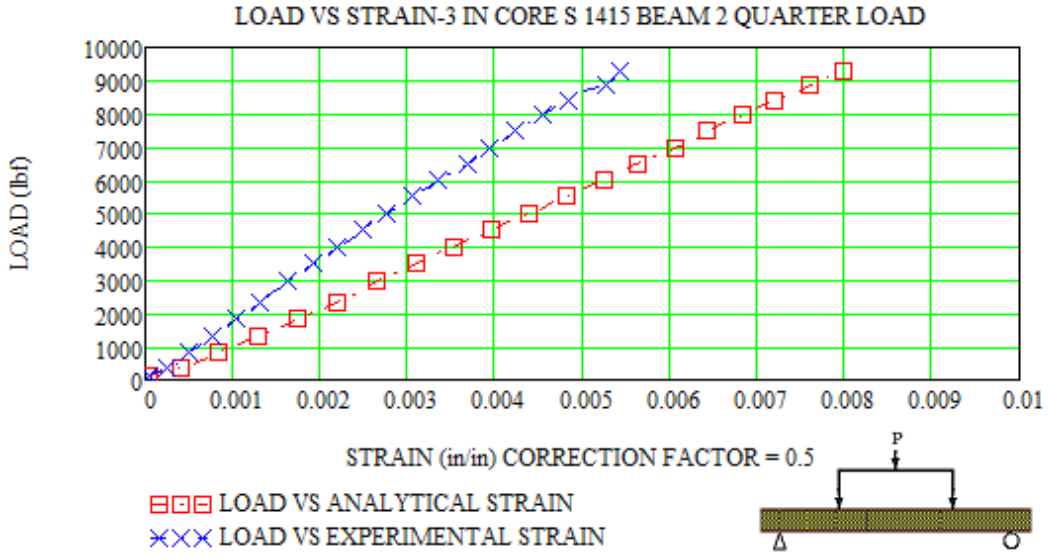
LOAD VS STRAIN-3 IN CORE S 1415 BEAM 2 QUARTER LOAD
LOAD (lbf)
10000
9000
8000
7000
6000
5000
4000
3000
2000
1000
0
0
0.001
0.002
0.003
0.004
0.005
0.006
0.007
0.008
0.009
0.01
STRAIN (in/in) CORRECTION FACTOR = 0.5
LOAD VS ANALYTICAL STRAIN
LOAD VS EXPERIMENTAL STRAIN
P

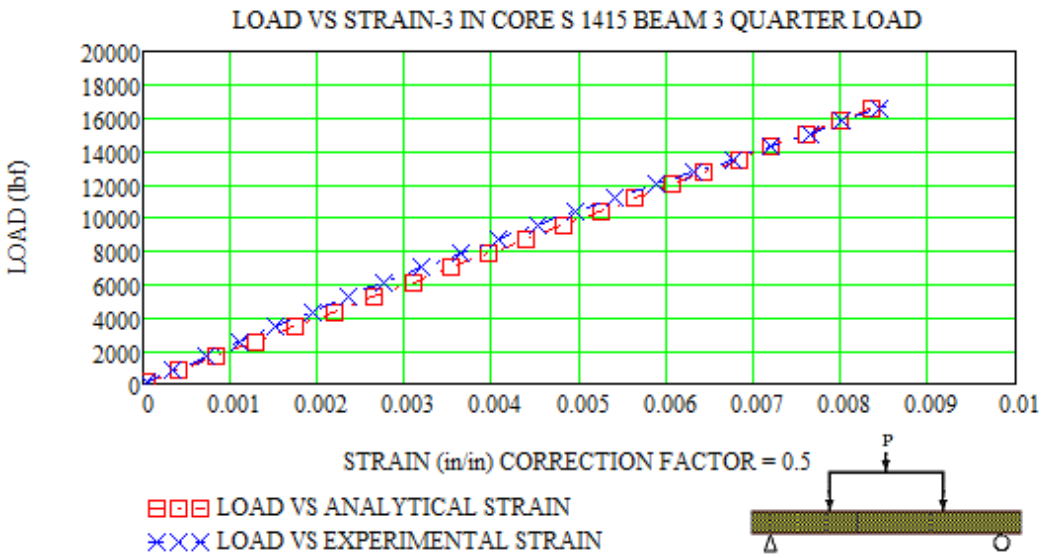

Load vs. Strain-3 in. core-S 1415-quarter load Beam # 1, 2, 3

Analytical vs. Experimental Deflection Data-Group II Center-Point Load

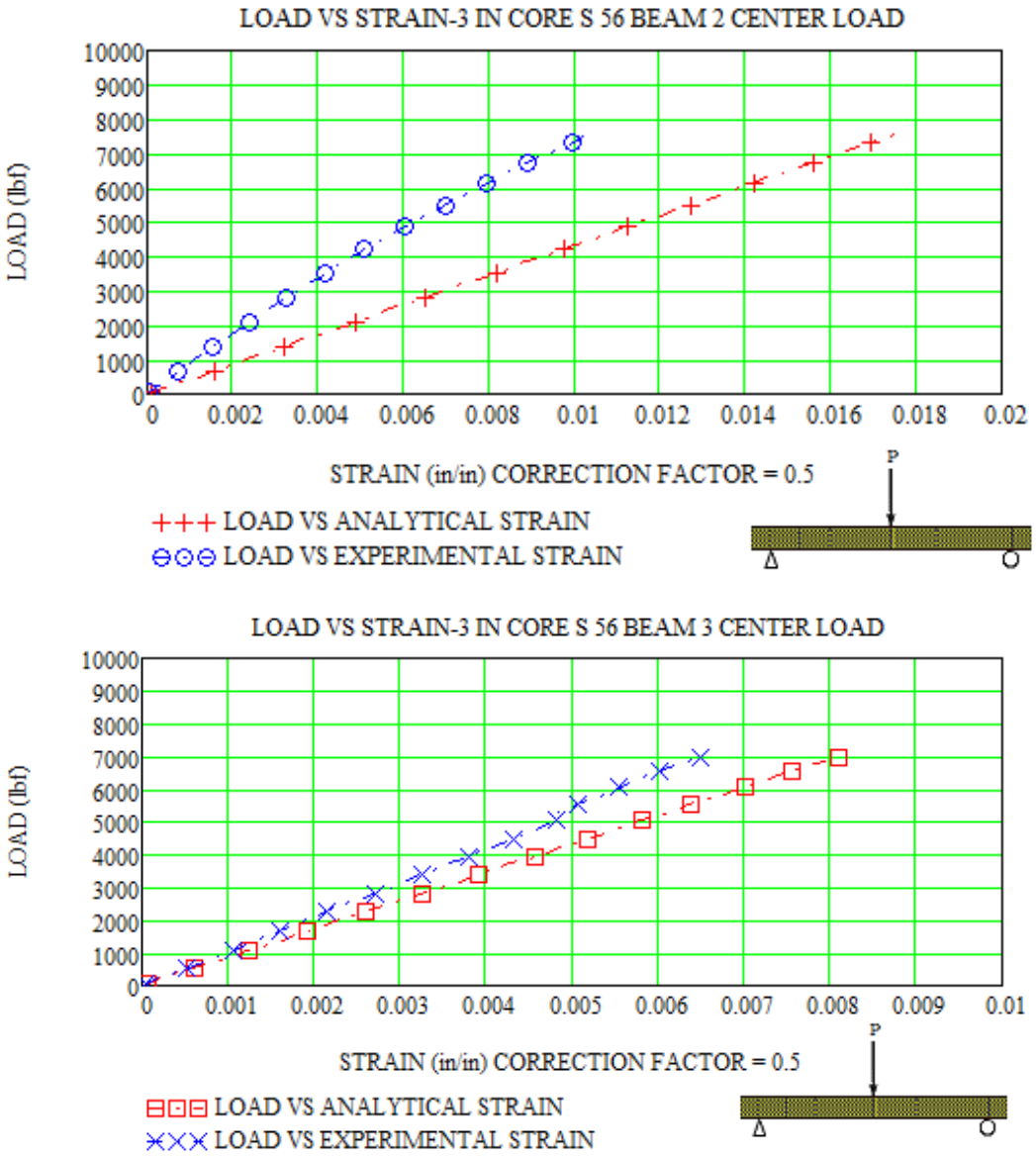

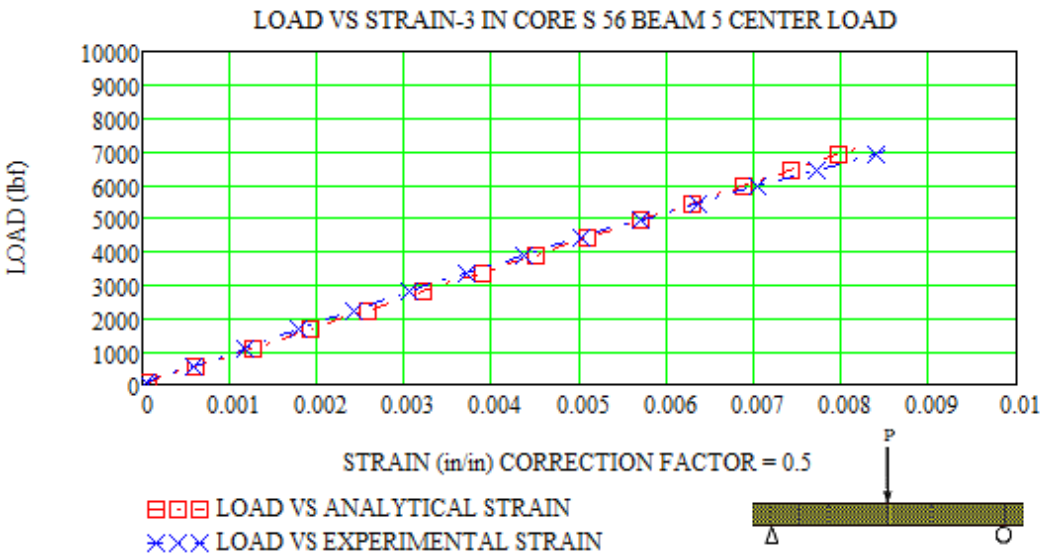

Load vs. Deflection-3 in. core-S 56-center load Beam 2, 3, 5

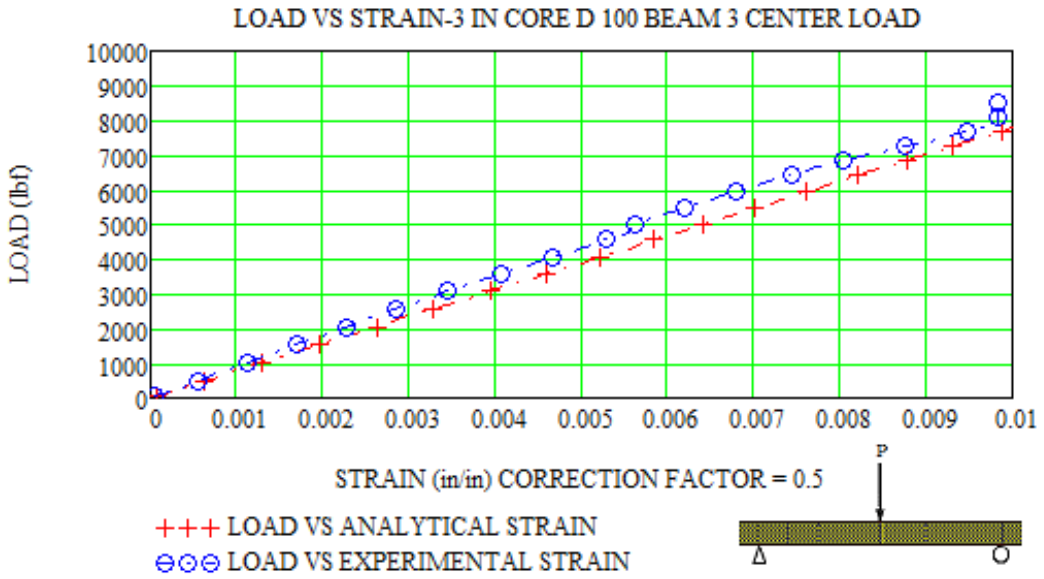

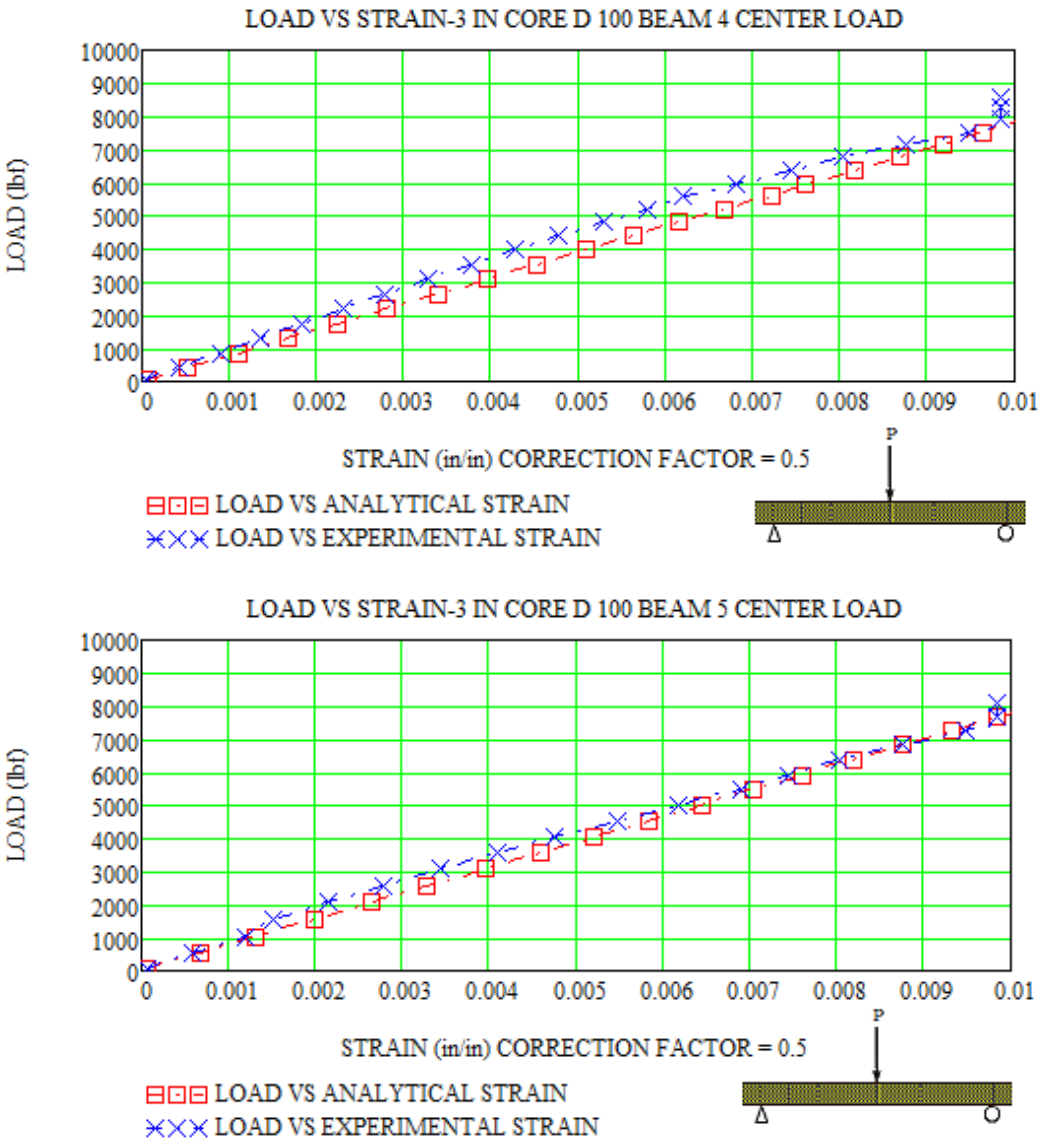

Load vs. Deflection-3 in. core-D 100-center load Beam # 3, 4, 5

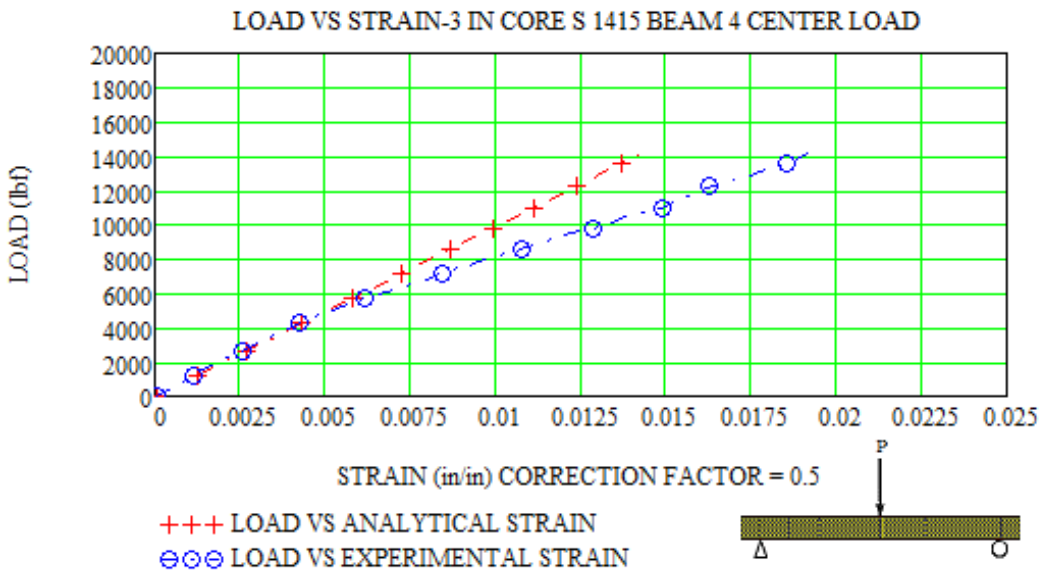
LOAD VS STRAIN-3 IN CORE S 1415 BEAM 4 CENTER LOAD
LOAD (lbf)
20000
18000
16000
14000
12000
10000
8000
6000
4000
2000
0
0
0.0025
0.005
0.0075
0.01
0.0125
0.015
0.0175
0.02
0.0225
0.025
STRAIN (in/in) CORRECTION FACTOR = 0.5
P
LOAD VS ANALYTICAL STRAIN
LOAD VS EXPERIMENTAL STRAIN

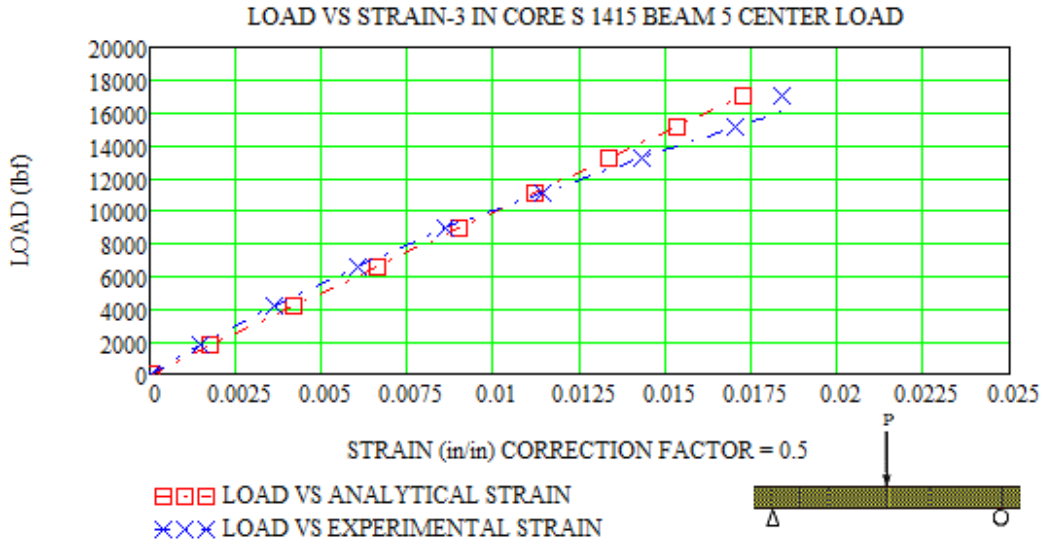
LOAD VS STRAIN-3 IN CORE S 1415 BEAM 5 CENTER LOAD
LOAD (lbf)
20000
18000
16000
14000
12000
10000
8000
6000
4000
2000
0
0
0.0025
0.005
0.0075
0.01
0.0125
0.015
0.0175
0.02
0.0225
0.025
STRAIN (in/in) CORRECTION FACTOR = 0.5
P
LOAD VS ANALYTICAL STRAIN
LOAD VS EXPERIMENTAL STRAIN

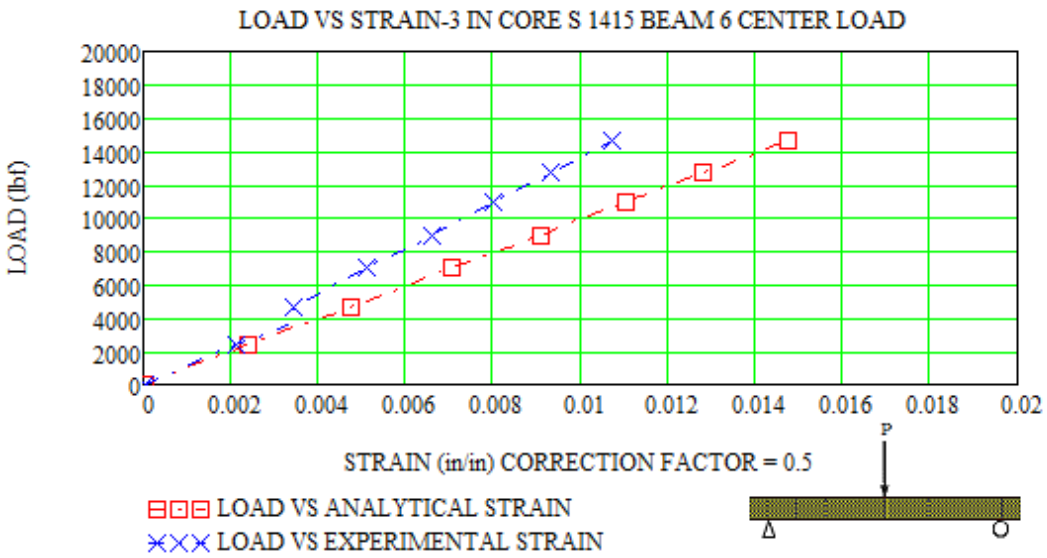

Load vs. Deflection-3 in. core-S 1415-center load Beam # 4, 5, 6

Analytical vs. Experimental Deflection Data-Group II Quarter-Point Load

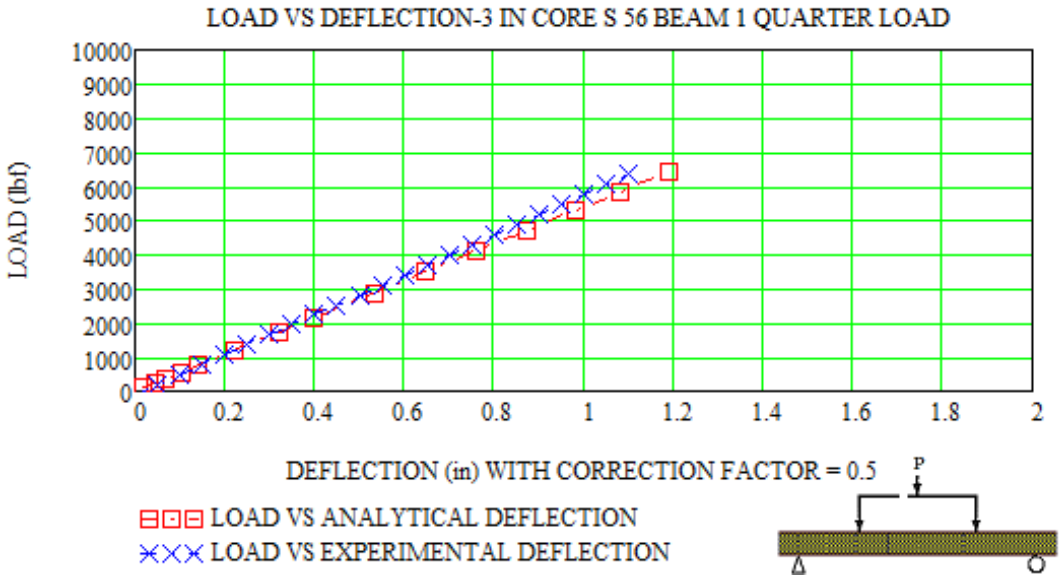

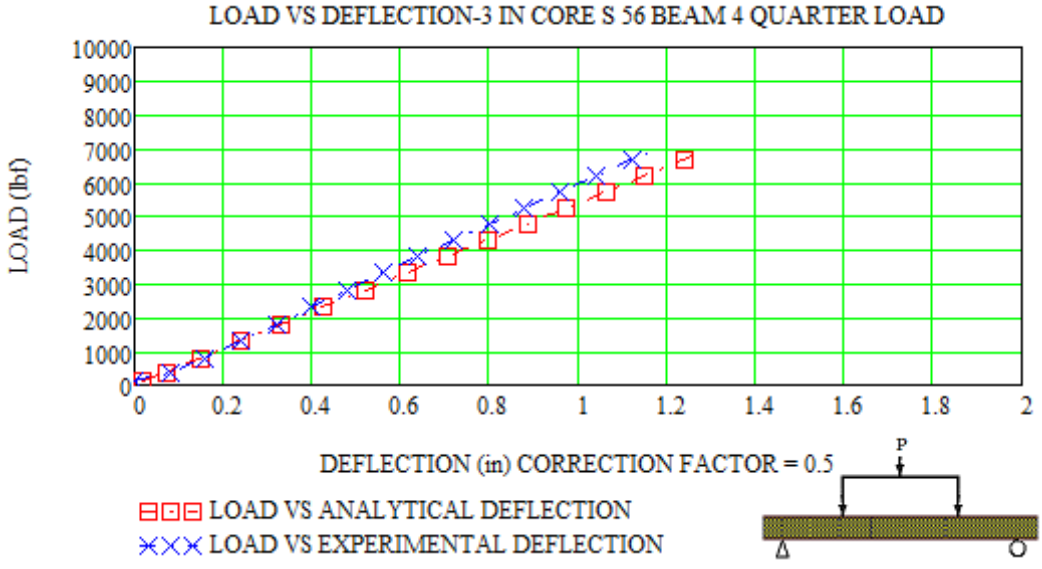

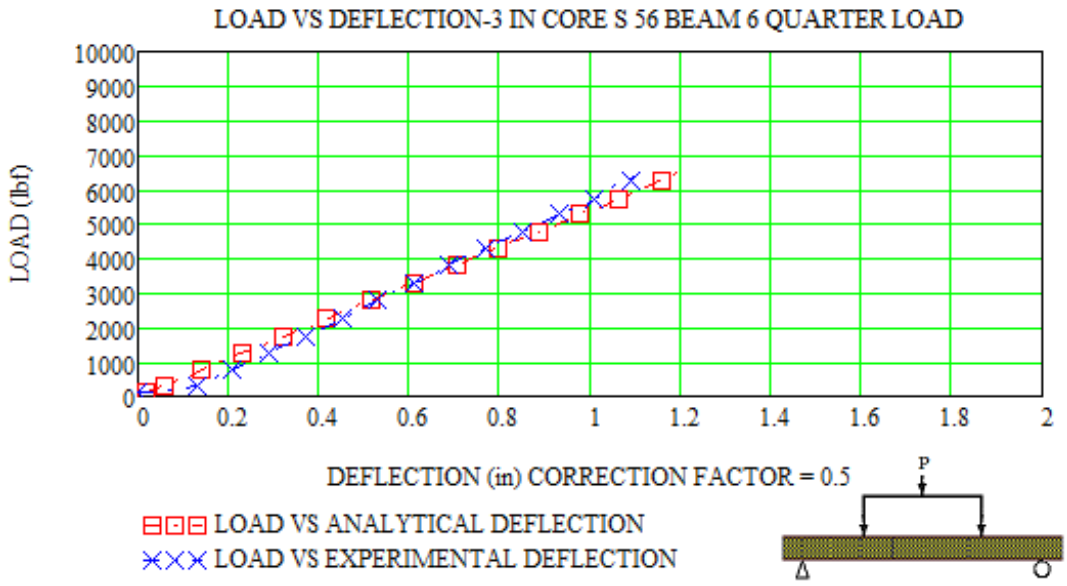

Load vs. Deflection-3 in. core-S 56-quarter load Beam # 1, 4, 6

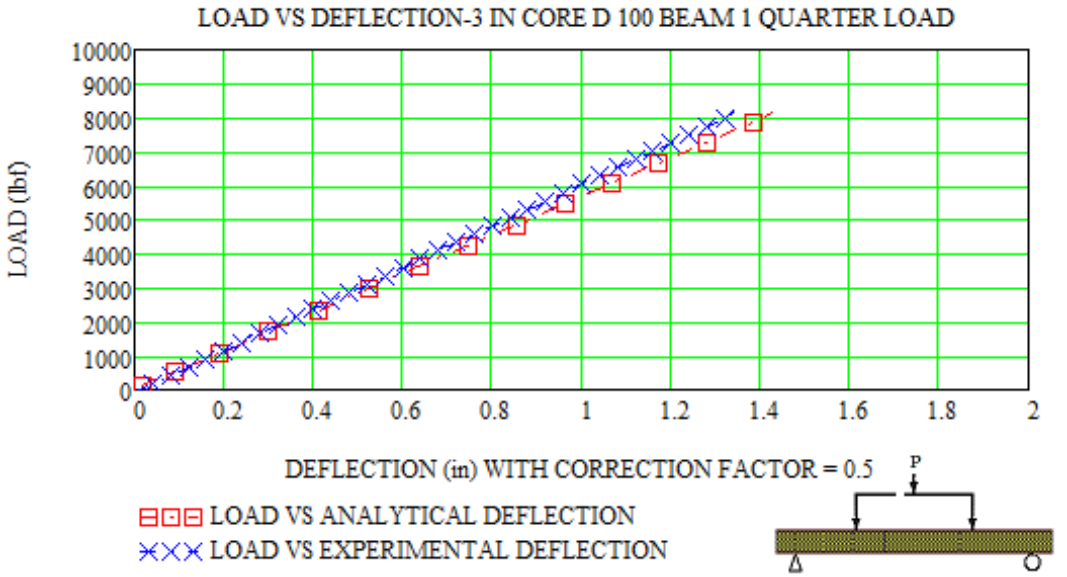

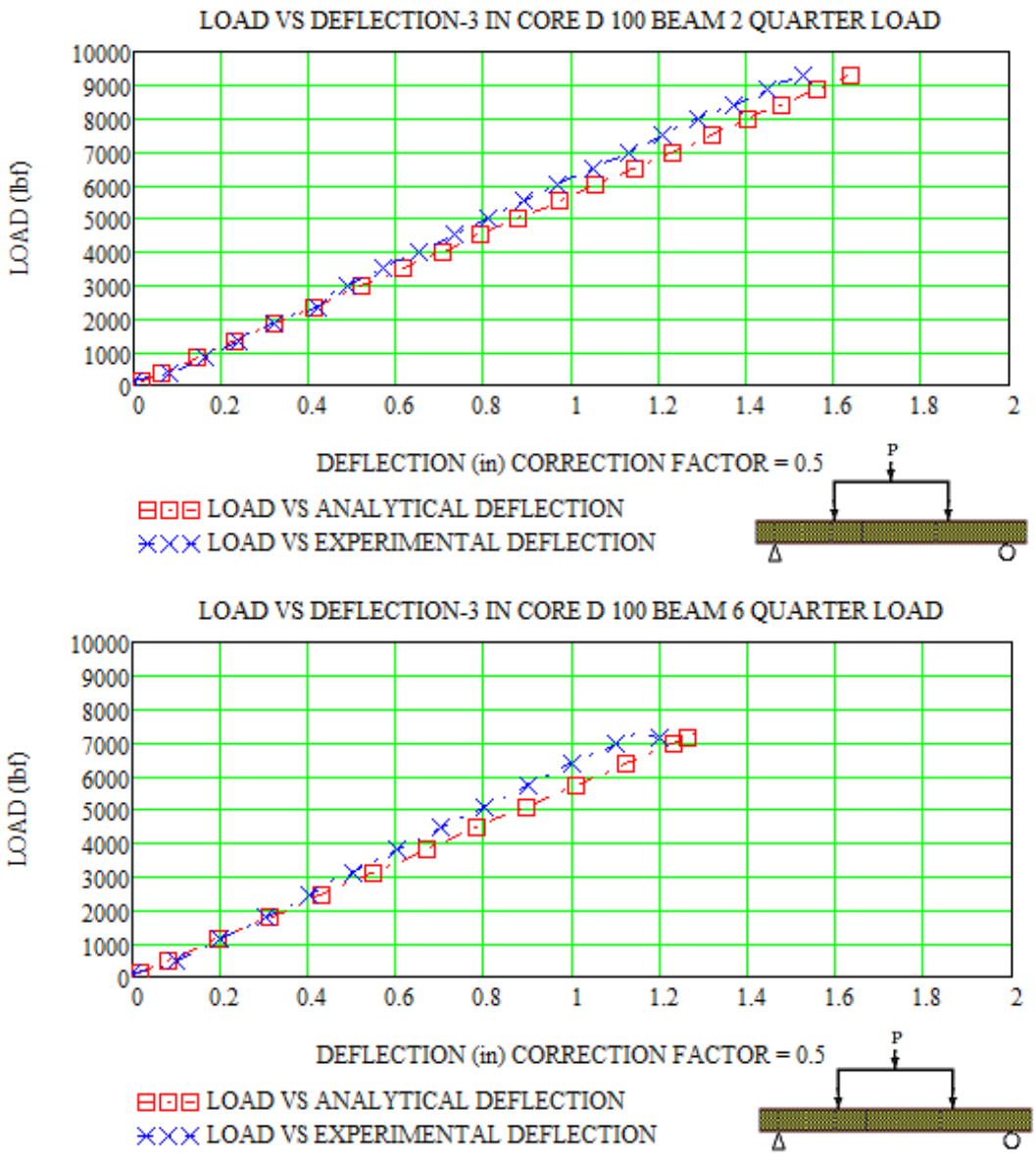

Load vs. Deflection-3 in. core-D 100-quarter load Beam # 1, 2, 6

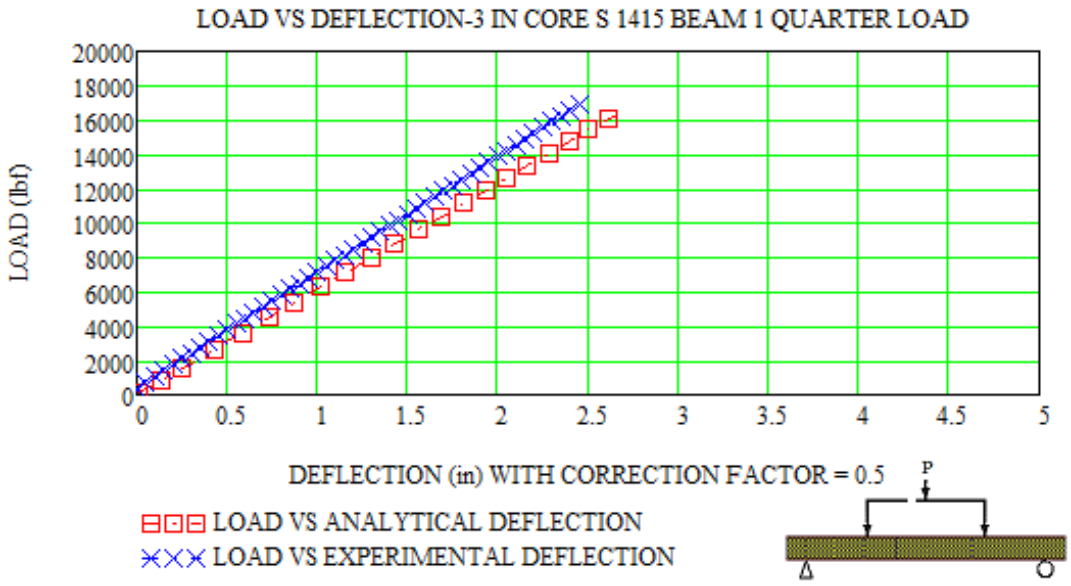
LOAD VS DEFLECTION-3 IN CORE S 1415 BEAM 1 QUARTER LOAD
LOAD (lbf)
20000
18000
16000
14000
12000
10000
8000
6000
4000
2000
0
0
0.5
1
1.5
2
2.5
3
3.5
4
4.5
5
DEFLECTION (in) WITH CORRECTION FACTOR = 0.5
LOAD VS ANALYTICAL DEFLECTION
LOAD VS EXPERIMENTAL DEFLECTION
P

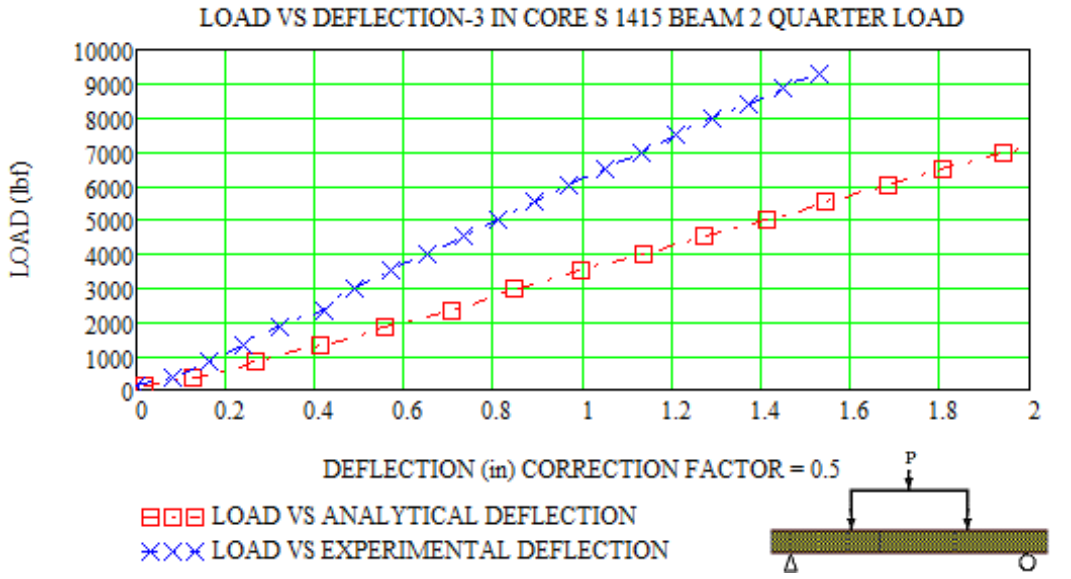
LOAD VS DEFLECTION-3 IN CORE S 1415 BEAM 2 QUARTER LOAD
LOAD (lbf)
10000
9000
8000
7000
6000
5000
4000
3000
2000
1000
0
0
0.2
0.4
0.6
0.8
1
1.2
1.4
1.6
1.8
2
DEFLECTION (in) CORRECTION FACTOR = 0.5
LOAD VS ANALYTICAL DEFLECTION
LOAD VS EXPERIMENTAL DEFLECTION
P

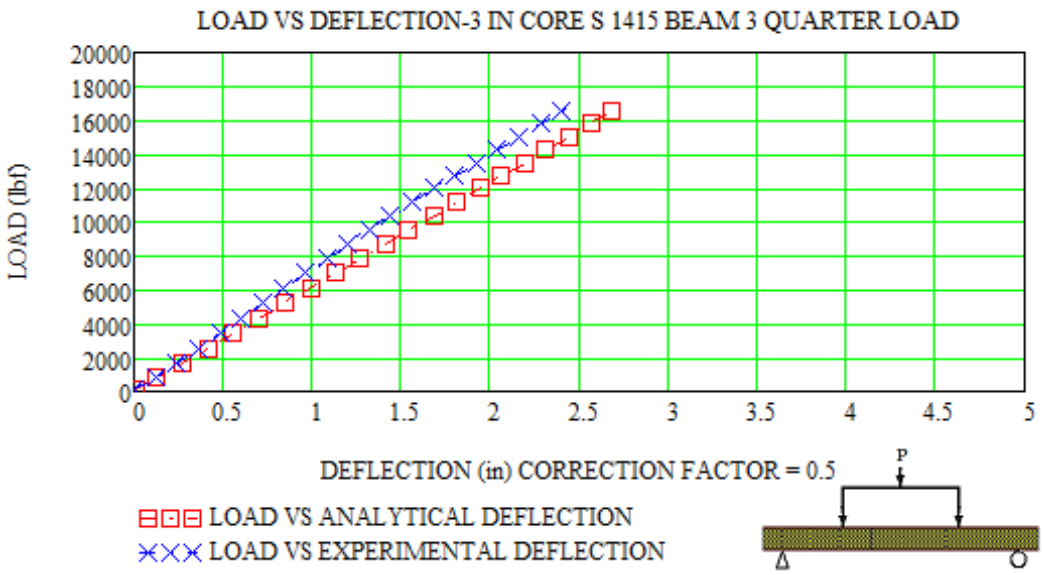

Load vs. Deflection-3 in. core-S 1415-quarter load Beam # 1, 2, 3

VITA

Ho Dac Qui Nhon was born in Qui Nhon, Viet Nam. He attended the Louisiana State University School of Architecture and the University of New Orleans. He graduated from the University of New Orleans with a Bachelor of Science in Civil Engineering. He served as a Civil/Hydraulic Engineer for the U.S. Army Corps of Engineers-New Orleans District with a focus on Hydrologic and Hydraulic modeling. He is presently a Program Coordinator at the Houston Community College, Houston, Texas.